Thermoresponsive Polymer Brushes via Grafting-To Procedures

Lucas W. Teunissen

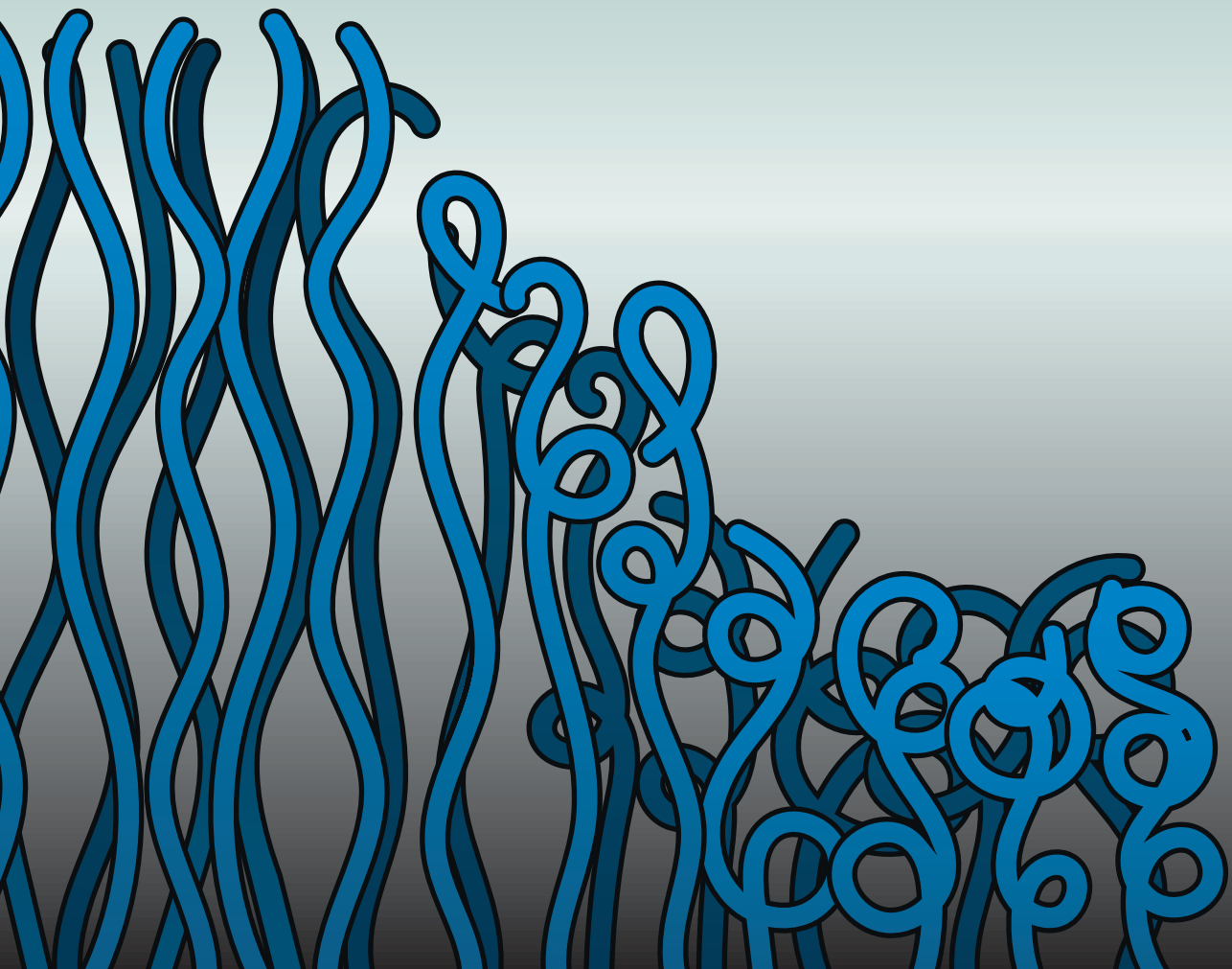

Propositions

1. Polymer brushes synthesized by grafting-to techniques reach 'grafting-from' heights. (this thesis)
2. Polymer brush grafting density and polymer molecular weight are of equal importance for antifouling properties as chemical functionality. (this thesis)
3. Use of anthropomorphisms in science is not appropriate.
4. Social media platforms are the main instigators of societal distrust towards academia.
5. The early division of the Dutch student population into separated high school programs catalyzes societal polarization.
6. Soccer is no industry.

Propositions belonging to the thesis, entitled

Thermoresponsive Polymer Brushes via Grafting-To Procedures

Lucas W. Teunissen
Wageningen, 05-07-2023

Thermoresponsive Polymer Brushes via Grafting-To Procedures

Lucas W. Teunissen

Thesis committee

Promotor
Prof. Dr H. Zuilhof
Professor of Organic Chemistry
Wageningen University & Research

Co-promotor
Dr M.M.J. Smulders
Associate Professor at the Laboratory of Organic Chemistry
Wageningen University & Research

Other members
Prof. Dr J.R. de Vries, Wageningen University & Research
Prof. Dr J. Huskens, University of Twente, Enschede
Prof. Dr M. Weinhart, Freie Universität Berlin, Germany
Dr H. Van der Weijde, Tata Steel Nederland, Velsen

This research was conducted under the auspices of VLAG Graduate School (Biobased, Biomolecular, Chemical, Food and Nutrition Sciences)

Thermoresponsive Polymer Brushes via Grafting-To Procedures

Lucas W. Teunissen

Thesis
submitted in fulfilment of the requirements of the degree of doctor
at Wageningen University
by the authority of the Rector Magnificus,
Prof. Dr A.P.J. Mol,
in the presence of the
Thesis Committee appointed by the Academic Board
to be defended in public
on Wednesday 5 July 2023
at 1:30 p.m. in the Omnia Auditorium.

Lucas W. Teunissen
Thermoresponsive Polymer Brushes via Grafting-To Procedures,
202 pages

PhD thesis, Wageningen University, Wageningen, the Netherlands (2023)
With references, with summary in English

ISBN 978-94-6447-672-9
DOI 10.18174/629341

Table of Contents

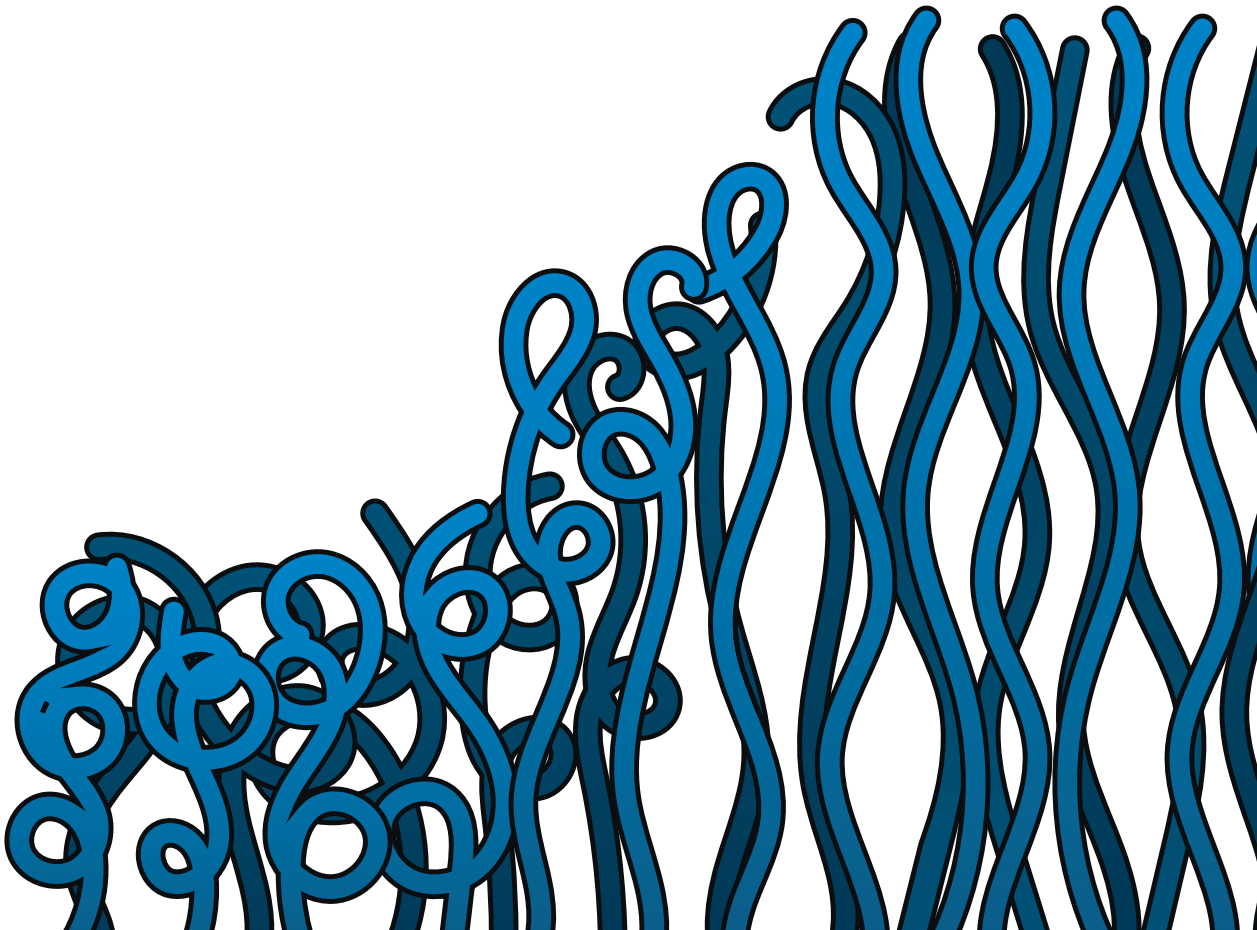

Chapter 1

Introduction

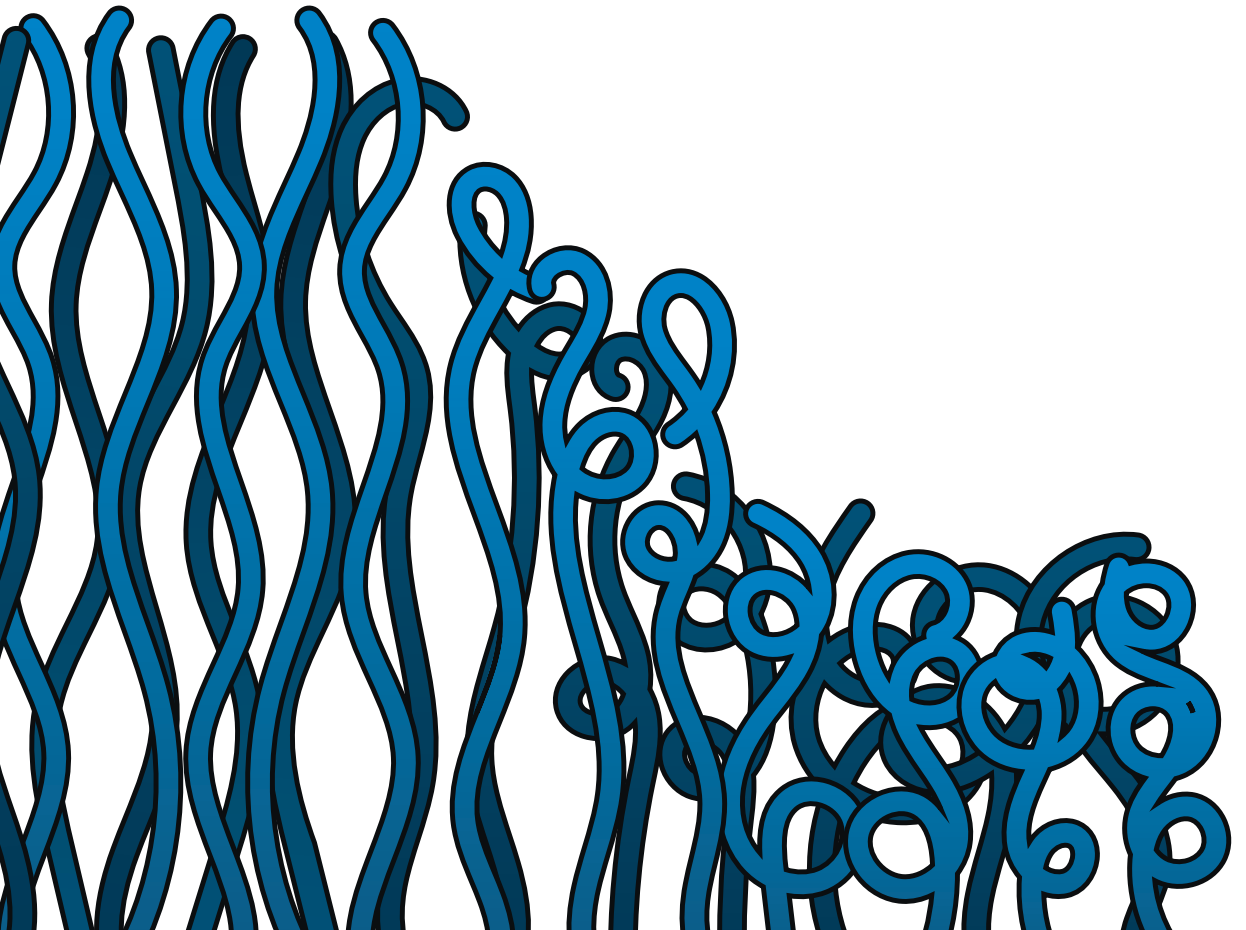

1.1 Surfaces in biomedical applications

1.1.1 Biofouling

Undesired, nonspecific adsorption of proteins, cell adhesion and biofilm formation – known as biofouling – represents a serious challenge in many types of devices (Figure 1.1).[1,2] Adsorption of proteins and cells on medical implants can cause blood clotting, bacterial infections and inflammation, which will lead to rejection of the device.[3,4] The accumulation of proteins and cells in membranes used in hemodialysis and artificial kidneys significantly reduces permittivity, selectivity and membrane lifetime.[5–7] Likewise, nonspecific deposition of biological material on biosensors leads to a decrease and eventually a complete loss in sensitivity towards the analyte.[8–10] Evidently, nonspecific protein adsorption is a regularly occurring phenomenon and ongoing challenge in biomedical applications. Production of biomedical devices therefore requires careful engineering of the device surface to control the interactions with the complex biological media they are exposed to.

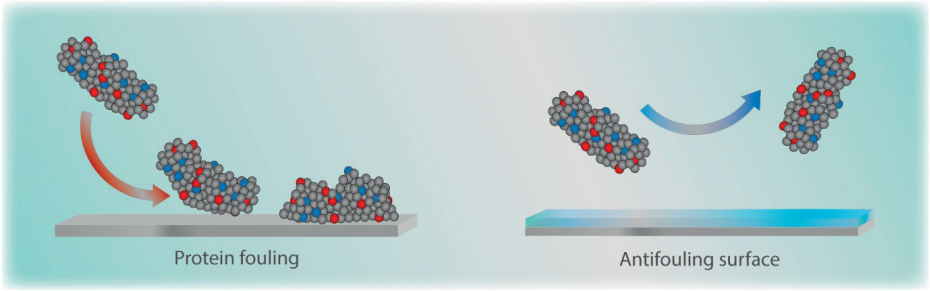

Figure 1.1 Protein adsorption on surfaces, known as biofouling, which can be prevented by introduction of an antifouling layer.

Although biofouling occurs ubiquitously on surfaces of biodevices that are brought in contact with biological media, the exact process of biofouling is complex and different for each situation. It has, however, been determined that most fouling processes are initiated by the adhesion of singular, high-mobility proteins on the substrate surface.[11–14] The deposition of these biological proteins on the surface is governed by a complex interplay of hydrophobic, electrostatic, hydrogen bonding and Van der Waals interactions.[15] Overall, protein adsorption is believed to be a combination of enthalpy gain involving the latter three, close-contact interactions, and - for functionalized surface an often larger - gain in

entropy that is caused by the replacement and release of surface-bound water molecules and salt ions.[15,16] As a result, hydrophobic surfaces are generally more prone to protein adsorption due to weak surface-water interactions.[17] Conversely, protein adsorption on hydrophilic substrates that strongly bind water through hydrogen bonding is inhibited due to the enthalpic penalty linked to the displacement of the coordinating water molecules.[18,19]

1.1.2 Antifouling surfaces

The desire to overcome the complications of protein fouling in biomedical devices has led to numerous studies on the subject of antifouling surfaces.[2,8,12,20–25] The design of these surfaces aims to minimize interactions between the exposed substrate and the fouling species in a particular medium.[20] Currently, the most efficient approach to produce such surfaces is by introduction of a thin organic coating to the device surface. A wide range of organic, antifouling coatings has been developed over the past years with varying chemical compositions. Hydrophilic coatings, that derive their antifouling capabilities primarily from their ability to strongly bind water, were produced based on amino acids,[26] peptides,[27,28] poly(saccharides),[29,30] poly(ethylene glycol) (PEG) derivatives,[31,32] zwitterionics,[33,34] and hydroxypropyl methacrylamide (HPMA).[35–37] In contrast, strongly hydrophobic, low surface energy coatings based on fluorinated polymers have been demonstrated to resist protein adsorption based on the self-cleaning effect.[38,39] This effect occurs due to the weak adhesion of proteins to low surface energy coatings, which causes their release under dynamic conditions.[38]

Apart from the chemical composition of the antifouling layers, a distinction can be made with respect to structural organization of the organic material. The two most commonly employed types of architectures in antifouling layers are self-assembled monolayers (SAMs) and polymer brushes.[23] SAMs are molecular layers that adsorb and self-assemble to form organized surface structures.[40,41] Polymer brushes, in contrast, consist of polymers end-grafted to a surface at high grafting density that, at a sufficiently high surface density, stretch away from the surface.[42,43] Surface modification with SAMs, and specifically SAMs based on PEG derivatives, was long considered the most efficient approach to prevent nonspecific protein adsorption.[44,45] These monolayers performed outstandingly in fouling studies involving single protein solutions.[46,47] However, in more realistic experiments involving complex media such as blood plasma or human serum, SAMs could not prevent biofilm formation.[36,48] Following the development of surface-initiated controlled radical polymerization (SI-CRP) methods, the synthesis of polymer brush coatings became a more prominent approach to introduce surface coatings. Shortly after, polymer brushes based on PEG, zwitterionic and HPMA monomers were produced and found to prevent

protein adsorption more successfully than SAMs.[35,49] In fact, exposure of poly(HPMA) and zwitterionic poly(carboxybetaine methacrylate) brushes to blood plasma did not result in protein adsorption altogether.[36,49] The promising results reported in these studies are illustrative of the advancements that have been made in the field of antifouling surfaces for biomedical applications and underline the potential of polymer brushes in future devices.

In addition to superior resistance to protein adsorption with respect to SAMs, polymer brushes offer greater versatility in terms of chemical components and polymer architecture (discussed in further detail in Section 1.2).[50–52] The currently available controlled radical polymerization techniques allow meticulous design of polymer structure and, thus, integration of multiple functionalities. One of the more exciting options for such added functionality is the incorporation of stimuli-responsive polymers, which paves the way for new technologies in biomedical devices.

1.1.3 Thermoresponsive polymers

One of the main strongpoints of polymers is the wide variety of properties (structural, chemical, mechanical, conformational, electrical, optical) that can be obtained, which is illustrated by the extremely diverse types of polymers applied in industry and day-to-day life. The majority of these polymer materials are produced with specific properties that are intended to persist for at least the lifetime that is expected of its application.

Although most polymers are synthesized to have unchanging properties, there has been increasingly more attention for polymers that respond to changes in their environment.[53] The chemical or physical properties of these materials, commonly addressed as stimuli-responsive polymers, are affected by changes in their environment. To date, many types of responsive polymers have been synthesized, with a diverse set of applicable stimuli including temperature,[54–59] pH,[60,61] solvent type,[62] ionic strength,[63] magnetic and electric fields,[64] mechanical stress,[65,66] and light irradiation.[62,67,68]

Out of the available classes of stimuli-responsive polymers, thermoresponsive polymers have been investigated most intensively, primarily due to the ease of applying changes in temperature.[69] Although several types of temperature-responsive behavior have been reported, the majority of the applied thermoresponsive polymers exhibit a temperature-dependent solubility gap in aqueous solutions (Figure 1.2).[57,59] The temperatures at which the transition occurs between solubility and insolubility are defined as the upper critical solution temperature (UCST) and lower critical solution temperature (LCST).[54,70,71] Polymers that possess a UCST do not dissolve at temperatures below this point due to strong intermolecular interactions between the polymer chains.[56,72] These interactions are reduced with increasing temperature and eventually overcome, resulting in mixing of

polymer and solvent. Reports on UCST-type materials are limited as the conditions required for the phase transition are typically not appropriate for practical applications.[70,72,73] Scientific research that focuses on LCST behavior, on the other hand, has generated considerable momentum over the past decades. In contrast to the enthalpy-governed UCST, the LCST transition is an entropy-driven phenomenon.[54] At temperatures below the LCST, favorable enthalpy due to hydrogen bonds between the polymers and water molecules dominates the free energy of mixing and leads to solvation. The coordination of water molecules, however, is accompanied by an entropic penalty due to increased ordering. With increasing temperature, this entropic contribution grows and eventually results in a positive free energy of mixing and, therefore, phase separation.[54,59] Both the UCST and LCST phase transitions induce a conformational change of the polymer structure, called the coil-globule transition (Figure 1.2).[54,73] Polymer chains that are dissolved adopt a swollen and randomized coil conformation. Upon desolvation, the polymers collapse to form globule-like structures that will aggregate and precipitate unless they are stabilized by added surfactants.[74]

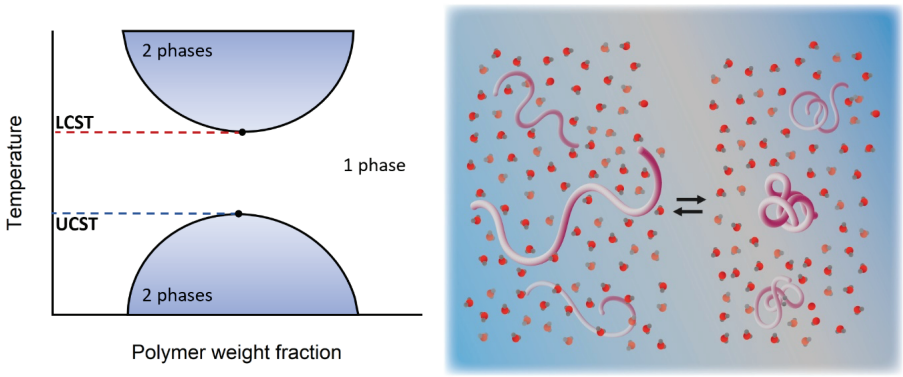

Figure 1.2 (A) Phase diagrams for aqueous solutions of polymers that exhibit LCST- and UCST-type behavior. **(B)** Representation of the coil-globule transition of a LCST-type polymer, which is hydrated and swollen at T < LCST and collapsed and dehydrated at T > LCST.

The theory on thermoresponsive polymers described thus far in this document mainly considered polymer material navigating freely through aqueous solutions. Interestingly, in addition to applications in solution, this class of polymers can be immobilized on surfaces to produce temperature-responsive polymer brush coatings.[56,59,75–79]

1.2 Polymer brush coatings

Polymer brush coatings consist of polymer chains end-grafted to a surface and are typically between 10–100 nm thick.[80] Strictly speaking, the term polymer brushes is reserved for polymer chains that are end-grafted to an interface at sufficiently high grafting density, or chains per unit area.[81] The grafting density and corresponding surface conformation is commonly described by the ratio between the polymer radius of gyration, R_g, and the average distance between chains on the surface, D.[82–84] At low grafting densities, where $D > 2R_g$, there is no interaction between chains and the polymers reside in the "pancake" or "mushroom" regime (Figure 1.3), depending on interactions with solvent and surface.[84,85] In the "brush" regime, the inter-chain distance is smaller than the radius of gyration ($D < 2R_g$), which leads to steric interactions between chains that affect their conformation and direct them away from the surface.[83,86] Further increase of the number of chains per unit area yields high-density brushes, in which the chains are in highly stretched conformations.[83]

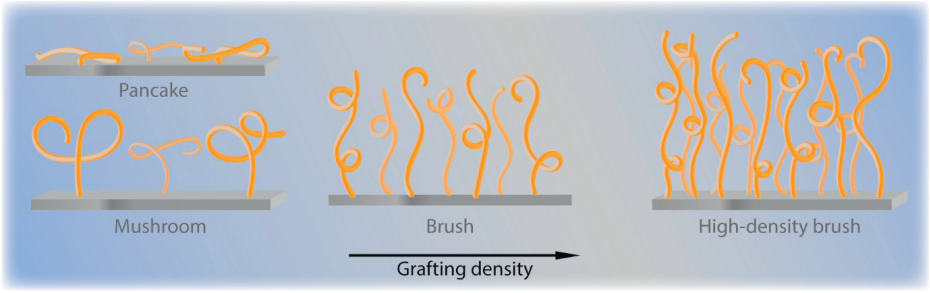

Figure 1.3 Representation of the pancake, mushroom, brush and high-density brush grafting regimes that can be obtained following attachment of polymers to a surface.

The grafting density of the polymer brush has significant impact on the final coating properties.[18,87,88] Likewise, chemical functionality of the monomer, thickness of the brush and type of brush architecture strongly influence the qualities of the resulting coating.[50,89] The design process therefore requires careful consideration of the desired features of the polymer brush, followed by selection of an appropriate synthesis method.

1.2.1 Grafting-to and grafting-from

There are two main strategies that are generally employed to synthesize polymer brushes, the grafting-to and the grafting-from approach (Figure 1.4).[50,90] In the grafting-to approach, pre-synthesized polymer chains are grafted to a surface from solution or melt.[90] The grafting-from approach, on the other hand, involves introduction of polymerization initiator molecules on the target substrate and subsequent polymerization performed from the surface.[50]

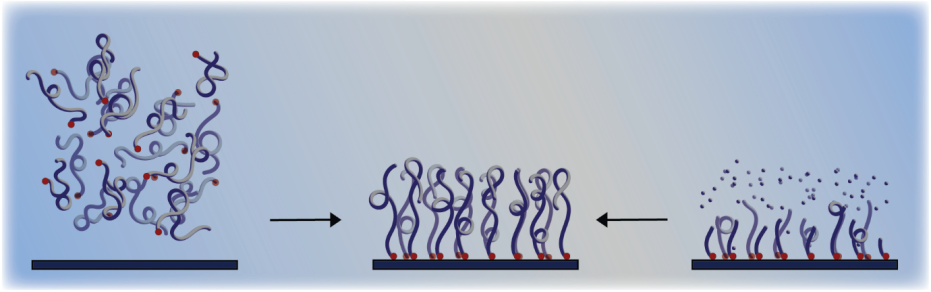

Figure 1.4 Strategies for the synthesis of polymer brushes: grafting-to approach in which pre-synthesized polymers are attached to the surface (left), and grafting-from approach in which polymerization is performed from surface-immobilized polymerization initiators (right).

The primary advantages of the grafting-to approach are increased control over polymer properties and the ability to accurately determine these properties prior to the grafting step.[83] These aspects become considerably more difficult once the polymers are attached to the surface.[91] An additional asset is the relative simplicity of the procedure, which is of importance for potential upscaling of the synthesis process.[50,89] At the same time, the grafting-to approach is met with a prominent drawback. The grafting densities that can be achieved via grafting-to procedures are typically low due to excluded volume interactions between the incoming polymer chains (Figure 1.5).[83] In other words, the attachment of every polymer chain makes it increasingly more difficult for additional incoming chains to bind to the surface. As a result, the grafted polymer chains are frequently in the "mushroom" regime. Increased grafting densities can be achieved by cloud point grafting or grafting from melt, but these techniques require highly specific reactions conditions that limit their general applicability.[92–95] Easy-to-apply grafting-to techniques that can achieve polymer brushes of high grafting density and layer thickness belong to the ultimate goals in this field, yet were scarce at the start of this project.

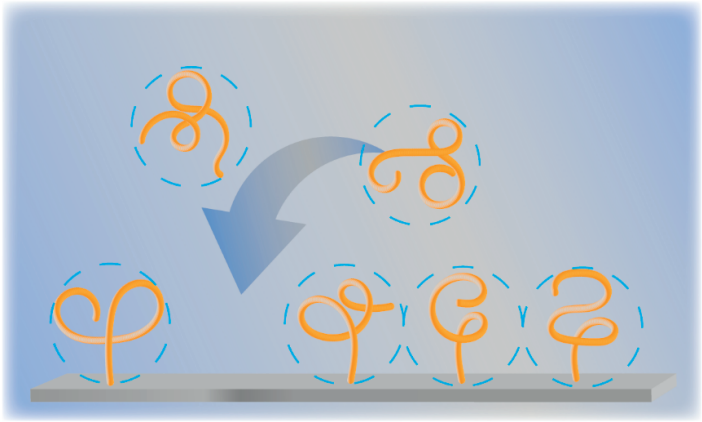

Figure 1.5 Excluded volume interactions of the polymer coils hamper the production of high-grafting density polymer brushes via the grafting-to approach.

Synthesis of polymer brushes using the grafting-from technique does not experience the same limitation in grafting density. During surface-initiated polymerization reactions, relatively small monomer molecules react at initiator sites and, as such, polymer chains are grown from the substrate.[50,51,89] Due to the higher grafting densities and layer thicknesses that can be achieved via the grafting-from synthesis, it has been the preferred method for polymer brush synthesis.[50] In spite of its popularity, the grafting-from approach also has its shortcomings. As mentioned above, thorough determination of polymer properties such as molecular weight, polydispersity and grafting density is challenging as the chains are immediately attached to the surface.[83,91] Moreover, polymerization from a surface is typically more complicated experimentally, especially for larger substrates, which limits its potential in future commercial applications.[96]

Evidently, both strategies have their strongpoints and their suitability will depend on the particular situation. Despite their differences, grafting-from and grafting-to methods have one procedural step in common, the polymerization. In fact, most synthesis procedures employ the exact same polymerization techniques.

1.2.2 Reversible-deactivation radical polymerization

One of the main reasons for the huge interest in polymer brush coatings is the ability to accurately control the properties of the polymers and therefore those of the coating. The origin of this control lies within the development of reversible-deactivation radical polymerization (RDRP) techniques, such as atom transfer radical polymerization (ATRP),

reversible addition-fragmentation chain-transfer polymerization (RAFT), nitroxide-mediated polymerization (NMP) and photoiniferter-mediated polymerization (PIMP).[97–100] For grafting-to approaches, these polymerization techniques are generally applied in solution, whereas grafting-from approaches rely on surface-initiated reactions.[43,50,66] The improved control over RDRP reactions in comparison with free radical polymerization reactions stems from the reversible deactivation reactions that take place during the polymerization. The growing polymer chains are constantly activated and then quickly deactivated again. Monomers can only be added to the growing chains when they are in the active state, whereas in deactivated state, the chains are dormant. Throughout the polymerization, the polymer chains mainly reside in the dormant state and the concentration of active species at any point during the reaction is low.[100] Due to the low concentration of active species, chain termination reactions occur to minimal extent. RDRP polymerization reactions therefore yield polymers of narrow molecular dispersity, in contrast with polymers synthesized using free radical polymerization. Moreover, the deactivation of growing chains and corresponding absence of termination reactions ensures end-group fidelity and makes RDRP polymerization reactions the technique of choice for synthesis of (multi) block copolymers and other more complex polymer architectures.[97,101] Additionally, RDRP techniques are compatible with a wide range of monomers, which allows the synthesis of many different types of polymers.[101]

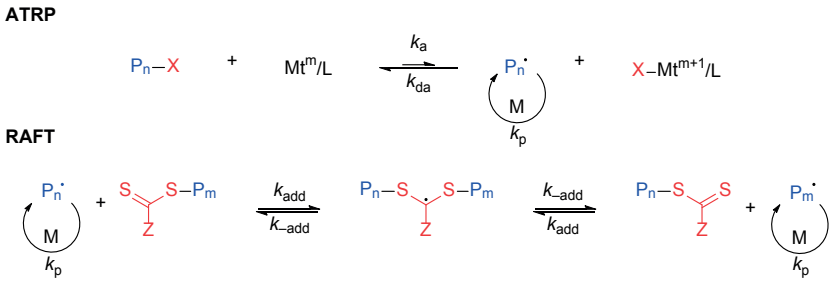

Scheme 1.1 Mechanisms for atom transfer radical polymerization (ATRP) and reversible addition-fragmentation chain-transfer (RAFT) polymerization. P_n/P_m = growing chains, X = halide, Mt^m/L = transition metal complex, M = monomer, Z = CTA side group.

The most popular of the RDRP techniques in polymer brush synthesis are atom transfer radical polymerization (ATRP) and reversible addition-fragmentation chain-transfer (RAFT) polymerization.[97] ATRP is a metal-catalyzed radical polymerization reaction, in which the catalyst is a redox-active transition metal catalyst. Copper is by far the most

frequently employed metal, although the reaction can also be performed using alternatives including ruthenium, iron and molybdenum catalysts.[102] The ATRP mechanism proceeds via activation of alkyl halides by the transition metal catalyst, which removes the halogen atom and generates the active radical species (Scheme 1.1). Return of the subtracted halide to the growing chain removes the free radical species and deactivates the growing chain. The fast reversible deactivation of the growing chains strongly limits the number of termination reactions that occur during polymerization. The produced polymers therefore typically have low polydispersity and display high end-group fidelity, which can be used for further polymerization or post-polymerization functionalization.[103] The extensive control during polymerization, in combination with the low-cost and easily available catalyst complexes and initiators, has seen ATRP become the most commonly applied RDRP technique.[104] RAFT polymerization, however, is arguably the most straightforward of the RDRP techniques in terms of experimental procedure.[105] The RAFT mechanism is different from that of ATRP, since the deactivation of the growing chains proceeds through degenerative chain transfer reactions induced by a chain-transfer agent (CTA) (Scheme 1.1).[103] Radicals are generated using initiator molecules which then react with monomers to form growing polymer chains. The CTA, a molecule carrying typically a thiocarbonylthio group, adds to the growing chains and thereby reversibly deactivates them. Similar to ATRP and other RDRP techniques, the reversible deactivation of the polymer chains provides control over the reaction and yields monodisperse polymers with high end-group fidelity. As mentioned above, RAFT polymerization is arguably the simplest of the RDRP techniques as it merely requires addition of CTA to a polymerization mixture.[97] In addition, RAFT has the broadest compatibility with monomer types.[97,106,107]

RDRP techniques have revolutionized polymer science and, accordingly, the field of polymer brush coatings. Application of the controlled polymerization methods on surfaces have greatly increased the possibilities for different polymer brush designs and architectures.[50,89] The high end-group fidelity that is characteristic for RDRP techniques can be employed to synthesize countless combinations of copolymers in varying compositions, including block, gradient and alternating copolymers (Figure 1.6).

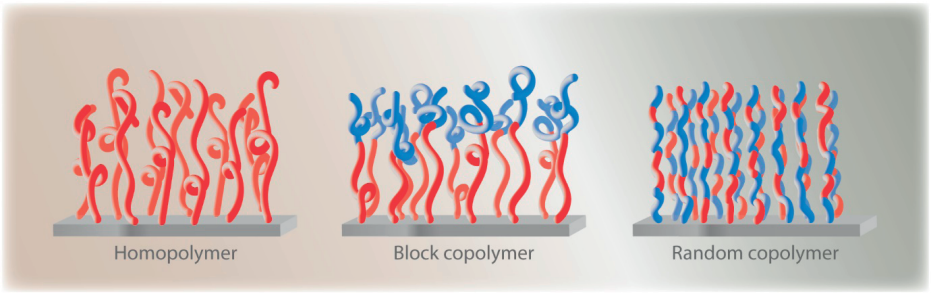

Figure 1.6 Examples of the polymer brush architectures that can be achieved using surface-initiated RDRP methods.

1.2.3 Antifouling polymer brushes

As was mentioned in Section 1.1.2, the most promising materials to prepare antifouling surfaces are polymer brush coatings. Numerous studies have been performed in which, using RDRP techniques, antifouling polymer brushes were synthesized and tested against biological media.[22] In certain studies, the antifouling polymer brush coatings displayed such strong antifouling properties that they succeeded in preventing adsorption from complex biological media, such as human blood plasma.[36,49] The outstanding performance of these antifouling polymer brushes is believed to originate from two contributing factors. First of all, the polymer brushes are of hydrophilic nature and, in aqueous environment, form a hydration barrier of coordinated water molecules.[44,45] Approaching proteins will need to displace these water molecules in order to adsorb to the surface molecules, but this is thermodynamically unfavorable. Secondly, the adsorption of the protein on the surface will cause compression of the densely-grafted polymer chains, which is unfavorable due to a decrease in conformational entropy and a coinciding osmotic pressure penalty.[23,108,109] As can be intuitively grasped, and as confirmed by theoretical studies, the compression of polymer brushes becomes increasingly unfavorable with higher grafting densities.[108] This theory was indeed confirmed experimentally by demonstrating that protein adsorption occurs more easily on polymer brushes of lower grafting density.[18,110]

1.2.4. Thermoresponsive polymer brushes

The introduction of thermoresponsive properties to polymer brush coatings has resulted in the development of many innovative coating technologies.[56,79] As was observed in solution, described in Section 1.1.3, surface-grafted thermoresponsive polymers undergo the coil-globule transition when crossing the LCST.[56,79,111] At temperatures below the LCST,

the polymer brush is solvated and the chains adopt a swollen conformation (Figure 1.7).[112] Then, when the temperature exceeds the LCST, the polymers are desolvated and collapse towards the surface to form globule-like structures.

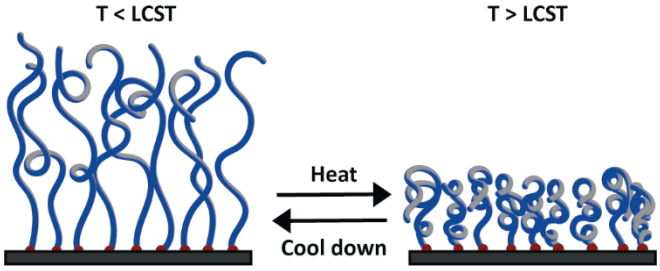

Figure 1.7 Representation of the LCST transition for thermoresponsive polymer brush coatings.

The conformational change that occurs within the brush is strongly affected by the grafting density and molecular weight of the polymers.[87,88,110,113] For extremely dense brushes, only a slight decrease in thickness is observed when the temperature is raised above the LCST.[88] The high grafting density of these brushes does not leave much space for the polymer chains to collapse. Surprisingly, brushes of low grafting densities were also found to have a limited conformational change following the phase transition, because below the LCST the chains were not forced into a stretched brush regime, but adopted a mushroom conformation. The largest conformational change is therefore detected for brushes at intermediate grafting densities. At these densities, the polymers are grafted close enough to force chains away from the surface below the LCST, but distant enough to allow adoption of a collapsed state above the LCST.[113]

Along with the conformational change of thermoresponsive polymer brushes, the surface properties of the material change during the phase transition. The altered surface properties affect the interactions of the polymer material with its surroundings.[79] This feature has been exploited in recent years for the development of new coating technologies in biomedical devices.[56,77–79,114] The ability to control adsorption of biological material with variation of temperature has allowed the development of cutting-edge applications that facilitate controlled cell sheet release in culture dishes,[115–117] kill-and-release of bacteria in bactericidal coatings,[118] and switchable protein adsorption in biosensor devices.[119]

The polymer that is most frequently employed in thermoresponsive surface coatings is poly(*N*-isopropylacrylamide) (poly(NIPAM)).[78,120,121] The characteristic LCST of 32 °C led to the immense interest in this particular polymer, more so as the critical temperature

is hardly sensitive to changes in its environment, such as pH or salt concentration.[121,122] Consequently, the thermoresponsive properties of poly(NIPAM) can be addressed in applications that operate at near-physiological temperatures. Poly(NIPAM) is therefore an ideal candidate for applications in biomedical devices and has been at the heart of many innovative polymer brush technologies.[56,77–79,114] It should, however, be mentioned that the success of poly(NIPAM) has limited studies of other thermoresponsive polymers in polymer brush coatings. Investigation of complementary thermoresponsive polymers will not only diversify the field of thermoresponsive polymer brushes, but can also overcome limitations involving polymerization of NIPAM. For instance, the synthesis of block copolymer brushes using poly(NIPAM) as the first block is restricted, as only a limited number of monomers can be successfully polymerized from poly(acrylamide) structures using RDRP reactions.[123] Termination reactions that occur during polymerization of NIPAM further complicate its use.[124] Review of novel candidates for thermoresponsive polymer brushes is therefore sure to complement the presently employed materials.

1.3 The link to the surface

Apart from the synthesis of the polymers, either via grafting-from or grafting-to, the method of binding between the target substrate and the polymer brush is an extremely important factor in coating performance. Generally, polymer brushes are attached to a surface via either physisorption or chemisorption.[42,89,90] Increasingly, the polymer brush coatings are linked covalently to the target substrate to achieve increased stability and durability of the coating.[50,90] In terms of attachment chemistries for polymer brush synthesis, a distinction can be made between attachment of polymerization initiators for grafting-from polymerization, or introduction of reactive handles to facilitate binding of polymers via the grafting-to approach.

1.3.1 Common anchors

Typically employed anchoring groups for the immobilization of polymerization initiators on a target substrate include silanes and thiols/disulfides.[50] Silanes are extremely effective modification agents for silicon oxide and various metal oxides and, under appropriate conditions, form SAMs.[125] Thiol- and disulfide-containing compounds, on the other hand, bind strongly to noble metal surfaces, arranging themselves in highly ordered SAMs.[125] Polymerization initiators can thus efficiently be introduced to noble metal surfaces such as gold and platinum utilizing the affinity between sulfur and noble metals.[126] Other func-

tional groups that are employed to a lesser extent for the introduction of polymerization initiators to a target substrate include phosphonic acids, alkenes and carboxylates.[125]

The most straightforward procedure to attach polymers via a grafting-to approach is likely grafting of thiol-capped polymers to noble metal surfaces. This strategy does not require functionalization of the substrate with anchoring groups and merely involves dip-coating in polymer solution.[87,93] Unfortunately, grafting of polymer brushes to other surface types generally does require surface activation, *i.e.* the prior introduction of reactive functional groups at the substrate.[90] A commonly employed procedure involves functionalization of the surface with epoxide groups via attachment of epoxide-functionalized silanes.[127,128] The resulting epoxide groups then act as reactive handle that can be addressed to covalently bind the polymer material. Alternatively, functional groups that allow linking through click chemistry are regularly utilized to perform grafting-to reactions.[129–131]

1.3.2 Substrate-independent coating techniques

The large differences in chemical and physical properties between various types of materials complicate the development of modularly applicable surface modification methods. Nevertheless, there are several approaches that appear to successfully modify most materials.[132] These techniques include surface modifications from the gas phase, such as chemical vapor deposition polymerization and plasma polymerization deposition, as well as solution-phase methods, such as layer-by-layer deposition and spin coating.[132]

Chemical vapor deposition employs volatile monomers which are vaporized and then polymerized on the target surface.[133] This technique is frequently employed to produce polymer films with specific functionality, but the layers regularly only weakly adhere to the substrate.[134] Plasma polymerization deposition also utilizes monomer vapor to synthesize polymer films on a substrate. However, this technique typically enables covalent anchoring and crosslinking of the monomers on the surface of interest, increasing the adhesion strength to the surface.[135,136] Large-scale application of this techniques is not straightforward, though, as high-end equipment is required to perform the deposition.[133]

Layer-by-layer assembly of polymer material to introduce thin films to a surface is experimentally simple, and can be employed to substrates of all shapes and sizes.[137] The procedure involves sequential exposure of the substrate to solutions containing the layering materials. The classic example of layer-by-layer assemblies is the alternating layer stack of positively and negatively charged polyelectrolytes that rely on electrostatic interactions.[138] Alternatives do exist, in which for example hydrogen bonding, charge transfer interactions or host-guest interactions provide attractive forces between layers and the

interface.[139] The non-covalent interactions between the assembly and the substrate are prone to stability issues, especially in the presence of high ion concentrations.[139] Finally, spin coating allows highly uniform deposition of polymer films by placing polymer solution in the middle of a substrate which is rotated at high speed.[140] Although a popular lab technique, spin coating becomes more difficult with increasing substrate size and is not very suitable for large-scale applications.[140]

1.3.3 Poly(dopamine)

None of the methods described in Section 1.3.2 is as simple or as universally applicable on different surface types as poly(dopamine) deposition.[141] Since the first report, which introduced the extraordinary adhesive properties of poly(dopamine) films after a study of the adhesive proteins in mussels, poly(dopamine) films have had enormous impact on surface science.[142,143] The types of surfaces that can be modified is seemingly limitless and ranges from metals and metal oxides to carbon structures and polymer surfaces.[143]

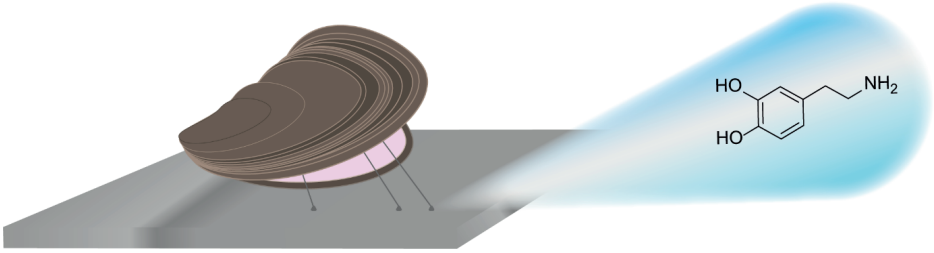

Figure 1.8 Adhesive films based on dopamine mimic the adhesive plaque in mussel byssal threads that enables mussels to stick to almost any kind of surface, even in cold water.

Despite several investigations, the exact poly(dopamine) structure and mechanism of formation have not yet been fully established.[144–147] It is commonly argued that it is indeed impossible to elucidate these facets completely, as they are affected by the conditions of deposition and the nature of the substrate.[147–151] The starting point for poly(dopamine) formation is evident, however, and involves the oxidation of dopamine to form dopamine quinone and further derivatives.[147,151] These species can form C–C crosslinks in a seemingly random manner to form a highly complicated network of poly(dopamine) structures. Additional linkages can be formed by Michael addition and Schiff-base reactions involving the amine groups present in dopamine.[152] These reactions yield primarily oligomeric structures that, in turn, are interconnected via supramolecular interactions.[144,151] The adhesive

strength of this complex poly(dopamine) network is, like its polymerization mechanism, not yet fully understood.[153] It is currently believed, however, that interplay between the catechol and amino groups in the structure play a prominent roll.[146,152,154,155]

In addition to a near-universal applicability, poly(dopamine)-based surface modification is of immense interest because it is a low-cost and experimentally straightforward method to introduce reactive functional groups to a substrate.[142,143,147] The poly(dopamine) structure is known to contain catechols, quinones, amines and arenes that can be targeted for reactions to introduce specific functionalities to the surface.[147] Amongst others, these reactive sites provide the possibility to attach polymer brush coatings on poly(dopamine) films.[156–162]

1.3.4 Modular polymer brush synthesis

The easy, fast, and substrate-independent applicability of poly(dopamine) films constitutes an outstanding means to attach polymer brush coatings to various surfaces. In polymer brush research, poly(dopamine) films have been employed in combination with the grafting-from approach.[156–164] Polymerization initiators were attached to poly(dopamine) and surface-initiated polymerization reactions were performed from the poly(dopamine) film. Using this approach, polymer brush coatings were synthesized that displayed antibacterial,[163] controlled cell-adhesion,[156,161] and antifouling properties.[162] The unique adhesive properties of poly(dopamine) have led to the development of modular procedures for the synthesis of polymer brushes.[159,160,162] The availability of a modular and simple synthesis technique will broaden the applicability and relevance of polymer brushes in general. Several studies have demonstrated substrate-independent grafting-from methods, in which polymer brushes were synthesized from various poly(dopamine)-modified substrate types.[159,160,162] In some cases, the modularity could even be extended to polymer functionality, as different types of substrate were coated with various polymer brush types.[159,164]

In addition to grafting-from procedures, polymer brush synthesis can also be performed by grafting polymers to poly(dopamine).[165–169] Using various attachment chemistries, functional polymers were successfully grafted to poly(dopamine)-modified substrates. Applicability to multiple substrate types, however, has rarely been demonstrated for grafting-to approaches.[168] Furthermore, modular grafting-to methods that are substrate-independent and, in addition, allow introduction of a variety of functional groups are currently lacking. A method like that would provide the field of surface engineering with a highly versatile tool to produce polymer brush coatings with extensive control over polymer properties and functionality, suitable for a wide range of substrates.

1.4 Thesis outline

The development of thermoresponsive polymer brush coatings has introduced a new phase in the design of biomedical devices. Exciting and innovative applications for poly(NIPAM) polymer brushes have already been developed, and the first examples of commercial applications have been reported.[77] However, for the research field to continue making progress, it is important to further study alternative, thermoresponsive polymer brush coatings. Additionally, it is of immense value to study the design of a substrate-independent grafting-to approach that produces functional polymer brush coatings and can potentially contribute to future large-scale production methods.

The synthesis and characterization of a novel thermoresponsive brush is described in **Chapter 2**. Poly(*N*-(2-methacryloyloxyethyl)pyrrolidone (poly(NMEP)) brushes are synthesized using surface-initiated ATRP (SI-ATRP). The height profiles of the polymer brush obtained using atomic force microscopy in aqueous environment clearly demonstrate reversible thermoresponsiveness. Furthermore, we show that poly(NMEP) brushes can be used as basis for the synthesis of block copolymer brushes and, finally, demonstrate the antifouling properties of the coating.

In **Chapter 3**, we introduce a grafting-to procedure that allows the synthesis of thermoresponsive polymer brush coatings with appreciable grafting density and brush thickness. The two-step procedure involves deposition of a poly(dopamine) primer layer and subsequent grafting-to of poly(GMA)-*b*-poly(NIPAM) block copolymers. The influence of the size of the poly(NIPAM) block, and inherently the grafting density of the brushes, on the thermoresponsive behavior of the coating is discussed based on measurements carried out using a quartz crystal microbalance with dissipation monitoring (QCM-D). We demonstrate that these polymer brush properties affect the switchable protein adsorption above and below the LCST.

The optimization of the grafting-to procedure is reported in **Chapter 4**, based on analysis of the properties of the poly(dopamine) primer layer and on their effect on the subsequent grafting step. Experimental results, including XPS, AFM, spectroscopic ellipsometry and contact angle measurements, indicate that the poly(dopamine) deposition conditions strongly influence the physical and chemical features of the poly(dopamine) films. We demonstrate that these conditions play a crucial role in the success of the grafting step and stability of the coating. We show that, under optimized conditions, it is possible to obtain layer thicknesses of up to 19 nm for the grafted polymers, which is very high for grafted-to polymer brushes, and bring a wide range of further applications into view.

The universally applicable adhesive properties of poly(dopamine) films prompted us to broaden the scope of the two-step grafting to procedure, as is described in **Chapter 5**. We show that this procedure can be employed independent of surface type by successful modification of gold, silicon oxide and polyester-coated substrates. Moreover, we reveal that the modularity of the approach can be extended even further by grafting a range of block copolymers containing various functional groups. Finally, we demonstrate how this method can be used without adaptations to produce binary brush systems.

The work described in this thesis is brought into perspective in **Chapter 6**. The current state of the polymer brush research field is discussed and linked to the advancements that were made during this project.

1.5 References

1. Chen, S., Li, L., Zhao, C. & Zheng, J. Surface hydration: Principles and applications toward low-fouling/nonfouling biomaterials. *Polymer (Guildf).* **51**, 5283–5293 (2010).
2. Bixler, G. D. & Bhushan, B. Biofouling: lessons from nature. *Philos. Trans. R. Soc. A Math. Phys. Eng. Sci.* **370**, 2381–2417 (2012).
3. Liu, S. & Guo, W. Anti-Biofouling and Healable Materials: Preparation, Mechanisms, and Biomedical Applications. *Adv. Funct. Mater.* **28**, 1800596 (2018).
4. Harding, J. L. & Reynolds, M. M. Combating medical device fouling. *Trends Biotechnol.* **32**, 140–146 (2014).
5. Yang, Q. & Mi, B. Nanomaterials for Membrane Fouling Control: Accomplishments and Challenges. *Adv. Chronic Kidney Dis.* **20**, 536–555 (2013).
6. Deppisch, R., Storr, M., Buck, R. & Göhl, H. Blood material interactions at the surfaces of membranes in medical applications. *Sep. Purif. Technol.* **14**, 241–254 (1998).
7. Rana, D. & Matsuura, T. Surface modifications for antifouling membranes. *Chem. Rev.* **110**, 2448–2471 (2010).
8. Vaisocherová, H., Brynda, E. & Homola, J. Functionalizable low-fouling coatings for label-free biosensing in complex biological media: advances and applications. *Anal. Bioanal. Chem.* **407**, 3927–3953 (2015).
9. Wisniewski, N. & Reichert, M. Methods for reducing biosensor membrane biofouling. *Colloids Surfaces B Biointerfaces* **18**, 197–219 (2000).
10. Rong, G., Corrie, S. R. & Clark, H. A. In Vivo Biosensing: Progress and Perspectives. *ACS Sensors* **2**, 327–338 (2017).
11. Yang, W. J., Neoh, K., Kang, E., Teo, S. L. & Rittschof, D. Polymer brush coatings for combating marine biofouling. *Prog. Polym. Sci.* **39**, 1017–1042 (2014).
12. Blaszykowski, C., Sheikh, S. & Thompson, M. A survey of state-of-the-art surface chemistries to minimize fouling from human and animal biofluids. *Biomater. Sci.* **3**, 1335–1370 (2015).
13. Thevenot, P., Hu, W. & Tang, L. Surface Chemistry Influences Implant Biocompatibility. *Curr. Top. Med. Chem.* **8**, 270–280 (2008).
14. Blaszykowski, C., Sheikh, S. & Thompson, M. Surface chemistry to minimize fouling from blood-based fluids. *Chem. Soc. Rev.* **41**, 5599–5612 (2012).
15. Norde, W. Driving forces for protein adsorption at solid surfaces. *Macromol. Symp.* **103**, 5–18 (1996).
16. Rabe, M., Verdes, D. & Seeger, S. Understanding protein adsorption phenomena at solid surfaces. *Adv. Colloid Interface Sci.* **162**, 87–106 (2011).
17. Malmsten, M. Formation of Adsorbed Protein Layers. *J. Colloid Interface Sci.* **207**, 186–199 (1998).
18. Wang, Y. M. *et al.* Grafting density and antifouling properties of poly[N-(2-hydroxypropyl) methacrylamide] brushes prepared by "grafting to" and "grafting from". *Polym. Chem.* **13**, 3815–3826 (2022).
19. Rosenhahn, A., Schilp, S., Kreuzer, H. J. & Grunze, M. The role of inert surface chemistry in marine biofouling prevention. *Phys. Chem. Chem. Phys.* **12**, 4273–4274 (2010).
20. Zhang, H. & Chiao, M. Anti-fouling coatings of poly(dimethylsiloxane) devices for biological and biomedical applications. *J. Med. Biol. Eng.* **35**, 143–155 (2015).

21. Higaki, Y., Kobayashi, M., Murakami, D. & Takahara, A. Anti-fouling behavior of polymer brush immobilized surfaces. *Polym. J.* **48**, 325–331 (2016).

22. Maan, A. M. C., Hofman, A. H., de Vos, W. M. & Kamperman, M. Recent Developments and Practical Feasibility of Polymer-Based Antifouling Coatings. *Adv. Funct. Mater.* **30**, 2000936 (2020).

23. Banerjee, I., Pangule, R. C. & Kane, R. S. Antifouling coatings: Recent developments in the design of surfaces that prevent fouling by proteins, bacteria, and marine organisms. *Adv. Mater.* **23**, 690–718 (2011).

24. Liu, L., Li, W. & Liu, Q. Recent development of antifouling polymers: structure, evaluation, and biomedical applications in nano/micro-structures. *Wiley Interdiscip. Rev. Nanomedicine Nanobiotechnology* **6**, 599–614 (2014).

25. Faustino, C. M. C., Lemos, S. M. C., Monge, N. & Ribeiro, I. A. C. A scope at antifouling strategies to prevent catheter-associated infections. *Adv. Colloid Interface Sci.* **284**, 102230 (2020).

26. Lee, D. U. *et al.* Amino acid-mediated negatively charged surface improve antifouling and tribological characteristics for medical applications. *Colloids Surfaces B Biointerfaces* **211**, 112314 (2022).

27. Bolduc, O. R., Clouthier, C. M., Pelletier, J. N. & Masson, J.-F. Peptide Self-Assembled Monolayers for Label-Free and Unamplified Surface Plasmon Resonance Biosensing in Crude Cell Lysate. *Anal. Chem.* **81**, 6779–6788 (2009).

28. Li, G. *et al.* Ultra low fouling zwitterionic polymers with a biomimetic adhesive group. *Biomaterials* **29**, 4592–4597 (2008).

29. Holland, N. B., Qiu, Y., Ruegsegger, M. & Marchant, R. E. Biomimetic engineering of non-adhesive glycocalyx-like surfaces using oligosaccharide surfactant polymers. *Nature* **392**, 799–801 (1998).

30. Mohan, T. *et al.* Highly Protein Repellent and Antiadhesive Polysaccharide Biomaterial Coating for Urinary Catheter Applications. *ACS Biomater. Sci. Eng.* **5**, 5825–5832 (2019).

31. Lowe, S., O'Brien-Simpson, N. M. & Connal, L. A. Antibiofouling polymer interfaces: poly(ethylene glycol) and other promising candidates. *Polym. Chem.* **6**, 198–212 (2015).

32. Knop, K., Hoogenboom, R., Fischer, D. & Schubert, U. S. Poly(ethylene glycol) in drug delivery: Pros and cons as well as potential alternatives. *Angew. Chemie - Int. Ed.* **49**, 6288–6308 (2010).

33. Cao, Z. & Jiang, S. Super-hydrophilic zwitterionic poly(carboxybetaine) and amphiphilic non-ionic poly(ethylene glycol) for stealth nanoparticles. *Nano Today* **7**, 404–413 (2012).

34. Zheng, L., Sundaram, H. S., Wei, Z., Li, C. & Yuan, Z. Applications of zwitterionic polymers. *React. Funct. Polym.* **118**, 51–61 (2017).

35. Rodriguez-Emmenegger, C., Houska, M., Alles, A. B. & Brynda, E. Surfaces Resistant to Fouling from Biological Fluids: Towards Bioactive Surfaces for Real Applications. *Macromol. Biosci.* **12**, 1413–1422 (2012).

36. Rodriguez-Emmenegger, C. *et al.* Polymer brushes showing non-fouling in blood plasma challenge the currently accepted design of protein resistant surfaces. *Macromol. Rapid Commun.* **32**, 952–957 (2011).

37. Kuzmyn, A. R., Nguyen, A. T., Teunissen, L. W., Zuilhof, H. & Baggerman, J. Antifouling Polymer Brushes via Oxygen-Tolerant Surface-Initiated PET-RAFT. *Langmuir* **36**, 4439–4446 (2020).

38. Krishnan, S. *et al.* Comparison of the fouling release properties of hydrophobic fluorinated and hydrophilic PEGylated block copolymer surfaces: Attachment strength of the diatom Navicula and the green alga Ulva. *Biomacromolecules* **7**, 1449–1462 (2006).

39. Koguchi, R., Jankova, K. & Tanaka, M. Fluorine-containing bio-inert polymers: Roles of intermediate water. *Acta Biomater.* **138**, 34–56 (2022).

40. Ulman, A. Formation and Structure of Self-Assembled Monolayers. *Chem. Rev.* **96**, 1533–1554 (1996).

41. Gooding, J. J., Mearns, F., Yang, W. & Liu, J. Self-assembled monolayers into the 21st century: Recent advances and applications. *Electroanalysis* **15**, 81–96 (2003).

42. Zhao, B. & Brittain, W. J. Polymer brushes: Surface-immobilized macromolecules. *Prog. Polym. Sci.* **25**, 677–710 (2000).

43. Barbey, R. & Klok, H. A. Room temperature, aqueous post-polymerization modification of glycidyl methacrylate-containing polymer brushes prepared via surface-initiated atom transfer radical polymerization. *Langmuir* **26**, 18219–18230 (2010).

44. Ostuni, E., Chapman, R. G., Holmlin, R. E., Takayama, S. & Whitesides, G. M. A survey of structure-property relationships of surfaces that resist the adsorption of protein. *Langmuir* **17**, 5605–5620 (2001).

45. Chapman, R. G. *et al.* Surveying for Surfaces that Resist the Adsorption of Proteins. *J. Am. Chem. Soc.* **122**, 8303–8304 (2000).

46. Prime, K. L. & Whitesides, G. M. Self-assembled organic monolayers: Model systems for studying adsorption of proteins at surfaces. *Science (80-.).* **252**, 1164–1167 (1991).

47. Desai, N. P. & Hubbell, J. A. Solution technique to incorporate polyethylene oxide and other water-soluble polymers into surfaces of polymeric biomaterials. *Biomaterials* **12**, 144–153 (1991).

48. Vaisocherová, H. *et al.* Functionalized ultra-low fouling carboxy- and hydroxy-functional surface platforms: functionalization capacity, biorecognition capability and resistance to fouling from undiluted biological media. *Biosens. Bioelectron.* **51**, 150–157 (2014).

49. Rodriguez Emmenegger, C. *et al.* Interaction of Blood Plasma with Antifouling Surfaces. *Langmuir* **25**, 6328–6333 (2009).

50. Zoppe, J. O. *et al.* Surface-Initiated Controlled Radical Polymerization: State-of-the-Art, Opportunities, and Challenges in Surface and Interface Engineering with Polymer Brushes. *Chem. Rev.* **117**, 1105–1318 (2017).

51. Azzaroni, O. Polymer brushes here, there, and everywhere: Recent advances in their practical applications and emerging opportunities in multiple research fields. *J. Polym. Sci. Part A Polym. Chem.* **50**, 3225–3258 (2012).

52. Pyun, J., Kowalewski, T. & Matyjaszewski, K. Synthesis of Polymer Brushes Using Atom Transfer Radical Polymerization. *Macromol. Rapid Commun.* **24**, 1043–1059 (2003).

53. Wei, M., Gao, Y., Li, X. & Serpe, M. J. Stimuli-responsive polymers and their applications. *Polym. Chem.* **8**, 127–143 (2017).

54. Aseyev, V., Tenhu, H. & Winnik, F. M. Non-ionic Thermoresponsive Polymers in Water. *Adv. Polym. Sci.* **242**, 29–89 (2011).

55. Bikram, M. & West, J. L. Thermo-responsive systems for controlled drug delivery. *Expert Opin. Drug Deliv.* **5**, 1077–1091 (2008).

56. Doberenz, F., Zeng, K., Willems, C., Zhang, K. & Groth, T. Thermoresponsive polymers and their biomedical application in tissue engineering-a review. *J. Mater. Chem. B* **8**, 607 (2020).

57. Zhang, Q., Weber, C., Schubert, U. S. & Hoogenboom, R. Thermoresponsive polymers with lower critical solution temperature: from fundamental aspects and measuring techniques to recommended turbidimetry conditions. *Mater. Horizons* **4**, 109–116 (2017).

58. Roy, D., Brooks, W. L. A. & Sumerlin, B. S. New directions in thermoresponsive polymers. *Chem. Soc. Rev.* **42**, 7214 (2013).

59. Kim, Y.-J. & Matsunaga, Y. T. Thermo-responsive polymers and their application as smart biomaterials. *J. Mater. Chem. B* **5**, 4307–4321 (2017).

60. Kocak, G., Tuncer, C. & Bütün, V. pH-Responsive polymers. *Polym. Chem.* **8**, 144–176 (2017).

61. Dai, S., Ravi, P. & Tam, K. C. pH-Responsive polymers: synthesis, properties and applications. *Soft Matter* **4**, 435 (2008).

62. Yerushalmi, R., Scherz, A., Van Der Boom, M. E. & Kraatz, H. B. Stimuli responsive materials: New avenues toward smart organic devices. *J. Mater. Chem.* **15**, 4480–4487 (2005).

63. Xiao, S. *et al.* Salt-responsive zwitterionic polymer brushes with anti-polyelectrolyte property. *Curr. Opin. Chem. Eng.* **19**, 86–93 (2018).

64. Zhang, Q. M. & Serpe, M. J. Stimuli-Responsive Polymers for Actuation. *ChemPhysChem* **18**, 1451–1465 (2017).

65. Weder, C. Polymers react to stress. *Nature* **459**, 45–46 (2009).

66. Azzaroni, O. *et al.* Mechanically Induced Generation of Counterions Inside Surface-Grafted Charged Macromolecular Films: Towards Enhanced Mechanotransduction in Artificial Systems. *Angew. Chemie* **118**, 7600–7603 (2006).

67. Jochum, F. D. & Theato, P. Temperature- and light-responsive smart polymer materials. *Chem. Soc. Rev.* **42**, 7468–7483 (2013).

68. Stoychev, G., Kirillova, A. & Ionov, L. Light-Responsive Shape-Changing Polymers. *Adv. Opt. Mater.* **7**, 1900067 (2019).

69. Schattling, P., Jochum, F. D. & Theato, P. Multi-stimuli responsive polymers-the all-in-one talents. *Polym. Chem.* **5**, 25–36 (2014).

70. Seuring, J. & Agarwal, S. Polymers with Upper Critical Solution Temperature in Aqueous Solution. *Macromol. Rapid Commun.* **33**, 1898–1920 (2012).

71. Niskanen, J. & Tenhu, H. How to manipulate the upper critical solution temperature (UCST)? *Polym. Chem.* **8**, 220–232 (2017).

72. Zhang, Q. & Hoogenboom, R. Polymers with upper critical solution temperature behavior in alcohol/water solvent mixtures. *Prog. Polym. Sci.* **48**, 122–142 (2015).

73. Seuring, J. & Agarwal, S. Polymers with Upper Critical Solution Temperature in Aqueous Solution: Unexpected Properties from Known Building Blocks. *ACS Macro Lett.* **2**, 597–600 (2013).

74. Podewitz, M. *et al.* Coil–Globule Transition Thermodynamics of Poly(N-isopropylacrylamide). *J. Phys. Chem. B* **123**, 8838–8847 (2019).

75. Minko, S. Responsive Polymer Brushes. *J. Macromol. Sci. Part C Polym. Rev.* **46**, 397–420 (2006).

76. Uhlmann, P. *et al.* Surface functionalization by smart coatings: Stimuli-responsive binary polymer brushes. *Prog. Org. Coatings* **55**, 168–174 (2006).

77. Nagase, K., Okano, T. & Kanazawa, H. Poly(N-isopropylacrylamide) based thermoresponsive polymer brushes for bioseparation, cellular tissue fabrication, and nano actuators. *Nano-Structures & Nano-Objects* **16**, 9–23 (2018).

78. Nagase, K., Yamato, M., Kanazawa, H. & Okano, T. Poly(N-isopropylacrylamide)-based thermoresponsive surfaces provide new types of biomedical applications. *Biomaterials* **153**, 27–48 (2018).

79. Nastyshyn, S. *et al.* Temperature-Responsive Polymer Brush Coatings for Advanced Biomedical Applications. *Polymers (Basel).* **14**, 4245 (2022).

80. Buhl, K. B. *et al.* Polymer Brush Coating and Adhesion Technology at Scale. *Polymers (Basel).* **12**, 1475 (2020).

81. Brittain, W. J. & Minko, S. A structural definition of polymer brushes. *J. Polym. Sci. Part A Polym. Chem.* **45**, 3505–3512 (2007).

82. Dalsin, J. L. *et al.* Protein resistance of titanium oxide surfaces modified by biologically inspired mPEG-DOPA. *Langmuir* **21**, 640–646 (2005).

83. Michalek, L., Barner, L. & Barner-Kowollik, C. Polymer on Top: Current Limits and Future Perspectives of Quantitatively Evaluating Surface Grafting. *Adv. Mater.* **30**, 1706321 (2018).

84. Moh, L. C. H., Losego, M. D. & Braun, P. V. Solvent quality effects on scaling behavior of poly(methyl methacrylate) brushes in the moderate- and high-density regimes. *Langmuir* **27**, 3698–3702 (2011).

85. Liu, G., Cheng, H., Yan, L. & Zhang, G. Study of the Kinetics of the Pancake-to-Brush Transition of Poly(N-isopropylacrylamide) Chains. *J. Phys. Chem. B* **109**, 22603–22607 (2005).

86. Zhou, F. & Huck, W. T. S. Surface grafted polymer brushes as ideal building blocks for "smart" surfaces. *Phys. Chem. Chem. Phys.* **8**, 3815–3823 (2006).

87. Schweigerdt, A., Heinen, S., Stöbener, D. D. & Weinhart, M. Grafting Density-Dependent Phase Transition Mechanism of Thermoresponsive Poly(glycidyl ether) Brushes: A Comprehensive QCM-D Study. *Langmuir* **37**, 7087–7096 (2021).

88. Yim, H. *et al.* Effects of Grafting Density and Molecular Weight on the Temperature-Dependent Conformational Change of Poly(N-isopropylacrylamide) Grafted Chains in Water. *Macromolecules* **39**, 3420–3426 (2006).

89. Barbey, R. *et al.* Polymer brushes via surface-initiated controlled radical polymerization: synthesis, characterization, properties, and applications. *Chem. Rev.* **109**, 5437–5527 (2009).

90. Zdyrko, B. & Luzinov, I. Polymer brushes by the 'grafting to' method. *Macromol. Rapid Commun.* **32**, 859–869 (2011).

91. Patil, R. R., Turgman-Cohen, S., Šrogl, J., Kiserow, D. & Genzer, J. Direct measurement of molecular weight and grafting density by controlled and quantitative degrafting of surface-anchored poly(methyl methacrylate). *ACS Macro Lett.* **4**, 251–254 (2015).

92. Kingshott, P., Thissen, H. & Griesser, H. J. Effects of cloud-point grafting, chain length, and density of PEG layers on competitive adsorption of ocular proteins. *Biomaterials* **23**, 2043–56 (2002).

93. Heinen, S. & Weinhart, M. Poly(glycidyl ether)-Based Monolayers on Gold Surfaces: Control of Grafting Density and Chain Conformation by Grafting Procedure, Surface Anchor, and Molecular Weight. *Langmuir* **33**, 2076–2086 (2017).

94. Minko, S. *et al.* Synthesis of adaptive polymer brushes via 'grafting to' approach from melt. *Langmuir* **18**, 289–296 (2002).

95. Iyer, K. S. & Luzinov, I. Effect of macromolecular anchoring layer thickness and molecular weight on polymer grafting. *Macromolecules* **37**, 9538–9545 (2004).

96. Edmondson, S., Osborne, V. L. & Huck, W. T. S. Polymer brushes via surface-initiated polymerizations. *Chem. Soc. Rev.* **33**, 14–22 (2004).

97. Corrigan, N. *et al.* Reversible-deactivation radical polymerization (Controlled/living radical polymerization): From discovery to materials design and applications. *Prog. Polym. Sci.* **111**, 101311 (2020).

98. Braunecker, W. A. & Matyjaszewski, K. Controlled/living radical polymerization: Features, developments, and perspectives. *Prog. Polym. Sci.* **32**, 93–146 (2007).

99. Shipp, D. A. Reversible-Deactivation Radical Polymerizations. *Polym. Rev.* **51**, 99–103 (2011).

100. Goto, A. & Fukuda, T. Kinetics of living radical polymerization. *Prog. Polym. Sci.* **29**, 329–385 (2004).

101. Braunecker, W. A. & Matyjaszewski, K. Controlled/living radical polymerization: Features, developments, and perspectives. *Prog. Polym. Sci.* **32**, 93–146 (2007).

102. Matyjaszewski, Krzysztof & Xia, J. Atom Transfer Radical Polymerization (ATRP). *Chem. Rev.* **101**, 2921–2990 (2001).

103. Keddie, D. J. A guide to the synthesis of block copolymers using reversible-addition fragmentation chain transfer (RAFT) polymerization. *Chem. Soc. Rev* **43**, 496 (2014).

104. Matyjaszewski, K. Advanced Materials by Atom Transfer Radical Polymerization. *Adv. Mater.* **30**, 1–22 (2018).

105. Moad, G., Rizzardo, E. & Thang, S. H. Toward Living Radical Polymerization. *Acc. Chem. Res.* **41**, 1133–1142 (2008).

106. Perrier, S. 50th Anniversary Perspective : RAFT Polymerization—A User Guide. *Macromolecules* **50**, 7433–7447 (2017).

107. Sofia, S. J., Premnath, V. & Merrill, E. W. Poly(ethylene oxide) grafted to silicon surfaces: Grafting density and protein adsorption. *Macromolecules* **31**, 5059–5070 (1998).

108. Halperin, A. Polymer Brushes that Resist Adsorption of Model Proteins: Design Parameters. *Langmuir* **15**, 2525–2533 (1999).

109. Hadjesfandiari, N., Yu, K., Mei, Y. & Kizhakkedathu, J. N. Polymer brush-based approaches for the development of infection-resistant surfaces. *J. Mater. Chem. B* **2**, 4968–4978 (2014).

110. Xue, C. *et al.* Protein adsorption on poly(N -isopropylacrylamide) brushes: Dependence on grafting density and chain collapse. *Langmuir* **27**, 8810–8818 (2011).

111. Weir, M. P. & Parnell, A. J. Water Soluble Responsive Polymer Brushes. *Polymers (Basel).* **3**, 2107–2132 (2011).

112. Li, D., Xu, L., Wang, J. & Gautrot, J. E. Responsive Polymer Brush Design and Emerging Applications for Nanotheranostics. *Adv. Healthc. Mater.* **10**, 2000953 (2021).

113. Plunkett, K. N., Zhu, X., Moore, J. S. & Leckband, D. E. PNIPAM Chain Collapse Depends on the Molecular Weight and Grafting Density. *Langmuir* **22**, 4259–4266 (2006).

114. Nagase, K., Watanabe, M., Kikuchi, A., Yamato, M. & Okano, T. Thermo-Responsive Polymer Brushes as Intelligent Biointerfaces: Preparation via ATRP and Characterization. *Macromol. Biosci.* **11**, 400–409 (2011).

115. Takahashi, H., Nakayama, M., Itoga, K., Yamato, M. & Okano, T. Micropatterned Thermoresponsive Polymer Brush Surfaces for Fabricating Cell Sheets with Well-Controlled Orientational Structures. *Biomacromolecules* **12**, 1414–1418 (2011).

116. Kwon, O. H., Kikuchi, A., Yamato, M., Sakurai, Y. & Okano, T. Rapid cell sheet detachment from Poly(N-isopropylacrylamide)-grafted porous cell culture membranes. *J. Biomed. Mater. Res.* **50**, 82–89 (2000).

117. Akiyama, Y., Kikuchi, A., Yamato, M. & Okano, T. Ultrathin Poly(N -isopropylacrylamide) Grafted Layer on Polystyrene Surfaces for Cell Adhesion/Detachment Control. *Langmuir* **20**, 5506–5511 (2004).

118. Wang, X. *et al.* Temperature-Responsive Hierarchical Polymer Brushes Switching from Bactericidal to Cell Repellency. *ACS Appl. Mater. Interfaces* **9**, 40930–40939 (2017).

119. Burkert, S. *et al.* Protein Resistance of PNIPAAm Brushes: Application to Switchable Protein Adsorption. *Langmuir* **26**, 1786–1795 (2010).

120. Lanzalaco, S. & Armelin, E. Poly(N-isopropylacrylamide) and Copolymers: A Review on Recent Progresses in Biomedical Applications. *Gels* **3**, 36 (2017).

121. Halperin, A., Kröger, M. & Winnik, F. M. Poly(N-isopropylacrylamide) Phase Diagrams: Fifty Years of Research. *Angew. Chemie - Int. Ed.* **54**, 15342–15367 (2015).

122. Schild, H. G. Poly(N-isopropylacrylamide): experiment, theory and application. *Prog. Polym. Sci.* **17**, 163–249 (1992).

123. Rademacher, J. T., Baum, M., Pallack, M. E., Brittain, W. J. & Simonsick, W. J. Atom Transfer Radical Polymerization of N,N-Dimethylacrylamide. *Macromolecules* **33**, 284–288 (2000).

124. Herberg, A., Yu, X. & Kuckling, D. End Group Stability of Atom Transfer Radical Polymerization (ATRP)-Synthesized Poly(N-isopropylacrylamide): Perspectives for Diblock Copolymer Synthesis. *Polymers (Basel).* **11**, 678 (2019).

125. Pujari, S. P., Scheres, L., Marcelis, A. T. M. & Zuilhof, H. Covalent surface modification of oxide surfaces. *Angew. Chemie - Int. Ed.* **53**, 6322–6356 (2014).

126. Inkpen, M. S. *et al.* Non-chemisorbed gold–sulfur binding prevails in self-assembled monolayers. *Nat. Chem.* **11**, 351–358 (2019).

127. Huang, H. & Penn, L. S. Dense tethered layers by the 'grafting-to' approach. *Macromolecules* **38**, 4837–4843 (2005).

128. Minko, S. *et al.* Bidisperse mixed brushes: Synthesis and study of segregation in selective solvent. *Macromolecules* **36**, 7268–7279 (2003).

129. Hansson, S. *et al.* Grafting efficiency of synthetic polymers onto biomaterials: A comparative study of grafting- from versus grafting- to. *Biomacromolecules* **14**, 64–74 (2013).

130. Soto-Cantu, E. *et al.* Versatility of alkyne-modified poly(glycidyl methacrylate) layers for click reactions. *Langmuir* **27**, 5986–5996 (2011).

131. Gao, H. & Matyjaszewski, K. Synthesis of molecular brushes by 'grafting onto' method: Combination of ATRP and click reactions. *J. Am. Chem. Soc.* **129**, 6633–6639 (2007).

132. Wei, Q. & Haag, R. Universal polymer coatings and their representative biomedical applications. *Mater. Horizons* **2**, 567–577 (2015).

133. Choy, K. Chemical vapour deposition of coatings. *Prog. Mater. Sci.* **48**, 57–170 (2003).

134. Alf, M. E. *et al.* Chemical Vapor Deposition of Conformal, Functional, and Responsive Polymer Films. *Adv. Mater.* **22**, 1993–2027 (2009).

135. Yameen, B., Khan, H. U., Knoll, W., Förch, R. & Jonas, U. Surface Initiated Polymerization on Pulsed Plasma Deposited Polyallylamine: A Polymer Substrate-Independent Strategy to Soft Surfaces with Polymer Brushes. *Macromol. Rapid Commun.* **32**, 1735–1740 (2011).

136. Coad, B. R., Lu, Y., Glattauer, V. & Meagher, L. Substrate-Independent Method for Growing and Modulating the Density of Polymer Brushes from Surfaces by ATRP. *ACS Appl. Mater. Interfaces* **4**, 2811–2823 (2012).

137. Hammond, P. T. Building biomedical materials layer-by-layer. *Mater. Today* **15**, 196–206 (2012).

138. Li, Y., Wang, X. & Sun, J. Layer-by-layer assembly for rapid fabrication of thick polymeric films. *Chem. Soc. Rev.* **41**, 5998 (2012).

139. Zhang, X. *et al.* Progress on the layer-by-layer assembly of multilayered polymer composites: Strategy, structural control and applications. *Prog. Polym. Sci.* **89**, 76–107 (2019).

140. Butt, M. A. Thin-Film Coating Methods: A Successful Marriage of High-Quality and Cost-Effectiveness—A Brief Exploration. *Coatings* **12**, (2022).

141. Dreyer, D. R., Miller, D. J., Freeman, B. D., Paul, D. R. & Bielawski, C. W. Perspectives on poly(dopamine). *Chem. Sci.* **4**, 3796–3802 (2013).

142. Ryu, J. H., Messersmith, P. B. & Lee, H. Polydopamine Surface Chemistry: A Decade of Discovery. *ACS Appl. Mater. Interfaces* **10**, 7523–7540 (2018).

143. Lee, H., Dellatore, S. M., Miller, W. M. & Messersmith, P. B. Mussel-Inspired Surface Chemistry for Multifunctional Coatings. *Science (80-.).* **318**, 426–430 (2007).

144. Liebscher, J. *et al.* Structure of polydopamine: A never-ending story? *Langmuir* **29**, 10539–10548 (2013).

145. D'Ischia, M., Napolitano, A., Ball, V., Chen, C. T. & Buehler, M. J. Polydopamine and eumelanin: From structure-property relationships to a unified tailoring strategy. *Acc. Chem. Res.* **47**, 3541–3550 (2014).

146. Della Vecchia, N. F. *et al.* Building-block diversity in polydopamine underpins a multifunctional eumelanin-type platform tunable through a quinone control point. *Adv. Funct. Mater.* **23**, 1331–1340 (2013).

147. Liebscher, J. Chemistry of Polydopamine – Scope, Variation, and Limitation. *European J. Org. Chem.* **2019**, 4976–4994 (2019).

148. Svoboda, J., Král, M., Dendisová, M., Matějka, P. & Pop-Georgievski, O. Unraveling the influence of substrate on the growth rate, morphology and covalent structure of surface adherent polydopamine films. *Colloids Surfaces B Biointerfaces* **205**, 111897 (2021).

149. Ball, V., Frari, D. Del, Toniazzo, V. & Ruch, D. Kinetics of polydopamine film deposition as a function of pH and dopamine concentration: Insights in the polydopamine deposition mechanism. *J. Colloid Interface Sci.* **386**, 366–372 (2012).

150. Ponzio, F. *et al.* Oxidant Control of Polydopamine Surface Chemistry in Acids: A Mechanism-Based Entry to Superhydrophilic-Superoleophobic Coatings. *Chem. Mater.* **28**, 4697–4705 (2016).

151. Yang, J., Cohen Stuart, M. A. & Kamperman, M. Jack of all trades: Versatile catechol crosslinking mechanisms. *Chem. Soc. Rev.* **43**, 8271–8298 (2014).

152. Saiz-Poseu, J., Mancebo-Aracil, J., Nador, F., Busqué, F. & Ruiz-Molina, D. The Chemistry behind Catechol-Based Adhesion. *Angew. Chemie Int. Ed.* **58**, 696–714 (2019).

153. El Yakhlifi, S. & Ball, V. Polydopamine as a stable and functional nanomaterial. *Colloids Surfaces B Biointerfaces* **186**, 110719 (2020).

154. Alfieri, M. L. *et al.* The chemistry of polydopamine film formation: The amine-quinone interplay. *Biomimetics* **3**, 26 (2018).

155. Maier, G. P., Rapp, M. V., Waite, J. H., Israelachvili, J. N. & Butler, A. Adaptive synergy between catechol and lysine promotes wet adhesion by surface salt displacement. *Science (80-.).* **349**, 628–632 (2015).

156. Rodriguez-Emmenegger, C. *et al.* Controlled Cell Adhesion on Poly(dopamine) Interfaces Photopatterned with Non-Fouling Brushes. *Adv. Mater.* **25**, 6123–6127 (2013).

157. Hafner, D. *et al.* Mussel-Inspired Polymer Carpets: Direct Photografting of Polymer Brushes on Polydopamine Nanosheets for Controlled Cell Adhesion. *Adv. Mater.* **28**, 1489–1494 (2016).

158. Liu, C., Lee, J., Ma, J. & Elimelech, M. Antifouling Thin-Film Composite Membranes by Controlled Architecture of Zwitterionic Polymer Brush Layer. *Environ. Sci. Technol.* **51**, 2161–2169 (2017).

159. Hafner, D. & Jordan, R. Substrate-independent Cu(0)-mediated controlled radical polymerization: Grafting of block copolymer brushes from poly(dopamine) modified surfaces. *Polym. Chem.* **11**, 2129–2136 (2020).

160. Zhu, B. & Edmondson, S. Polydopamine-melanin initiators for Surface-initiated ATRP. *Polymer (Guildf).* **52**, 2141–2149 (2011).

161. Alas, G. R., Agarwal, R., Collard, D. M. & García, A. J. Peptide-functionalized poly[oligo(ethylene glycol) methacrylate] brushes on dopamine-coated stainless steel for controlled cell adhesion. *Acta Biomater.* **59**, 108–116 (2017).

162. Li, N. *et al.* Universal Strategy for Efficient Fabrication of Blood Compatible Surfaces via Polydopamine-Assisted Surface-Initiated Activators Regenerated by Electron Transfer Atom-Transfer Radical Polymerization of Zwitterions. *ACS Appl. Mater. Interfaces* **12**, 12337–12344 (2020).

163. Wang, S. *et al.* Grafting antibacterial polymer brushes from titanium surface via polydopamine chemistry and activators regenerated by electron transfer ATRP. *React. Funct. Polym.* **140**, 48–55 (2019).

164. Sheng, W. *et al.* Brushing up from "anywhere" under sunlight: a universal surface-initiated polymerization from polydopamine-coated surfaces. *Chem. Sci.* **6**, 2068–2073 (2015).

165. Pop-Georgievski, O. *et al.* Nonfouling poly(ethylene oxide) layers end-tethered to polydopamine. *Langmuir* **28**, 14273–14283 (2012).

166. Pop-Georgievski, O. *et al.* Poly(ethylene oxide) layers grafted to dopamine-melanin anchoring layer: Stability and resistance to protein adsorption. *Biomacromolecules* **12**, 3232–3242 (2011).

167. Xu, G. *et al.* Antifouling and Antimicrobial Coatings from Zwitterionic and Cationic Binary Polymer Brushes Assembled via 'click' Reactions. *Ind. Eng. Chem. Res.* **56**, 14479–14488 (2017).

168. Yameen, B. *et al.* A facile avenue to conductive polymer brushes via cyclopentadiene–maleimide Diels–Alder ligation. *Chem. Commun.* **49**, 8623–8625 (2013).

169. Heinen, S. *et al.* Transfer of functional thermoresponsive poly(glycidyl ether) coatings for cell sheet fabrication from gold to glass surfaces. *J. Mater. Chem. B* **6**, 1489–1500 (2018).

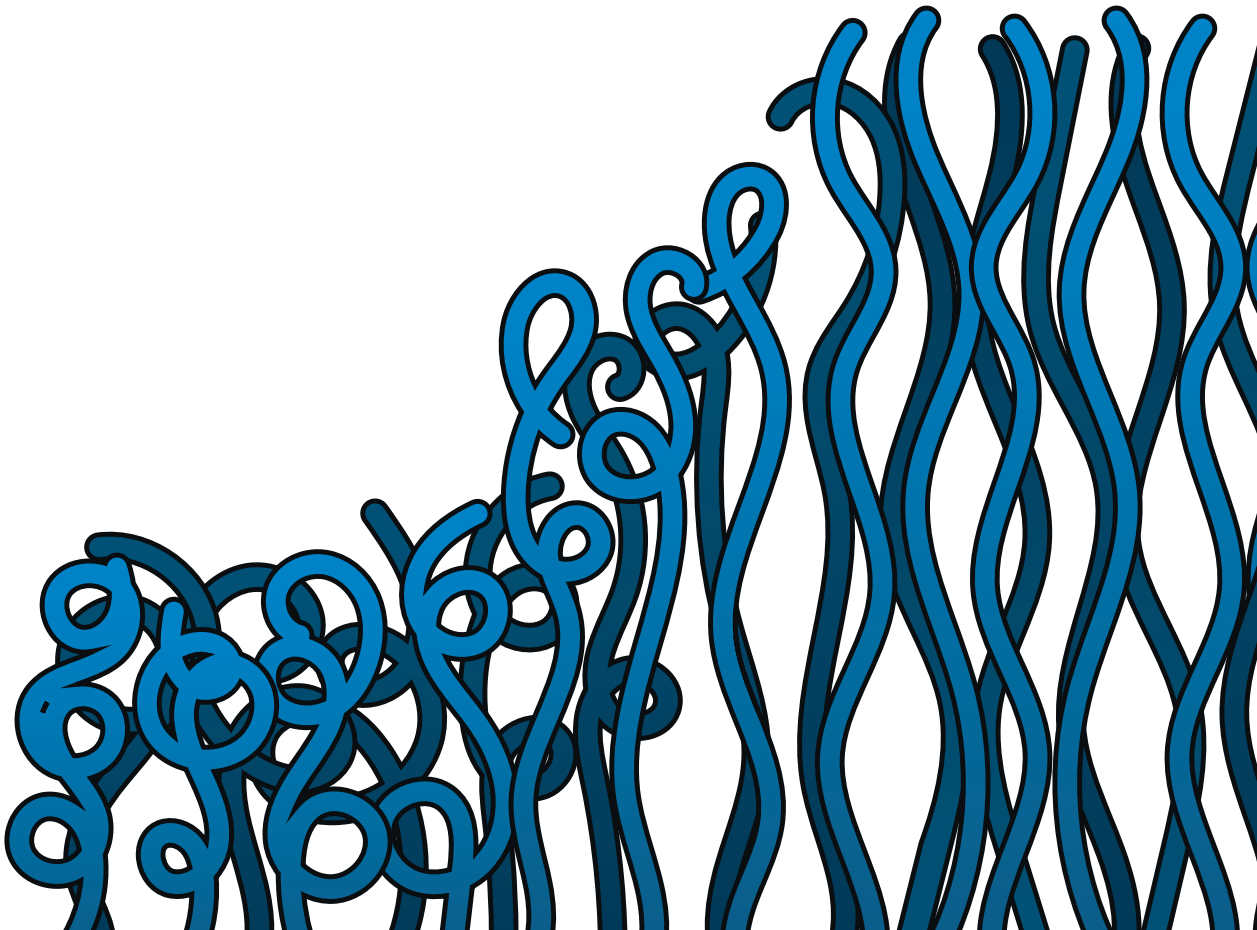

Chapter 2

Thermoresponsive, Pyrrolidone-based Antifouling Polymer Brushes

Teunissen, L. W., Kuzmyn, A. R., Ruggeri, F. S., Smulders, M. M. J. & Zuilhof, H. Thermoresponsive, Pyrrolidone-Based Antifouling Polymer Brushes. *Adv. Mater. Interfaces* **9**, *2101717 (2022).*

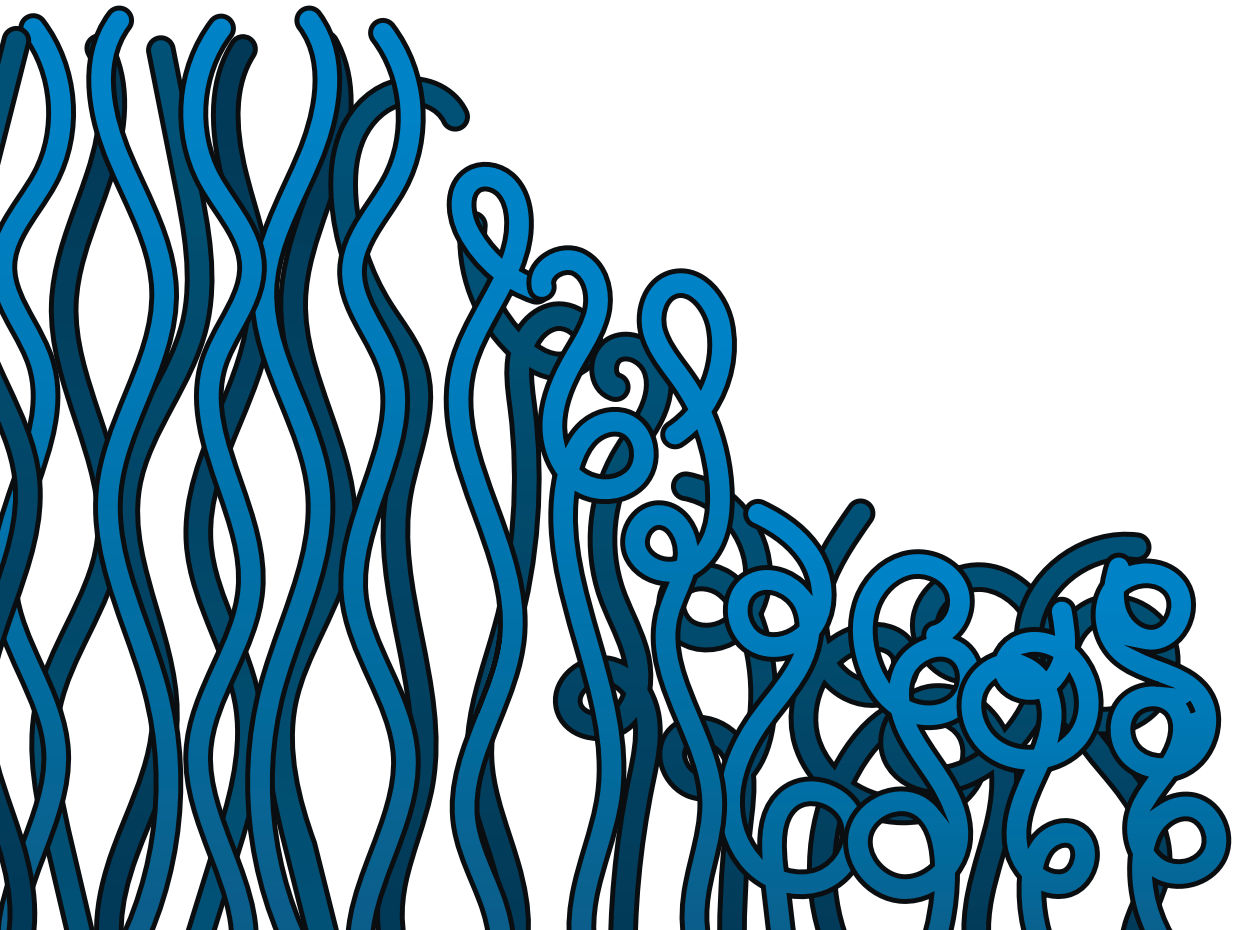

Abstract

Commonly, modification of surfaces with thermoresponsive polymers is performed using poly(*N*-isopropylacrylamide) (poly(NIPAM)). However, integration of poly(NIPAM) with a second polymer to obtain more complex copolymer structures has proven challenging due to inherently poorly controllable polymerization characteristics of acrylamides. In this Chapter, we present the synthesis of *N*-(2-methacryloyloxyethyl)pyrrolidone (NMEP) and subsequent polymerization under controlled conditions from silicon oxide substrates via surface-initiated atom transfer radical polymerization (SI-ATRP) to produce thermoresponsive poly(NMEP) brushes. The livingness of the brushes is demonstrated by reinitiation of poly(NMEP) brushes using oligo(ethylene glycol) methyl ether methacrylate to obtain diblock copolymer brushes. Following extensive characterization, the reversible thermoresponsive behavior of these poly(NMEP) brushes is demonstrated using phase-controlled AFM topography measurements in an aqueous liquid environment. These measurements indicate that at 27 °C the poly(NMEP) brushes are solvated and extend away from the surface, whereas at 60 °C the polymers are insoluble and reside in a collapsed conformation. Finally, to investigate the potential applicability of poly(NMEP) brushes in biomedical devices, the antifouling properties of the coating are tested in aqueous media containing BSA, fibrinogen, or 10% diluted human serum using quartz crystal microbalance with dissipation monitoring (QCM-D). These measurements reveal very good antifouling properties, even when exposed to 10% diluted human serum.

2.1 Introduction

Thermoresponsive polymers are rapidly becoming more important in the development of smart materials and devices due to their addressable properties.[1–3] For this type of polymers, solubility in a certain medium is dependent on the temperature of the system. The ability to control polymer solubility is of great interest in, for example, drug delivery,[4] tissue engineering,[5] or membrane technology.[6] Commonly employed thermoresponsive polymers are those that exhibit a lower critical solution temperature (LCST).[7–9] Such polymers are soluble at temperatures below that critical temperature, whereas they are insoluble at temperatures exceeding the LCST.[10] This change in solubility is accompanied by a conformational transformation, with a coil-to-globule transition from soluble to insoluble polymers.[11]

For thermoresponsive polymers end-grafted to a surface, specifically polymer brushes, this conformational change manifests itself by chains that point away from the surface when soluble, whereas insoluble chains collapse and minimize interaction with solvent molecules (Figure 2.1).[12,13] This behavior results in addressable surface wettability and adhesive properties, which open the door to smart applications in cell-culture substrates,[14] temperature-dependent chromatography,[15] on-off membranes,[16] and microfluidic systems.[17] Typically, in order to obtain sufficiently high grafting densities and brush thicknesses, such polymer brushes are synthesized by surface-initiated polymerization techniques.[18]

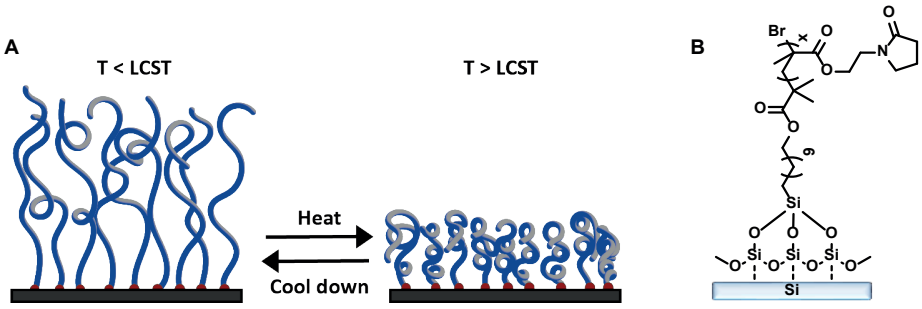

Figure 2.1 (A) Illustration of the conformational change of a polymer brush with an LCST that collapses when *T* > LCST and extends again when *T* < LCST. **(B)** The molecular structure of the poly(NMEP) brushes under current study grown from ATRP initiators on silicon oxide.

Commonly employed controlled surface-initiated polymerization procedures involve surface-initiated atom transfer radical polymerization (SI-ATRP) and surface-initiated radical addition-fragmentation chain transfer (SI-RAFT) polymerization.[18,19] These techniques allow precise tuning of brush height with low dispersity and limited termination. A recent addition to the field of controlled surface-initiated polymerization procedures is surface-initiated photoinduced electron transfer-reversible addition–fragmentation chain transfer polymerization (SI-PET-RAFT).[20] This light-triggered technique allows surface-initiated polymerization of a wide range of monomers into various types of brush architectures without the need of rigorous degassing.[21–25]

Among the thermoresponsive polymers employed in polymer brush coatings, poly(*N*-isopropylacrylamide) (poly(NIPAM)) is –by far– the most intensively investigated, mainly due to its LCST at 32 °C.[26] This LCST renders poly(NIPAM) highly relevant for biomedical applications. However, it has also become apparent that maintaining control during grafting-from polymerization of NIPAM, and acrylamides in general, is difficult to achieve due to several possible termination reactions.[27–29] That lack of control hampers the synthesis of more complex polymer brush structures, such as block copolymers, that incorporate poly(NIPAM). As a result, there is only a relatively limited number of reports in which poly(NIPAM) polymer brushes could successfully be reinitiated with a second monomer; and in the few cases in which reinitiation was described, the thickness of the second block did not exceed 3 nm.[30–32] Spencer *et al.* successfully reinitiated poly(NIPAM) brushes with a second block of poly(*N,N*-dimethylacrylamide (poly(DMAM)) of 22 nm thick.[33] However, the polymerization reactions had to be under highly specific conditions (a closed flow system) and required addition of halide salts, making them harder to apply in a highly general matter.

In an attempt to produce more complex polymer brush structures incorporating a thermoresponsive polymer layer and a second layer of appreciable thickness (*e.g.*, > 10 nm in dry conditions) under standard surface-initiated polymerization conditions, we set out to explore alternatives for poly(NIPAM) that would combine thermoresponsiveness with a more controlled polymerization behavior. Substantially less investigated than poly(NIPAM) is the thermoresponsive polymer poly(*N*-(2-methacryloyloxyethyl) pyrrolidone) (poly(NMEP), see Scheme 2.1).[34–41] Poly(NMEP) has been reported to possess thermoresponsive properties in aqueous solutions with an LCST ranging between 51 and 72 °C, depending on the molecular weight of the polymer.[36,38,39] Unlike NIPAM, the polymerizable group in NMEP is a methacrylate (Scheme 2.1), which enables significantly more straightforward reinitiation using acrylamides, acrylates, and other methacrylates via controlled polymerization methods (such as ATRP and RAFT).[42,43]

The structure of poly(NMEP) resembles that of poly(vinyl pyrrolidone) (PVP), as both contain the pyrrolidone functional group (Scheme 2.1). Surface modifications using PVP have been increasingly investigated over the past years.[44–49] Polymer brushes of PVP have been fabricated on silicon using SI-ATRP,[46] with thicknesses up to 35 nm. Nevertheless, maintaining a high level of control over the polymerization of *N*-vinyl pyrrolidone (NVP) is known to be hampered by the non-conjugated, vinylic nature of the monomer.[50]

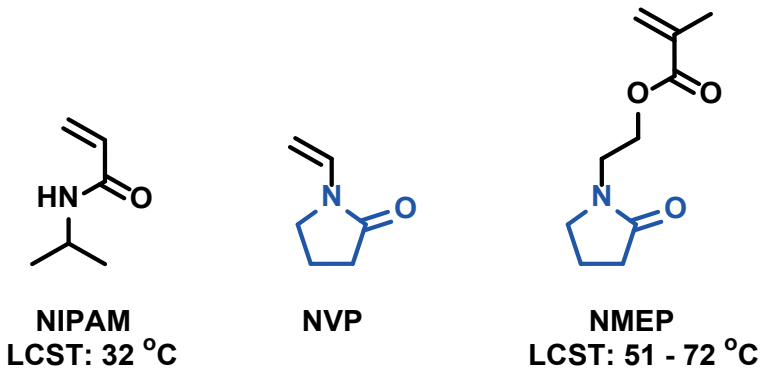

Scheme 2.1 Molecular structures of, from left to right, *N*-isopropylacrylamide (NIPAM), *N*-vinyl pyrrolidone (NVP) and *N*-(2-methacryloyloxyethyl)pyrrolidone (NMEP). The reported LCST values are for the polymers in solution.

In this study, we demonstrate for the first time the synthesis of thermoresponsive poly(NMEP) brushes using controlled SI-ATRP from silicon oxide-coated silicon, which can be used as a platform for further polymerization reactions to create multi-functional block copolymer brushes. We achieve a high level of control over the polymerization reaction, as indicated by linear polymerization kinetics during the first 90 minutes, as well as demonstrated by the successful reinitiation using poly(methyl oligo ethylene glycol methacrylate) (poly(MeOEGMA)) for the creation of diblock structures. The reversible thermoresponsive behavior of the polymer brush in aqueous solution was demonstrated with high statistical significance at the nanoscale using phase-controlled atomic force microscopy (AFM) measurements of 3-D topography.[51,52] Finally, we report the anti-biofouling properties of poly(NMEP) brushes synthesized on gold sensors, which were investigated using a quartz crystal microbalance with dissipation monitoring (QCM-D) and compared to bare gold substrates.

2.2 Results and Discussion

2.1.1 SI-ATRP of NMEP

Polymer brushes of poly(NMEP) were synthesized according to the procedure outlined in Scheme 2.2. The pyrrolidone-containing monomer (NMEP) was synthesized on a 30-gram scale following a procedure adapted from Savelyeva and Marić.[40] To this aim, 2-hydroxyethyl pyrrolidone was reacted with freshly-distilled methacryloyl chloride in the presence of a stoichiometric amount of triethylamine. The monomer was purified by column chromatography and characterized using NMR, GC-MS and IR spectroscopy (see Materials and Methods (Section 2.4) and Supporting Information (Section 2.6) for full details of the monomer synthesis and characterization).

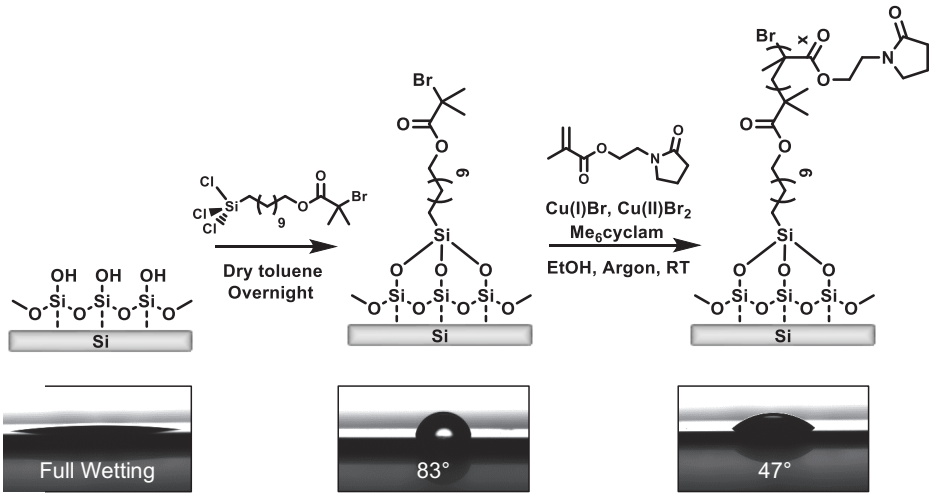

Scheme 2.2 Procedure for the synthesis of poly(NMEP) brushes from silicon surfaces using SI-ATRP. Static water contact angle measurements were performed for plasma-cleaned silicon (full wetting); initiator-modified silicon (83 ± 1°) and poly(NMEP) brushes (47 ± 2°).

Silicon wafer was selected as the planar substrate for its low initial roughness and widespread use in biomedical applications.[53] To grow the poly(NMEP) brushes from silicon, the first step was to attach a self-assembled monolayer (SAM) of the bromine-terminated ATRP-initiator to plasma-cleaned silicon surfaces (Scheme 2.2).[54] The XPS wide scan spectrum of the resulting surface clearly showed the Br_{3d} signal, which confirms the presence of the ATRP initiator group (Figure 2.2, Initiator-Si). The static water contact angle of this initiator-modified silicon surface was 83 ± 1°, in line with the literature

value for this SAM.[55] From these functionalized surfaces, a copper-catalyzed SI-ATRP of the NMEP monomer was performed in ethanol under argon at room temperature (RT, 19 ± 2°C). To avoid potential complexation of the growing chain to the catalyst and its ensuing deactivation, Me_6cyclam was selected as the ligand.[56] Using this procedure, it was possible to produce poly(NMEP) brushes with dry thicknesses of over 50 nm within 2 h (Figure 2.3A). The static water contact angle for the brush-modified surfaces decreased significantly with respect to the initiator-modified surfaces to 47 ± 2°. XPS wide scan spectra of the surfaces further confirmed the synthesis of poly(NMEP) brushes through the emergence of a characteristic signal at 400.0 eV, arising from the nitrogen present in the pyrrolidone ring of the monomer (Figure 2.2A).

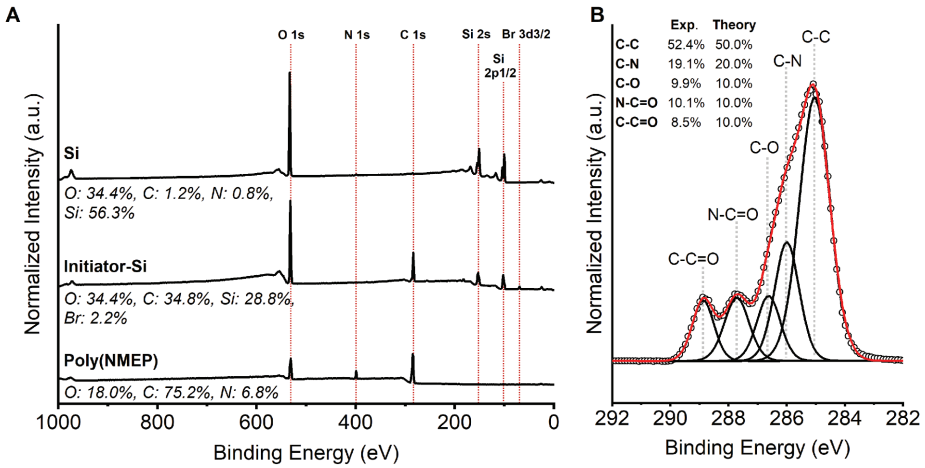

Figure 2.2 (A) XPS wide scan spectra of air plasma-cleaned silicon wafer (top), ATRP-initiator functionalized silicon (middle) and poly(NMEP) brushes (dry thickness of 23.6 ± 0.2 nm by ellipsometry) on silicon (bottom). **(B)** XPS C 1s narrow scan spectrum of poly(NMEP) brushes on silicon.

The measured atomic ratio for C : N : O of 11 : 3 : 1 was close to the theoretical ratio of 10 : 3 : 1. The small discrepancy is believed to originate from the presence of adventitious carbon following air exposure. The XPS C 1s narrow scan spectrum supports this hypothesis as a higher ratio of C–C bonds is observed than the theoretical ratio predicts (Figure 2.2B). Clearly visible are the signals arising from the N–C=O bond of the pyrrolidone ring at 287.7 eV and the C–C=O bond of the methacrylate moiety at 288.9 eV. Furthermore, the experimentally obtained XPS C1s narrow scan spectrum corresponds strongly

with the XPS C 1s narrow scan spectrum that was simulated using DFT calculations (see Supporting Information).[57,58]

2.2.2 Polymerization kinetics

The kinetics of the polymerization reaction were investigated in detail as they provide insights into whether the polymerization is of a 'living' nature and proceeds in a controlled manner. As the chains are grown from the surface, the polymerization rate was assessed by relating the dry brush thickness, as determined by ellipsometry, to reaction time (Figure 2.3A).

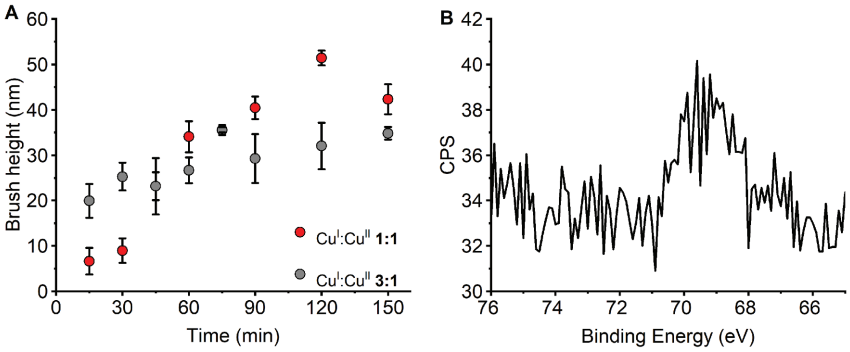

Figure 2.3 (A) Polymerization kinetics for SI-ATRP of NMEP from initiator-modified silicon for two Cu^{I}:Cu^{II} ratios, as determined by ellipsometry in dry conditions. **(B)** XPS Br 3d$^{3/2}$ narrow scan spectrum of poly(NMEP) brushes after 60 minutes of polymerization. Bromine accounted for 0.3% of the elemental composition of the polymer brush, which proved to be sufficient for successful reinitiation.

Two polymerization series were performed that varied in the ratio Cu^{I}:Cu^{II}, which were 3:1 and 1:1. The series with an increased Cu^{I}:Cu^{II} ratio of 3:1 exhibited a fast initial polymerization rate, but leveled off after approximately 30 min at dry brush thicknesses of ca. 35 nm. For the series with an equimolar Cu^{I}:Cu^{II} ratio, initiation occurred more slowly and a dry brush thickness of more than 50 nm could be achieved. These observations are in accordance with findings that an increased content of Cu^{II} present at the start of the reaction slows down the polymerization rate, but decreases the amount of chain termination due to a more controlled polymerization.[59] During the first 90 min of polymerization, the brush height appears to increase linearly. After longer polymerization times, however,

the growth rate drops and a plateau is reached. It can be assumed that this is caused by termination reactions that start to dominate the polymerization reaction.

2.2.3 Synthesis of poly(NMEP)-*b*-poly(MeOEGMA) brushes

To verify the persisting living nature of the growing polymer chains after 60 minutes of polymerization, a second monomer, MeOEGMA, was polymerized from poly(NMEP) brushes (Scheme 2.3). More generally, the ability to add a second block of a polymer of choice to poly(NMEP) brush surfaces provides access to more complex polymer (brush) structures incorporating multiple monomers that can be specifically designed towards their application.

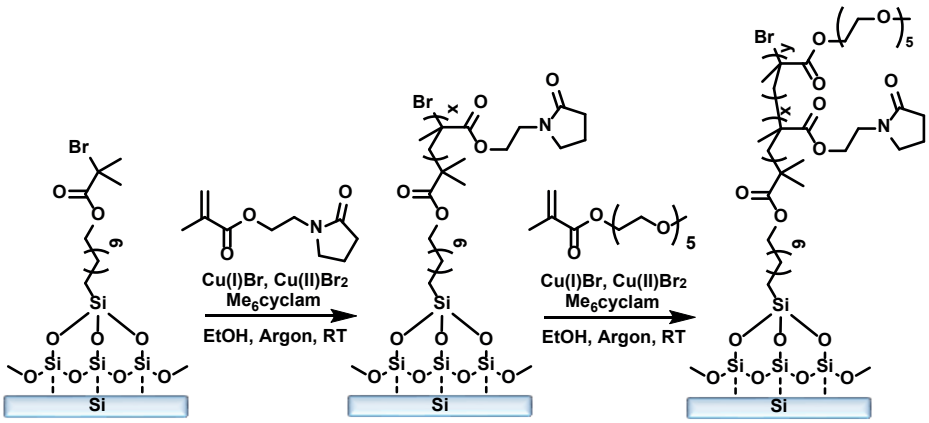

Scheme 2.3 Procedure for the synthesis of poly(NMEP)-*b*-poly(MeOEGMA) brushes by two-step SI-ATRP of NMEP and MeOEGMA.

Practically, reinitiation of the first block requires the presence of bromine at each chain-end of the polymers. After one hour of polymerization using a 1:1 ratio of Cu^{I}:Cu^{II}, poly(NMEP) had reached a dry thickness of 32 ± 4 nm, as was determined using ellipsometry. Notably, the XPS Br $3d_{3/2}$ narrow scan spectrum of the poly(NMEP) homopolymer brushes confirmed retention of the tertiary bromide groups necessary for reinitiation (Figure 2.3B). After the synthesis of the first block, the silicon substrates modified with the poly(NMEP) polymer brush were removed from the reactor, cleaned, and then cut in two halves: One half was used for characterization of the first poly(NMEP) block, the other was used as a base for the growth of the second polymer block. The polymerization of MeOEGMA was then performed using the same procedure, although the

reaction time was increased to 16 h. After the second polymerization step, the overall dry thickness of the polymer brush had increased to 43 ± 2 nm. This implies a thickness of 11 ± 6 nm for the poly(MeOEGMA) block. The static water contact angle for poly(NMEP)-*b*-poly(MeOEGMA) brush was 51 ± 1°, which corresponds to previously reported values for poly(MeOEGMA) brushes.[24,60] The XPS wide scan spectrum showed a significant decrease in nitrogen content, which is in accordance with the addition of a poly(MeOEGMA) block to the brush (Figure 2.4A). The presence of this second block could also be inferred from the XPS C 1s narrow scan spectrum (Figure 2.4B), which revealed a marked increase in the signal at 286.5 eV, originating from the multiple C–O bonds that are present in the structure of MeOEGMA.

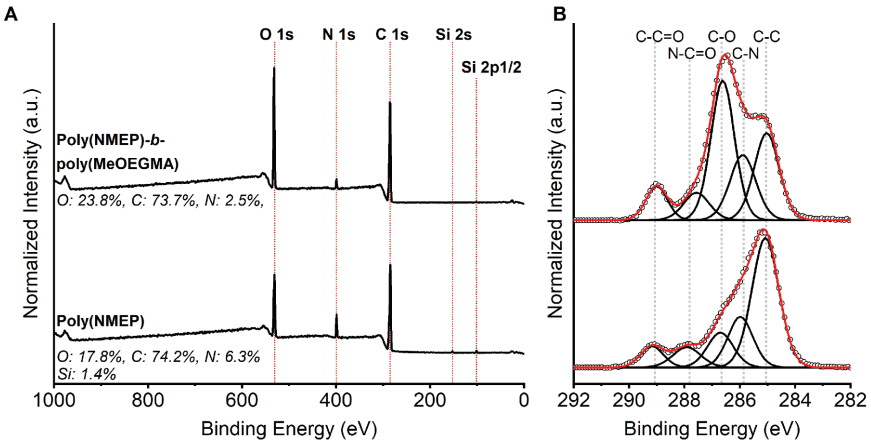

Figure 2.4 (A) XPS wide scan spectrum for poly(NMEP) brush and block copolymer poly(NMEP)-*b*-poly(MeOEGMA) brush. **(B)** XPS C 1s narrow scans of block copolymer poly(NMEP)*b*-poly(MeOEGMA) brush (top) and poly(NMEP) brush (bottom) on silicon.

2.2.4 Thermoresponsive properties of poly(NMEP) brushes

Following the synthesis and characterization of the newly synthesized poly(NMEP) brushes, we investigated the thermoresponsive properties of these polymer brushes by phase-controlled AFM in an aqueous liquid environment as a function of the temperature. In water, the brushes will collapse when the temperature exceeds the LCST. We thus expect a controllable variation in thickness of our poly(NMEP) brushes because of their temperature-dependent conformation. To assess the thermoresponsiveness, in line with previously reported measurements,[61,62] we first gently scratched a poly(NMEP) brush

surface (dry ellipsometric thickness = 42.5 ± 1.7 nm) to locally remove the polymer layer and expose the underlying silicon surface, as reference for the measurement of height. Then, we acquired 3-D topology maps of the scratched area and surrounding polymer brush whilst immersed in water and as a function of temperature (Figure 2.5 and Supporting Information). After initial processing of the acquired images (see Section 2.4 and Supporting Information for details on image analysis), the height of the polymer brush in solution was determined relative to the level of the uncovered silicon surface. According to previous reports, the LCST of poly(NMEP) in aqueous solutions is dependent on polymer molecular weight and ranges from 53 °C (105 kDa) to 72 °C (20 kDa).[36,38,39] For poly(NMEP) brushes, however, we determined that the LCST lies between 40 °C and 50 °C (Figure 2.5C and Supporting Information). It is likely that the relatively low LCST results from the combination of surface effects, such as short inter-chain distances, and a high degree of polymerization. The ensuing thermoresponsive studies were performed at temperatures sufficiently lower and higher than the LCST to ensure brush extension and collapse, respectively. At 27 °C, in the solvated state, the thickness of the poly(NMEP) brush was determined at 91 ± 3 nm (Figure 2.5). Upon increasing the temperature to 60 °C, the brushes collapsed to 69 ± 4 nm. Furthermore, the collapse at 60 °C and subsequent extension of the polymer chains at 27 °C was observed in two consecutive cycles, demonstrating good reversibility (Figure 2.5D).

Our measurements demonstrate that the expulsion of water reduces the brush thickness by ~25%. Overall, the AFM measurements demonstrate the thermoresponsiveness of the poly(NMEP) brush. This level of collapse closely resembled the level reported for poly(NIPAM) brushes (ca. 20%), which were synthesized following a nearly identical procedure using the same initiator layer followed by SI-ATRP.[63] In that same range, the brush height for thermoresponsive poly((di(ethylene glycol)methyl ether methacrylate)-co-MeOEGMA) brushes synthesized using SI-ATRP from silicon has been reported to decrease by ~16%.[64] The extent of swelling and collapsing of thermoresponsive polymer brushes has been shown to depend on several variables, such as grafting density and brush thickness,[12] which thus can lead to a wide range of swelling/collapsing ratios.

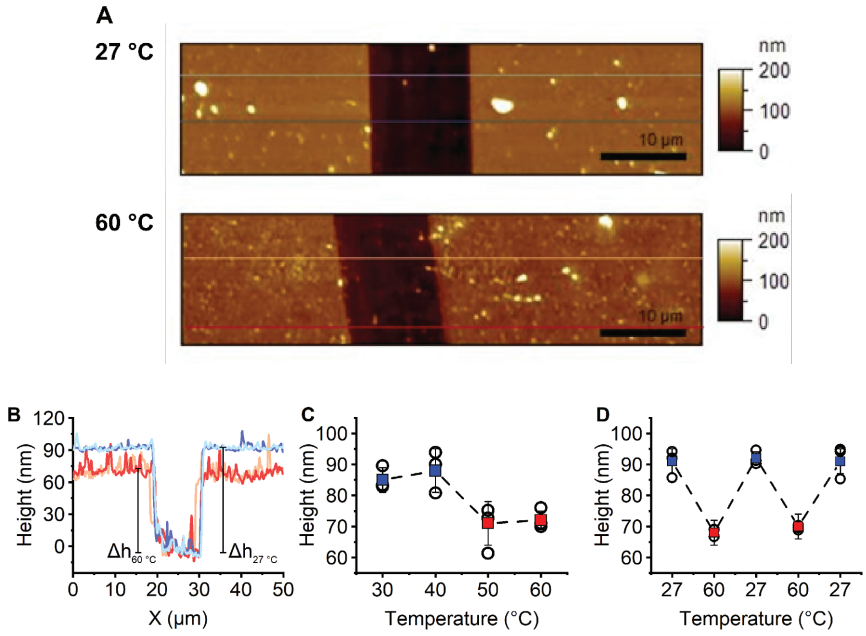

Figure 2.5 (A) AFM 3-D morphology map of the scratched surface with on either side poly(NMEP) brush; **(B)** Height profiles of the AFM maps, taken along the cross-sectional lines in the AFM maps; Brush average height arising from the height distributions of selected areas of interest (detailed description in Supporting Information) with increasing solution temperature **(C)** and during two and a half cycles of increasing and lowering the solution temperature **(D)**.

2.2.5 Protein fouling studies

Essential in the development of efficient and durable biomedical devices is control over the interactions between the device surface and biological media. To prevent deactivation and losses in sensitivity of such applications, non-specific adsorption by components of biological media should be minimized. Modification of the exposed surfaces using low-fouling polymer brushes has provided a solution to this matter.[54,65,66] For the development of so-called 'smart' biomedical devices polymer brush coatings that combine responsiveness with non-fouling character might be advantageous, for example for the reversible binding of cells.[14,32,67] For this reason, the antifouling properties of poly(NMEP) brushes on gold sensors were prepared (XPS data in Supporting Information) and tested against bovine serum albumin (BSA, 5 mg/mL), fibrinogen (Fbg, 1 mg/mL), and diluted human serum (10% in PBS) solutions using QCM-D. Gold-coated sensors were selected as substrate as gold is a commonly employed material in analysis techniques such as sur-

face plasmon resonance (SPR) and electrochemical sensing.[68–70] Polymerization of NMEP from the gold sensors requires the use of a thiol-terminated ATRP-initiator. Compared to the poly(NMEP) brushes on silicon, the grafting density of the poly(NMEP) on these substrates is therefore likely to differ to a certain extent. BSA and fibrinogen were selected as these proteins represent major constituents of blood and are believed to play a key role in surface adhesion.[71] The concentrations of the BSA and fibrinogen solutions employed in this study correspond to the concentrations of the proteins present in 10× diluted human serum.[72,73] Additionally, poly(NMEP) brushes were exposed to dilute human serum to investigate their antifouling properties against more complex biological media. For comparison, the same antifouling experiments were also performed against the unmodified gold QCM-D sensors.

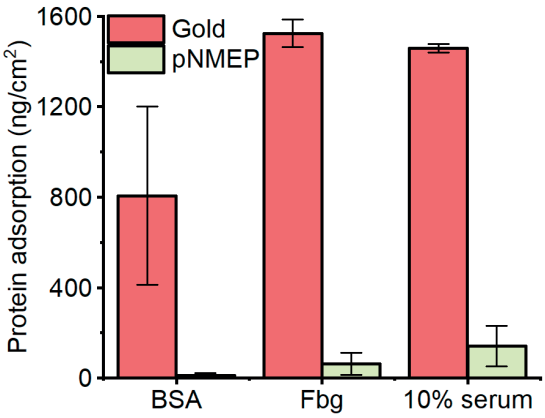

Figure 2.6 Adsorption of BSA (5 mg/mL), fibrinogen (1 mg/mL) and diluted human serum on gold and poly(NMEP)-modified gold, as measured by QCM-D.

The poly(NMEP) brushes showed a 95% decrease in adsorption of BSA and fibrinogen protein solutions, as well as more than 90% reduction in adsorption of 10% human serum when compared to the unmodified gold substrates (Figure 2.6). For the single-protein solutions, it was possible to compare the antifouling performance of poly(NMEP) brushes to the previously reported performance of several oligo(ethylene glycol)-based self-assembled monolayers (SAMs),[74] a frequently employed type of protein-resistant surface.[75,76] In the reference study, the oligo(ethylene glycol) SAMs were exposed to 1 mg/mL solutions of BSA or fibrinogen for 5 min before switching back to buffer solution. The amount of BSA

adsorbed on the SAMs after exposure ranged from 5 to 18 ng/cm^2, whereas the amount of fibrinogen ranged from effectively non-fouling to 27 ng/cm^2.[74] Despite having both a higher concentration and longer exposure time, the amount of accumulated BSA on poly(NMEP) brushes (12 ng/cm^2) was comparable to the values reported for the oligo(ethylene glycol) SAMs.[74] During the fouling experiments with fibrinogen, the poly(NMEP) brushes collected 63 ± 43 ng/cm^2 in 15 min. Although the amount of adsorbed protein on the poly(NMEP) brushes is drastically reduced when compared to the adsorption on bare gold, there is less accumulation of fibrinogen on the oligo(ethylene glycol) SAMs.[74] This may be explained by the longer exposure time of the poly(NMEP) to the protein solution. Following these results, the strongly reduced non-specific adsorption of proteins and serum implies that poly(NMEP) brushes represent a good candidate for smart, responsive coatings in biomedical applications.

2.3 Conclusions

In this Chapter, the monomer NMEP was synthesized and then, for the first time, polymerized from surfaces using SI-ATRP to form polymer brushes. Within 2 hours, a poly(NMEP) brush thickness of 50 nm could be achieved. The living nature of the polymerization procedure was confirmed by the synthesis of block copolymer brushes, through reinitiation of poly(NMEP) with MeOEGMA.

We showed that poly(NMEP) brushes are thermoresponsive by measuring the brush height as a function of temperature from 27 °C to 60 °C by AFM in liquid environment. At increased temperature, the poly(NMEP) brushes collapse and brush height is reduced with ~25%. In addition, the responsive properties of the poly(NMEP) brushes are complemented by promising antifouling performance against BSA, fibrinogen and diluted serum. The combination of thermoresponsive properties, antifouling properties and the possibility to include it in complex polymer structures makes poly(NMEP) of great interest as a smart coating in biomedical devices.

2.4 Materials and Methods

2.4.1 Materials

All chemical reagents were used without further purification unless otherwise specified. Triethylamine (TEA), oligo(ethylene glycol) methyl ether methacrylate (MeOEGMA,

average M_n 300) (MeOEGMA), heptane, Na_2CO_3, $MgSO_4$, Cu(I)Br (99.99% trace metals basis), Cu(II)Br_2 (99.99% trace metals basis), phosphate buffered-saline (PBS, pH 7.2 – 7.4), bovine serum albumin (BSA), fibrinogen (Fbg) and human serum were purchased from Sigma-Aldrich. 2-Hydroxyethyl-*N*-pyrrolidone (>98.0%), 2-(2-bromoisobutyryloxy)undecyl thiol and 1,4,8,11-tetramethyl-1,4,8,11-tetraazacyclotetradecane (Me_6cyclam >98.0%) were purchased from Tokyo Chemical Industry. 11-(Trichlorosilyl)undecyl 2-bromo-2-methylpropanoate was purchased from Gelest, Inc. Methacryloyl chloride (97%) was purchased from Thermo Fisher Scientific. α-bromobutyrate-11-undecanethiol was purchased from ProChimia Surfaces. Deionized water was produced with Milli-Q Integral 3 system Millipore, Molsheim, France (Milli-Q water). Dichloromethane (DCM, >98.0%) and toluene (HPLC grade, 99.9%) were acquired from Sigma-Aldrich and dried using a PureSolv solvent purification system. Silicon single side-polished wafers (Si(100), N-type, phosphorus-doped) were obtained from Siltronix.

2.4.2 Synthesis of N-(2-methacryloyloxy)ethyl pyrrolidone (NMEP)

The synthesis of NMEP was based on previously reported methods by Savelyeva and Marić.[40] 2-Hydroxyethyl-N-pyrrolidone (32.3 g, 250 mmol) and TEA (25.3 g, 250 mmol) were added to a 100 mL three-neck round bottom flask containing 30 mL dry DCM. The reaction setup was purged with argon for 30 min. Then, methacryloyl chloride (26.1 g, 250 mmol) in 30 mL dry DCM was added dropwise to the flask over a period of 30 min while stirring and cooling on an ice bath. The reaction mixture was stirred while cooling for 6 h after which the formed triethylammonium chloride was filtered off. The filtrate was concentrated under reduced pressure and subsequently washed with 50 mL 5% Na_2CO_3 solution, 50 mL brine, and 50 mL deionized water. The organic phase was dried over $MgSO_4$ and concentrated under reduced pressure. The crude product was purified by column chromatography with heptane:ethyl acetate (1:1) as eluent (R_f = 0.1), yielding 29.7 g (60%). **^{1}H NMR** (400 MHz, $CDCl_3$) δ 6.11 (s, 1H), 5.59 (s, 1H), 4.29 (t, J = 5.4 Hz, 4H), 3.60 (t, J = 5.4 Hz, 5H), 3.48 (t, J = 7.0 Hz, 4H), 2.38 (t, J = 8.1 Hz, 5H), 2.10 – 1.98 (m, 5H), 1.95 (s, 3H). **^{13}C NMR** (101 MHz, $CDCl_3$) δ 175.21, 166.97, 135.86, 125.95, 62.13, 47.92, 41.58, 30.66, 18.19, 18.07. **GC-MS** (m/z): 197.1 (M^+), 128.1 ($M^+ - C_4H_5O$), 111.1 ($M^+ - C_4H_5O_2$), 98.1 ($M^+ - C_4H_5O_2$), 69.0 ($M^+ - C_6H_{10}O_2N$). **IR** ν (cm^{-1}) = 2957*m* (CH_3), 2928*m* (CH_2), 2896*m* (CH_3), 1716*s* (C=O), 1683*s* (N–C=O), 1637*m* (C=C), 1424*m* (C–H), 1289*m* (C–N).

2.4.3 Functionalization of Si substrates

Silicon surfaces were cut in squares (approx. 1 × 1 cm), rinsed using acetone, ethanol, and Milli-Q and dried under a gentle stream of argon. They were then subjected to air plasma (Femto, Diener Electronic) for 5 min. After plasma activation, the surfaces were quickly transferred to a solution of 11-(trichlorosilyl)undecyl 2-bromo-2-methylpropanoate (10 µL) in dry toluene (4 mL) and left at RT (19 ± 2 °C) for 16 h. The initiator-functionalized surfaces were then removed from the solution and rinsed using acetone, ethanol, and Milli-Q. Finally, the surfaces were dried under a gentle stream of argon.

2.4.4 SI-ATRP of NMEP

For a typical polymerization experiment, ethanol was degassed by three freeze-pump-thaw cycles. Simultaneously, a septum-sealed flask containing Cu(I)Br (5.7 mg, 0.040 mmol), Cu(II)Br_2 (8.9 mg, 0.040 mmol) and Me_6cyclam (10.2 mg, 0.080 mmol) and a septum-sealed flask containing NMEP (0.660 g, 3.35 mmol) were purged with argon for 30 min. Degassed ethanol (5 mL) was then transferred to the catalyst mixture using a syringe that was purged with argon. The mixture was stirred for 15 min under argon until a dark-blue solution had formed. The catalyst solution was then transferred to the flask containing the monomer using a syringe that had been purged with argon, after which the mixture was stirred for 15 min. The polymerization solution was then transferred under argon to the polymerization reactors that contained initiator-functionalized Si surfaces and had been purged by three evacuate-argon refill cycles. Polymerization reactions were then performed for the desired period at RT (19 ± 2 °C). To stop the reaction, the reactors were opened to the atmosphere. The surfaces were then taken out, rinsed thoroughly with acetone, ethanol, and Milli-Q, and finally dried under a gentle stream of argon.

2.4.5 Block copolymerization: Synthesis of poly(NMEP)-block-poly(MeOEGMA) brushes

SI-ATRP of the first block, poly(NMEP), was carried out as described above for 60 min. After the substrate was removed from the reactor, it was rinsed with acetone, ethanol, and Milli-Q and dried under a gentle stream of argon. The substrate was then cut into two halves; one half was stored for analysis, the other was used for the second polymerization step. Thus, the latter was placed in a second reactor, which was then purged by three evacuate-argon refill cycles. A polymerization solution of Cu(I)Br (5.7 mg, 0.040 mmol), Cu(II)Br_2 (8.9 mg, 0.040 mmol), Me_6cyclam (10.2 mg, 0.080 mmol), and the second monomer, MeOEGMA (1.01 g, 3.35 mmol), was prepared as described above and added to the reactor under argon. The polymerization reaction was performed for 16 h

at RT (19 ± 2 °C). To stop the reaction, the reactor was opened to the atmosphere. The silicon wafer was then taken out, rinsed thoroughly with acetone, ethanol, and Milli-Q, and finally dried under a gentle stream of argon.

2.4.6 Functionalization of Au QCM-D sensor

To facilitate polymerization of NMEP on gold-coated quartz sensors, an ATRP initiator was immobilized on the gold surface. Briefly, gold-coated quartz sensors (QSX 301 Gold, QSense) that have a fundamental frequency (f_0) of 5 MHz were subjected to UV-ozone cleaning (Procleaner UV.PC.220, Bioforce Nanosciences) for 10 min. The sensors were then submerged in a 2% solution of sodium dodecyl sulfate in Milli-Q for 30 min followed by washing with Milli-Q. Subsequently, the sensors were dried with a gentle flow of argon and subjected to oxygen plasma for 10 min. The sensors were taken from the plasma cleaner and placed in a solution of 2-(2-bromoisobutyryloxy)undecyl thiol in methanol (2 µL in 4 mL) for 16 h. After, the sensors were removed from the solution, rinsed with ethanol, and dried under a gentle stream of argon. SI-ATRP of NMEP was then performed as described above.

2.4.7 X-ray photoelectron spectroscopy (XPS)

XPS measurements were performed using a JPS-9200 photoelectron spectrometer (JEOL Ltd., Japan). All samples were analyzed using a focused monochromated Al Kα X-ray source (spot size of 300 µm) at a constant dwelling time for wide-scan 50 ms and narrow scan of 100 ms and pass energy: wide-scan 50 eV narrow scan: 10 eV, under UHV conditions (base pressure: $3 \cdot 10^{-7}$ Pa). The power of the X-ray source was 240 W (20 mA and 12 kV). Charge compensation was applied during the XPS scans with an accelerating voltage of 2.8 eV and a filament current of 4.8 A. All narrow range spectra were corrected with a linear background before fitting. The spectra were fitted with symmetrical Gaussian/Lorentzian (GL(30)) line shapes using CasaXPS. All spectra were referenced to the C 1s peak attributed to C–C and C–H atoms at 285.0 eV.

2.4.8 Static water contact angle measurements

The wettability of the modified surfaces was determined by automated static water contact angle measurements using a DSA 100 goniometer (Krüss, Germany). The volume of a drop of demineralized water employed was 3 µL. Contact angles from sessile drops measured by the tangent method were estimated using a standard error propagation technique involving partial derivatives.

2.4.9 Ellipsometry

Ellipsometric angles Δ and Ψ of the synthesized polymer brushes were measured using an EP4 imaging ellipsometer (Accurion, Germany). The measurements were performed in air at room temperature in the wavelength range of λ = 400.6 – 761.3 nm at an angle of incidence of 50°. The acquired Δ and Ψ were fitted in the EP4 modeling software using a multilayer model to obtain dry polymer brush thickness and refraction index values. The model consisted of a silicon (Si) bottom layer covered with a thin SiO_2 layer of 2.9 nm. Then, the NMEP polymer layer was described using a Cauchy model with parameters A = 1.498 and B = 3000. For all measurements at least two different surfaces were prepared independently, and per surface at least three randomly selected areas were used for thickness measurements.

2.4.10 Atomic Force Microscopy (AFM) measurements

Atomic Force Microscopy was performed using an Asylum MFP-3D Origin AFM (Oxford Instruments, United Kingdom) equipped with a BioHeater Closed Fluid Cell Accessory and Environmental Controller. The instrument was operated in tapping mode and equipped with a silicon cantilever (AC240TS-R3, k = 1.3 N/m) with a nominal tip radius of ~7 nm. Prior to loading the polymer brush substrates into the cell, the surfaces were gently scratched with a scalpel to partly remove the polymer film and expose the silicon. Measurements were performed in a Milli-Q solution, at 27 °C, 30 °C, 40 °C, 50 °C, or 60 °C, and triplicated to measure the average thickness of the polymeric film and its standard deviation (SD) upon cooling and heating (Figure 2.5 and Supporting Information). Before measurements at each temperature, 60 min was taken to obtain AFM thermal stability. The acquired images were processed and analyzed using MountainsSPIP (DigitalSurf, France).

2.4.11 QCM-D measurements

Measurements were performed by using Q-Sense E4 QCM-D (Biolin Scientific, Sweden). All experiments were conducted at 20 °C. Before each experiment, the buffer and protein solutions were bubbled with argon to eliminate dissolved oxygen, which may interfere with the experiment. The PBS buffer solution was pumped via a peristaltic pump (Ismatec high precision multichannel dispenser) with a flow rate of 400 µL/min for at least 15 min before each experiment. Fouling experiments were performed at a flow rate of 25 µL/min. Pristine gold-coated sensors and gold-coated sensors with poly(NMEP) brushes with thicknesses of approximately 20 nm were subjected to a protein solution for 15 min, after which the buffer solution was pumped over the sensors again until the signal stabilized.

Frequency shifts (Δf) and dissipation shifts (ΔD) were acquired at the 3rd (15 MHz), 5th (25 MHz), 7th (35 MHz), 9th (45 MHz), and 11th (55 MHz) harmonic overtone. For data analysis, only the 3rd (15 MHz) overtone was used. QSoft software was used during data acquisition and DFind (version 1.2.7) for analysis of the data. The 'wet' mass (thickness) of the sensor surfaces after protein fouling was estimated from the decrease of the frequency of the quartz crystal with the Sauerbrey equation (1):[77]

$$\Delta m = (-C \times \Delta f_n) / n \quad (1)$$

In this equation, Δm is the areal mass density of the adsorbed foulant, Δf_n the frequency shift, C (17.7 ng/cm^2/Hz) the mass sensitivity constant for a 5 MHz quartz crystal, and n the harmonic number (3, 5, 7, 9 or 11).

2.4.12 Simulation of XPS C 1s Narrow Scan Spectra

Electronic core-level calculations were performed using the Gaussian 16 system.[78] The molecular geometry was optimized at the B3LYP/6-311G(d,p) level of theory. The core orbital energies were then calculated using natural bond order (NBO) analysis and used to simulate the XPS C1s spectrum of poly(NMEP) brushes.[57,58]

2.5 Acknowledgements

This research was carried out under project number C16030a in the framework of the Partnership Program of the Materials innovation institute M2i (www.m2i.nl) and the NWO Domain Science, which is part of the Netherlands Organization for Scientific Research (www.nwo.nl).

2.6 Supporting Information

The supporting information is available from the Wiley Online Library: https://doi.org/10.1002/admi.202101717

2.7 References

1. Mendes, P. M. Stimuli-responsive surfaces for bio-applications. *Chem. Soc. Rev.* **37**, 2512 (2008).
2. Chen, T., Ferris, R., Zhang, J., Ducker, R. & Zauscher, S. Stimulus-responsive polymer brushes on surfaces : Transduction mechanisms and applications. *Prog. Polym. Sci.* **35**, 94–112 (2010).
3. Peng, S. & Bhushan, B. Smart polymer brushes and their emerging applications. *RSC Adv.* **2**, 8557 (2012).
4. Bikram, M. & West, J. L. Thermo-responsive systems for controlled drug delivery. *Expert Opin. Drug Deliv.* **5**, 1077–1091 (2008).
5. Doberenz, F., Zeng, K., Willems, C., Zhang, K. & Groth, T. Thermoresponsive polymers and their biomedical application in tissue engineering-a review. *J. Mater. Chem. B* **8**, 607 (2020).
6. Chu, L. Y., Niitsuma, T., Yamaguchi, T. & Nakao, S. ichi. Thermoresponsive transport through porous membranes with grafted PNIPAM gates. *AIChE J.* **49**, 896–909 (2003).
7. Wei, M., Gao, Y., Li, X. & Serpe, M. J. Stimuli-responsive polymers and their applications. *Polym. Chem.* **8**, 127–143 (2017).
8. Roy, D., Brooks, W. L. A. & Sumerlin, B. S. New directions in thermoresponsive polymers. *Chem. Soc. Rev.* **42**, 7214 (2013).
9. Kim, Y.-J. & Matsunaga, Y. T. Thermo-responsive polymers and their application as smart biomaterials. *J. Mater. Chem. B* **5**, 4307–4321 (2017).
10. Zhang, Q., Weber, C., Schubert, U. S. & Hoogenboom, R. Thermoresponsive polymers with lower critical solution temperature: from fundamental aspects and measuring techniques to recommended turbidimetry conditions. *Mater. Horizons* **4**, 109–116 (2017).
11. Aseyev, V., Tenhu, H. & Winnik, F. M. Non-ionic Thermoresponsive Polymers in Water. *Adv. Polym. Sci.* **242**, 29–89 (2011).
12. Plunkett, K. N., Zhu, X., Moore, J. S. & Leckband, D. E. PNIPAM Chain Collapse Depends on the Molecular Weight and Grafting Density. *Langmuir* **22**, 4259–4266 (2006).
13. Yim, H. *et al.* Effects of Grafting Density and Molecular Weight on the Temperature-Dependent Conformational Change of Poly(N-isopropylacrylamide) Grafted Chains in Water. *Macromolecules* **39**, 3420–3426 (2006).
14. Nagase, K., Watanabe, M., Kikuchi, A., Yamato, M. & Okano, T. Thermo-Responsive Polymer Brushes as Intelligent Biointerfaces: Preparation via ATRP and Characterization. *Macromol. Biosci.* **11**, 400–409 (2011).
15. Nagase, K. *et al.* Interfacial Property Modulation of Thermoresponsive Polymer Brush Surfaces and Their Interaction with Biomolecules. *Langmuir* **23**, 9409–9415 (2007).
16. Frost, S. & Ulbricht, M. Thermoresponsive ultrafiltration membranes for the switchable permeation and fractionation of nanoparticles. *J. Memb. Sci.* **448**, 1–11 (2013).
17. Huber, D. L., Manginell, R. P., Samara, M. A., Kim, B.-I. & Bunker, B. C. Programmed Adsorption and Release of Proteins in a Microfluidic Device. *Science (80-.).* **301**, 352–354 (2003).
18. Zoppe, J. O. *et al.* Surface-Initiated Controlled Radical Polymerization: State-of-the-Art, Opportunities, and Challenges in Surface and Interface Engineering with Polymer Brushes. *Chem. Rev.* **117**, 1105–1318 (2017).

19. Olivier, A., Meyer, F., Raquez, J. M., Damman, P. & Dubois, P. Surface-initiated controlled polymerization as a convenient method for designing functional polymer brushes: From self-assembled monolayers to patterned surfaces. *Prog. Polym. Sci.* **37**, 157–181 (2012).

20. Li, M. *et al.* SI-PET-RAFT: Surface-Initiated Photoinduced Electron Transfer-Reversible Addition–Fragmentation Chain Transfer Polymerization. *ACS Macro Lett.* **8**, 374–380 (2019).

21. Xu, X. *et al.* Antifouling Surfaces Enabled by Surface Grafting of Highly Hydrophilic Sulfoxide Polymer Brushes. *Biomacromolecules* **22**, 330–339 (2020).

22. Seo, S. E., Discekici, E. H., Zhang, Y., Bates, C. M. & Hawker, C. J. Surface-initiated PET-RAFT polymerization under metal-free and ambient conditions using enzyme degassing. *J. Polym. Sci.* **58**, 70–76 (2020).

23. Roeven, E. *et al.* PLL–Poly(HPMA) Bottlebrush-Based Antifouling Coatings: Three Grafting Routes. *Langmuir* **36**, 10187–10199 (2020).

24. Kuzmyn, A. R., Nguyen, A. T., Teunissen, L. W., Zuilhof, H. & Baggerman, J. Antifouling Polymer Brushes via Oxygen-Tolerant Surface-Initiated PET-RAFT. *Langmuir* **36**, 4439–4446 (2020).

25. Kuzmyn, A. R. *et al.* Diblock and Random Antifouling Bioactive Polymer Brushes on Gold Surfaces by Visible-Light-Induced Polymerization (SI-PET-RAFT) in Water. *Adv. Mater. Interfaces* **9**, (2022).

26. Kubota, K., Fujishige, S. & Ando, I. Solution Properties of Poly(N-isopropylacrylamide) in Water. *Polym. J.* **22**, 15–20 (1990).

27. Rademacher, J. T., Baum, M., Pallack, M. E., Brittain, W. J. & Simonsick, W. J. Atom Transfer Radical Polymerization of N,N-Dimethylacrylamide. *Macromolecules* **33**, 284–288 (2000).

28. Teodorescu, M. & Matyjaszewski, K. Atom Transfer Radical Polymerization of (Meth)acrylamides. *Macromolecules* **32**, 4826–4831 (1999).

29. Herberg, A., Yu, X. & Kuckling, D. End Group Stability of Atom Transfer Radical Polymerization (ATRP)-Synthesized Poly(N-isopropylacrylamide): Perspectives for Diblock Copolymer Synthesis. *Polymers (Basel).* **11**, 678 (2019).

30. Idota, N., Ebara, M., Kotsuchibashi, Y., Narain, R. & Aoyagi, T. Novel temperature-responsive polymer brushes with carbohydrate residues facilitate selective adhesion and collection of hepatocytes. *Sci. Technol. Adv. Mater.* **13**, (2012).

31. Yu, Q. *et al.* Protein Adsorption and Cell Adhesion/Detachment Behavior on Dual-Responsive Silicon Surfaces Modified with Poly(N-isopropylacrylamide)-block-polystyrene Copolymer. *Langmuir* **26**, 8582–8588 (2010).

32. Takahashi, H., Nakayama, M., Yamato, M. & Okano, T. Controlled Chain Length and Graft Density of Thermoresponsive Polymer Brushes for Optimizing Cell Sheet Harvest. *Biomacromolecules* **11**, 1991–1999 (2010).

33. Mandal, J., Arcifa, A. & Spencer, N. D. Synthesis of acrylamide-based block-copolymer brushes under flow: monitoring real-time growth and surface restructuring upon drying. *Polym. Chem* **11**, 3209 (2020).

34. Nash, M. E. *et al.* Synthesis and characterization of a novel thermoresponsive copolymer series and their application in cell and cell sheet regeneration) Synthesis and characterization of a novel thermoresponsive copolymer series and their application in cell and cell sheet. *J. Biomater. Sci. Polym. Ed.* **24**, 253–268 (2013).

35. Cunningham, V. J., Ning, Y., Armes, S. P. & Musa, O. M. Poly(N-2-(methacryloyloxy)ethyl pyrrolidone)-poly(benzyl methacrylate) diblock copolymer nano-objects via RAFT alcoholic dispersion polymerisation in ethanol. *Polymer (Guildf).* **106**, 189–199 (2016).

36. Cunningham, V. J., Derry, M. J., Fielding, L. A., Musa, O. M. & Armes, S. P. RAFT Aqueous Dispersion Polymerization of N-(2-(Methacryloyloxy)ethyl)pyrrolidone: A Convenient Low Viscosity Route to High Molecular Weight Water-Soluble Copolymers. *Macromolecules* **49**, 4520–4533 (2016).

37. Cunningham, V. J., Armes, S. P. & Musa, O. M. Synthesis, characterisation and Pickering emulsifier performance of poly(stearyl methacrylate)–poly(N-2-(methacryloyloxy)ethyl pyrrolidone) diblock copolymer nano-objects via RAFT dispersion polymerisation in n-dodecane. *Polym. Chem.* **7**, 1882 (2016).

38. Sun, J. *et al.* Effect of Molecular Structure on Thermoresponsive Behaviors of Pyrrolidone-Based Water-Soluble Polymers. *Macromolecules* **43**, 4041–4049 (2010).

39. Peng, Y. *et al.* Facile Synthesis and Thermoresponsive Behaviors of a Well-Defined Pyrrolidone Based Hydrophilic Polymer. *Macromolecules* **41**, 3007–3014 (2008).

40. Savelyeva, X. & Marić, M. Pyrrolidone-functional smart polymers via nitroxide-mediated polymerization. *J. Polym. Sci. Part A Polym. Chem.* **52**, 2011–2024 (2014).

41. Iskander, G. M., Baker, L. E., Wiley, D. E. & Davis, T. P. Synthesis and polymerization of new pyrrolidone-containing methacrylate monomers. *Polymer (Guildf).* **39**, 4165–4169 (1998).

42. Krys, P. & Matyjaszewski, K. Kinetics of Atom Transfer Radical Polymerization. *Eur. Polym. J.* **89**, 482–523 (2017).

43. Keddie, D. J. A guide to the synthesis of block copolymers using reversible-addition fragmentation chain transfer (RAFT) polymerization. *Chem. Soc. Rev* **43**, 496 (2014).

44. Liu, X., Xu, Y., Wu, Z. & Chen, H. Poly(N-vinylpyrrolidone)-Modified Surfaces for Biomedical Applications. *Macromol. Biosci.* **13**, 147–154 (2013).

45. Yuan, H., Qian, B., Zhang, W. & Lan, M. Protein adsorption resistance of PVP-modified polyurethane film prepared by surface-initiated atom transfer radical polymerization. *Appl. Surf. Sci.* **363**, 483–489 (2016).

46. Wu, Z. *et al.* Protein Adsorption on Poly(N-vinylpyrrolidone)-Modified Silicon Surfaces Prepared by Surface-Initiated Atom Transfer Radical Polymerization. *Langmuir* **25**, 2900–2906 (2009).

47. Liu, X. *et al.* Facile Synthesis of Thermally Stable Poly(N-vinylpyrrolidone)-Modified Gold Surfaces by Surface-Initiated Atom Transfer Radical Polymerization. *Langmuir* **28**, 9451–9459 (2012).

48. Au-Duong, A.-N., Vo, D.-T. & Lee, C.-K. Bactericidal magnetic nanoparticles with iodine loaded on surface grafted poly(N-vinylpyrrolidone). *J. Mater. Chem. B* **3**, 840–848 (2015).

49. Xiang, T. *et al.* Surface hydrophilic modification of polyethersulfone membranes by surface-initiated ATRP with enhanced blood compatibility. *Colloids Surfaces B Biointerfaces* **110**, 15–21 (2013).

50. Yusa, S. I. *et al.* Thermo-responsive diblock copolymers of poly(N-isopropylacrylamide) and poly(N-vinyl-2-pyrroridone) synthesized via organotellurium-mediated controlled radical polymerization (TERP). *Macromolecules* **40**, 5907–5915 (2007).

51. Ruggeri, F. S., Šneideris, T., Vendruscolo, M. & Knowles, T. P. J. Atomic force microscopy for single molecule characterisation of protein aggregation. *Archives of Biochemistry and Biophysics* **664**, 134–148 (2019).

52. Ruggeri, F. S. *et al.* Nanoscale studies link amyloid maturity with polyglutamine diseases onset. *Sci. Rep.* **6**, 31155 (2016).

53. Shergujri, M. A. *et al.* Paper-Based Sensors for Biomedical Applications. in *Biomedical Engineering and its Applications in Healthcare* **19**, 355–376 (Springer Singapore, 2019).

54. Kuzmyn, A. R., Nguyen, A. T., Zuilhof, H. & Baggerman, J. Bioactive Antifouling Surfaces by Visible-Light-Triggered Polymerization. *Adv. Mater. Interfaces* **6**, 1900351 (2019).

55. Obstals, F. *et al.* Improving Hemocompatibility of Membranes for Extracorporeal Membrane Oxygenators by Grafting Nonthrombogenic Polymer Brushes. *Macromol. Biosci.* **18**, 1700359 (2018).

56. Lu, X. *et al.* Controllable synthesis of poly(N-vinylpyrrolidone) and its block copolymers by atom transfer radical polymerization. *Polymer (Guildf).* **48**, 2835–2842 (2007).

57. Giesbers, M., Marcelis, A. T. M. & Zuilhof, H. Simulation of XPS C1s Spectra of Organic Monolayers by Quantum Chemical Methods. *Langmuir* **29**, 4782–4788 (2013).

58. Zhao, J., Gao, F., Pujari, S. P., Zuilhof, H. & Teplyakov, A. V. Universal Calibration of Computationally Predicted N 1s Binding Energies for Interpretation of XPS Experimental Measurements. *Langmuir* **33**, 10792–10799 (2017).

59. Tang, W. & Matyjaszewski, K. Kinetic Modeling of Normal ATRP, Normal ATRP with [CuII]0 , Reverse ATRP and SR&NI ATRP. *Macromol. Theory Simulations* **17**, 359–375 (2008).

60. Gevrek, T. N., Bilgic, T., Klok, H.-A. & Sanyal, A. Maleimide-Functionalized Thiol Reactive Copolymer Brushes: Fabrication and Post-Polymerization Modification. *Macromolecules* **47**, 7842–7851 (2014).

61. Motornov, M., Sheparovych, R., Katz, E. & Minko, S. Chemical Gating with Nanostructured Responsive Polymer Brushes: Mixed Brush versus Homopolymer Brush. *ACS Nano* **2**, 41–52 (2021).

62. Steenackers, M. *et al.* Structured Polymer Brushes on Silicon Carbide. *Chem. Mater* **22**, 272–278 (2010).

63. Xue, C. *et al.* Protein adsorption on poly(N -isopropylacrylamide) brushes: Dependence on grafting density and chain collapse. *Langmuir* **27**, 8810–8818 (2011).

64. Jonas, A. M., Glinel, K., Oren, R., Nysten, B. & Huck, W. T. S. Thermo-Responsive Polymer Brushes with Tunable Collapse Temperatures in the Physiological Range. *Macromolecules* **40**, 4403–4405 (2007).

65. van Andel, E. *et al.* Systematic Comparison of Zwitterionic and Non-Zwitterionic Antifouling Polymer Brushes on a Bead-Based Platform. *Langmuir* **35**, 1181–1191 (2019).

66. Kuzmyn, A. R. *et al.* Exploiting end group functionalization for the design of antifouling bioactive brushes. *Polym. Chem.* **5**, 4124 (2014).

67. Takahashi, H., Nakayama, M., Itoga, K., Yamato, M. & Okano, T. Micropatterned Thermoresponsive Polymer Brush Surfaces for Fabricating Cell Sheets with Well-Controlled Orientational Structures. *Biomacromolecules* **12**, 1414–1418 (2011).

68. Homola, J., Yee, S. S. & Gauglitz, G. Surface plasmon resonance sensors: review. *Sensors Actuators, B Chem.* **54**, 3–15 (1999).

69. Vaisocherova-Lísalová, H. *et al.* Copolymer Brush-Based Ultralow-Fouling Biorecognition Surface Platform for Food Safety. *Anal. Chem.* **88**, 10533–10539 (2016).

70. Kotlarek, D. *et al.* Compact Grating-Coupled Biosensor for the Analysis of Thrombin. *ACS Sensors* **4**, 2109–2116 (2019).

71. Riedel, T. *et al.* Complete Identification of Proteins Responsible for Human Blood Plasma Fouling on Poly(ethylene glycol)-Based Surfaces. *Langmuir* **29**, 3388–3397 (2013).

72. Lowe, G. D. O., Rumley, A. & Mackie, I. J. Plasma Fibrinogen. *Ann Clin Biochem* **41**, 430–440 (2004).

73. Quinlan, G. J., Martin, G. S. & Evans, T. W. Albumin: Biochemical properties and therapeutic potential. *Hepatology* **41**, 1211–1219 (2005).

74. Hayashi, T., Tanaka, Y., Koide, Y., Tanaka, M. & Hara, M. Mechanism underlying bioinertness of self-assembled monolayers of oligo(ethyleneglycol)-terminated alkanethiols on gold: protein adsorption, platelet adhesion, and surface forces. *Phys. Chem. Chem. Phys* **14**, 10196–10206 (2012).

75. Ekblad, T. & Liedberg, B. Protein adsorption and surface patterning. *Curr. Opin. Colloid Interface Sci.* **15**, 499–509 (2010).

76. Ogaki, R., Alexander, M. & Kingshott, P. Chemical patterning in biointerface science. *Mater. Today* **13**, 22–35 (2010).

77. Sauerbrey, G. *Verwendung von Schwingquarzen zur Wägung dünner Schichten und zur Mikrowägung*. *Zeitschrift für Physik* **55**, (1959).

78. Frisch, M. J. *et al.* Gaussian 16, revision C.01. (2016).

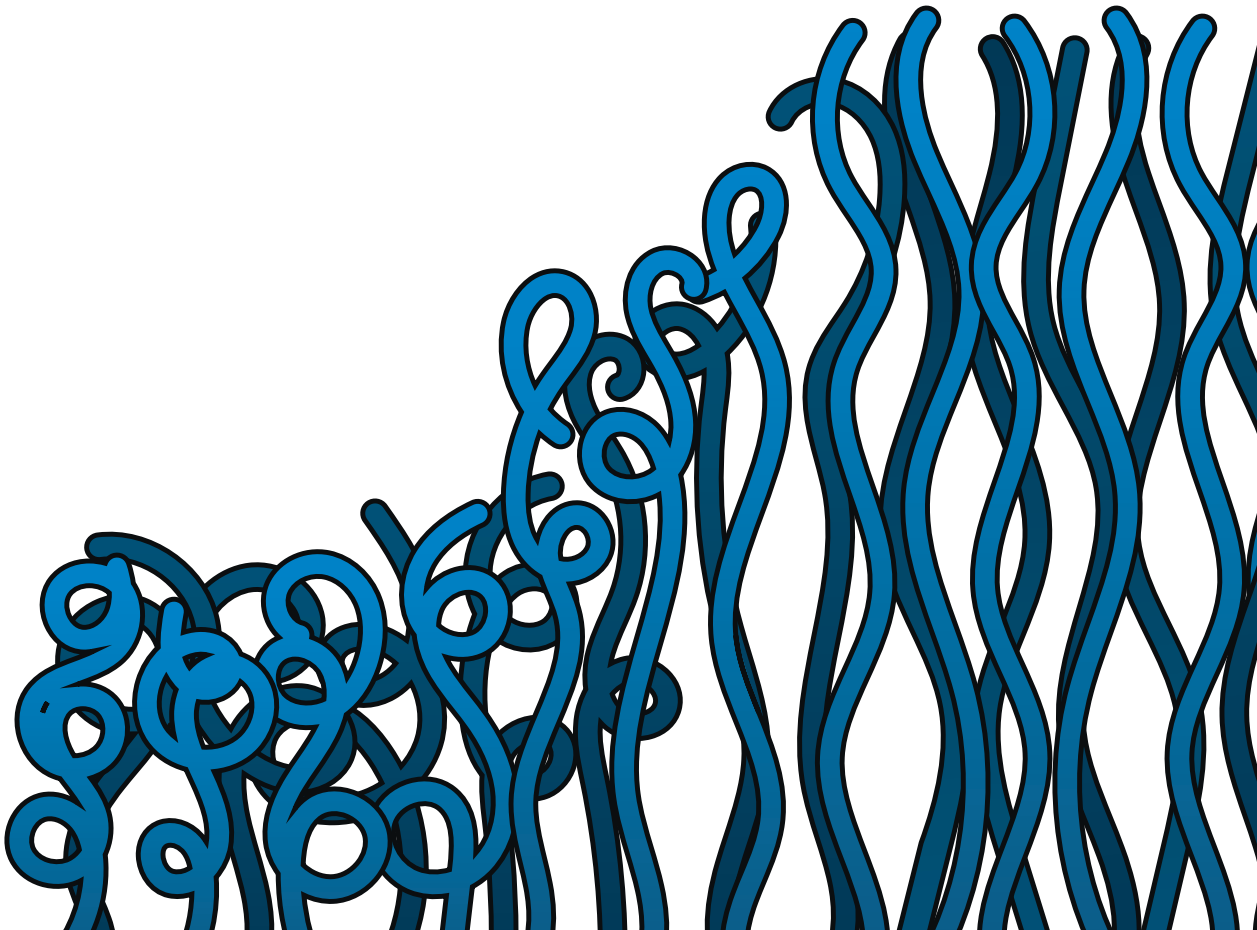

Chapter 3

Thermoresponsive Polymer Brushes for Switchable Protein Adsorption via Dopamine-Assisted Grafting-To Strategy

Teunissen, L. W., van den Beukel, J., Smulders, M. M. J. & Zuilhof, H.
Thermoresponsive Polymer Brushes for Switchable Protein Adsorption via Dopamine-Assisted Grafting-To Strategy.
Adv. Mater. Interfaces 9, 2201198 (2022).

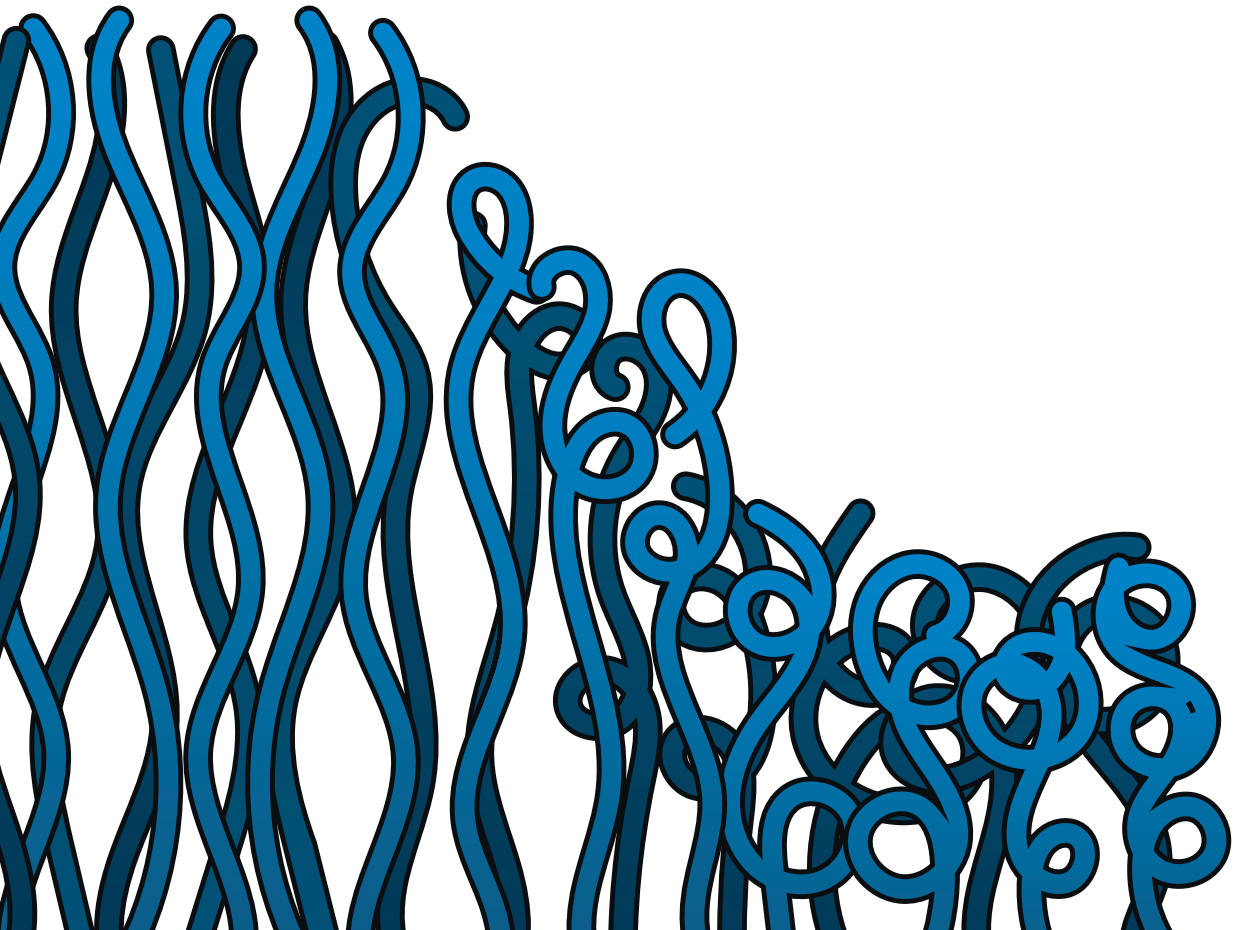

Abstract

Surface modifications using responsive polymers give access to biomedical applications that rely on switchable properties, such as smart sensors and actuator systems. In this Chapter, thermoresponsive polymer coatings are synthesized on silicon oxide surfaces using a facile and effective two-step grafting-to strategy. Briefly, the substrates are first functionalized with a poly(dopamine) primer layer. Subsequently, block copolymers of poly(glycidyl methacrylate) and poly(*N*-isopropylacrylamide) (poly(GMA)$_{20}$-block-poly(NIPAM)$_n$ (n = 263, 528 and 705)) synthesized via reversible addition-fragmentation chain-transfer (RAFT) polymerization, are grafted to the poly(dopamine)-modified surfaces. Characterization using ellipsometry, X-ray photoelectron spectroscopy (XPS) and contact angle measurements confirmed polymer attachment with appreciable grafting densities. Quartz crystal microbalance with dissipation monitoring (QCM-D) is employed to investigate the thermoresponsive properties and degree of hydration of the polymers below and above their lower critical solution temperature (LCST). The longer the polymer chain, the more water is lost per repeating unit upon increasing the temperature above the LCST. The surfaces are exposed to diluted and undiluted human serum at 20 °C and 40 °C to demonstrate for all three polymer brushes switchable protein adsorption-repellence. In a broader perspective, this study presents a straightforward, robust and efficient procedure to modify virtually any surface type with a thermoresponsive coating.

3.1 Introduction

A key aspect in the design and production of functional materials is precise control over surface properties. In many applications, including microfluidics,[1] sensing[2] and membrane technology,[3] modification of the interface to either promote or inhibit certain surface interactions is essential. In the biomedical field, for instance, exposure of device surfaces to complex biological species such as proteins, cells and bacteria is inevitable.[4–6] Evidently, control over the interactions with the constituents of such biological media is paramount.

Modification of interfaces using functional polymers can be employed to promote or inhibit such interactions.[7–9] Numerous types of antifouling polymer coatings have been developed for biomedical applications to prevent unspecific adsorption of biological components that may lead to internal complications or degradation of the instrument.[10–12] In contrast, polymer films may also be introduced to promote adhesion of specific biomacromolecules to an interface.[13–15]

In addition to surface modifications that are able to either promote or inhibit adsorption of biologic material, the use of stimuli-responsive polymers enables the creation of "smart" surfaces that can switch between adhesive and non-adhesive states.[16–18] Among the available options, temperature is likely one of the most practical stimuli to apply.[19] Through functionalization of surfaces with thermoresponsive polymer coatings, it is possible to tune the degree of surface adhesive properties with respect to proteins and cells through variation of the applied temperature.[20–25] When the system temperature is below the lower critical solution temperature (LCST), the polymers are hydrated and swollen. In this state, adhesion of proteins and cells is typically low. At temperatures exceeding the LCST, however, hydrogen bonding is disrupted and the polymers expulse water and adopt a collapsed conformation. As a result, adhesion of biological constituents is then consistently higher. This addressable feature of thermoresponsive polymer coatings shows great promise in membrane applications,[26–28] functional antifouling surface technology[21,29] and cell-sheet engineering.[24,30,31]

Investigations of thermoresponsive polymer brush surfaces and their interactions with protein solutions have been performed mainly for coatings synthesized using surface-initiated grafting-from polymerization techniques, as discussed in Chapter 2,[22,23] that can yield high grafting densities.[32,33] The main, inherent disadvantage to surface-initiated polymerization reactions, however, is that detailed characterization of the produced polymers, feasible in most detail (*e.g.*, in terms of polydispersity and degree of polymerization) by degrafting, is challenging as the grown polymer is strongly (covalently) bound to the surface.[34,35] Depending on the surface such analysis may require harsh degrafting

conditions that are not compatible with all functional groups in the polymer, especially for highly functional polymers. Synthesis of the polymers in solution and subsequent grafting to a substrate circumvents this and is more readily scalable, but the resulting grafting densities are typically lower. For such procedures, the final number of polymer chains per unit area depends greatly on the polymer coil size.[36,37] Large polymer coils will cover a substantial area of the substrate, thereby obstructing attachment of other polymers which then results in lower grafting densities. Although the number of chains per surface area is lower than for grafting-from techniques, tuning of polymer length in grafting-to procedures does provide control over grafting density, which in turn will influence the coating's properties.

Several grafting-to procedures have been developed that yield functional polymer coatings of relatively high grafting densities.[37–40] To yield such high grafting densities, excluded volume effects are minimized by grafting under cloud point conditions or grafting from melt. Cloud point grafting has been employed predominantly to graft polymer chains to gold surfaces.[40–42] Although effective in achieving high grafting densities, application requires strict solubility conditions governed by polymer type and size, which also strongly limits the amount of applicable grafting chemistries. Alternatively, high grafting densities can be achieved by grafting polymers from melt.[38,43] During this procedure, the polymers occupy a much smaller volume and therefore higher amounts of chains bind per unit area.[43–46] Although grafting from melt is advantageous in terms of grafting density, the procedure requires elevated temperatures, especially for longer polymers, which can result in degradation of the polymer.[47,48] When compared to grafting under cloud point conditions and grafting-to from melt, grafting-to strategies from polymer solutions can be considered as more robust as the reaction conditions are more easily governable by choice of solvent and grafting reaction.

To achieve increased stability and grafting density of a grafted-to polymer brush, a primer layer can be used that strongly binds to the substrate and holds functional groups to which the polymer chains can be covalently attached.[49,50] Deposition of, by now widely investigated, poly(dopamine) provides such attachment sites through the amine groups present in its structure.[51,52] Use of poly(dopamine) is especially advantageous when compared to other modifying agents as it can form a stable primer layer onto virtually any substrate.[50,53,54] The poly(dopamine) layer can be simply deposited from aqueous solutions, does not require harsh pretreatment by, *e.g.*, plasma activation or strong acid, and the free amine groups present can conveniently be used for reactions with several chemical functional groups, including epoxides,[55] which thus also allow polymer attachment.[56–58] The epoxide functionality can be introduced to polymer chains as end group functionality

or by incorporation of epoxide-containing monomers during the polymerization step.[59,60] We thus hypothesized that a block copolymer design that combines a short poly(glycidyl methacrylate) (poly(GMA)) segment with a longer thermoresponsive polymer segment would provide for the effective covalent attachment of fully characterizable, thermoresponsive block copolymers to poly(dopamine)-functionalized surfaces.[61]

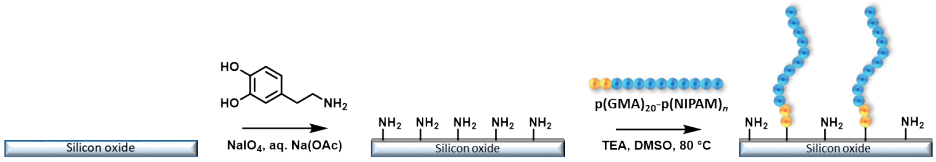

Scheme 3.1 Schematic overview of the surface modification steps undertaken in this study: Two-step grafting procedure that involves functionalizing the target substrate with a poly(dopamine) layer containing free amines, followed by grafting of poly(GMA)$_{20}$-*b*-poly(NIPAM)$_n$ to the surface.

In this Chapter, we demonstrate a facile grafting-to procedure for grafting poly(glycidyl methacrylate)-*b*-poly(*N*-isopropylacrylamide) –abbreviated herein to poly(GMA)-*b*-poly(NIPAM)– using poly(dopamine) as a priming layer (Scheme 3.1).[50,53,54] This approach aims to combine robust surface attachment, ease of use, thermoresponsiveness and high degree of molecular control. Three block copolymers of varying poly(NIPAM) block size are synthesized via consecutive reversible addition-fragmentation chain-transfer (RAFT) polymerization reactions and fully characterized in solution, after which they are grafted to poly(dopamine)-modified silicon oxide substrates. The thermoresponsive properties of the resultant surfaces in dependence of the size of the poly(NIPAM) blocks are investigated using quartz crystal microbalance with dissipation monitoring (QCM-D). Protein adsorption as a function of this thermoresponsive behavior is then assessed to investigate whether protein adsorption can be switched "on" and "off" with temperature changes, and how that property is dependent on the poly(NIPAM) block size.

3.2 Results and Discussion

3.2.1 Synthesis of block copolymers

The RAFT polymerization was carried out in two steps, starting with the polymerization of GMA (Scheme 3.2) to form short polymer chains of approximately 20 GMA units. Char-

acterization and determination of the chain length of the poly(GMA)$_{20}$ was performed using ^{1}H NMR spectrometry (see Supporting Information), confirming an average chain length of 20 units. From this poly(GMA)$_{20}$, which was used as a macro-RAFT agent, block copolymers of three distinct lengths were synthesized by variation in monomer (NIPAM) concentration. The targeted degree of polymerization (*DP*) for the poly(NIPAM) segments were 200, 400 and 600. The three synthesized block copolymers were characterized using ^{1}H NMR spectrometry and GPC (Table 3.1 and Supporting Information).

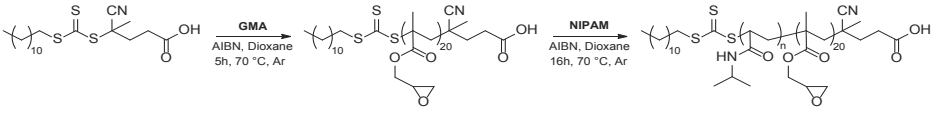

Scheme 3.2 Procedure for the synthesis of poly(GMA)$_{20}$-block-poly(NIPAM)$_n$.

The molecular weights, M_n, for the polymers obtained from GPC suggested poly(NIPAM) blocks consisting of 263, 528 and 705 repeating units (poly(GMA)$_{20}$-*b*-poly(NIPAM)$_{263}$ [in short: pG$_{20}$N$_{263}$], poly-(GMA)$_{20}$-*b*-poly(NIPAM)$_{528}$ [pG$_{20}$N$_{528}$] and poly(GMA)$_{20}$-*b*-poly(NIPAM)$_{705}$ [pG$_{20}$N$_{705}$]), respectively (Table 3.1). The slightly higher than expected degrees of polymerization are attributed to slight differences in the GPC behavior of the block copolymers compared to the poly(methyl methacrylate) calibration standards. The rather high PDI values for the block copolymers are believed to be the result of the use of poly(GMA) as macro-RAFT agent,[62] as well as the high degree of polymerization for these polymers. Since the carboxylic acid functionality present in the RAFT agent may also react with the amine groups of poly(dopamine), a homopolymer of poly(NIPAM) with *DP* of 651 [pN$_{651}$] was synthesized as a control polymer to verify the role in achieving a strong surface binding of the poly(GMA) segment during the grafting-to process.

Table 3.1 Analysis of the synthesized block copolymers, based on GPC data.

	Polymer	Targeted DP	M_n (kDa)	M_w (kDa)	Đ
1	**pG$_{20}$N$_{263}$**	200	33	50	1.53
2	**pG$_{20}$N$_{528}$**	400	63	94	1.51
3	**pG$_{20}$N$_{705}$**	600	83	145	1.75
4	**pN$_{651}$**	600	74	105	1.43

3.2.2 Poly(dopamine) deposition

In parallel, coating of silicon oxide substrates with poly(dopamine) was performed in the presence of oxidizing agent $NaIO_4$, as this approach is known to yield highly homogeneous thin films in short reaction times (5 min at room temperature) and to achieve a higher amount of free amine groups when compared to typical dopamine deposition methods performed in basic NaOAc solutions.[63,64] The thickness of the poly(dopamine) thin films was determined at 2.2 ± 0.8 nm using ellipsometry, in agreement with earlier findings.[63] Emergence of the N 1s signal in the X-ray photoelectron spectroscopy wide scan spectrum confirmed the presence of poly(dopamine) on the surface (Figure 3.1A). Deconvolution of the peak in the N 1s narrow scan of the poly(dopamine) spectrum revealed the presence of free amine groups (402.0 eV) –which are available for subsequent surface functionalization– in the polymerized dopamine material (Figure 3.1B).[65,66] Finally, static water contact angle measurements revealed a more hydrophobic character for the poly(dopamine) surface [52° ± 7°] as compared to pristine silicon oxide substrates [32° ± 1°] (Table 3.2).

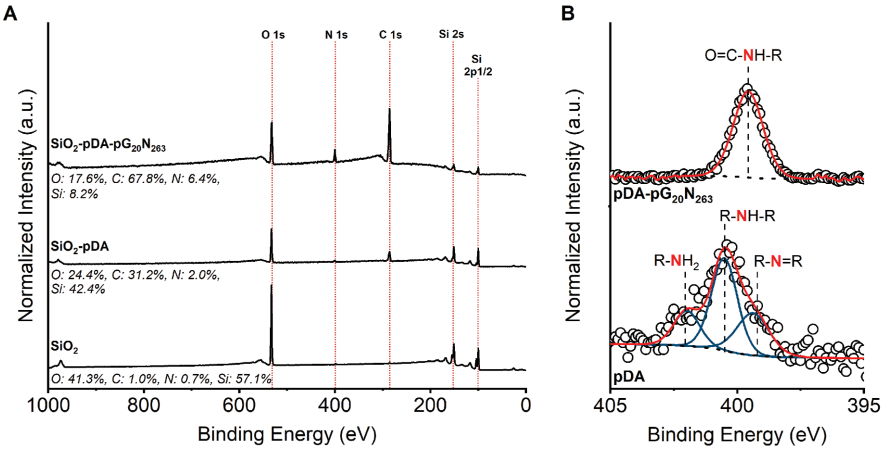

Figure 3.1 (A) XPS wide scan spectra of pristine SiO_2 substrate (bottom), poly(dopamine)-modified SiO_2 (middle) and $pG_{20}N_{263}$ grafted to poly(dopamine)-modified SiO_2 (top). **(B)** XPS N 1s narrow scan spectrum of SiO_2-poly(dopamine) (bottom) and $pG_{20}N_{263}$ grafted to poly(dopamine)-modified SiO_2 (top).

3.2.3 Grafting-to reactions

Block copolymers $pG_{20}N_{263}$, $pG_{20}N_{528}$ and $pG_{20}N_{705}$ were then grafted to the poly(dopamine)-modified SiO_2 surfaces. The substrates were placed in a solution of polymer and

triethylamine in DMSO at 80 °C overnight. Triethylamine was added to promote the nucleophilic epoxide ring opening reaction in the poly(glycidyl methacrylate) block.[55,58] XPS wide scan analysis of the block copolymer-functionalized substrates revealed a relative increase in nitrogen content, caused by the amide groups present in the NIPAM structure (Figure 3.1A and Supporting Information). Additionally, the decrease of the silicon signal indicates an increase in layer thickness. The nitrogen narrow scan spectrum showed a peak at 399.0 eV (Figure 3.1B), characteristic for the amide functionality present in poly(NIPAM).[67] Dry film thicknesses of the block copolymer-modified surfaces were determined using ellipsometry after extensive drying under nitrogen flow (Figure 3.2 and Table 3.2). The obtained values of 5.9 ± 1.1, 5.0 ± 1.0 and 6.3 ± 0.3 nm for grafted $pG_{20}N_{263}$, $pG_{20}N_{528}$ and $pG_{20}N_{705}$, respectively, show that comparable layer thicknesses were achieved for all three polymer lengths. This result indicates that the dry thickness, and thus added polymer content, does not depend on the size of the three grafted polymers, since comparable values were found for all three polymer sizes. Similar observations have been made previously for grafting-to procedures performed from solution, for which the grafted polymer thickness was roughly the same for grafting-to performed with different polymer chain lengths.[68–70]

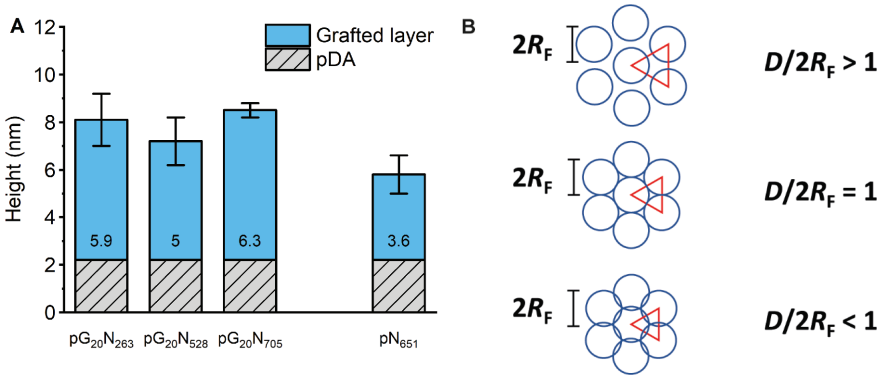

Figure 3.2 (A) Dry layer thickness (in nm) of the polymer-modified surfaces as determined by ellipsometry. Value inside the blue bar represents the dry layer thickness of the second poly(NIPAM) block. Data are shown with a ± SD (n = 6). **(B)** Top view of the polymer's Flory radius (R_F) and its relation to inter-chain distance (D). The sides of the red triangles have lengths D.

As a control experiment, to verify the advantage of including a poly(GMA) segment, a COOH-terminated $poly(NIPAM)_{651}$ (pN_{651}) homopolymer was immobilized on the

surface via the same procedure. Analysis of the grafted pN_{651} layer using ellipsometry showed a thickness increase of 3.6 ± 0.8 nm. This is not only significantly lower than the thicknesses achieved for the block copolymers (Figure 3.2A, Table 3.2), but in contrast to the covalently bound polymer brushes also does not survive a series of simple washing steps (see Supporting Information). This result indeed confirmed that incorporation of the poly(GMA) segment in the block copolymers is advantageous during attachment of the polymers.

3.2.4 Grafting density and brush regime

Calculation of the grafting density, σ, was performed based on the description provided by Alexander-de Gennes' theory, taking into account the polymer length, dry layer thickness and polymer bulk density (see Supporting Information for details).[71] The highest number of polymer chains per nm² was found for $pG_{20}N_{263}$, followed by $pG_{20}N_{528}$ and lastly $pG_{20}N_{705}$. The Flory radius, R_F, which describes the effective size of the polymer brush coils was calculated for each of the block copolymers, based on the number of repeating units and the segment length of NIPAM, for both good (R_{F_Good}) and poor (R_{F_Bad}) solvent conditions (Table 3.2).[22,72–74] These conditions correspond to temperatures lower and higher than the LCST of the block copolymers, respectively.

Table 3.2 Characterization of polymer-modified substrates: Dry layer thickness, static water contact angles, grafting densities σ, inter-chain distance *D*, and interaction between grafted polymers based on their Flory radius for good ($D/2R_{F\_good}$) and bad ($D/2R_{F\_bad}$) solvent conditions. Data are shown with a ± SD ($n = 6$).

	Thickness (nm)	SWCA (°)	σ (nm^{-2})	*D* (nm)	$D/2R_{F\_good}$	$D/2R_{F\_bad}$
poly (dopamine)	2.2 ± 0.8	52 ± 7				
$pG_{20}N_{263}$	5.9 ± 1.1[a]	57 ± 2	0.12 ± 0.02	3.2 ± 0.4	0.18 ± 0.02	0.82 ± 0.1
$pG_{20}N_{528}$	5.0 ± 1.0[a]	60 ± 2	0.053 ± 0.010	4.9 ± 0.5	0.19 ± 0.02	1.00 ± 0.1
$pG_{20}N_{705}$	6.3 ± 0.3[a]	59 ± 2	0.051 ± 0.003	5.0 ± 0.1	0.16 ± 0.004	0.93 ± 0.02
pN_{651}	3.6 ± 0.8[a]	61 ± 2	0.032 ± 0.009	6.3 ± 0.7	0.22 ± 0.02	1.21 ± 0.1

[a] Thickness of grafted layer on top of the poly(dopamine) film.

To understand the extent to which the surface-tethered polymers interact with their neighboring chains, the relation between the polymers' Flory radius, R_F, and the inter-chain distance, *D*, was determined (see Supporting Information).[22,37,72] The $D/2R_F$ value was used to determine the conformational state of the grafted polymers (Table 3.2).[22,23,39,41,42,74,75] At

$D/2R_F > 1$, there is no overlap between the chains and the polymers reside in a mushroom regime with little interaction between the chains (Figure 3.2B). $D/2R_F = 1$ marks the point at which chain segments start to overlap and the polymers reside in the mushroom-to-brush regime. Grafted polymer films that possess $D/2R_F < 0.5$ are generally considered to be in the brush regime, where extensive overlap between the polymer segments forces the chains to stretch away from the surface.[39,76,77] The calculations in which good solvent conditions are assumed yield $D/2R_{F\_good} < 0.2$ for the three grafted block copolymers, indicating that the surface-grafted polymers interact with each other extensively and reside in the brush regime. The results obtained from these calculations confirm that the method employed here is able to achieve high grafting densities and layer thickness when compared to other grafting-to from solution procedures.[37] In fact, grafting densities that were reported for polymer brushes grafted from melt were achieved.[78,79]

The volume occupied by the polymers, and therefore the interaction between chains, decreases significantly when R_F values for poor solvent conditions are considered. In such an environment, the $D/2R_{F\_bad}$ values for the grafted block copolymers approach 1, which implies that the grafted block copolymers reside in the mushroom-to-brush regime.[39,76,77] In contrast, for the grafted COOH-terminated poly(NIPAM)$_{651}$, $D/2R_{F\_bad} > 1$, which implies that there is no more overlap between the polymer segments in bad solvent conditions and the polymers reside in a mushroom conformation.

3.2.5 Thermal response

Although the total mass of polymer material that is grafted to the poly(dopamine) layer is comparable for all of the three block copolymer-functionalized surfaces, the grafting densities and size of polymers differ greatly. This provides the opportunity to compare the thermoresponsive behavior of the three films as a function of grafting density and, indirectly, polymer molecular weight. To investigate this relation, QCM-D measurements were performed between 20 and 40 °C. SiO_2-coated QCM-D sensors were firstly modified with poly(dopamine) after which the block copolymers were grafted to the poly(dopamine)-modified sensors using the procedure described above. Additionally, reference experiments were performed using pristine SiO_2 QCM-D sensors as well as poly(dopamine)-modified SiO_2 QCM-D sensors. The measurements of the poly(dopamine)-modified SiO_2 sensors are essential as they allow the data acquired for the polymer-functionalized surfaces to be corrected for the influence of water density, water viscosity and the temperature-dependent behavior of poly(dopamine)-modified SiO_2 sensors.[41,80–82]

The QCM-D data show that the resonance frequencies of all sensors increase with increasing temperature (Figure 3.3A). The frequency changes for pristine SiO_2 and poly(dopamine)modified sensors are linear with temperature and arise mainly from the decreasing viscosity and density of water with temperature.[83]

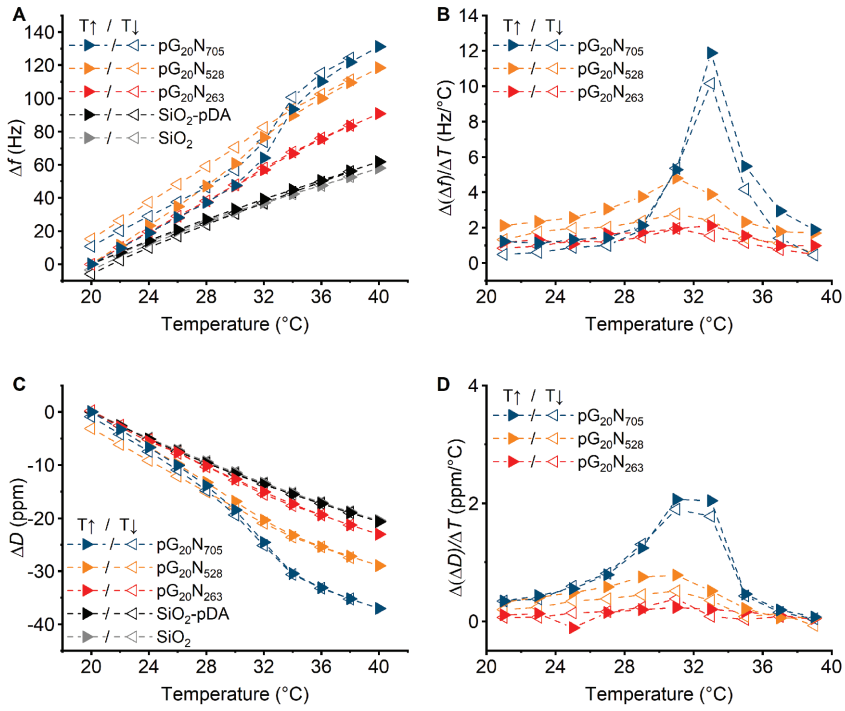

Figure 3.3 (A) Frequency shift, measured by QCM-D, as a function of temperature for pristine SiO_2 sensors, poly(dopamine)-modified SiO_2 sensors and polymer functionalized sensors. **(B)** The slope of the frequency shift, $\Delta(\Delta f)/\Delta T$, for the polymer-functionalized sensors after subtracting values for poly(dopamine)-modified SiO_2 sensors. **(C)** Dissipation shift, measured by QCM-D, as a function of temperature for pristine SiO_2 sensors, poly(dopamine)-modified SiO_2 sensors and polymer-functionalized sensors. **(D)** The slope of the dissipation shift $\Delta(\Delta D)/\Delta T$, for the polymer-functionalized sensors after subtracting values for poly(dopamine)-modified SiO_2 sensors . Note: The error bars for these plots were here omitted for clarity, but are displayed in the Supporting Information, ($n = 3$).

As opposed to the linear trend observed for the pristine SiO_2 and poly(dopamine)-modified SiO_2 sensors, the QCM-D data for the $pG_{20}N_{263}$-, $pG_{20}N_{528}$- and $pG_{20}N_{705}$-modified sensors displayed a clear nonlinear trend. The nonlinearity of the data is caused by the thermoresponsive character of the poly(NIPAM) segment of the polymers. With increas-

ing temperature, the LCST is crossed and the grafted polymers collapse. This conformational change is accompanied by the expulsion of solvent molecules that were initially coordinated to the polymer chains. The release of solvent molecules amounts to a decrease in mass of the polymer film and thus leads to an increase in the resonance frequency of the QCMD sensor.[81,84] This process is reversible, as witnessed by lowering the temperature from 40 to 20 °C, which induces rehydration and swelling of the polymers, and concomitant increase in mass and decrease of the resonance frequency.

The nonlinear trends were investigated in more detail by calculating the slopes for the frequency change, $\Delta(\Delta f)/\mathrm{D}T$, for each temperature step and correcting the data by subtracting the slopes determined for the poly(dopamine)-modified SiO_2 sensors (Figure 3.3B). The resulting plots show increased values between 26 °C and 38 °C with distinct maxima around 32 °C, the LCST of poly(NIPAM).[73] It is in this range that the collapse of the poly(NIPAM) polymers occurs and water molecules are driven out of the grafted layer. The data indicates that the collapse occurs gradually with increasing temperature, which agrees with previous reports,[85] and that the bulk of the transition occurs around 32 °C. The clear differences in peak heights visible in Figure 3.3B arise from varying amounts of water loss and uptake by the polymer-modified sensors.

The dissipation plots agree with these findings, as a marked decrease in dissipation is observed with increasing temperature, from 26 °C to 36 °C (Figure 3.3C and Figure 3.3D). Again, the transition is most distinct for the $pG_{20}N_{705}$-modified sensors, caused by higher dissipation for long chains and therefore a more pronounced difference between extended and collapsed state.

Table 3.3 Quantification of the dehydration for the grafted block copolymers upon increasing temperature from 20 °C to 40 °C using QCM-D. Data are shown with a ± SD (n = 3).

	$\Delta f_{20\text{-}40°C}$ (Hz)	Δm (H_2O) (ng/cm^2)	$\Delta N_{n/chain}$ (H_2O/chain)	$\Delta N_{n/monomer}$ (H_2O/monomer)
$pG_{20}N_{263}$	29.0 ± 12.1	–75 ± 31	–208 ± 87	–1.1 ± 0.5
$pG_{20}N_{528}$	56.6 ± 9.9	–146 ± 25	–921 ± 161	–4.9 ± 0.9
$pG_{20}N_{705}$	69.3 ± 14.9	–179 ± 38	–1174 ± 252	–6.3 ± 1.3

Since changes in resonance frequency are related to increases or decreases in mass on the sensor, it is possible to approximate the mass of solvent molecules lost upon polymer collapse (Table 3.3).[41,80] Using the Sauerbrey equation, the absolute frequency change measured between 20 °C and 40 °C, $\Delta f_{20\text{-}40°C}$, can be translated into the mass

lost within that temperature range (Δm (H_2O)).[86] From these calculations, it followed that the $pG_{20}N_{705}$-modified sensors expulse the largest amount of water followed by the $pG_{20}N_{528}$-modified sensors. The amount of water lost from the more densely grafted $pG_{20}N_{263}$ is significantly lower. Since the grafting densities of the coated surfaces are known, the amount of lost water that was coordinated per chain can then be determined ($\Delta N_{n/chain}$ (H_2O/chain)). It follows that the amount of water lost per chain is lowest for the shorter $pG_{20}N_{263}$ polymers and increases with polymer length. To make a more appropriate comparison between the grafted layers, the amount of water lost per monomer unit ($\Delta N_{n/monomer}$ (H_2O/monomer)) was calculated. It is then clear that the more densely grafted $pG_{20}N_{263}$ loses significantly less water per monomer unit than the larger polymers grafted at lower grafting densities, which corresponds to findings reported previously.[41] The larger loss of water for polymer coatings of lower grafting density can be explained by the larger amount of available space between the polymer chains for the solvent molecules to settle. Additionally, the data presented here implies that, for the same absolute amount of polymer (*i.e.*, in grams of material) attached to the surface, hydration occurs to a larger extent for grafted polymers of high molecular weight and low grafting density than for those of low molecular weight and high grafting density. Consideration of that correlation is highly valuable to obtain the desired surface properties when producing polymer coatings using grafting-to from solution. For example, the differences between the polymer coatings presented in this paper are expected to play a central role in their protein adhesive properties, as the hydration layer is considered a prominent prerequisite for antifouling polymer coatings.[7,9] This relation was investigated for the $pG_{20}N_{263}$, $pG_{20}N_{528}$ and $pG_{20}N_{705}$-modified surfaces.

3.2.6 Protein fouling studies

To assess the coatings' antifouling properties, polymer-modified SiO_2 QCM-D sensors were exposed to a flow of 10% human serum (0.25 µL min^{-1}) for 15 min. Control experiments were carried out using both poly(dopamine)-modified QCM-D sensors and pristine QCM-D sensors. The experiments were performed at 20 °C as well as at 40 °C, to analyze the effect of the thermoresponsive behavior on protein adsorption (Figure 3.4). For the untreated SiO_2-coated sensors, significant unspecific adsorption of human serum components was observed, reaching 832 ± 59 ng/cm^2 at 20 °C. Deposition of proteins on the poly(dopamine)-modified QCM-D sensors was 378 ± 159 ng/cm^2, a decrease of more than 50% when compared to the pristine SiO_2-coated sensors. The comparatively large variation in this data point is likely the result of the granular and rough surface morphology, typical for poly(dopamine) coatings.[87] During the fouling measurements

on the polymer-modified sensors at 20 °C, the surface-grafted polymers are solvated and stretch away from the surface, strongly reducing the adsorption protein, in line with literature.[21,88] The $pG_{20}N_{263}$ and $pG_{20}N_{528}$-modified surfaces inhibited unspecific adsorption to a comparable degree, binding 156 ± 19 ng/cm^2 and 209 ± 43 ng/cm^2, respectively. The $pG_{20}N_{705}$-modified surface outperformed both other polymer-modified surfaces in terms of antifouling behavior at 20 °C, with 30 ± 5 ng/cm^2 of bound protein measured. The lower adsorption may be due to the more extensive hydration per repeating unit for the longer polymer chains, as demonstrated using QCM-D (Table 3.3). The solvent molecules form a barrier that incoming proteins need to displace to make contact with the surface. The difference in the amount of coordinated water molecules for $pG_{20}N_{705}$ with respect to $pG_{20}N_{528}$, however, appears to be too small to be solely responsible for this difference in adsorption behavior. A second contributing factor may be the length of the $pG_{20}N_{705}$ polymers that stretch away from the poly(dopamine)-modified SiO_2 surface when the temperature is below the LCST. Longer chains provide a larger poly(NIPAM) barrier between the poly(dopamine)-modified SiO_2 and the protein solution. This explanation agrees with previous studies that have shown that a minimal film thickness is required to obtain optimal antifouling properties.[10,89,90] Following the strong antifouling results of $pG_{20}N_{705}$ against the protein adsorption, the $pG_{20}N_{705}$-modified surfaces were also subjected to undiluted human serum. At 20 °C, 128 ± 24 ng/cm^2 of protein was adsorbed from the undiluted human serum, comparable to the values found for $pG_{20}N_{263}$ and $pG_{20}N_{528}$-modified surfaces after exposure to 10% human serum.

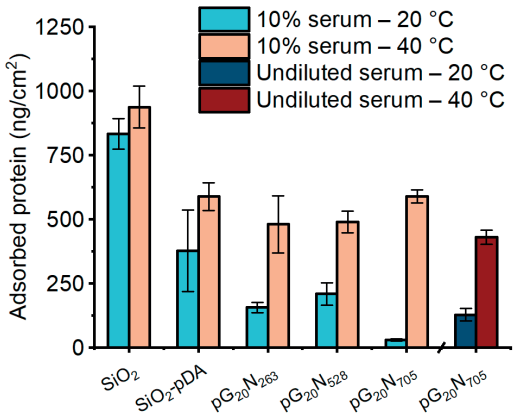

Figure 3.4 Adsorption of protein for pristine and polymer functionalized SiO_2-sensors after exposure to diluted human serum (10% in PBS) and undiluted human serum at 20 °C and 40 °C measured by QCM-D. Data are shown with a ± SD (*n* = 2).

The same experiments were performed at 40 °C to study the effect of the conformational change of the grafted polymers above their LCST on protein adsorption. Again, control experiments were performed for poly(dopamine)-modified QCM-D sensors and untreated SiO_2-coated QCM-D sensors. The amount of protein deposited on the untreated sensors at 40 °C, 937 ± 81 ng/cm^2, was similar to the fouling experiment at 20 °C. For the poly(dopamine)-modified sensors, more protein was deposited on the surface than at lower temperature, reaching 589 ± 54 ng/cm^2. The $pG_{20}N_{263}$, $pG_{20}N_{528}$ and $pG_{20}N_{705}$-modified surfaces now display a comparable degree of fouling when exposed to diluted human serum at 40 °C: 480 ± 111, 491 ± 43 and 590 ± 25 ng/cm^2, respectively. The similar amounts of protein adsorption –that was for each copolymer also at least 2.5 × higher than at 20 °C– can be attributed to the matching physical properties of the polymers in the collapsed state, where layer thickness corresponds to the dry layer thickness, and the monomer density is near-identical.[25] Practically, increasing the temperature above the LCST "switches off" the influence of grafting density or polymer chain length and yields near-identical amounts of protein adsorption.

The experiment performed with $pG_{20}N_{705}$-modified surfaces at 40 °C in the presence of undiluted human serum showed adsorption of 430 ± 24 ng/cm^2, which is in the same range as was found for the adsorption of diluted serum on the polymer modified surfaces at 40 °C. As was found for the diluted serum, a clear difference in adsorption of protein from undiluted human serum on the $pG_{20}N_{705}$-modified surfaces was observed for measurements performed at 20 °C and 40 °C. Comparison of all fouling experiments for the polymer-modified surfaces performed at 20 °C and 40 °C plainly illustrates the ability of these systems to switch between minimal protein adsorption at temperatures below the LCST and increased protein adsorption at temperature exceeding the LCST.

3.3 Conclusion

A straightforward and versatile two-step grafting-to approach for the immobilization of block copolymers featuring epoxide-containing poly(glycidyl methacrylate) (poly-GMA) on silicon oxide wafers was presented in this Chapter. First, SiO_2 surfaces were functionalized by amine-presenting polydopamine, which was followed by grafting poly(GMA)-*b*-poly(NIPAM) block copolymers of different lengths. High grafting densities, in the same range as have been reported for polymer brushes grafted from melt, were achieved. The amount of surface-attached polymer was independent of polymer length, which allowed comparison for thermoresponsive and antifouling character. It

was demonstrated that the highest molecular weight polymer under study, $pG_{20}N_{705}$, was hydrated most strongly and showed the most promising switching ability with respect to protein adsorption. This surface functionalization procedure shows great promise for applications in which commonly employed coating procedures, such as surface-initiated polymerizations, spin-coating or grafting from melt, are not applicable. Finally, the potential of this procedure in terms of modularity in surface type as well as final coating properties, invoked by the broad applicability of poly(dopamine) and the possibility to vary the polymer used for the longer chain segment of the block copolymers, respectively, is evident.

3.4 Materials and Methods

3.4.1 Materials

All chemical reagents were used without further purification unless otherwise specified. Triethylamine (TEA), 2,2′-azobis(2-methylpropionitrile) (AIBN) (98%), phosphate buffered-saline (PBS, pH 7.2 – 7.4), NaOAc (>99%), 1,4-dioxane (99.8%, anhydrous, non-stabilized) and human serum were purchased from Sigma-Aldrich. 4-Cyano-4-[(-dodecylsulfanylthiocarbonyl)sulfanyl]pentanoic acid (CDPA) (> 95.0%), dopamine.HCl (> 98.0%) and *N*isopropylacrylamide (NIPAM) (> 98.0%, stabilized) were purchased from TCI Chemicals Europe. Glycidyl methacrylate (GMA) (97%, stabilized) was purchased from Thermo Fisher Scientific. $NaIO_4$ (99%) was purchased from ACROS Organics. Deionized water was produced with Milli-Q Integral 3 system Millipore, Molsheim, France (Milli-Q water). Silicon single side-polished wafers (Si(100), N-type, phosphorus-doped) were obtained from Siltronix.

Prior to use, GMA was purified by washing with 0.1% m/v KOH solution and NIPAM was recrystallized from hexane.

3.4.2 RAFT polymerization of $pGMA_{20}$

To a 100 mL Schlenk flask were added AIBN (7.19 mg, 0.0438 mmol, 1 equiv.), CDPA (0.353 g, 0.88 mmol, 20 equiv.), GMA (3.6 mL, 27.6 mmol, 630 equiv.), and 1,4-dioxane (10 mL). The solution was degassed through three freeze-pump-thaw cycles. Following the last cycle, the flask was charged with argon. The flask was heated at 70 °C for 5.5 h, after which the flask was quenched in liquid nitrogen to deactivate the radical polymerization. To the solution was then added acetone (5 mL) and the product was precipitated in ice-cold diethyl ether, resulting in a pink paste. The paste was obtained via centrifugation,

redissolved in acetone (15 mL), and once again precipitated from ice-cold diethyl ether to remove the last remnants of monomer. The product, a fine yellow powder, was obtained through filtration. It was then dried over air (Yield: 1.32 g, 59%). **^{1}H NMR** (400 MHz, $CDCl_3$) δ 7.92 – 7.83 (d, 2H), 7.57 – 7.48 (t, 1H), 7.40 – 7.32 (t, 2H), 4.38 – 4.24 (m, 20H), 3.86 – 3.72 (dt, 20H), 3.26 – 3.19 (m, 21H), 2.87 – 2.79 (dt, 21H), 2.68 – 2.59 (tt, 21H), 2.17 – 1.72 (m, 37H), 1.11 – 1.07 (s, 19H), 0.94 – 0.90 (s, 26H).

3.4.3 Block copolymerization

To a 100 mL Schlenk flask was added AIBN (2.0 mg; 0.012 mmol; 0.1 equiv.), $pGMA_{20}$ (374 mg; 0.12 mmol; 1 equiv.), NIPAM (2.99 g; 26.5 mmol; 220 equiv.), and 1,4-dioxane (10 mL). The solution was deoxygenated by three freeze-pump-thaw cycles. After the last cycle, the flask was charged with argon. The flask was then heated at 70 °C and left to stir overnight. Subsequently, the solution was quenched in liquid nitrogen to deactivate the radical polymerization. To the reaction mixture was then added acetone (10-30 mL), after which the polymer was purified by precipitation from hexane twice. Analogously: For the $pG_{20}N_{528}$ polymer, the following reactants were used: AIBN (2.0 mg, 0.012 mmol, 0.1 equiv.), $pGMA_{20}$ (374 mg, 0.12 mmol, 1 equiv.) and NIPAM (5.98 g, 52.9 mmol, 440 equiv.) in 1,4 dioxane (10 mL). For $pG_{20}N_{705}$ polymer, the following reactants were used: AIBN (0.67 mg, 0.004 mmol, 0.2 equiv.), $pGMA_{20}$ (62.3 mg, 0.019 mmol, 1 equiv.), NIPAM (1.43 g, 22.1 mmol, 660 equiv.) in 1,4-dioxane (5 mL).

$pG_{20}N_{263}$: **^{1}H NMR** (400 MHz, $CDCl_3$) δ 4.30 (s), 4.01 (s), 3.82 (s), 3.23 (s), 2.84 (s), 2.64 (s), 2.09 (s), 1.67 (s), 1.14 (s). $pG_{20}N_{528}$: **^{1}H NMR** (400 MHz, $CDCl_3$) δ 4.29 (s), 4.00 (s), 3.84 (s), 3.23 (s), 2.84 (s), 2.64 (s), 1.63 (s), 1.14 (s). $pG_{20}N_{705}$: **^{1}H NMR** (400 MHz, $CDCl_3$) δ 6.49 (s, 1H), 3.93 (s, 1H), 2.07 (s, 1H), 1.74 (s, 0H), 1.57 (s, 1H), 1.07 (s, 6H).

3.4.4 RAFT homopolymerization of NIPAM

To a 100 mL Schlenk flask was added AIBN (2.0 mg, 0.012 mmol, 0.2 equiv.), CDPA (27 mg, 0.067 mmol, 1 equiv.), NIPAM (5.43 g, 48 mmol, 720 equiv.), and 1,4-dioxane (10 mL). The solution was deoxygenated by three freeze-pump-thaw cycles. After the last cycle, the flask was charged with argon. The flask was then heated at 70 °C and left to stir overnight. Subsequently, the solution was quenched in liquid nitrogen to deactivate the radical polymerization. To the reaction mixture was then added acetone (10-30 mL), after which the polymer was purified by precipitation from hexane twice.

Modification of SiO_2 substrates with poly(dopamine). 1 × 1 cm SiO_2 substrates were rinsed using acetone, ethanol and Milli-Q and then dried under a gentle stream of argon. The SiO_2 substrates were placed in a petri dish containing freshly prepared solution of

dopamine.HCl (50 mg, 0.26 mmol, 1 equiv.), $NaIO_4$ (81.2 mg, 0.38 mmol, 1.46 equiv.) in 60 mM NaOAc solution (20 mL). The petri dish was closed, sealed using parafilm and placed on an automated shaker at RT, 60 RPM, for 5 min. The surfaces were then removed from the solution, cleaned using Milli-Q and subsequently dried.

3.4.5 Grafting of polymers to poly(dopamine)-modified SiO_2 substrates

A stock solution of polymer (10 mg/mL) and TEA (0.16 g/mL) in DMSO was prepared. The stock solution was added to a reaction vial containing a poly(dopamine)-modified SiO_2 substrate. The vial was heated to 80 °C overnight, after which the surface was taken from the vial, cleaned using acetone, ethanol and water and subsequently dried.

3.4.6 Gel permeation chromatography (GPC)

The polymer molecular weight and polydispersity index (PDI) were determined using gel permeation chromatography (Agilent 1200 Organic GPC + refractive index detector, equipped with PLgel 5 μm MIXED-D column), The column was calibrated with a poly(methyl methacrylate) polymer set. The selected eluent was DMF + 0.1% LiBr, pumped at a constant flow of 0.5 mL/min.

3.4.7 Ellipsometry

Ellipsometric angles Δ and Ψ of the synthesized polymer brushes were measured using an EP4 imaging ellipsometer (Accurion, Germany). The measurements were performed in air at room temperature in the wavelength range of λ = 400.6 – 761.3 nm at an angle of incidence of 50°. The acquired Δ and Ψ were fitted in the EP4 modeling software using a multilayer model to obtain dry polymer brush thickness and refraction index values. The model consisted of a silicon (Si) bottom layer covered with a thin SiO_2 layer of 2.9 nm. The poly(dopamine) layer was described using a Cauchy model with parameters A = 1.70 and B = 3000. The organic layer for polymer-modified substrates was described using a Cauchy model with parameters A = 1.50 and B = 3000.

3.4.8 X-ray photoelectron spectroscopy

XPS measurements were performed as described in Chapter 2.

3.4.9 Static water contact angle measurements

Static water contact angle measurements were performed as described in Chapter 2.

3.4.10 Quartz-crystal microbalance with dissipation monitoring (QCM-D) measurements

Measurements were performed by using Q-Sense E4 QCM-D (Biolin Scientific, Sweden).

Prior to the temperature-dependent measurements, Milli-Q was pumped via a peristaltic pump (Ismatec high precision multichannel dispenser) with a flow rate of 400 µL/min for at least 15 min. The flow rate was then reduced to 25 µL/min. The temperature was set at 20 °C and the system was left to stabilize for 1 h. The temperature was then increased with steps of 2 °C with a rate of 1 °C/min, where each step was followed by a stabilization period of 1 h. After reaching 40 °C and stabilization of 1 h, the temperature was decreased with steps of 2 °C with a rate of 1 °C/min, where again each step was followed by a stabilization period of 1 h. The measurement was stopped following 1 h of stabilization after returning to 20 °C.

Before each fouling experiment, the buffer and protein solutions were bubbled with argon to eliminate dissolved oxygen, which may interfere with the experiment. The PBS buffer solution was pumped via a peristaltic pump (Ismatec high precision multichannel dispenser) with a flow rate of 400 µL/min for at least 15 min before each experiment. Fouling experiments were performed at a flow rate of 25 µL/min. Pristine SiO_2-coated sensors, poly(dopamine)-modified SiO_2 coated sensors and polymer-modified SiO_2 sensors were subjected to a 10% human serum in PBS solution or undiluted human serum for 15 min, after which the PBS buffer solution was pumped over the sensors again until the signal stabilized.

Frequency shifts (Δf) and dissipation shifts (ΔD) were acquired at the 3rd (15 MHz), 5th (25 MHz), 7th (35 MHz), 9th (45 MHz), and 11th (55 MHz) harmonic overtone. For data analysis, only the 5th (25 MHz) overtone was used for the fouling measurements and the 7th (35 MHz) overtone was used for the temperature-dependent measurements. QSoft software was used during data acquisition and DFind (version 1.2.7) for analysis of the data. The 'wet' mass (thickness) of the sensor surfaces after protein fouling was estimated from the decrease of the frequency of the quartz crystal with the Sauerbrey equation (1):[86]

$$\Delta m = -C \frac{\Delta f_n}{n} \tag{1}$$

In this equation, Δm is the areal mass density of the adsorbed foulant, Δf_n the frequency shift, C (17.7 ng/cm^2/Hz) the mass sensitivity constant for a 5 MHz quartz crystal, and n the harmonic number (3, 5, 7, 9 or 11).

3.4.11 Statistical analysis

All statistical results were calculated using Origin 2019 software. Data were displayed as average values ± standard deviation.

3.5 Acknowledgements

Sevil Şahin is acknowledged for assistance with the QCM-D measurements. This research was carried out under project number C16030a in the framework of the Partnership Program of the Materials innovation institute M2i (www.m2i.nl) and the NWO Domain Science, which is part of the Netherlands Organization for Scientific Research (www.nwo.nl).

3.6 Supporting Information

The supporting information is available from the Wiley Online Library:
https://doi.org/10.1002/admi.202201198

3.7 References

1. Zhou, J., Ellis, A. V. & Voelcker, N. H. Recent developments in PDMS surface modification for microfluidic devices. Electrophoresis 31, 2–16 (2010).
2. Yüce, M. & Kurt, H. How to make nanobiosensors: Surface modification and characterisation of nanomaterials for biosensing applications. RSC Adv. 7, 49386–49403 (2017).
3. Rana, D. & Matsuura, T. Surface modifications for antifouling membranes. Chem. Rev. 110, 2448–2471 (2010).
4. Ferreira, P., Alves, P., Coimbra, P. & Gil, M. H. Improving polymeric surfaces for biomedical applications: a review. J. Coatings Technol. Res. 12, 463–475 (2015).
5. Banerjee, I., Pangule, R. C. & Kane, R. S. Antifouling coatings: Recent developments in the design of surfaces that prevent fouling by proteins, bacteria, and marine organisms. Adv. Mater. 23, 690–718 (2011).
6. Sun, T. & Qing, G. Biomimetic smart interface materials for biological applications. Adv. Mater. 23, 57–77 (2011).
7. Wei, Q. et al. Protein interactions with polymer coatings and biomaterials. Angew. Chemie - Int. Ed. 53, 8004–8031 (2014).
8. Maan, A. M. C., Hofman, A. H., de Vos, W. M. & Kamperman, M. Recent Developments and Practical Feasibility of Polymer-Based Antifouling Coatings. *Adv. Funct. Mater.* **30**, 2000936 (2020).
9. Chen, S., Li, L., Zhao, C. & Zheng, J. Surface hydration: Principles and applications toward low-fouling/nonfouling biomaterials. *Polymer (Guildf).* **51**, 5283–5293 (2010).
10. Rodriguez-Emmenegger, C. *et al.* Polymer brushes showing non-fouling in blood plasma challenge the currently accepted design of protein resistant surfaces. *Macromol. Rapid Commun.* **32**, 952–957 (2011).
11. Kuzmyn, A. R., Nguyen, A. T., Teunissen, L. W., Zuilhof, H. & Baggerman, J. Antifouling Polymer Brushes via Oxygen-Tolerant Surface-Initiated PET-RAFT. *Langmuir* **36**, 4439–4446 (2020).
12. Kuzmyn, A. R. *et al.* Diblock and Random Antifouling Bioactive Polymer Brushes on Gold Surfaces by Visible-Light-Induced Polymerization (SI-PET-RAFT) in Water. *Adv. Mater. Interfaces* **9**, (2022).
13. Buck, E., Lee, S., Stone, L. S. & Cerruti, M. Protein Adsorption on Surfaces Functionalized with COOH Groups Promotes Anti-inflammatory Macrophage Responses. *ACS Appl. Mater. Interfaces* **13**, 7021–7036 (2021).
14. Takasu, K. *et al.* Polymer brush biointerfaces for highly sensitive biosensors that preserve the structure and function of immobilized proteins. *Sensors Actuators, B Chem.* **216**, 428–433 (2015).
15. Hou, J., Shi, Q., Ye, W., Stagnaro, P. & Yin, J. Micropatterning of hydrophilic polyacrylamide brushes to resist cell adhesion but promote protein retention. *Chem. Commun.* **50**, 14975–14978 (2014).
16. Kim, Y.-J. & Matsunaga, Y. T. Thermo-responsive polymers and their application as smart biomaterials. *J. Mater. Chem. B* **5**, 4307–4321 (2017).
17. Mendes, P. M. Stimuli-responsive surfaces for bio-applications. *Chem. Soc. Rev.* **37**, 2512 (2008).
18. Murdoch, T. J., Humphreys, B. A., Johnson, E. C., Webber, G. B. & Wanless, E. J. Specific ion effects on thermoresponsive polymer brushes: Comparison to other architectures. *J. Colloid Interface Sci.* **526**, 429–450 (2018).

19. Ward, M. A. & Georgiou, T. K. Thermoresponsive polymers for biomedical applications. *Polymers (Basel).* **3**, 1215–1242 (2011).

20. Psarra, E. *et al.* Nanostructured Biointerfaces: Nanoarchitectonics of Thermoresponsive Polymer Brushes Impact Protein Adsorption and Cell Adhesion. *ACS Appl. Mater. Interfaces* **7**, 12516–12529 (2015).

21. Burkert, S. *et al.* Protein Resistance of PNIPAAm Brushes: Application to Switchable Protein Adsorption. *Langmuir* **26**, 1786–1795 (2010).

22. Xue, C., Choi, B. C., Choi, S., Braun, P. V. & Leckband, D. E. Protein adsorption modes determine reversible cell attachment on poly(N-isopropyl acrylamide) brushes. *Adv. Funct. Mater.* **22**, 2394–2401 (2012).

23. Xue, C. *et al.* Protein adsorption on poly(N -isopropylacrylamide) brushes: Dependence on grafting density and chain collapse. *Langmuir* **27**, 8810–8818 (2011).

24. Nagase, K., Okano, T. & Kanazawa, H. Poly(N-isopropylacrylamide) based thermoresponsive polymer brushes for bioseparation, cellular tissue fabrication, and nano actuators. *Nano-Structures & Nano-Objects* **16**, 9–23 (2018).

25. Halperin, A. & Kröger, M. Collapse of thermoresponsive brushes and the tuning of protein adsorption. *Macromolecules* **44**, 6986–7005 (2011).

26. Frost, S. & Ulbricht, M. Thermoresponsive ultrafiltration membranes for the switchable permeation and fractionation of nanoparticles. *J. Memb. Sci.* **448**, 1–11 (2013).

27. Chu, L. Y., Niitsuma, T., Yamaguchi, T. & Nakao, S. ichi. Thermoresponsive transport through porous membranes with grafted PNIPAM gates. *AIChE J.* **49**, 896–909 (2003).

28. Yang, M. *et al.* A thermoresponsive membrane for chiral resolution. *Adv. Funct. Mater.* **18**, 652–663 (2008).

29. Wang, X. *et al.* Temperature-Responsive Hierarchical Polymer Brushes Switching from Bactericidal to Cell Repellency. *ACS Appl. Mater. Interfaces* **9**, 40930–40939 (2017).

30. Annaka, M., Yahiro, C., Nagase, K., Kikuchi, A. & Okano, T. Real-time observation of coil-to-globule transition in thermosensitive poly(N-isopropylacrylamide) brushes by quartz crystal microbalance. *Polymer (Guildf).* **48**, 5713–5720 (2007).

31. Nagase, K., Watanabe, M., Kikuchi, A., Yamato, M. & Okano, T. Thermo-Responsive Polymer Brushes as Intelligent Biointerfaces: Preparation via ATRP and Characterization. *Macromol. Biosci.* **11**, 400–409 (2011).

32. Zoppe, J. O. *et al.* Surface-Initiated Controlled Radical Polymerization: State-of-the-Art, Opportunities, and Challenges in Surface and Interface Engineering with Polymer Brushes. *Chem. Rev.* **117**, 1105–1318 (2017).

33. Chen, W. L., Cordero, R., Tran, H. & Ober, C. K. 50th Anniversary Perspective: Polymer Brushes: Novel Surfaces for Future Materials. *Macromolecules* **50**, 4089–4113 (2017).

34. Patil, R. R., Turgman-Cohen, S., Šrogl, J., Kiserow, D. & Genzer, J. On-Demand Degrafting and the Study of Molecular Weight and Grafting Density of Poly(methyl methacrylate) Brushes on Flat Silica Substrates. *Langmuir* **31**, 2372–2381 (2015).

35. Patil, R. R., Turgman-Cohen, S., Šrogl, J., Kiserow, D. & Genzer, J. Direct measurement of molecular weight and grafting density by controlled and quantitative degrafting of surface-anchored poly(methyl methacrylate). *ACS Macro Lett.* **4**, 251–254 (2015).

36. Michalek, L., Mundsinger, K., Barner-Kowollik, C. & Barner, L. The long and the short of polymer grafting. *Polym. Chem.* **10**, 54–59 (2019).

37. Michalek, L., Barner, L. & Barner-Kowollik, C. Polymer on Top: Current Limits and Future Perspectives of Quantitatively Evaluating Surface Grafting. *Adv. Mater.* **30**, 1706321 (2018).

38. Pop-Georgievski, O. *et al.* Nonfouling poly(ethylene oxide) layers end-tethered to polydopamine. *Langmuir* **28**, 14273–14283 (2012).

39. Dalsin, J. L. *et al.* Protein resistance of titanium oxide surfaces modified by biologically inspired mPEG-DOPA. *Langmuir* **21**, 640–646 (2005).

40. Emilsson, G. *et al.* Strongly stretched protein resistant poly(ethylene glycol) brushes prepared by grafting-to. *ACS Appl. Mater. Interfaces* **7**, 7505–7515 (2015).

41. Schweigerdt, A., Heinen, S., Stöbener, D. D. & Weinhart, M. Grafting Density-Dependent Phase Transition Mechanism of Thermoresponsive Poly(glycidyl ether) Brushes: A Comprehensive QCM-D Study. *Langmuir* **37**, 7087–7096 (2021).

42. Heinen, S. & Weinhart, M. Poly(glycidyl ether)-Based Monolayers on Gold Surfaces: Control of Grafting Density and Chain Conformation by Grafting Procedure, Surface Anchor, and Molecular Weight. *Langmuir* **33**, 2076–2086 (2017).

43. Jones, R. A. L., Lehnert, R. J., Schönherr, H. & Vancso, J. Factors affecting the preparation of permanently end-grafted polystyrene layers. *Polymer (Guildf).* **40**, 525–530 (1999).

44. Luzinov, I., Julthongpiput, D., Malz, H., Pionteck, J. & Tsukruk, V. V. Polystyrene layers grafted to epoxy-modified silicon surfaces. *Macromolecules* **33**, 1043–1048 (2000).

45. Iyer, K. S. & Luzinov, I. Effect of macromolecular anchoring layer thickness and molecular weight on polymer grafting. *Macromolecules* **37**, 9538–9545 (2004).

46. Minko, S. *et al.* Synthesis of adaptive polymer brushes via 'grafting to' approach from melt. *Langmuir* **18**, 289–296 (2002).

47. Kim, M., Schmitt, S., Choi, J., Krutty, J. & Gopalan, P. From Self-Assembled Monolayers to Coatings: Advances in the Synthesis and Nanobio Applications of Polymer Brushes. *Polymers (Basel).* **7**, 1346–1378 (2015).

48. Widin, J. M. *et al.* Bulk and thin film morphological behavior of broad dispersity poly(styrene-b-methyl methacrylate) diblock copolymers. *Macromolecules* **46**, 4472–4480 (2013).

49. Gundberg, C. M., Clough, M. E. & Carpenter, T. O. Development and validation of a radioimmunoassay for mouse osteocalcin: paradoxical response in the Hyp mouse. *Endocrinology* **130**, 1909–15 (1992).

50. Pujari, S. P., Scheres, L., Marcelis, A. T. M. & Zuilhof, H. Covalent surface modification of oxide surfaces. *Angew. Chemie - Int. Ed.* **53**, 6322–6356 (2014).

51. Liebscher, J. *et al.* Structure of polydopamine: A never-ending story? *Langmuir* **29**, 10539–10548 (2013).

52. Hong, S. *et al.* Non-covalent self-assembly and covalent polymerization co-contribute to polydopamine formation. *Adv. Funct. Mater.* **22**, 4711–4717 (2012).

53. Lee, H., Dellatore, S. M., Miller, W. M. & Messersmith, P. B. Mussel-Inspired Surface Chemistry for Multifunctional Coatings. *Science (80-.).* **318**, 426–430 (2007).

54. Dreyer, D. R., Miller, D. J., Freeman, B. D., Paul, D. R. & Bielawski, C. W. Perspectives on poly(dopamine). *Chem. Sci.* **4**, 3796–3802 (2013).

55. Benaglia, M., Alberti, A., Giorgini, L., Magnoni, F. & Tozzi, S. Poly(glycidyl methacrylate): A highly versatile polymeric building block for post-polymerization modifications. *Polym. Chem.* **4**, 124–132 (2013).

56. Fowler, P. M. P. T. *et al.* Surface Zwitterionization of Expanded Poly(tetrafluoroethylene) via Dopamine-Assisted Consecutive Immersion Coating. *ACS Appl. Mater. Interfaces* **12**, 41000–41010 (2020).

57. Barbey, R., Laporte, V., Alnabulsi, S. & Klok, H. A. Postpolymerization modification of poly(glycidyl methacrylate) brushes: An XPS depth-profiling study. *Macromolecules* **46**, 6151–6158 (2013).

58. Mao, S., Zhang, D., Zhang, Y., Yang, J. & Zheng, J. A Universal Coating Strategy for Controllable Functionalized Polymer Surfaces. *Adv. Funct. Mater.* **30**, 2004633 (2020).

59. Gadwal, I. & Khan, A. Protecting-group-free synthesis of chain-end multifunctional polymers by combining ATRP with thiol-epoxy 'click' chemistry. *Polym. Chem.* **4**, 2440–2444 (2013).

60. Muzammil, E. M., Khan, A. & Stuparu, M. C. Post-polymerization modification reactions of poly(glycidyl methacrylate)s. *RSC Adv.* **7**, 55874–55884 (2017).

61. Höhne, S. & Uhlmann, P. Synthesis of functional block copolymers and terpolymers containing polyglycidyl methacrylate blocks. *J. Polym. Sci. Part A Polym. Chem.* **53**, 675–684 (2015).

62. Gudipati, C. S. *et al.* Synthesis of poly(glycidyl methacrylate)-block-poly(pentafluorostyrene) by RAFT: Precursor to novel amphiphilic poly(glyceryl methacrylate)-block- poly(pentafluorostyrene). *Macromol. Rapid Commun.* **29**, 1902–1907 (2008).

63. Ponzio, F. *et al.* Oxidant Control of Polydopamine Surface Chemistry in Acids: A Mechanism-Based Entry to Superhydrophilic-Superoleophobic Coatings. *Chem. Mater.* **28**, 4697–4705 (2016).

64. Zhang, W. *et al.* Fast coating of hydrophobic upconversion nanoparticles by NaIO4-induced polymerization of dopamine: Positively charged surfaces and in situ deposition of Au nanoparticles. *Appl. Surf. Sci.* **527**, 146821 (2020).

65. Xuan, Y., Jiang, G., Li, Y., Wang, J. & Geng, H. Inhibiting effect of dopamine adsorption and polymerization on hydrated swelling of montmorillonite. *Colloids Surfaces A Physicochem. Eng. Asp.* **422**, 50–60 (2013).

66. Ding, Y. *et al.* Insights into the Aggregation/Deposition and Structure of a Polydopamine Film. *Langmuir* **30**, 12258–12269 (2014).

67. Alem, H. *et al.* Microstructure and thermo-responsive behavior of poly(N-isopropylacrylamide) brushes grafted in nanopores of track-etched membranes. *J. Memb. Sci.* **308**, 75–86 (2008).

68. Hansson, S. *et al.* Grafting efficiency of synthetic polymers onto biomaterials: A comparative study of grafting- from versus grafting- to. *Biomacromolecules* **14**, 64–74 (2013).

69. Huang, H. & Penn, L. S. Dense tethered layers by the 'grafting-to' approach. *Macromolecules* **38**, 4837–4843 (2005).

70. Jin, J. *et al.* Effect of grafted PEG chain conformation on albumin and lysozyme adsorption: A combined study using QCM-D and DPI. *Colloids Surfaces B Biointerfaces* **136**, 838–844 (2015).

71. de Gennes, P. G. Introduction to Probability Models. *J. Polym. Sci., Polym. Symp* **13**, 1821 (1980).

72. Israelachvili, J. N. *Steric (Polymer-Mediated) and Thermal Fluctuation Forces*. *Intermolecular and Surface Forces* (2011). doi:10.1016/b978-0-12-375182-9.10016-8

73. Kubota, K., Shouei, F. & Ando, I. Solution properties of poly(n-isopropylacrylamide) in water. *Polym. J.* **22**, 15–20 (1990).

74. Plunkett, K. N., Zhu, X., Moore, J. S. & Leckband, D. E. PNIPAM Chain Collapse Depends on the Molecular Weight and Grafting Density. *Langmuir* **22**, 4259–4266 (2006).

75. Zhu, X., Yan, C., Winnik, F. M. & Leckband, D. End-grafted low-molecular-weight PNIPAM does not collapse above the LCST. *Langmuir* **23**, 162–169 (2007).

76. Pasche, S., De Paul, S. M., Vörös, J., Spencer, N. D. & Textor, M. Poly(l-lysine)-graft-poly(ethylene glycol) Assembled Monolayers on Niobium Oxide Surfaces: A Quantitative Study of the Influence of Polymer Interfacial Architecture on Resistance to Protein Adsorption by ToF-SIMS and in Situ OWLS. *Langmuir* **19**, 9216–9225 (2003).

77. Sofia, S. J., Premnath, V. & Merrill, E. W. Poly(ethylene oxide) grafted to silicon surfaces: Grafting density and protein adsorption. *Macromolecules* **31**, 5059–5070 (1998).

78. Kumar Vyas, M., Schneider, K., Nandan, B. & Stamm, M. Switching of friction by binary polymer brushes. *Soft Matter* **4**, 1024–1032 (2008).

79. Minko, S. *et al.* Bidisperse mixed brushes: Synthesis and study of segregation in selective solvent. *Macromolecules* **36**, 7268–7279 (2003).

80. Adam, S. *et al.* Quartz crystal microbalance with coupled spectroscopic ellipsometry-study of temperature-responsive polymer brush systems. *Appl. Surf. Sci.* **421**, 843–851 (2017).

81. Liu, G. & Zhang, G. Collapse and Swelling of Thermally Sensitive Poly (N-isopropylacrylamide) Brushes Monitored with a Quartz Crystal Microbalance. *J. Phys. Chem. B* **109**, 743–747 (2005).

82. Plunkett, M. A., Wang, Z., Rutland, M. W. & Johannsmann, D. Adsorption of pNIPAM layers on hydrophobic gold surfaces, measured in situ by QCM and SPR. *Langmuir* **19**, 6837–6844 (2003).

83. Laloyaux, X., Mathy, B., Nysten, B. & Jonas, A. M. Bidimensional Response Maps of Adaptive Thermo-and pH-Responsive Polymer Brushes. *Macromolecules* **43**, 7744–7751 (2010).

84. Laloyaux, X., Mathy, B., Nysten, B. & Jonas, A. M. Surface and Bulk Collapse Transitions of Thermoresponsive Polymer Brushes. *Langmuir* **26**, 838–847 (2010).

85. Ishida, N. & Biggs, S. Effect of grafting density on phase transition behavior for poly(N-isopropylacryamide) brushes in aqueous solutions studied by AFM and QCM-D. *Macromolecules* **43**, 7269–7276 (2010).

86. Sauerbrey, G. *Verwendung von Schwingquarzen zur Wägung dünner Schichten und zur Mikrowägung*. *Zeitschrift für Physik* **55**, (1959).

87. Qie, R., Zajforoushan Moghaddam, S. & Thormann, E. Parameterization of the optical constants of polydopamine films for spectroscopic ellipsometry studies. *Phys. Chem. Chem. Phys.* **23**, 5516–5526 (2021).

88. Yu, Q. *et al.* Protein adsorption on poly(N-isopropylacrylamide)-modified silicon surfaces: Effects of grafted layer thickness and protein size. *Colloids Surfaces B Biointerfaces* **76**, 468–474 (2010).

89. Rodriguez-Emmenegger, C. *et al.* Substrate-independent approach for the generation of functional protein resistant surfaces. *Biomacromolecules* **12**, 1058–1066 (2011).

90. Zhao, C., Li, L., Wang, Q., Yu, Q. & Zheng, J. Effect of film thickness on the antifouling performance of poly(hydroxy-functional methacrylates) grafted surfaces. *Langmuir* **27**, 4906–4913 (2011).

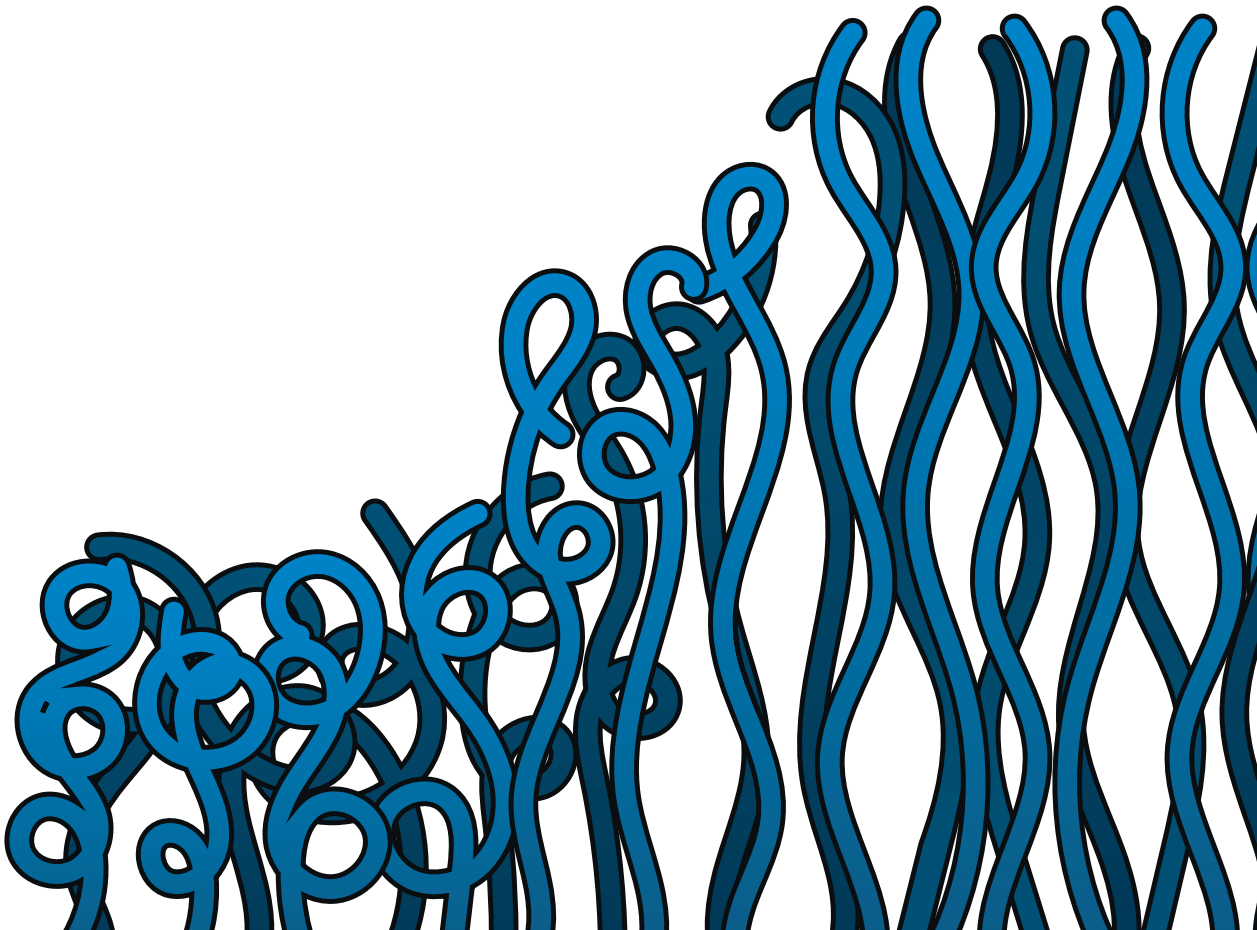

Chapter 4

Optimization of Poly(dopamine) Deposition for Grafting-To Polymer Brush Synthesis

Teunissen, L. W., Smulders, M. M. J. & Zuilhof, H.
19 nm-Thick Grafted-To Polymer Brushes onto Optimized Poly(Dopamine)-Coated Surfaces
Adv. Mater. Interfaces, Manuscript Accepted (2023).

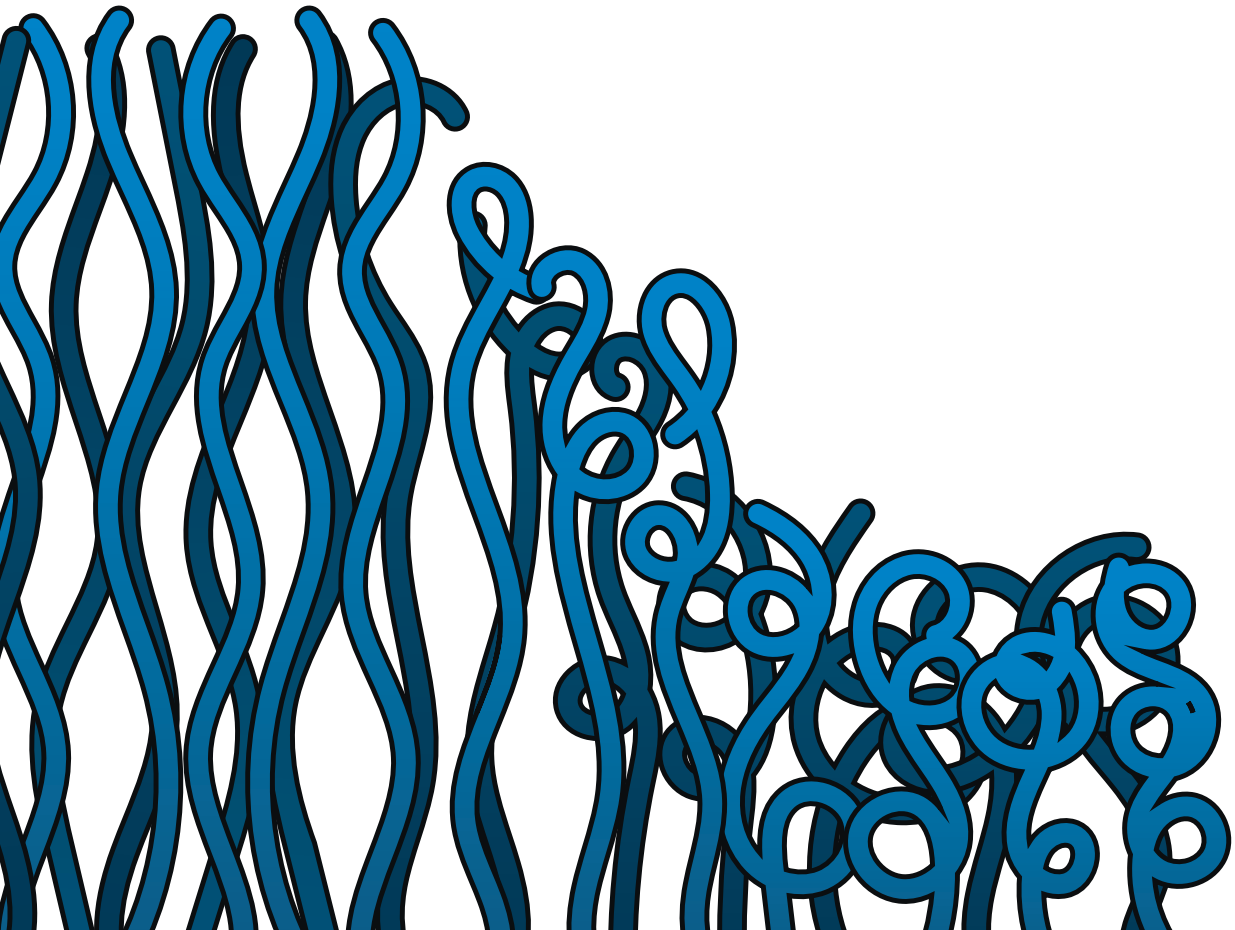

Abstract

Grafting-to polymer coatings are typically easy to apply, but the thickness of such coatings is generally limited to a few nanometers, which might hamper applications. This Chapter presents a grafting-to coating approach that yielded polymer brushes up to an unprecedented thickness of 19 nm. To this aim, we optimized an easy-to-apply poly(dopamine) primer layer. Poly(dopamine) is a readily attainable, but highly complex and chemically not well understood primer layer. In this study, poly(dopamine) was deposited on silicon substrates using several deposition protocols (pH 4–7 in presence of $NaIO_4$, and from Tris solution at pH 8.5). The modified surfaces were characterized using XPS, spectroscopic ellipsometry, static water contact angle measurements and AFM. Subsequently, block copolymers of poly(glycidyl methacrylate)$_{20}$-*b*-poly(*N*-isopropylacrylamide)$_n$ were attached onto the poly(dopamine) films using a grafting-to approach. The results indicated that the conditions of poly(dopamine) deposition and the poly(dopamine) film thickness strongly influenced the stability and grafting efficiency of the block copolymers. Poly(dopamine) films deposited at pH 7 with $NaIO_4$ were stable, and yielded the most efficient grafting, with grafted polymer layers as thick as 19 nm. Polymer layers of such thickness are rarely achieved using grafting-to procedures from solution.

4.1 Introduction

To produce sophisticated devices such as biosensors,[1] purification systems[2] and antimicrobial coatings,[3] it is essential to carefully consider the interactions of the device's interfaces with the complex media it is subjected to. The type of interactions and their extent can be effectively controlled by modification of the surface using polymer chains. Polymer brush coatings, in particular, can be employed to introduce specific surface properties with great accuracy due to extensive control over variables such as brush thickness, grafting density, polymer architecture and functional groups.[4–6] Polymer brush coatings have therefore been used to equip surfaces with, e.g., antifouling,[7–14] lubricating,[15] and/or (thermo)responsive properties.[16]

Polymer brushes are most commonly synthesized by a grafting-from procedure, in which the chains are grown bottom-up from surface-bound initiators.[17,18] This approach is primarily selected because high grafting densities and brush thicknesses can be readily achieved. Additionally, the advent of surface-initiated, controlled polymerization techniques that allow for both the presence of water and oxygen has greatly expanded the potential of grafting-from approaches.[10,19–22] However, polymer brushes obtained via surface-initiated polymerization are difficult to characterize, and detailed analysis would optimally involve degrafting of the polymer chains. Degrafting reactions typically require harsh conditions that may damage the polymers and, in addition, large surface areas are needed to obtain sufficient amounts of detached polymer for detailed analysis.[23,24]

The primary alternative synthesis route towards polymer brushes is the grafting-to approach.[25] This strategy involves the synthesis of desired polymers in solution followed by their attachment to the target substrate. In contrast with surface-grown polymers, characterization of solution-grown polymers can be easily performed using straightforward analysis techniques. As a result, valuable information such as polymer molecular weight, polydispersity and, after immobilization, the grafting density of the polymer brush can be routinely determined. The major disadvantage to the grafting-to strategy is the inherent limitation in attainable layer thicknesses, which generally do not exceed 10 nm.[26] That limitation is at least partially the result of the excluded volume of each polymer chain on the surface, which hinders subsequent, incoming polymers to reach reactive sites on the surface. This thickness limitation might hamper several applications, such as optimal antifouling and self-healing options, and as such is a highly desirable hurdle to tackle. Grafting from melt,[27–34] or cloud-point grafting,[35–40] can partially overcome these limitations, but these procedures typically require highly specific reaction conditions.

Aside from selecting the most optimal grafting conditions, the means of binding the polymer to the substrate requires careful consideration during the development of a grafting-to procedure. One of the prerequisites for achieving stable and dense polymer coatings is the ability of the polymer chains to efficiently and permanently bind to reactive sites on the surface. These reactive sites are often introduced by modification of the target substrate with a primer layer.[25] A modification agent with high potential is poly(dopamine), mainly due to its ease of use, applicability on virtually any surface type and low cost.[41,42] Modification of a target substrate with poly(dopamine) introduces functional groups to the surface, such as amine and hydroxyl moieties, which can then be employed for further modification.

The chemical structure of poly(dopamine) has been the subject of many studies and is notoriously complex.[43–47] Despite extensive analysis using a range of different techniques, the exact structure of the highly cross-linked material as well as a complete understanding of the preceding polymerization mechanism remain elusive.[43,45–49] To add to the complexity, it has been demonstrated that the chemical structure and morphological features of a poly(dopamine) film are influenced by both the type of substrate and the deposition conditions.[49–53] These properties can be expected to strongly influence the reactivity of the poly(dopamine) towards any subsequent modification steps. Evidently, insight in these factors is of great value for any procedure that involves modification of poly(dopamine) films.

One of the most commonly employed procedures for the synthesis of poly(dopamine) layers relies on polymerization induced by oxidation of dopamine in a basic Tris buffer.[41,42,54] For this procedure, control over thickness and roughness of the resulting film can be obtained by variation of deposition time and dopamine concentration.[55] Alternatively, the polymerization can be initiated by oxidizing agents, such as $CuSO_4$, $CuSO_4$/H_2O_2,[56] $(NH_4)_2S_2O_8$,[57] or $NaIO_4$.[50] Specifically, using $NaIO_4$ as oxidant can significantly speed up the deposition process, and yields low-roughness, highly hydrophilic surfaces.[50,58,59]

In Chapter 3, we introduced a highly efficient grafting-to procedure to synthesize polymer brushes based on attachment of poly(glycidyl methacrylate)-*b*-poly(*N*-isopropylacrylamide) (poly(GMA)-*b*-poly(NIPAM)) block copolymers to poly(dopamine)-modified silicon surfaces.[60] The grafting densities that could be achieved using this procedure were relatively high for grafting-to procedures from solution (up to 0.12 chains/nm^2). It is therefore of interest to investigate the potential of this procedure in more detail, explicitly scrutinizing the chemical and topological properties of the poly(dopamine) primer layer, and the effects those have on follow-up grafting-to polymer coating.

In this Chapter, we aim to investigate three facets: 1) to which degree do the properties of the underlying poly(dopamine) layer vary in response to the deposition conditions, and 2) to which degree do the properties (thickness, density, stability) vary of a grafted-to polymer coating that is deposited onto this poly(dopamine) layer, in dependence on such variations in the poly(dopamine) layer; 3) how thick can we make grafted-to polymer brushes in attempts to overcome the 10 nm-thickness limitation. To this aim, a simple two-step modification procedure (Scheme 4.1) was followed: silicon surfaces were coated with poly(dopamine) by deposition from Tris buffer (pH 8.5) or acetate buffer (pH 4 and 7), in the presence of $NaIO_4$. Next, three poly(GMA)$_{20}$-*b*-poly(NIPAM)$_n$ block copolymers were grafted to the thus obtained set of poly(dopamine)-coated substrates. The influence of the poly(dopamine) deposition conditions on the block copolymer grafting step was studied thoroughly, using X-ray photoelectron spectroscopy (XPS), spectroscopic ellipsometry, static water contact angle measurements and atomic force microscopy (AFM), and pointed to the exceptional efficacy of this grafting-to coating method.

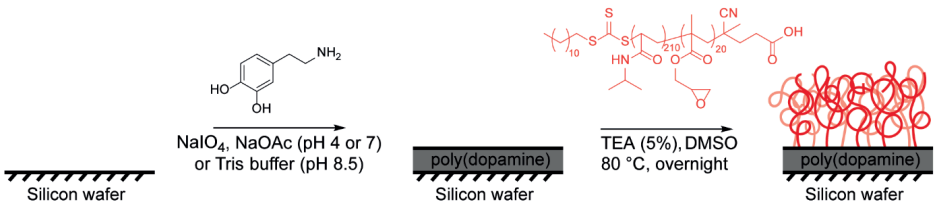

Scheme 4.1 Schematic representation of the silicon surface modification procedure employed in this study.

4.2 Results and Discussion

4.2.1 Polydopamine film formation

As the first step (Scheme 4.1), various deposition methods of poly(dopamine) onto (native oxide-covered) silicon substrates were investigated. Firstly, poly(dopamine) was deposited from a Tris-HCl buffer solution at pH 8.5. Alternatively, the deposition was carried out in the presence of oxidizing agent $NaIO_4$ at pH 4, 5, 6 or 7. For the experiments in the presence of $NaIO_4$, the pH was regulated using a HOAc/NaOAc buffer solution. It has been demonstrated previously that the pH strongly influences both the oxidation of catechols and formation of poly(dopamine) films, specifically: a low pH reduces the rate

of both.[53,59,60] Additionally, the deposition pH has been reported to affect the adhesive strength of the poly(dopamine) film.[61,62]

The kinetics of the poly(dopamine) film deposition were investigated using spectroscopic ellipsometry (Figure 4.1A). The evolution of layer thickness for poly(dopamine) from basic Tris solution onto (native) silicon oxide surfaces was relatively slow and reached 21 ± 2 nm after 4 h, which agrees well with previous reports for deposition on silicon surfaces.[39,63] The deposition reaction was found to be much faster for poly(dopamine) films deposited at pH 7 in the presence of $NaIO_4$. Film formation was visibly observed within a few minutes, reaching thicknesses >40 nm within 1 h, and with kinetics that did not vary significantly upon changing from 10 to 20 mM $NaIO_4$ or from pH 7 to 6. These overlapping kinetic plots suggest that under these reaction conditions, film growth rate is not limited by $NaIO_4$ concentration or pH, but by the starting concentration of dopamine.[59] In contrast, when performing the reaction under more acidic conditions, pH 4 and 5, an induction period (up to 40 min at pH 4) was observed after which film formation accelerated. Under these conditions poly(dopamine) film formation is apparently governed by two processes, first, adhesion of poly(dopamine) to the surface, and second, growth of the poly(dopamine) film.[52,64] The observed induction period for deposition at pH 4 is attributed to a lower oxidation rate of dopamine in acidic environment, as was reported in several previous studies.[57,59,61] While the ellipsometric thickness suggested little dopamine attachment during the induction period, the emergence of the N 1s signal in the XPS wide scan spectrum reveals that some dopamine attachment does take place (Supp. Figure 4.1). However, the low oxidation rate strongly hampered the cross-linking between dopamine species, and film formation was practically inhibited for the first 40 min. With time, dopamine is increasingly oxidized, allowing film thickness-increasing cross-linking reactions to become prevalent.

Static water contact angles (CA) were measured for poly(dopamine) layers deposited from $NaIO_4$-containing acetate buffer, at pH 4 and 7, and for poly(dopamine) layers deposited from Tris buffer, at pH 8.5 (Figure 4.1B). The CA for poly(dopamine) deposited from the Tris buffer decreased slightly with increasing layer thickness, from 58 ± 7° at a layer thickness of 3 ± 1 nm to 40 ± 6° at the thickness of 21 ± 2 nm. Poly(dopamine) films deposited at pH 7 in the presence of $NaIO_4$ exhibited a contact angle of 51 ± 2° at a layer thickness of 3 ± 1 nm, which dropped substantially with increasing layer thickness to 24 ± 2° at 23 ± 1 nm, in accordance with previous findings.[48] The poly(dopamine) films deposited in the presence of $NaIO_4$ at pH 4 demonstrated roughly constant static water contact angles, around 28°, irrespective of layer thickness.

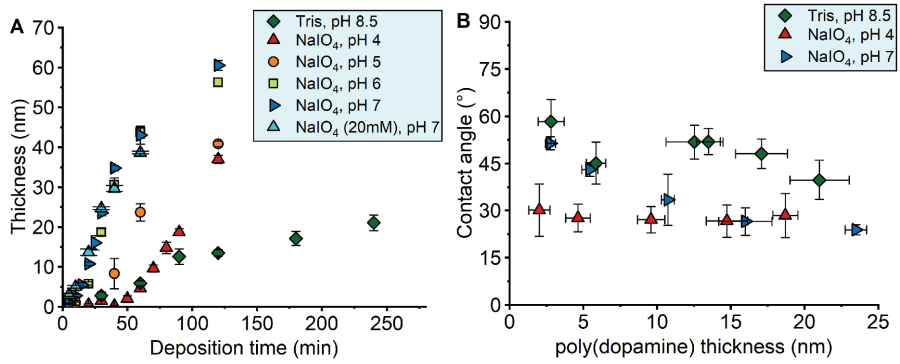

Figure 4.1 (A) Deposition kinetics for the deposition of poly(dopamine) from acetate buffers of various pH in the presence of $NaIO_4$, or from Tris buffer, pH 8.5 (thicknesses from spectroscopic ellipsometry). **(B)** Static water contact angles for poly(dopamine)-coated silicon substrates as a function of the poly(dopamine) layer thickness.

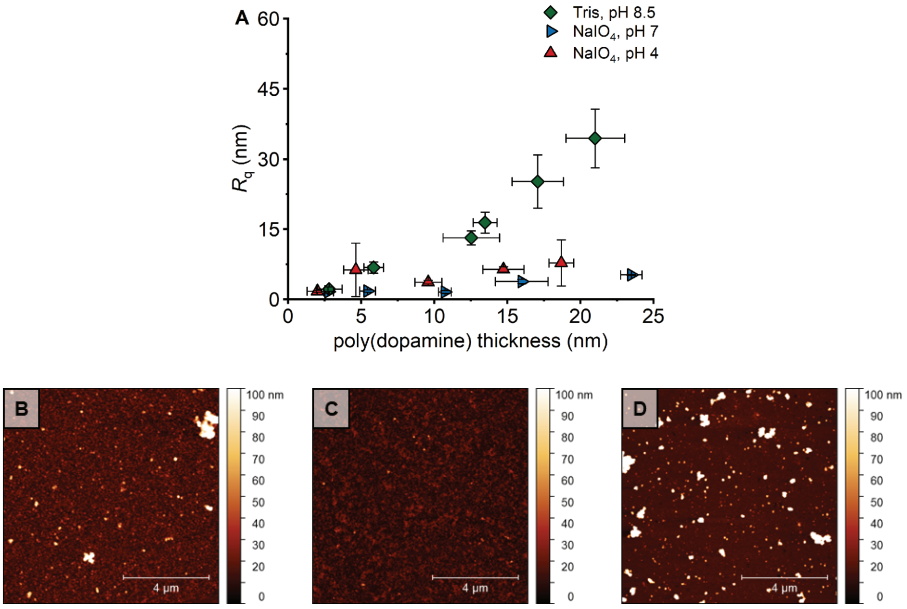

Figure 4.2 (A) Surface roughness R_q of poly(dopamine) films deposited from NaOAc buffers of varying pH in the presence of $NaIO_4$, or from Tris buffer, pH 8.5. Representative AFM images for silicon substrates modified with poly(dopamine) films at **(B)** pH 4 with $NaIO_4$ (thickness = 19 ± 1 nm); **(C)** pH 7 with $NaIO_4$ (thickness = 23 ± 1 nm) and **(D)** pH 8.5 (thickness = 21 ± 2 nm).

The surface roughness R_q of the different substrates was analyzed using atomic force microscopy (AFM) (Figure 4.2 and Supporting Information). In accordance with previous studies, poly(dopamine) films produced in the presence of $NaIO_4$ displayed lower R_q values (in the range of 5–7 nm for layer thicknesses of 20 nm) than poly(dopamine) films produced through self-oxidative polymerization in basic environment, which reached values up to 34 ± 6 nm.[64] For the substrates that were submerged in the basic Tris solution, large aggregates of poly(dopamine) were visible on the surface. It appears that during deposition from basic Tris buffer, polymerization – which can to a small degree also still occur from a surface-initiated polymer growth process – occurs extensively in solution, yielding large, insoluble particles that end up on the surface. The results obtained from AFM and CA measurements demonstrate that the deposition procedure strongly influences both chemical features (wettability) and morphological features (surface roughness) of the poly(dopamine) film.

The more hydrophilic character of the poly(dopamine) films deposited in the presence of $NaIO_4$, has been attributed to extensive oxidation of the poly(dopamine) film, which produces hydrophilic carboxylic acid groups and quinonoid structures.[48] Comparison of elemental ratios between C/N or C/O obtained from XPS wide scan did, however, not substantiate this hypothesis (Supp. Figure 4.8A). Remarkably, poly(dopamine) deposited at pH 7 in the presence of $NaIO_4$, exhibited a higher contact angle at low thicknesses, than observed for poly(dopamine) deposited at pH 4 in the presence of $NaIO_4$, despite their similar roughness values. In contrast, at increasing layer thickness, the contact angle for both films was around 25°. A possible explanation for this is that dopamine at pH 7 is oxidized at higher rate than at pH 4,[59] yielding an increased, oxidation-induced fraction of cyclized compounds in the polymer film than at pH 4, which in turn would provide a more hydrophobic film. Then, as the amount of available $NaIO_4$ decreases with longer deposition times, the oxidation rate of dopamine is lowered and therefore less cyclization occurs. Incorporation of the uncyclized dopamine, in combination with increasing layer thickness and roughness, finally yields contact angles comparable to those of poly(dopamine) deposited at pH 4.

To test this hypothesis, an extensive XPS study was performed on poly(dopamine)-coated substrates produced from $NaIO_4$-containing buffer, at pH 4 and 7, and for poly(dopamine) layers deposited from Tris buffer (Supp. Figure 4.5–4.8). The XPS study involved thorough analysis of the N 1s and C 1s narrow scan spectra of these samples. The spectra were deconvoluted to represent the binding energies reported previously for the different functional groups present in the poly(dopamine) structure,[47] but no significant

differences in chemical composition could be found between the films prepared using different procedures. This result implies that, to the degree that this is observable, the poly(dopamine) films exhibit roughly the same variety and ratios of functional groups. Yet, as the roughness values are highly similar, the differences observed in CA measurements are likely to originate from differences in chemical composition. Therefore, it is conceivable that due to the complex structure of poly(dopamine), which contains many different molecular structures each with their own binding energies, subtle differences in component ratios may go unnoticed using XPS analysis.

Overall, the poly(dopamine) deposition at pH 4 and pH 7 in the presence of $NaIO_4$ resulted in substantially more homogeneous and faster film formation than deposition from basic Tris solution. The remainder of this study will therefore focus on poly(dopamine)-modified substrates that were produced in the presence of $NaIO_4$. The results for the grafting-to studies on poly(dopamine) films deposited from Tris buffer are included in the Supporting Information (Section 4.7).

4.2.2 Grafting-to studies

Grafting-to reactions were performed using poly(GMA)$_{20}$-*b*-poly(NIPAM)$_{210}$ that had been separately synthesized using RAFT polymerization in solution, following an earlier published procedure.[58] Briefly, GMA was polymerized in the presence of RAFT agent to synthesize poly(GMA)$_{20}$, which then was used as macro-RAFT agent in a subsequent polymerization reaction of NIPAM, to yield poly(GMA)$_{20}$-*b*-poly(NIPAM)$_{210}$ (see Supporting Information for NMR, IR and GPC data). In Chapter 3, we demonstrated that for these polymers, the poly(GMA) block acts as an efficient anchoring segment, whereas the poly(NIPAM) block induces thermoresponsive and antifouling properties.[58] Here, the influence of poly(dopamine) deposition conditions and deposition time on the efficiency and rate of the grafting-to reaction were investigated.

Poly(GMA)$_{20}$-*b*-poly(NIPAM)$_{210}$ was attached to a range of poly(dopamine) substrates, obtained with various thicknesses and from several different preparation methods, via a grafting-to procedure in DMSO. Spectroscopic ellipsometry measurements were performed following these reactions to determine the total layer thickness of the resulting coatings, so as to infer the thickness of the poly(GMA)$_{20}$-*b*-poly(NIPAM)$_{210}$ layer, and these latter values for the top layer are given in Figure 4.3. From there we surmise that two factors determine the film thickness under these circumstances.

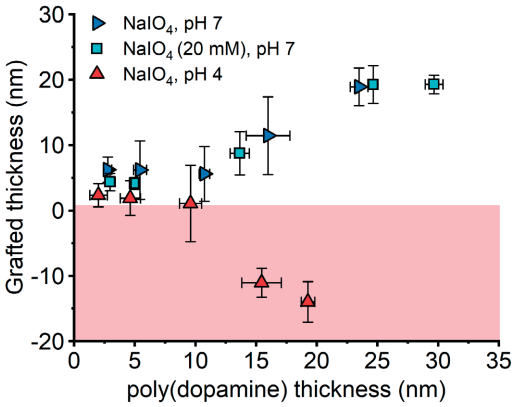

Figure 4.3 Change in film thickness following grafting of poly(GMA)$_{20}$-*b*-poly(NIPAM)$_{210}$ to poly(dopamine) layers as a function of poly(dopamine) thickness prior to reaction, as determined by spectroscopic ellipsometry. The red area in the graph indicates loss of material during reaction.

Firstly, the stability of the poly(dopamine) films is a clear issue under these conditions, and unstable attachments evidently yielded overall thinner films. All grafting reactions performed on poly(dopamine) layers that were deposited in the presence of $NaIO_4$ at pH 7 demonstrated an increase in film thickness after the polymer grafting reaction. In contrast, for the reactions performed on thicker poly(dopamine) layers deposited in the presence of $NaIO_4$ at pH 4, a loss of poly(dopamine) film was observed following the reaction. Despite the various literature reports on the use of poly(dopamine) as anchoring layer, reports on the stability of poly(dopamine) layers are scarce.[54,65] It is, however, apparent that the adhesive strength of poly(dopamine) depends strongly on the type of substrate employed, making it hard to draw general conclusions on the stability of poly(dopamine) layers.[49,65,66] In the current work, the stability against DMSO of the poly(dopamine) layer is highest when this was deposited at pH 7 in the presence of $NaIO_4$, and – as shown by a control experiment with twice the amount of $NaIO_4$ (20 mM) – not affected by the concentration of $NaIO_4$, similar to the observation made earlier on the deposition kinetics. Preliminary stability tests were performed on the produced surfaces, which turned out to be remarkably stable upon 24 h exposure to aqueous solutions in the pH range from 1 to 9 (Supp. Figure 4.16). In contrast, at pH 11 and 13, near-complete removal of the organic material was observed, and these latter results are in agreement with previous findings for poly(dopamine) films in strongly basic environments.[67]

The second factor that plays an important role during polymer grafting is the thickness of the poly(dopamine) layer. Grafting reactions performed on thin poly(dopamine)

films (< 10 nm) gave rise to poly(GMA)$_{20}$-*b*-poly(NIPAM)$_{210}$ layers of 6 ± 4 nm. Interestingly, for identical reactions performed on thicker poly(dopamine) films (> 10 nm), significantly higher poly(GMA)$_{20}$-*b*-poly(NIPAM)$_{210}$ layers could be achieved. In particular, grafted polymer layers reached thickness values up to 19 ± 3 nm, when deposited onto poly(dopamine) films thicker than 20 nm. A control experiment was performed to ensure that the observed increase in film thickness was not caused by swelling of the poly(dopamine) layer under the reaction conditions (Supp. Figure 4.17). Three poly(dopamine) substrates (average thickness 29.4 ± 0.7 nm) were exposed to grafting conditions without the presence of block copolymer. Following this experiment, the thickness of the poly(dopamine) layer remained virtually unchanged (average thickness 30.8 ± 2.4 nm). The increased thickness measured for the polymer grafting reactions must therefore indeed be caused by attachment of block copolymer.

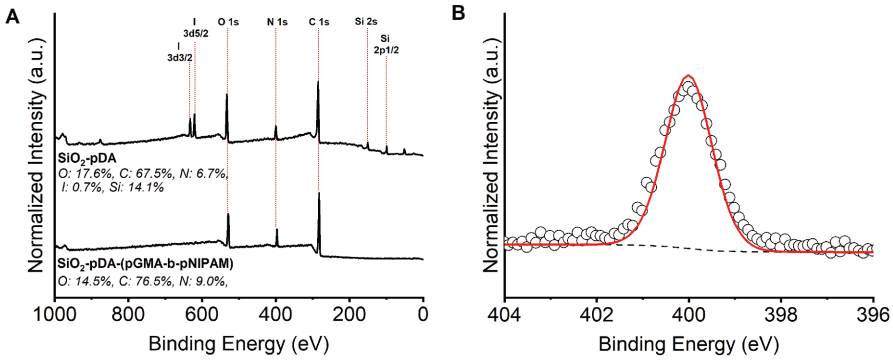

Figure 4.4 (A) XPS wide scan and **(B)** XPS N 1s narrow scan spectrum of a silicon substrate (with native oxide layer) coated with a layer of 23 ± 1 nm poly(dopamine) (NaOAc buffer (pH 7), 10 mM $NaIO_4$), and subsequently modified with poly(GMA)$_{20}$-*b*-poly(NIPAM)$_{210}$.

XPS analysis of the polymer-modified surfaces confirmed that the increase in layer thickness was indeed the result of addition of poly(GMA)$_{20}$-*b*-poly(NIPAM)$_{210}$ (Figure 4.4A), as the silicon signal was no longer visible in the wide scan spectrum of the block copolymer modified poly(dopamine) layer. Similarly, the iodine peak that was present after poly(dopamine) deposition had disappeared. It appears that any traces of iodate and iodic acid that were enclosed in the poly(dopamine) film leached out during the subsequent grafting step. Furthermore, the N 1s narrow scan spectrum showed a well-defined, narrow peak at 400.0 eV, arising from the amide functional groups present in the grafted block copolymer

(Figure 4.4B). In this N 1s XPS narrow scan, also no signals corresponding to C–N=C and C–NH_3^+ groups present in the poly(dopamine) structure were visible anymore, pointing to the presence of a significant overlayer on top of the poly(dopamine) layer.

The contact angles for the block polymer-modified substrates reached 59 ± 1° for the samples with the thickest block copolymer layers (Figure 4.5A), which compares well with the value of 58° found for poly(NIPAM)-modified silicon surfaces in literature.[68]

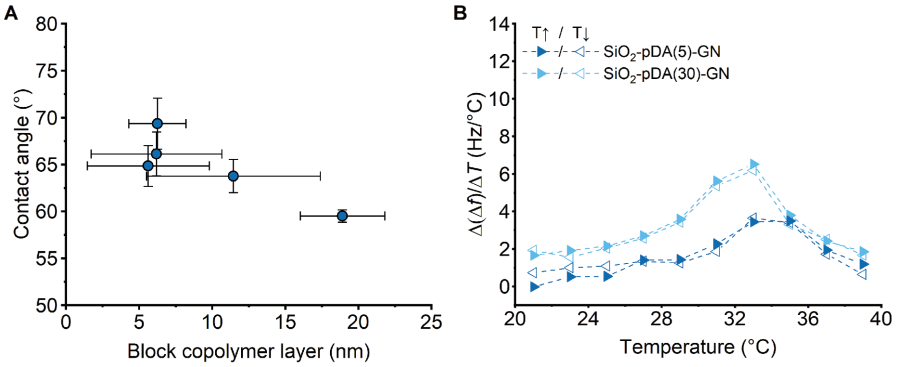

Figure 4.5 (A) Static water contact for poly(GMA)$_{20}$-*b*-poly(NIPAM)$_{210}$ that was grafted onto a poly(dopamine) layer (NaOAc buffer (pH 7), 10 mM $NaIO_4$), on silicon substrates. **(B)** Thermoresponsive character of the block copolymer-modified substrates demonstrated using QCM-D.

Quartz crystal microbalance with dissipation-monitoring (QCM-D) was employed to investigate whether the thermoresponsive properties, characteristic for poly(NIPAM), could be observed in the produced surfaces. Generally, when thermoresponsive polymers are brought in an aqueous environment where the temperature is lower than the polymer's lower critical solution temperature (LCST), water molecules will coordinate to the polymers and they swell.[71] Once the temperature is raised to exceed the LCST, water is entropically expelled and the polymers collapse. This reversible process can be monitored in polymer coatings using QCMD, as the expulsion of water is accompanied by a measurable change in the stagnant mass present on the surface.[33,60,72] Poly(dopamine) deposition was carried out on SiO_2-coated QCMD sensors for 5 and 30 min, followed by grafting the poly(GMA)$_{20}$-*b*-poly(NIPAM)$_{210}$ block copolymer. The sensors were then placed in an aqueous environment in the QCMD and subjected to a temperature program that adjusted the temperature from 20 °C to 40 °C, and then back to 20 °C. The produced surfaces indeed exhibited thermoresponsive behavior, with the LCST at ± 32 °C, as indi-

cated by the peaks in the plot (Figure 5B, raw data in Supporting Information), in line with previous studies.[60] Since $\Delta(\Delta f)/\Delta T$ is directly related to the mass change on the sensors, the data display the amount of water that is expulsed and again bound when increasing and decreasing the temperature.[33,60] The SiO_2 sensors that were coated with poly(dopamine) for 30 min show the greatest amount of water expulsed and coordinated again over the applied temperature cycle. These surfaces thus have a larger capacity to bind water and thus likely have more polymer material grafted to the surface, displaying agreement between these QCMD data and the ellipsometry data discussed above.

The grafted layer thickness of 19 ± 3 nm obtained in this study are exceptionally high for grafting-to procedures performed from solution, particularly considering the relatively high molecular weight of poly(GMA)$_{20}$-*b*-poly(NIPAM)$_{210}$.[24,30,31,71,72] Alexander-de Gennes' theory enables approximation of the grafting density, σ, based on the measured dry thickness of the polymer layer, the size of the polymers, Avogadro's number and the polymer bulk density.[73] Based on a layer thickness of 19 ± 3 nm, the grafting density, or chains per nm^2, can be approximated at 0.48 ± 0.07 chains/nm^2. Such high grafting densities for grafting-to reactions from solution have to our knowledge not yet been reported,[24] and are even more remarkable given the relatively large polymers (M_n = 38 kDa) used here.

To broaden the scope of this grafting procedure and further investigate the cause for the observed grafting densities, block copolymers of increased sizes were synthesized, specifically poly(GMA)$_{20}$-*b*-poly(NIPAM)$_{404}$ and poly(GMA)$_{20}$-*b*-poly(NIPAM)$_{566}$. These polymers were grafted to poly(dopamine) substrates under identical conditions as described for poly(GMA)$_{20}$-*b*-poly(NIPAM)$_{210}$. The thickness measured for the resulting grafted layers were highly similar to the results obtained earlier, showing an increase in block copolymer layer on thicker poly(dopamine) films (Figure 4.6A). Evidently, a change in poly(dopamine) features with increasing thickness is responsible for the higher grafting efficiency. We therefore hypothesize that at lower poly(dopamine) thickness, the grafting reaction is limited by the number of suitable reactive groups present in the poly(dopamine) layer. With increasing poly(dopamine) layer thickness, a larger total number of reactive groups will be available throughout the porous, granular structure of the poly(dopamine) film.[76]

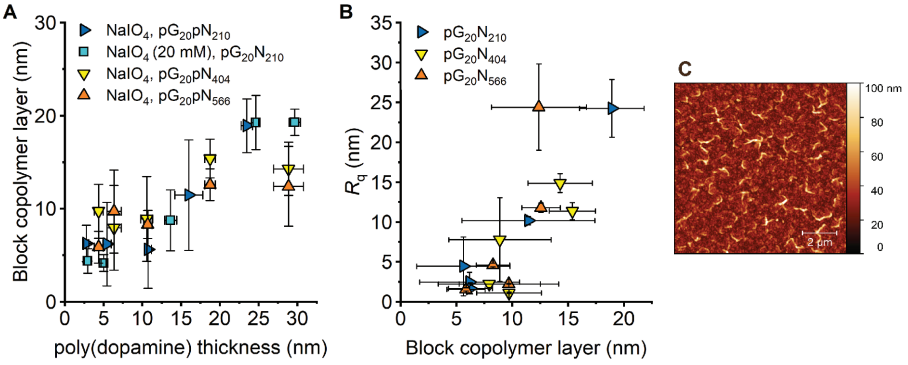

Figure 4.6 (A) Change in film thickness following grafting of various block copolymers to poly(dopamine) layers as a function of poly(dopamine) thickness prior to reaction, as determined by spectroscopic ellipsometry. **(B)** Roughness values for block copolymer-modified substrates measured by AFM. **(C)** AFM image of poly(GMA)$_{20}$-*b*-poly(NIPAM)$_{566}$-modified substrate with thread-like features.

AFM measurements were performed to determine the surface roughness of the substrates after polymer grafting (Figure 4.6B). The roughness increases markedly with increasing block copolymer layer thickness and follows the trend that was previously observed for roughness of poly(dopamine) (Figure 4.2A). To rule out a roughness increase caused by the poly(dopamine) layer during the reaction, the roughness of three poly(dopamine) substrates was measured before and after exposure to grafting conditions in the absence of the block copolymer (Supporting Information, Supp. Figure 4.17). The average roughness of these substrates did not increase, indicating that the increased roughness was a result of block copolymer attachment. The roughness values obtained for poly(GMA)$_{20}$-*b*-poly(NIPAM)$_{566}$ grafted on poly(dopamine) with film thickness of 18.7 ± 0.7 nm and 28.9 ± 1.9 nm are of particular interest. The attached block copolymer layers for these substrates have similar thicknesses of 12.6 ± 1.7 nm and 12.4 ± 4.3 nm, respectively. The R_q values differ significantly and are 11.8 ± 0.6 nm for grafting on the thinner – and relatively smoother – poly(dopamine) film and 24.4 ± 5.4 nm for grafting on the thicker – and relatively rougher – poly(dopamine) film. This implies that grafting of the block copolymer amplifies the topological features of the underlying poly(dopamine) films and thereby raises the surface roughness.

Interestingly, the AFM images obtained from the samples with thickest block copolymer layers showed thread-like regions that were not observed in the other samples (Figure 4.6C and Supporting Information) and could not be removed by extensive washing or sonication. The structures have a length and width of roughly 1–2 µm and 0.3 µm,

respectively, and are therefore too large to correspond to single polymer chains. Possible explanations for these features may be clustering of the surface-attached polymers, cross-linking between poly(glycidyl methacrylate) segments of the block copolymers or partial rupture of the poly(dopamine) layer. Crosslinking of the polymers would result in large, bottlebrush-like structures that correspond to the size range observed in the AFM image. A control experiment was performed to determine whether crosslinking of the block copolymers occurs in solution. Grafting conditions were simulated by heating a solution of poly(GMA)$_{20}$-*b*-poly(NIPAM)$_{210}$ in DMF with 5% TEA to 80 °C overnight without the presence of a poly(dopamine) substrate. GPC measurements were then performed and compared to the measurements taken before control experiment. The traces were near-identical, indicating that no reaction took place between the polymer chains in the reaction solution (Supp. Figure 4.24). Moreover, the previously described experiment in which thick poly(dopamine) films were exposed to grafting conditions without the presence of polymer did not result in thread-like features on the surface (Supp. Figure 4.17). Furthermore, sonication of a substrate with this thread motif in acetone for 10 minutes did not cause any further rupture of the film (Supp. Figure 4.25). As a result, the thread-like motifs are believed to be the result of clustering of the polymers on the topological features of the poly(dopamine) films.

In conclusion, the amount of polymer that can be grafted on poly(dopamine) and the resulting surface features are highly dependent on poly(dopamine) layer thickness. It is to be expected that such a dependence translates to any grafting-to reaction performed on poly(dopamine) films. Additionally, in a much broader sense, these findings plainly illustrate the strong influence that poly(dopamine) properties have on the outcome of any subsequent modification step. With poly(dopamine) on the forefront in the development of universally applicable coating procedures, it is of the essence for potential future application that studies of poly(dopamine) concerning modification efficiency and film stability are thoroughly investigated.[77] In that regard, this study contributes to development of a straightforward, substrate-independent grafting-to procedure for the synthesis of stable polymer brush coatings.

4.3 Conclusions

Poly(dopamine) deposition conditions greatly affect the properties of the poly(dopamine) film and, as a result, the efficiency of a subsequent grafting-to reaction using three block copolymers, specifically poly(GMA)$_{20}$-*b*-poly(NIPAM)$_{210}$, poly(GMA)$_{20}$-*b*-poly(NIPAM)$_{404}$

and poly(GMA)$_{20}$-*b*-poly(NIPAM)$_{566}$. Using optimized deposition conditions for both the poly(dopamine) layer and for the grafted-to polymer layer on top of this, we were able to graft polymer layers up to 19 nm thick. To get to this result, first poly(dopamine) was deposited at pH 4–7 in the presence of $NaIO_4$, and at pH 8.5 from Tris buffer, and distinct differences in deposition rate, hydrophilicity and surface roughness were observed. In addition, after grafting of the block copolymer poly(GMA)$_{20}$-*b*-poly(NIPAM)$_{210}$, variations in stability and grafting efficiency were apparent. Concerning the stability, poly(dopamine) deposited at pH 7 with $NaIO_4$ was the only film to survive the grafting conditions. Furthermore, the amount of block copolymer grafted to poly(dopamine) was shown to increase with poly(dopamine) layer thickness. The ultimate 19 ± 3 nm thick poly(GMA)$_{20}$-*b*-poly(NIPAM)$_{210}$ layers had an approximated grafting density of 0.48 ± 0.07 chains/nm^2. We expect such thicker and still easy to apply grafted-to surface coatings to have improved properties for a wide range of applications, including antifouling and self-healing coatings.

4.4 Materials and Methods

4.4.1 Materials

All chemical reagents were used without further purification unless otherwise specified. Triethylamine (TEA), 2,2′-azobis(2-methylpropionitrile) (AIBN) (98%), NaOAc (> 99%) and 1,4-dioxane (99.8%, anhydrous, non-stabilized) were purchased from Sigma-Aldrich. 4-Cyano-4-[(dodecylsulfanylthiocarbonyl)sulfanyl]pentanoic acid (CDPA) (> 95.0%), dopamine.HCl (> 98.0%) and *N*isopropylacrylamide (NIPAM) (> 98.0%, stabilized) were purchased from TCI Chemicals Europe. Glycidyl methacrylate (GMA) (97%, stabilized) and Tris base (≥ 99.8%) were purchased from Thermo Fisher Scientific. $NaIO_4$ (99%) was purchased from ACROS Organics. Deionized water was produced with Milli-Q Integral 3 system Millipore, Molsheim, France (Milli-Q water). Silicon single side-polished wafers (Si(100), N-type, phosphorus-doped) were obtained from Siltronix.

Prior to use, GMA was purified by washing with 0.1% m/v KOH solution and NIPAM was recrystallized from hexane.

4.4.2 Modification of silicon substrates with poly(dopamine)

1 × 1 cm Si substrates were rinsed using acetone, ethanol and Milli-Q and then dried under a gentle stream of argon. The Si substrates were placed in a petri dish containing freshly prepared solution of dopamine.HCl. For deposition in the presence of $NaIO_4$, this

solution consisted of dopamine.HCl (40 mg, 0.21 mmol, 10.5 mM) and $NaIO_4$ (10 or 20 mM) in 50 mM HOAc/NaOAc buffer (20 mL) of the desired pH. For deposition from basic Tris buffer, the solution consisted of dopamine.HCl (40 mg, 0.21 mol, 10.5 mM) in 10 mM Tris.HCl (Tris) buffer (pH 8.5). The petri dish was closed, sealed using parafilm and placed on an automated shaker at RT, 60 RPM. The surfaces were removed from the solution after the appropriate time, cleaned using Milli-Q and subsequently dried under nitrogen flow.

4.4.3 RAFT polymerization of poly(GMA)$_{20}$

The RAFT polymerization of GMA was performed according to the procedure previously described in Chapter 3.[58] The product, a fine yellow powder, was obtained through filtration. It was then dried over air (Yield: 0.99 g, 27%). **^{1}H NMR** (400 MHz, $CDCl_3$) δ 4.38 – 4.24 (m, 19H), 3.86 – 3.72 (m, 20H), 3.26 – 3.19 (m, 20H), 2.87 – 2.79 (dt, 19H), 2.68 – 2.59 (tt, 19iH), 2.17 – 1.72 (m, 34H), 1.45 – 1.23 (m, 18H), 1.11 – 1.07 (s, 19H), 0.94 – 0.80 (s, 34H). **IR** ν = 1740–1720 cm^{-1} (–C(=O)–O), 1470–1430 cm^{-1} (–CH_3), 1260 cm^{-1} (C–O), 903 cm^{-1} (epoxide C–O).[74–76]

4.4.4 Synthesis of poly(GMA)$_{20}$-*b*-poly(NIPAM)$_{210}$

To a 100 mL Schlenk flask was added AIBN (2.0 mg; 0.012 mmol; 0.1 equiv.), poly(GMA)$_{20}$ (374 mg; 0.12 mmol; 1 equiv.), NIPAM (2.99 g; 26.5 mmol; 220 equiv.), and 1,4-dioxane (10 mL). The solution was deoxygenated by three freeze-pump-thaw cycles. After the last cycle, the flask was charged with argon. The flask was then heated at 70 °C and left to stir for 3 h. Subsequently, the solution was quenched in liquid nitrogen to deactivate the radical polymerization. To the reaction mixture was then added acetone (10mL), after which the polymer was purified by precipitation from hexane twice. **^{1}H NMR** (400 MHz, CDCl3) δ 4.32 (s, 21H), 4.02 (s, 210H), 3.84 (s, 18H), 3.26 (s, 20H), 2.87 (s, 21H), 2.66 (s, 1H), 1.42 – 0.94 (m). **IR** ν = 3297 cm^{-1} (N–H), 1740–1720 cm^{-1} (–C(=O)–O), 1620–1560 cm^{-1} (–C(=O)–NH), 1542 cm^{-1} (N–H).[74,77,78]

4.4.5 Synthesis of poly(GMA)$_{20}$-b-poly(NIPAM)$_{404}$.

To a 50 mL Schlenk flask was added **AIBN** (0.38 mg; 0.0024 mmol; 0.1 equiv.), **pGMA$_{20}$** (0.37 mg; 0.012 mmol; 1 equiv.), **NIPAM** (0.78 g; 6.9 mmol; 575 equiv.), and 1,4-dioxane (6 mL). The solution was deoxygenated by three freeze-pump-thaw cycles. After the last cycle, the flask was charged with argon. The flask was then heated at 70 °C and left to stir for 3 h. Subsequently, the solution was quenched in liquid nitrogen to deactivate the radical polymerization. To the reaction mixture was then added acetone (5 mL), after which

the polymer was purified by precipitation from hexane twice. **^{1}H NMR** (400 MHz, $CDCl_3$) δ 6.28 (s), 4.23 (s, 23H), 3.93 (s, 404H), 3.79 – 3.70 (m), 3.17 (s, 20H), 2.77 (s, 27H), 2.58 (s, 383H), 1.06 (s, 2439H). **IR** ν = 3297 cm^{-1} (N–H), 1740–1720 cm^{-1} (–C(=O)–O), 1620–1560 cm^{-1} (–C(=O)–NH), 1542 cm^{-1} (N–H).[78,81,82]

4.5.6 Synthesis of poly(GMA)$_{20}$-b-poly(NIPAM)$_{566}$.

To a 50 mL Schlenk flask was added **AIBN** (0.38 mg; 0.0024 mmol; 0.1 equiv.), **pGMA$_{20}$** (0.37 mg; 0.012 mmol; 1 equiv.), **NIPAM** (1.17 g; 10.35 mmol; 860 equiv.), and 1,4-dioxane (9 mL). The solution was deoxygenated by three freeze-pump-thaw cycles. After the last cycle, the flask was charged with argon. The flask was then heated at 70 °C and left to stir for 5 h. Subsequently, the solution was quenched in liquid nitrogen to deactivate the radical polymerization. To the reaction mixture was then added acetone (5 mL), after which the polymer was purified by precipitation from hexane twice. **^{1}H NMR** (400 MHz, $CDCl_3$) δ 4.32 (s, 24H), 4.02 (s, 566H), 3.26 (s, 20H), 2.87 (s, 21H), 2.66 (s, 23H), 2.12 (s, 3374H), 1.16 (s, 1H). **IR** ν = 3297 cm^{-1} (N–H), 1740–1720 cm^{-1} (–C(=O)–O), 1620–1560 cm^{-1} (–C(=O)–NH), 1542 cm^{-1} (N–H).[78,81,82]

4.5.7 Grafting of polymers to poly(dopamine)-modified SiO$_2$ substrates.

The grafting-to reaction using poly(GMA)$_{20}$-*b*-poly(NIPAM)$_{210}$ was carried out according to the protocol described in Chapter 3.[58]

2.4.6 Control experiment cross-linking in solution.

A solution of 10 mg/mL poly(GMA)$_{20}$*b*poly(NIPAM)$_{210}$ in DMF with 5% TEA was prepared. The solution was heated to 80 °C overnight to mimic the reaction conditions of the grafting-to step. Following the reaction, GPC measurements were performed to determine the occurrence of crosslinking between polymer chains.

2.4.7 Gel permeation chromatography (GPC)

The polymer molecular weight and polydispersity index (PDI) were determined using gel permeation chromatography (Agilent 1200 Organic GPC + refractive index detector, equipped with PLgel 5 μm MIXED-D column), The column was calibrated with poly(methyl methacrylate) polymer set. The selected eluent was THF for poly(GMA)$_{20}$ and DMF + 0.1% LiBr for poly(GMA)$_{20}$-*b*-poly(NIPAM)$_{210}$, pumped at a constant flow of 0.5 mL/min.

2.4.8 Atomic Force Microscopy (AFM)

Atomic force microscopy was performed using an Asylum MFP-3D Origin AFM (Oxford Instruments, United Kingdom). The instrument was operated in tapping mode and equipped with a silicon cantilever (AC240TS-R3, k = 1.3 N m^{-1}) with a nominal tip radius of ~7 nm. The acquired images were processed and analyzed using Gwyddion open-source software for SPM data analysis.

2.4.9 Ellipsometry

Ellipsometric angles Δ and Ψ of the synthesized polymer brushes were measured using an EP4 imaging ellipsometer (Accurion, Germany). The measurements were performed in air at room temperature in the wavelength range of λ = 491 – 761.3 nm at an angle of incidence of 50°. The acquired Δ and Ψ were fitted in the EP4 modeling software using a multilayer model to obtain dry polymer brush thickness and refraction index values. The poly(dopamine) layer was describe using a Cauchy-Urbach model to account for the light absorption of poly(dopamine).

$$n(E) = A + BE^2; \qquad k(E) = \alpha e^{\beta(E-E_b)}$$

The following parameters were used: A = 1.54, B = 3000 nm^2, α = 0.161 ± 0.58, β = 0.242 ± 0.121 and E_b = 3.0 eV. The poly$(GMA)_{20}$-*b*-poly$(NIPAM)_{210}$ layer for polymer-modified substrates was described using a Cauchy model with parameters A = 1.50 and B = 3000 nm^2. Addition of an outermost layer to account for the roughness of the measured substrates using Bruggeman's effective medium approximation (EMA) did not improve the fit of the model.[79] Control experiments were carried out to verify the model by scratching the surface of a modified silicon oxide substrate and measuring the thickness using atomic force microscopy (AFM) (see Supporting Information).

Following Alexander-de Gennes' theory, the ellipsometric thickness, h_{dry}, was used to approximate the grafting density of the poly$(GMA)_{20}$-*b*-poly$(NIPAM)_{210}$ block copolymer chains on the poly(dopamine) films:[73]

$$\sigma \approx \frac{h_{\mathrm{dry}}\,\rho_b N_A}{M_n}$$

Here, σ is the grafting density in chains/nm^2, ρ_b is the density of the grafted polymer layer, N_A is Avogadro's constant and M_n is the polymer molecular weight. Bulk density of poly(NIPAM), ρ_b, was 1.07 g cm^{-3} used.[80]

2.4.10 ATR FT-IR spectroscopy

FT-IR spectra were obtained on a Bruker Tensor 27 spectrometer with platinum attenuated total reflection accessory. The samples were applied as powder or oil on top of the crystal. 64 scans were performed with a resolution of 4 cm^{-1}.

2.4.11 X-ray photoelectron spectroscopy

XPS measurements were performed as described in Chapter 2. The fits employed for deconvolution were attributed to C–C and C–H (285.0 eV), C–N (286.1 eV), C–O (286.8 eV), C=O (288.6 eV) and π-π* shake-up (291.1 eV).

The N 1s narrow scan spectrum was referenced to the N 1s peak attributed to C-NH-R at 400.0 eV. The fits employed for deconvolution were attributed to C–N=C (389.9 eV), C–NH–R (R = C,H; 400.0 eV) and C–NH_3^+ (401.5 eV).

2.4.12 Static water contact angle measurement

Static water contact angle measurements were performed as described in Chapter 2.

2.4.13 Quartz-crystal microbalance with dissipation monitoring (QCM-D) measurements

QCM-D measurements were performed as described in Chapter 3.

To account for any possible influence of the poly(dopamine) during these measurements, the experimental data was corrected by subtracting the frequency changes reference experiments were performed using poly(dopamine)-coated SiO_2 sensors.

2.4.14 Statistical analysis

All statistical results were calculated using Origin 2019 software. Data were displayed as average values ± standard deviation.

2.5 Acknowledgements

This research was carried out under project number C16030a in the framework of the Partnership Program of the Materials innovation institute M2i (www.m2i.nl) and the NWO Domain Science, which is part of the Netherlands Organization for Scientific Research (www.nwo.nl).

2.6 References

1. Takasu, K. *et al.* Polymer brush biointerfaces for highly sensitive biosensors that preserve the structure and function of immobilized proteins. *Sensors Actuators, B Chem.* **216**, 428–433 (2015).
2. Frost, S. & Ulbricht, M. Thermoresponsive ultrafiltration membranes for the switchable permeation and fractionation of nanoparticles. *J. Memb. Sci.* **448**, 1–11 (2013).
3. Kuzmyn, A. R. *et al.* Antiviral Polymer Brushes by Visible-Light-Induced, Oxygen-Tolerant Covalent Surface Coating. *ACS Omega* **7**, 38371–38379 (2022).
4. Zoppe, J. O. *et al.* Surface-Initiated Controlled Radical Polymerization: State-of-the-Art, Opportunities, and Challenges in Surface and Interface Engineering with Polymer Brushes. *Chem. Rev.* **117**, 1105–1318 (2017).
5. Chen, W. L., Cordero, R., Tran, H. & Ober, C. K. 50th Anniversary Perspective: Polymer Brushes: Novel Surfaces for Future Materials. *Macromolecules* **50**, 4089–4113 (2017).
6. Azzaroni, O. Polymer brushes here, there, and everywhere: Recent advances in their practical applications and emerging opportunities in multiple research fields. *J. Polym. Sci. Part A Polym. Chem.* **50**, 3225–3258 (2012).
7. Kuzmyn, A. R. *et al.* Diblock and Random Antifouling Bioactive Polymer Brushes on Gold Surfaces by Visible-Light-Induced Polymerization (SI-PET-RAFT) in Water. *Adv. Mater. Interfaces* **9**, 2101784 (2022).
8. Roeven, E. *et al.* PLL–Poly(HPMA) Bottlebrush-Based Antifouling Coatings: Three Grafting Routes. *Langmuir* **36**, 10187–10199 (2020).
9. Kuzmyn, A. R. *et al.* Exploiting end group functionalization for the design of antifouling bioactive brushes. *Polym. Chem.* **5**, 4124 (2014).
10. Kuzmyn, A. R., Nguyen, A. T., Zuilhof, H. & Baggerman, J. Bioactive Antifouling Surfaces by Visible-Light-Triggered Polymerization. *Adv. Mater. Interfaces* **6**, 1900351 (2019).
11. Kotlarek, D. *et al.* Compact Grating-Coupled Biosensor for the Analysis of Thrombin. *ACS Sensors* **4**, 2109–2116 (2019).
12. Rodriguez-Emmenegger, C. *et al.* Substrate-independent approach for the generation of functional protein resistant surfaces. *Biomacromolecules* **12**, 1058–1066 (2011).
13. Xu, X. *et al.* Antifouling and Antibacterial Surfaces Grafted with Sulfur-Containing Copolymers. *ACS Appl. Mater. Interfaces* **14**, 41400–41411 (2022).
14. Xu, X. *et al.* Antifouling Surfaces Enabled by Surface Grafting of Highly Hydrophilic Sulfoxide Polymer Brushes. *Biomacromolecules* **22**, 330–339 (2021).
15. Ritsema van Eck, G. C., Chiappisi, L. & de Beer, S. Fundamentals and Applications of Polymer Brushes in Air. *ACS Appl. Polym. Mater.* **4**, 3062–3087 (2022).
16. Teunissen, L. W., Kuzmyn, A. R., Ruggeri, F. S., Smulders, M. M. J. & Zuilhof, H. Thermoresponsive, Pyrrolidone-Based Antifouling Polymer Brushes. *Adv. Mater. Interfaces* **9**, 2101717 (2022).
17. Edmondson, S., Osborne, V. L. & Huck, W. T. S. Polymer brushes via surface-initiated polymerizations. *Chem. Soc. Rev.* **33**, 14–22 (2004).
18. Krishnamoorthy, M., Hakobyan, S., Ramstedt, M. & Gautrot, J. E. Surface-Initiated Polymer Brushes in the Biomedical Field: Applications in Membrane Science, Biosensing, Cell Culture, Regenerative Medicine and Antibacterial Coatings. *Chem. Rev.* **114**, 10976–11026 (2014).

19. Fromel, M., Benetti, E. M. & Pester, C. W. Oxygen Tolerance in Surface-Initiated Reversible Deactivation Radical Polymerizations: Are Polymer Brushes Turning into Technology? *ACS Macro Lett.* **11**, 415–421 (2022).

20. Li, M. *et al.* SI-PET-RAFT: Surface-Initiated Photoinduced Electron Transfer-Reversible Addition–Fragmentation Chain Transfer Polymerization. *ACS Macro Lett.* **8**, 374–380 (2019).

21. Xu, J., Jung, K., Atme, A., Shanmugam, S. & Boyer, C. A robust and versatile photoinduced living polymerization of conjugated and unconjugated monomers and its oxygen tolerance. *J. Am. Chem. Soc.* **136**, 5508–5519 (2014).

22. Kuzmyn, A. R., Nguyen, A. T., Teunissen, L. W., Zuilhof, H. & Baggerman, J. Antifouling Polymer Brushes via Oxygen-Tolerant Surface-Initiated PET-RAFT. *Langmuir* **36**, 4439–4446 (2020).

23. Patil, R. R., Turgman-Cohen, S., Šrogl, J., Kiserow, D. & Genzer, J. On-Demand Degrafting and the Study of Molecular Weight and Grafting Density of Poly(methyl methacrylate) Brushes on Flat Silica Substrates. *Langmuir* **31**, 2372–2381 (2015).

24. Patil, R. R., Turgman-Cohen, S., Šrogl, J., Kiserow, D. & Genzer, J. Direct measurement of molecular weight and grafting density by controlled and quantitative degrafting of surface-anchored poly(methyl methacrylate). *ACS Macro Lett.* **4**, 251–254 (2015).

25. Zdyrko, B. & Luzinov, I. Polymer brushes by the 'grafting to' method. *Macromol. Rapid Commun.* **32**, 859–869 (2011).

26. Michalek, L., Barner, L. & Barner-Kowollik, C. Polymer on Top: Current Limits and Future Perspectives of Quantitatively Evaluating Surface Grafting. *Adv. Mater.* **30**, 1706321 (2018).

27. Kingshott, P., Thissen, H. & Griesser, H. J. Effects of cloud-point grafting, chain length, and density of PEG layers on competitive adsorption of ocular proteins. *Biomaterials* **23**, 2043–56 (2002).

28. Ortiz, R., Olsen, S. & Thormann, E. Salt-Induced Control of the Grafting Density in Poly(ethylene glycol) Brush Layers by a Grafting-to Approach. *Langmuir* **34**, 4455–4464 (2018).

29. Unsworth, L. D., Sheardown, H. & Brash, J. L. Protein-resistant polyethylene oxide-grafted surfaces: Chain density-dependent multiple mechanisms of action. *Langmuir* **24**, 1924–1929 (2008).

30. Ghezzi, M. *et al.* Protein micropatterns by PEG grafting on dewetted PLGA films. *Langmuir* **30**, 11714–11722 (2014).

31. Emilsson, G. *et al.* Strongly stretched protein resistant poly(ethylene glycol) brushes prepared by grafting-to. *ACS Appl. Mater. Interfaces* **7**, 7505–7515 (2015).

32. Heinen, S. & Weinhart, M. Poly(glycidyl ether)-Based Monolayers on Gold Surfaces: Control of Grafting Density and Chain Conformation by Grafting Procedure, Surface Anchor, and Molecular Weight. *Langmuir* **33**, 2076–2086 (2017).

33. Schweigerdt, A., Heinen, S., Stöbener, D. D. & Weinhart, M. Grafting Density-Dependent Phase Transition Mechanism of Thermoresponsive Poly(glycidyl ether) Brushes: A Comprehensive QCM-D Study. *Langmuir* **37**, 7087–7096 (2021).

34. Michalek, L., Mundsinger, K., Barner, L. & Barner-Kowollik, C. Quantifying Solvent Effects on Polymer Surface Grafting. *ACS Macro Lett.* **8**, 800–805 (2019).

35. Luzinov, I., Minko, S. & Tsukruk, V. V. Adaptive and responsive surfaces through controlled reorganization of interfacial polymer layers. *Prog. Polym. Sci.* **29**, 635–698 (2004).

36. Iyer, K. S. & Luzinov, I. Effect of macromolecular anchoring layer thickness and molecular weight on polymer grafting. *Macromolecules* **37**, 9538–9545 (2004).

37. Minko, S. *et al.* Synthesis of adaptive polymer brushes via 'grafting to' approach from melt. *Langmuir* **18**, 289–296 (2002).

38. Laradji, A. M., McNitt, C. D., Yadavalli, N. S., Popik, V. V. & Minko, S. Robust, Solvent-Free, Catalyst-Free Click Chemistry for the Generation of Highly Stable Densely Grafted Poly(ethylene glycol) Polymer Brushes by the Grafting To Method and Their Properties. *Macromolecules* **49**, 7625–7631 (2016).

39. Pop-Georgievski, O. *et al.* Nonfouling poly(ethylene oxide) layers end-tethered to polydopamine. *Langmuir* **28**, 14273–14283 (2012).

40. Minko, S. *et al.* Bidisperse mixed brushes: Synthesis and study of segregation in selective solvent. *Macromolecules* **36**, 7268–7279 (2003).

41. Lee, H., Dellatore, S. M., Miller, W. M. & Messersmith, P. B. Mussel-Inspired Surface Chemistry for Multifunctional Coatings. *Science* **318**, 426–430 (2007).

42. Ryu, J. H., Messersmith, P. B. & Lee, H. Polydopamine Surface Chemistry: A Decade of Discovery. *ACS Appl. Mater. Interfaces* **10**, 7523–7540 (2018).

43. Dreyer, D. R., Miller, D. J., Freeman, B. D., Paul, D. R. & Bielawski, C. W. Elucidating the structure of poly(dopamine). *Langmuir* **28**, 6428–6435 (2012).

44. Dreyer, D. R., Miller, D. J., Freeman, B. D., Paul, D. R. & Bielawski, C. W. Perspectives on poly(dopamine). *Chem. Sci.* **4**, 3796–3802 (2013).

45. Hong, S. *et al.* Non-covalent self-assembly and covalent polymerization co-contribute to polydopamine formation. *Adv. Funct. Mater.* **22**, 4711–4717 (2012).

46. Liebscher, J. *et al.* Structure of polydopamine: A never-ending story? *Langmuir* **29**, 10539–10548 (2013).

47. Della Vecchia, N. F. *et al.* Building-block diversity in polydopamine underpins a multifunctional eumelanin-type platform tunable through a quinone control point. *Adv. Funct. Mater.* **23**, 1331–1340 (2013).

48. Ding, Y. *et al.* Insights into the Aggregation/Deposition and Structure of a Polydopamine Film. *Langmuir* **30**, 12258–12269 (2014).

49. D'Ischia, M., Napolitano, A., Ball, V., Chen, C. T. & Buehler, M. J. Polydopamine and eumelanin: From structure-property relationships to a unified tailoring strategy. *Acc. Chem. Res.* **47**, 3541–3550 (2014).

50. Ponzio, F. *et al.* Oxidant Control of Polydopamine Surface Chemistry in Acids: A Mechanism-Based Entry to Superhydrophilic-Superoleophobic Coatings. *Chem. Mater.* **28**, 4697–4705 (2016).

51. Svoboda, J., Král, M., Dendisová, M., Matějka, P. & Pop-Georgievski, O. Unraveling the influence of substrate on the growth rate, morphology and covalent structure of surface adherent polydopamine films. *Colloids Surfaces B Biointerfaces* **205**, 111897 (2021).

52. El Yakhlifi, S. *et al.* Oxidant-dependent antioxidant activity of polydopamine films: The chemistry-morphology interplay. *Colloids Surfaces A Physicochem. Eng. Asp.* **614**, 126134 (2021).

53. Della Vecchia, N. F. *et al.* Tris buffer modulates polydopamine growth, aggregation, and paramagnetic properties. *Langmuir* **30**, 9811–9818 (2014).

54. Liebscher, J. Chemistry of Polydopamine – Scope, Variation, and Limitation. *European J. Org. Chem.* **2019**, 4976–4994 (2019).

55. Ball, V., Frari, D. Del, Toniazzo, V. & Ruch, D. Kinetics of polydopamine film deposition as a function of pH and dopamine concentration: Insights in the polydopamine deposition mechanism. *J. Colloid Interface Sci.* **386**, 366–372 (2012).

56. Zhang, C. *et al.* CuSO4/H2O2-Induced Rapid Deposition of Polydopamine Coatings with High Uniformity and Enhanced Stability. *Angew. Chemie - Int. Ed.* **55**, 3054–3057 (2016).

57. Wei, Q., Zhang, F., Li, J., Li, B. & Zhao, C. Oxidant-induced dopamine polymerization for multifunctional coatings. *Polym. Chem.* **1**, 1430–1433 (2010).

58. Zhang, W. *et al.* Fast coating of hydrophobic upconversion nanoparticles by NaIO4-induced polymerization of dopamine: Positively charged surfaces and in situ deposition of Au nanoparticles. *Appl. Surf. Sci.* **527**, 146821 (2020).

59. Hong, S. H. *et al.* Sprayable Ultrafast Polydopamine Surface Modifications. *Adv. Mater. Interfaces* **3**, 1500857 (2016).

60. Teunissen, L. W., van den Beukel, J., Smulders, M. M. J. & Zuilhof, H. Thermoresponsive Polymer Brushes for Switchable Protein Adsorption via Dopamine-Assisted Grafting-To Strategy. *Adv. Mater. Interfaces* **9**, 2201198 (2022).

61. Weidman, S. W. & Kaiser, E. T. The Mechanism of the Periodate Oxidation of Aromatic Systems. III. A Kinetic Study of the Periodate Oxidation of Catechol. *J. Am. Chem. Soc.* **88**, 5820–5827 (1966).

62. Salomäki, M., Marttila, L., Kivelä, H., Ouvinen, T. & Lukkari, J. Effects of pH and Oxidants on the First Steps of Polydopamine Formation: A Thermodynamic Approach. *J. Phys. Chem. B* **122**, 6314–6327 (2018).

63. Cencer, M. *et al.* Effect of pH on the rate of curing and bioadhesive properties of dopamine functionalized poly(ethylene glycol) hydrogels. *Biomacromolecules* **15**, 2861–2869 (2014).

64. Yu, J. *et al.* Adhesion of mussel foot protein-3 to TiO2 surfaces: The effect of pH. *Biomacromolecules* **14**, 1072–1077 (2013).

65. Pop-Georgievski, O. *et al.* Poly(ethylene oxide) layers grafted to dopamine-melanin anchoring layer: Stability and resistance to protein adsorption. *Biomacromolecules* **12**, 3232–3242 (2011).

66. Alfieri, M. L. *et al.* The chemistry of polydopamine film formation: The amine-quinone interplay. *Biomimetics* **3**, 26 (2018).

67. Wei, H. *et al.* Stability of polydopamine and poly(DOPA) melanin-like films on the surface of polymer membranes under strongly acidic and alkaline conditions. *Colloids Surf. B. Biointerfaces* **110**, 22–28 (2013).

68. Saiz-Poseu, J., Mancebo-Aracil, J., Nador, F., Busqué, F. & Ruiz-Molina, D. The Chemistry behind Catechol-Based Adhesion. *Angew. Chemie Int. Ed.* **58**, 696–714 (2019).

69. Bernsmann, F. *et al.* Characterization of dopamine-melanin growth on silicon oxide. *J. Phys. Chem. C* **113**, 8234–8242 (2009).

70. Yu, Y. *et al.* Stretching of collapsed polymers causes an enhanced dissipative response of PNIPAM brushes near their LCST. *Soft Matter* **11**, 8508–8516 (2015).

71. Zhang, Q., Weber, C., Schubert, U. S. & Hoogenboom, R. Thermoresponsive polymers with lower critical solution temperature: from fundamental aspects and measuring techniques to recommended turbidimetry conditions. *Mater. Horizons* **4**, 109–116 (2017).

72. Laloyaux, X., Mathy, B., Nysten, B. & Jonas, A. M. Surface and Bulk Collapse Transitions of Thermoresponsive Polymer Brushes. *Langmuir* **26**, 838–847 (2010).

73. Julthongpiput, D., Lin, Y. H., Teng, J., Zubarev, E. R. & Tsukruk, V. V. Y-shaped polymer brushes: Nanoscale switchable surfaces. *Langmuir* **19**, 7832–7836 (2003).

74. Gao, H. & Matyjaszewski, K. Synthesis of molecular brushes by 'grafting onto' method: Combination of ATRP and click reactions. *J. Am. Chem. Soc.* **129**, 6633–6639 (2007).

75. de Gennes, P. G. Introduction to Probability Models. *J. Polym. Sci., Polym. Symp* **13**, 1821 (1980).

76. Qie, R., Zajforoushan Moghaddam, S. & Thormann, E. Parameterization of the optical constants of polydopamine films for spectroscopic ellipsometry studies. *Phys. Chem. Chem. Phys.* **23**, 5516–5526 (2021).

77. Wei, Q. & Haag, R. Universal polymer coatings and their representative biomedical applications. *Mater. Horizons* **2**, 567–577 (2015).

78. Soundararajan, S., Reddy, B. S. R. & Rajadurai, S. Synthesis and characterization of glycidyl methacrylate-styrene copolymers and determination of monomer reactivity ratios. *Polymer (Guildf).* **31**, 366–370 (1990).

79. Lillethorup, M., Shimizu, K., Plumeré, N., Pedersen, S. U. & Daasbjerg, K. Surface-attached poly(glycidyl methacrylate) as a versatile platform for creating dual-functional polymer brushes. *Macromolecules* **47**, 5081–5088 (2014).

80. Barbey, R. & Klok, H. A. Room temperature, aqueous post-polymerization modification of glycidyl methacrylate-containing polymer brushes prepared via surface-initiated atom transfer radical polymerization. *Langmuir* **26**, 18219–18230 (2010).

81. Hou, L. & Wu, P. Comparison of LCST-transitions of homopolymer mixture, diblock and statistical copolymers of NIPAM and VCL in water. *Soft Matter* **11**, 2771–2781 (2015).

82. Qi, X. *et al.* Development of novel hydrogels based on Salecan and poly(: N -isopropylacrylamide- co -methacrylic acid) for controlled doxorubicin release. *RSC Adv.* **6**, 69869–69881 (2016).

83. Aspnes, D. E., Theeten, J. B. & Hottier, F. Investigation of effective-medium models of microscopic surface roughness by spectroscopic ellipsometry. *Phys. Rev. B* **20**, 3292–3302 (1979).

84. Saunders, B. R. On the structure of poly(N-isopropylacrylamide) microgel particles. *Langmuir* **20**, 3925–3932 (2004).

2.7 Supporting Information

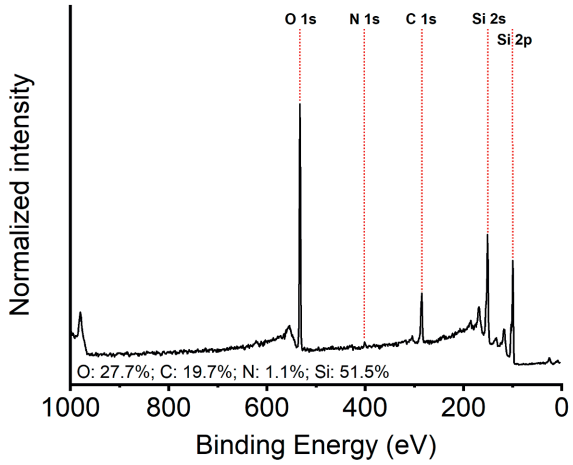

Supp. Figure 4.1 XPS wide scan of poly(dopamine) deposited in the presence of $NaIO_4$ from NaOAc buffer at pH 4 after 40 minutes.

pH 4 – $NaIO_4$ 50 min Thickness = 2.0 ± 0.7 nm RMS = 1.7 ± 0.2 nm	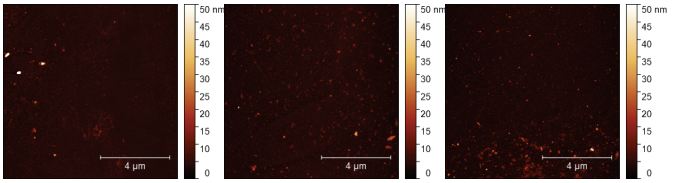
pH 4 – $NaIO_4$ 60 min Thickness = 4.6 ± 0.8 nm RMS = 6.3 ± 5.7 nm	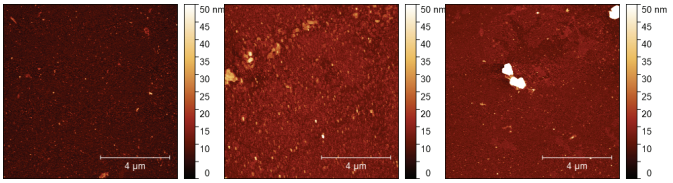
pH 4 – $NaIO_4$ 70 min Thickness = 9.6 ± 0.9 nm RMS = 3.7 ± 0.4 nm	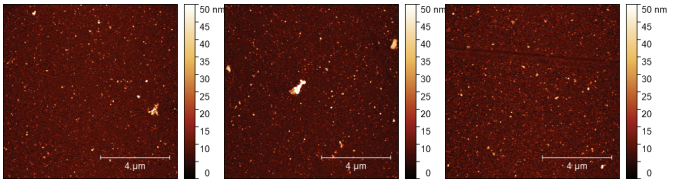
pH 4 – $NaIO_4$ 80 min Thickness = 14.7 ± 1.4 nm RMS = 6.4 ± 0.6 nm	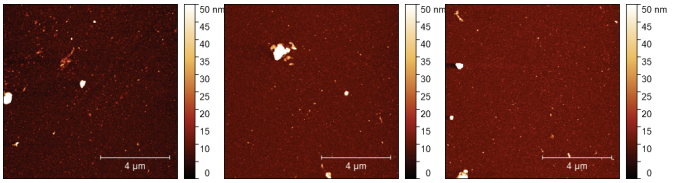
pH 4 – $NaIO_4$ 90 min Thickness = 18.7 ± 0.9 nm RMS = 7.8 ± 4.9 nm	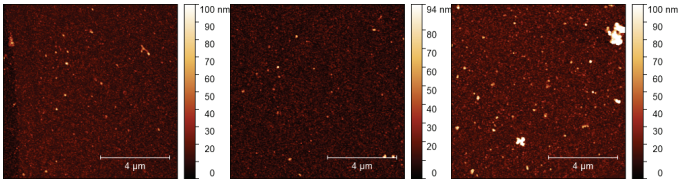

Supp. Figure 4.2 AFM images measured to determine the average roughness values (RMS) for poly(dopamine) films deposited from NaOAc buffer (pH 4) in the presence of 10 mM $NaIO_4$.

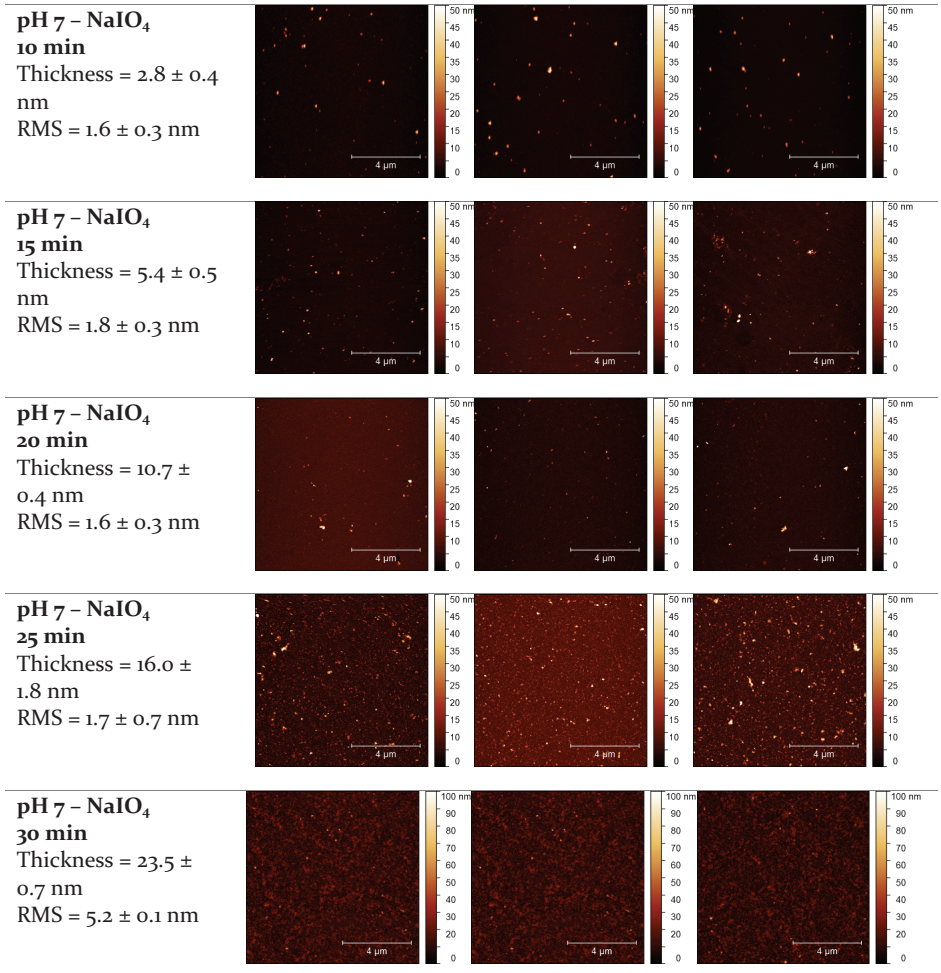

Supp. Figure 4.3 AFM images measured to determine the average roughness values (RMS) for poly(dopamine) films deposited from NaOAc buffer (pH 7) in the presence of 10 mM $NaIO_4$.

Tris **30 min** Thickness = 2.8 ± 0.9 nm RMS = 2.2 ± 0.5 nm	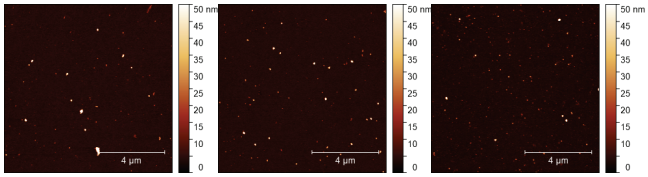
Tris **60 min** Thickness = 5.9 ± 0.7 nm RMS = 6.8 ± 1.2 nm	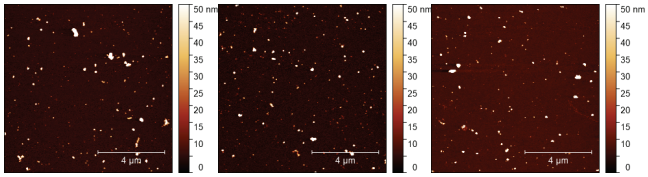
Tris **90 min** Thickness = 12.5 ± 1.9 nm RMS = 13.1 ± 1.5 nm	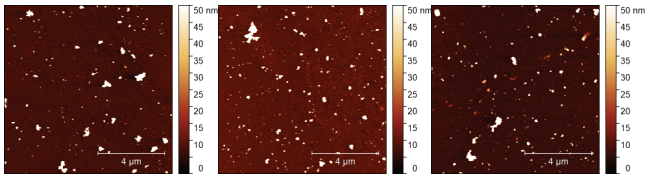
Tris **120 min** Thickness = 13.5 ± 0.8 nm RMS = 16.4 ± 2.2 nm	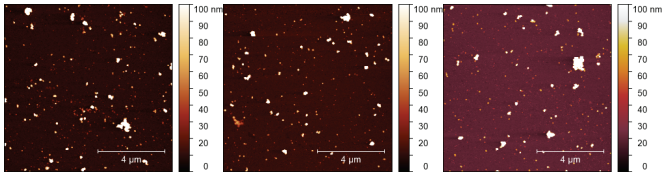
Tris **180 min** Thickness = 17.1 ± 1.8 nm RMS = 25.2 ± 5.7 nm	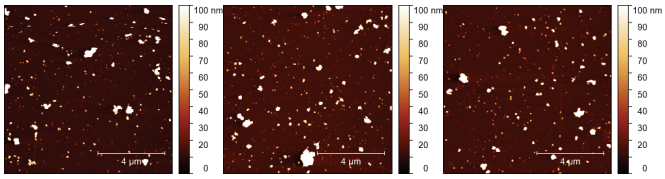
Tris **240 min** Thickness = 21.0 ± 2.0 nm RMS = 34.4 ± 6.3 nm	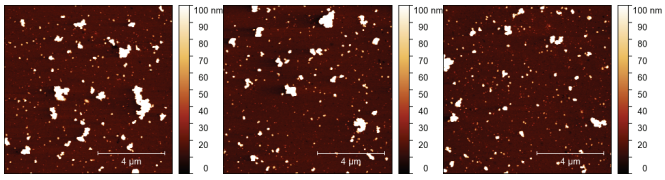

Supp. Figure 4.4 AFM images measured to determine the average roughness values (RMS) for poly(dopamine) films deposited from Tris buffer (pH 8.5).

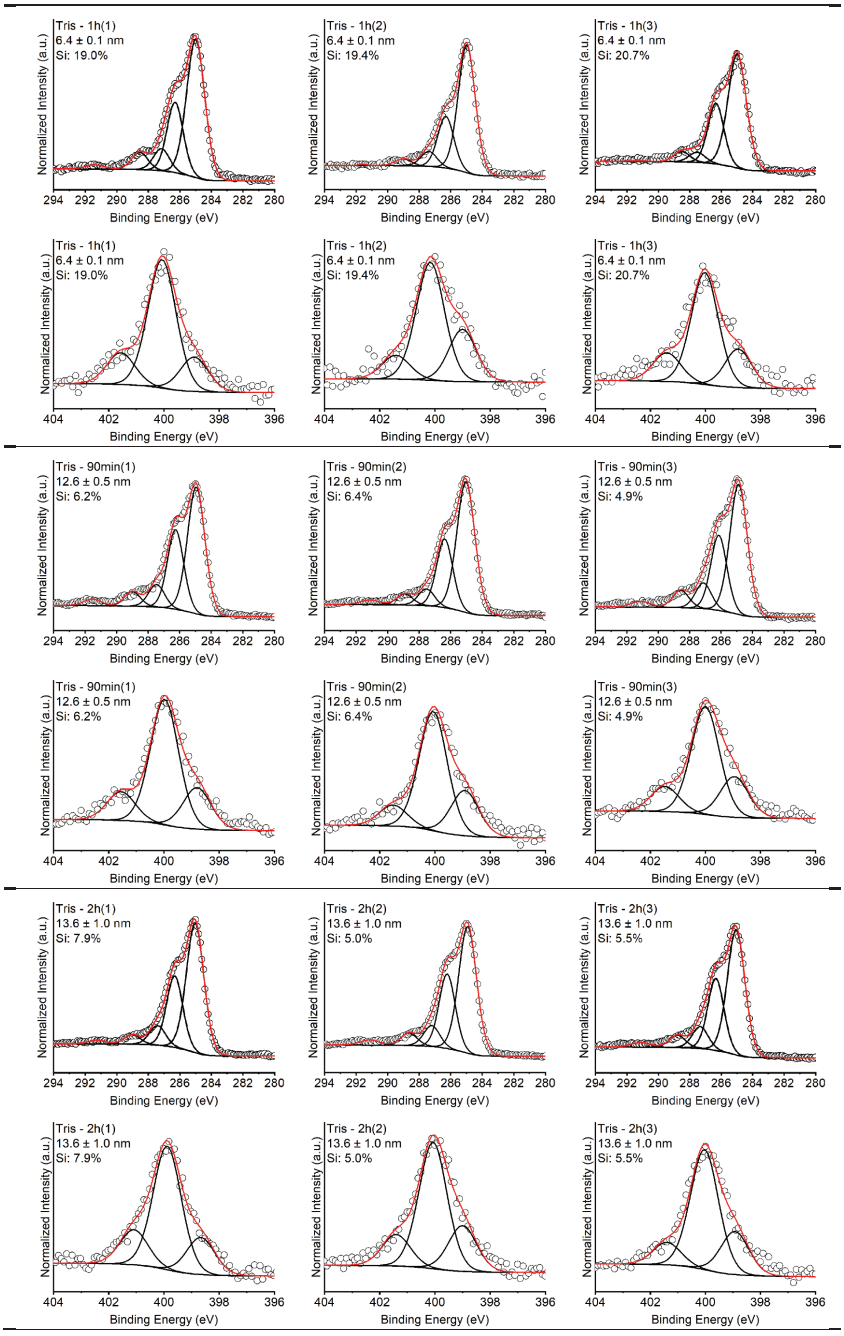

Supp. Figure 4.5 XPS C 1s and N 1s narrow scan spectra of poly(dopamine) deposited from Tris buffer (pH 8.5).

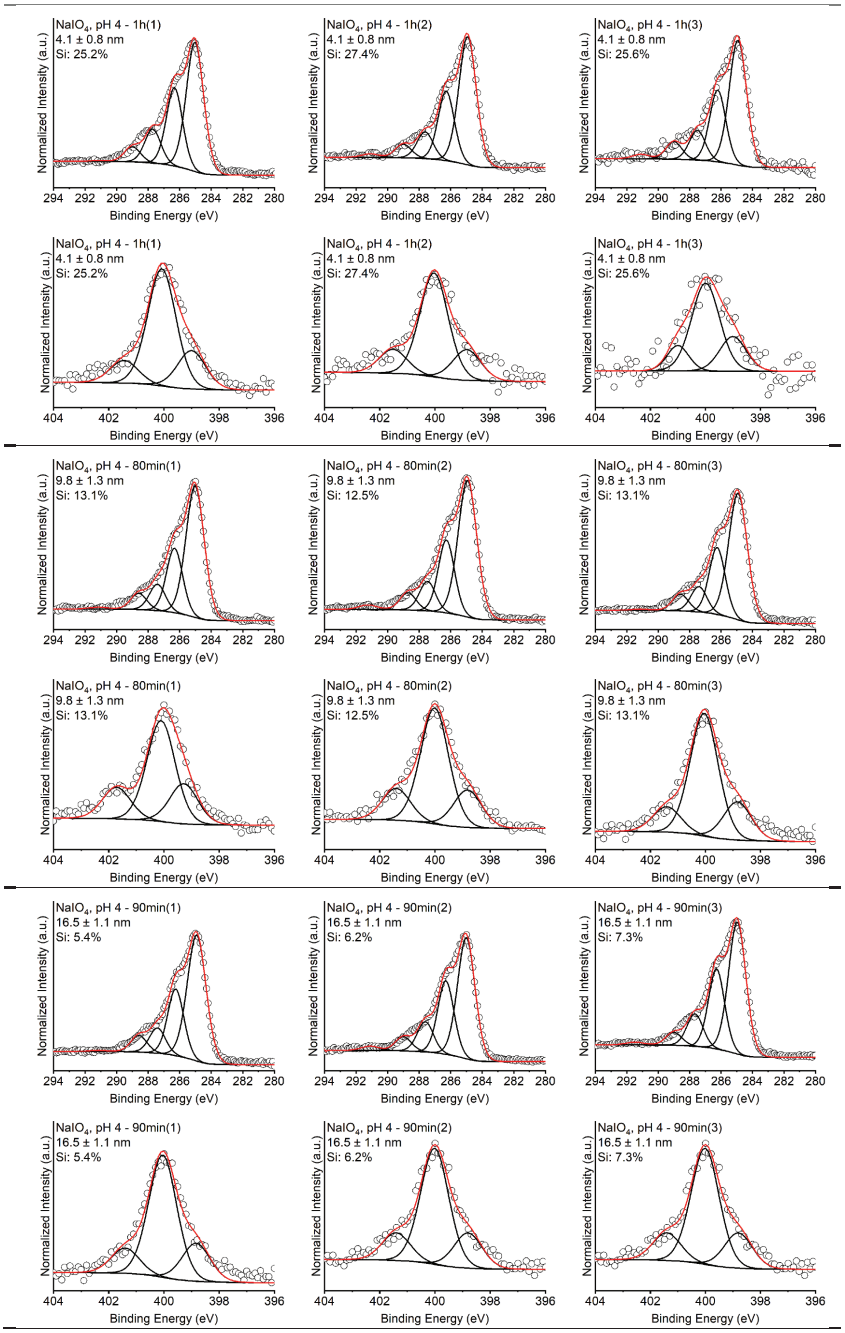

Supp. Figure 4.6 XPS C 1s and N 1s narrow scan spectra of poly(dopamine) deposited from NaOAc buffer in the presence of 10 mM $NaIO_4$ (pH 4).

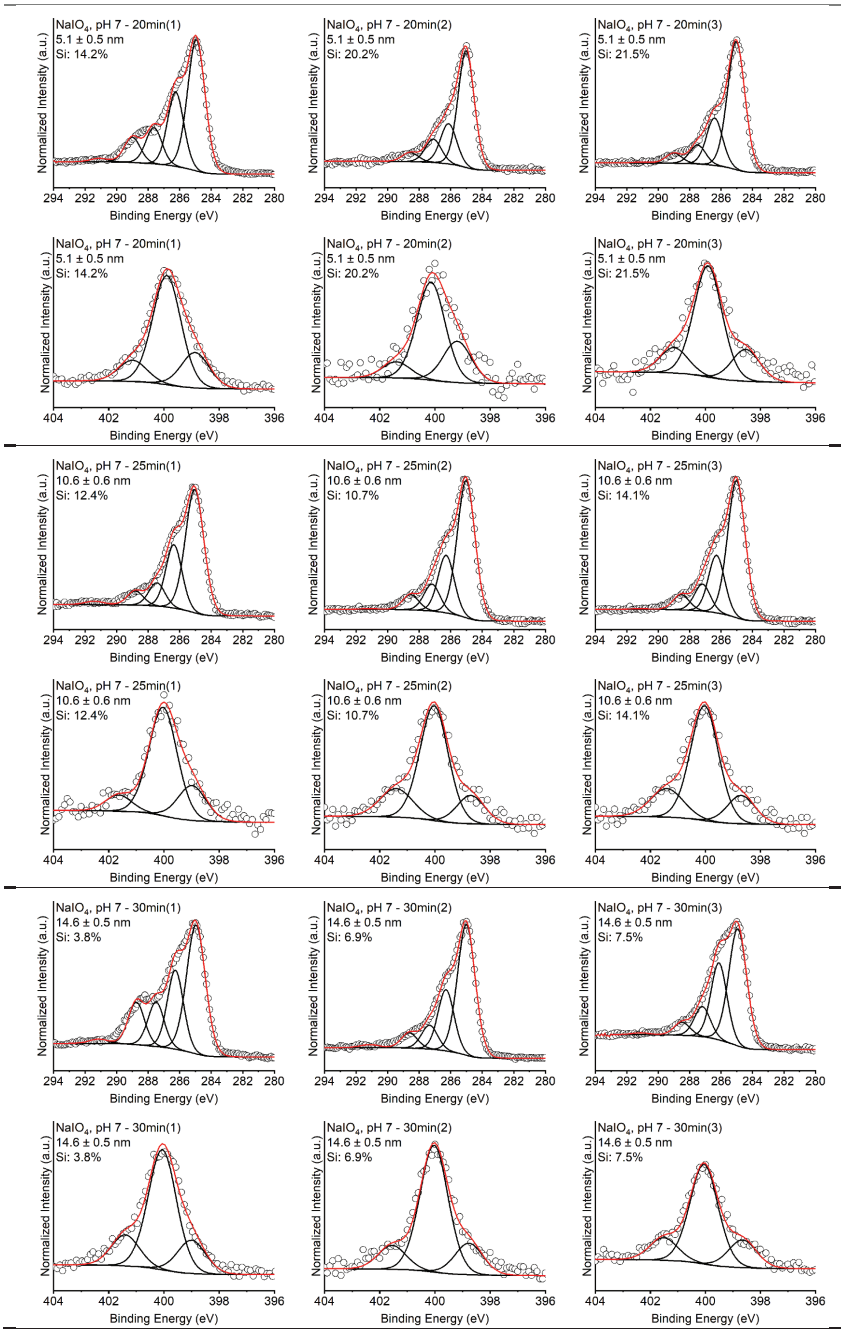

Supp. Figure 4.7 XPS C 1s and N 1s narrow scan spectra of poly(dopamine) deposited from NaOAc buffer in the presence of 10 mM $NaIO_4$ (pH 7).

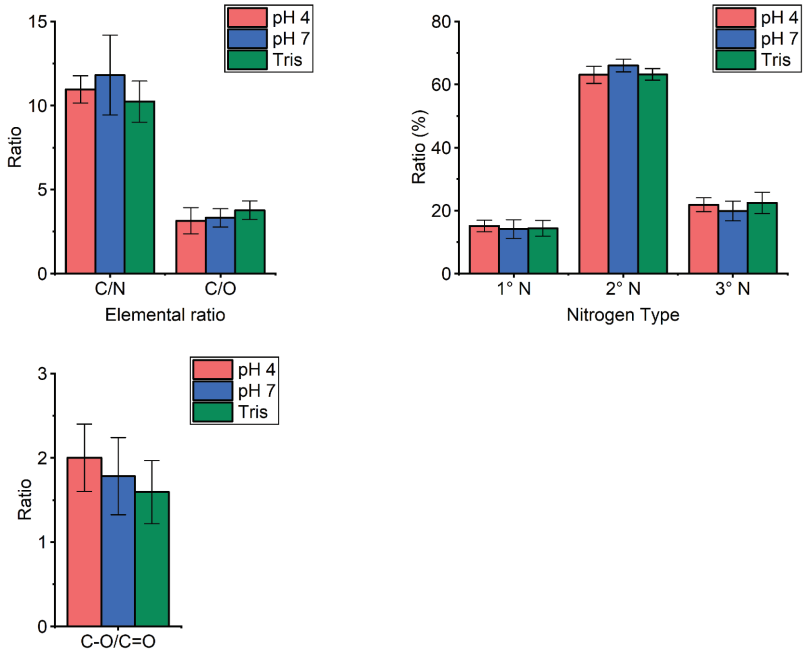

Supp. Figure 4.8 (A) Elemental ratio, **(B)** C–O/C=O ratio and **(C)** ratio between primary, secondary and tertiary nitrogen species obtained from XPS wide scan, C 1s narrow scan and N 1s narrow scan spectra.

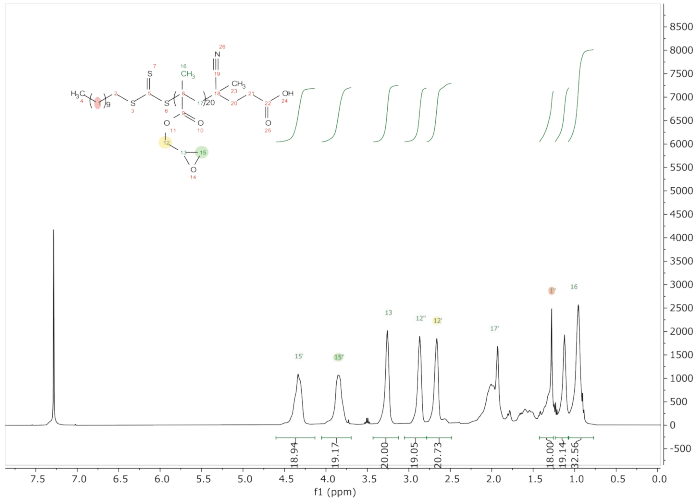

Supp. Figure 4.9 ^{1}H-NMR spectrum of poly(GMA)$_{20}$-MacroRAFT ($CDCl_3$, 400 MHz, 298 K).

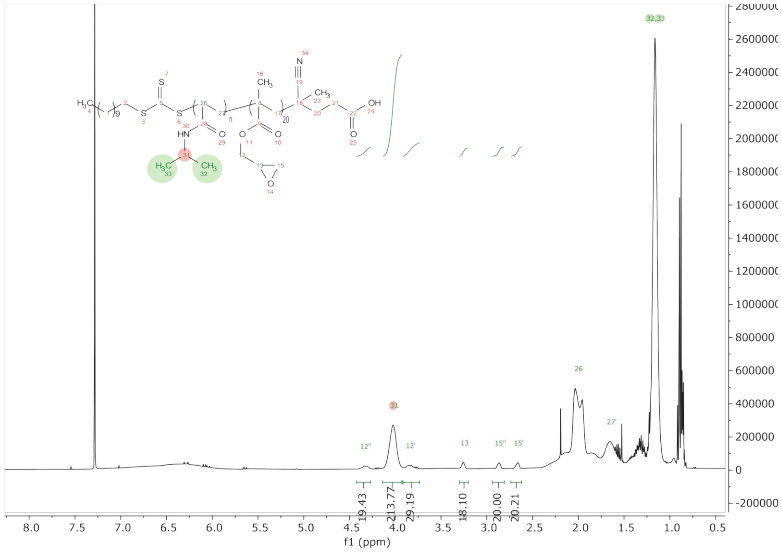

Supp. Figure 4.10 ^{1}H-NMR spectrum of poly(GMA)$_{20}$-*b*-poly(NIPAM)$_{210}$ ($CDCl_3$, 400 MHz, 298 K).

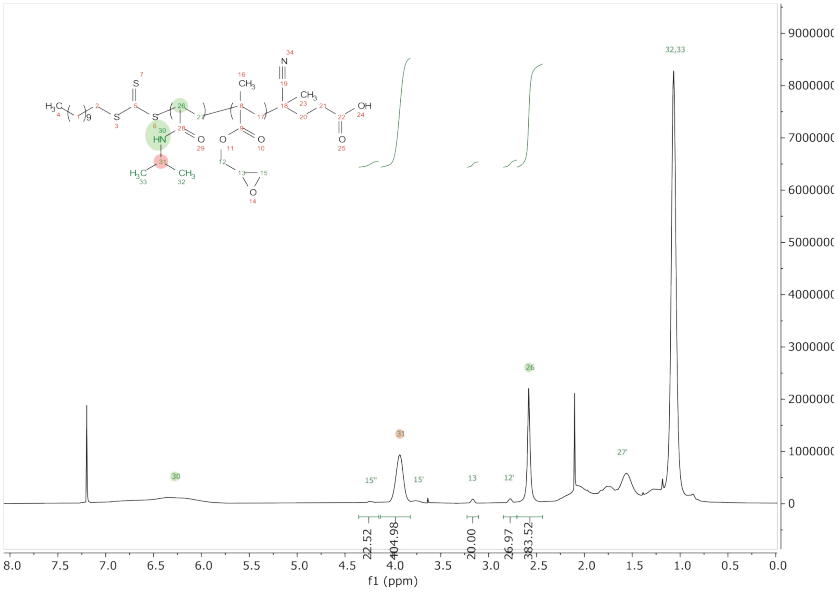

Supp. Figure 4.11 ^{1}H-NMR spectrum of poly(GMA)$_{20}$-*b*-poly(NIPAM)$_{404}$ ($CDCl_3$, 400 MHz, 298 K).

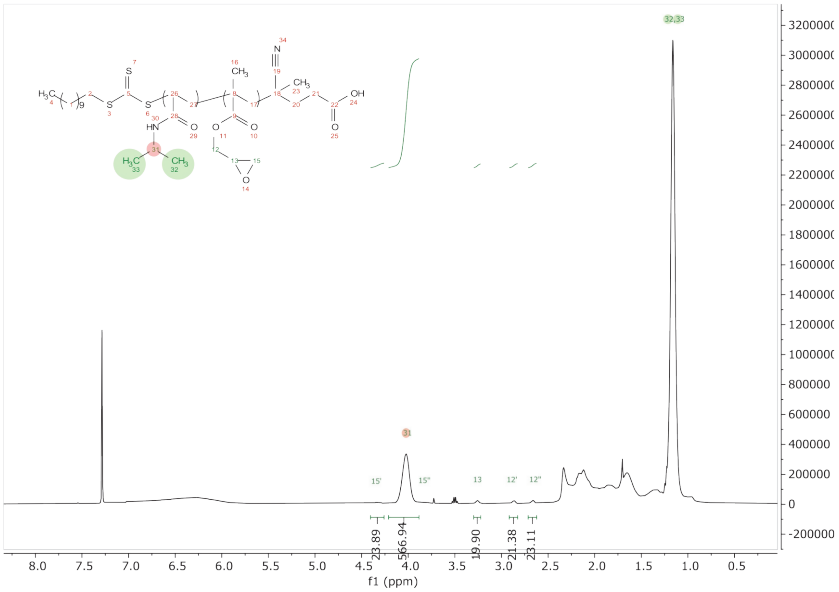

Supp. Figure 4.12 ^{1}H-NMR spectrum of poly(GMA)$_{20}$-*b*-poly(NIPAM)$_{566}$ ($CDCl_3$, 400 MHz, 298 K).

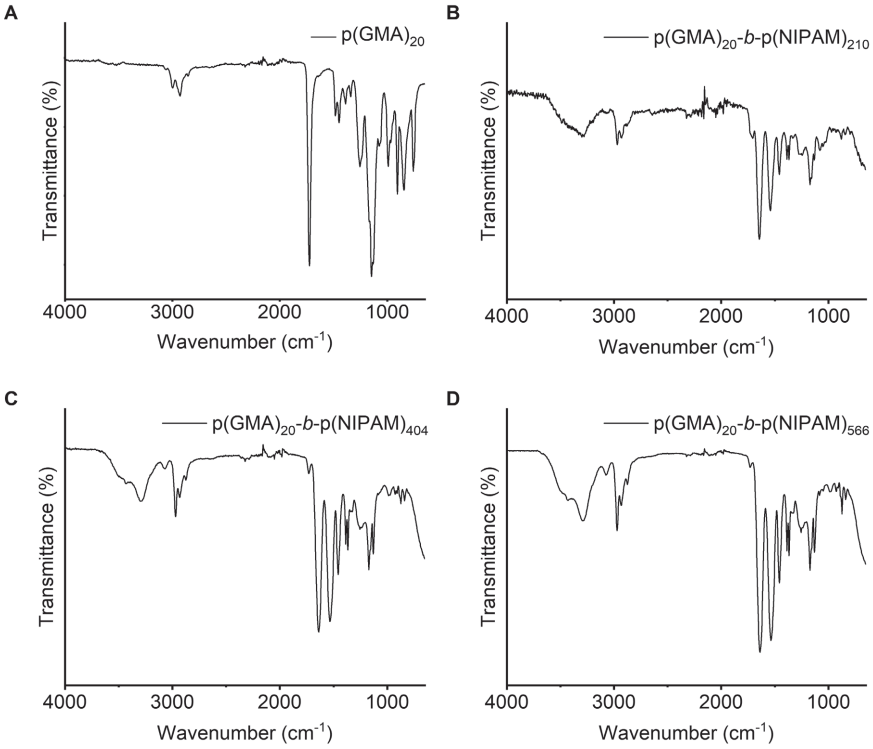

Supp. Figure 4.13 FT-IR spectra of **(A)** poly(GMA)$_{20}$, **(B)** poly(GMA)$_{20}$-*b*-poly(NIPAM)$_{210}$, **(C)** poly(GMA)$_{20}$-*b*-poly(NIPAM)$_{404}$ and **(D)** poly(GMA)$_{20}$-*b*-poly(NIPAM)$_{566}$.

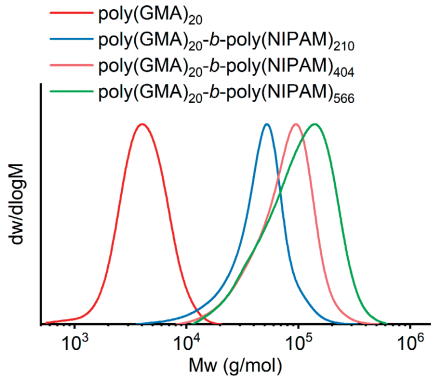

Supp. Figure 4.14 GPC traces of poly(GMA)$_{20}$ and poly(GMA)$_{20}$-*b*-poly(NIPAM)$_{210}$, poly(GMA)$_{20}$-*b*-poly(NIPAM)$_{404}$ and poly(GMA)$_{20}$-*b*-poly(NIPAM)$_{566}$.

Supp. Table 4.1 Analysis of poly(GMA)$_{20}$ and poly(GMA)$_{20}$-*b*-poly(NIPAM)$_{210}$, poly(GMA)$_{20}$-*b*-poly(NIPAM)$_{404}$ and poly(GMA)$_{20}$-*b*-poly(NIPAM)$_{566.}$

	M_n (kDa)	M_w (kDa)	Đ	n_{GPC}	n_{NMR}
Poly(GMA)$_{20}$	3.6	4.6	1.27	19.7	20
Poly(GMA)$_{20}$-*b*-poly(NIPAM)$_{210}$	37.9	51.9	1.37	295	210
Poly(GMA)$_{20}$-*b*-poly(NIPAM)$_{404}$	62.2	87.4	1.40	525	404
Poly(GMA)$_{20}$-*b*-poly(NIPAM)$_{566}$	78.3	124.2	1.58	661	566

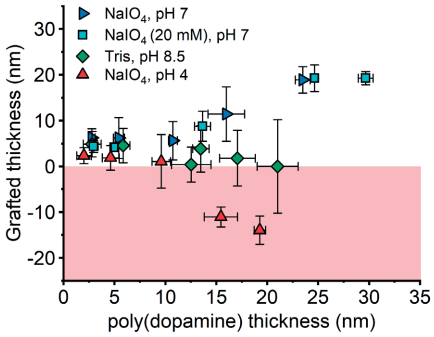

Supp. Figure 4.15 Change in film thickness following grafting of poly(GMA)$_{20}$-*b*-poly(NIPAM)$_{210}$ to poly(dopamine) layers as a function of poly(dopamine) thickness prior to reaction, as determined by spectroscopic ellipsometry. The red area in the graph indicates loss of material during reaction. Figure including grafting reactions on poly(dopamine) deposited from Tris buffer.

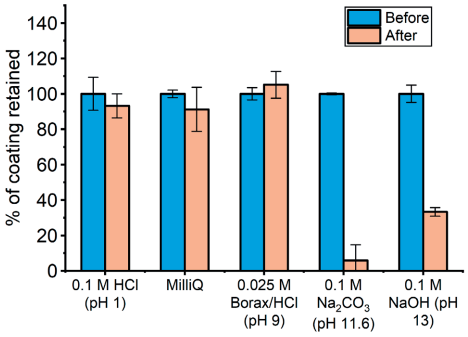

Supp. Figure 4.16 Stability measurements for poly(dopamine) films deposited from NaOAc buffer (pH 7) in the presence of 10 mM $NaIO_4$ and subsequently modified with poly(GMA)$_{20}$-*b*-poly(NIPAM)$_{210}$. The surfaces were exposed to aqueous solutions of varying pH for 24 h. The coating thickness was measured before and after exposure using spectroscopic ellipsometry.

Poly dopamine
Thickness = 29.4 ± 0.7 nm
R_q = 9.4 ± 0.5 nm

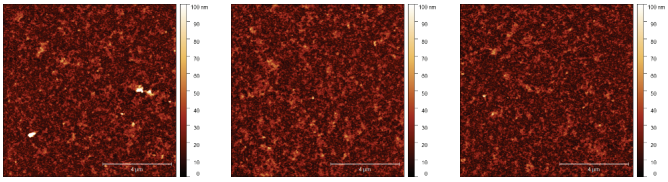

Control experiment
After DMSO, 5% TEA, 80 °C, overnight

Thickness = 30.8 ± 2.3 nm
R_q = 10.9 ± 0.3 nm

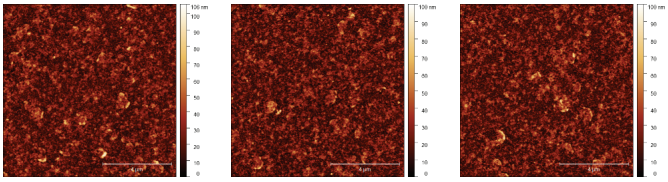

Supp. Figure 4.17 AFM images of poly(dopamine) before and after exposure to grafting conditions without the presence of block copolymer. Roughness values are obtained using AFM, thickness values were obtained using spectroscopic ellipsometry.

Grafted block copolymer thickness = 6.3 ± 2.0 nm RMS = 1.7 ± 0.7 nm	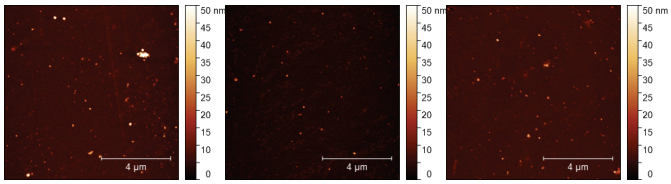
Grafted block copolymer thickness = 6.2 ± 4.5 nm RMS = 2.5 ± 1.2 nm	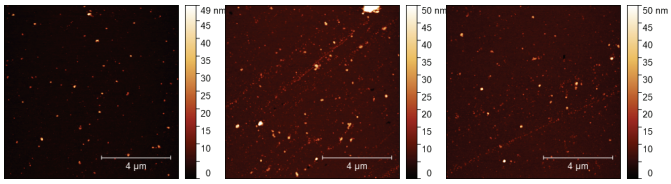
Grafted block copolymer thickness = 5.6 ± 4.2 nm RMS = 4.4 ± 3.7 nm	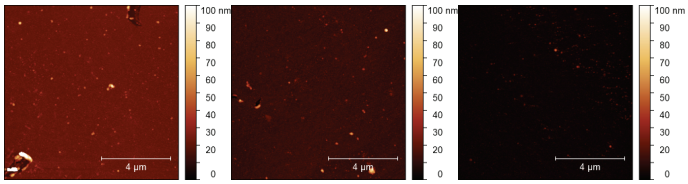
Grafted block copolymer thickness = 11.5 ± 5.9 nm RMS = 10.2 ± 0.5	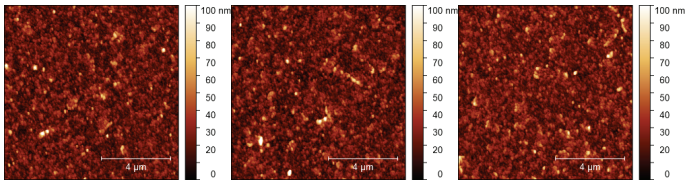
Grafted block copolymer thickness = 18.9 ± 2.9 nm RMS = 24.2 ± 3.6 nm	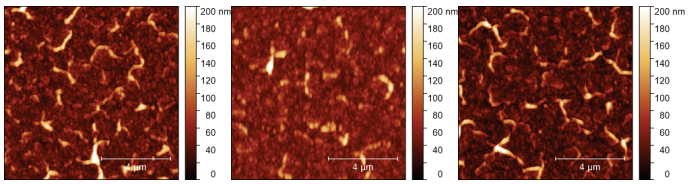

Supp. Figure 4.18 AFM images measured to determine the average roughness values (RMS) for poly(dopamine) films deposited from NaOAc buffer (pH 7) in the presence of 10 mM $NaIO_4$ and subsequently modified with poly(GMA)$_{20}$-*b*-poly(NIPAM)$_{210}$.

Grafted block copolymer thickness = 9.7 ± 2.9 nm RMS = 1.1 ± 0.1 nm	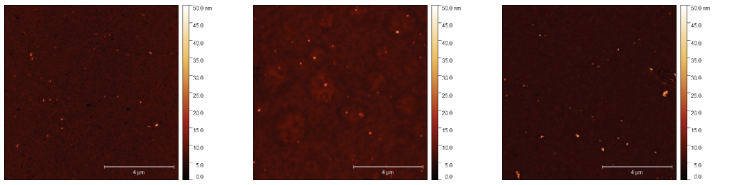
Grafted block copolymer thickness = 7.9 ± 4.6 nm RMS = 2.2 ± 0.5 nm	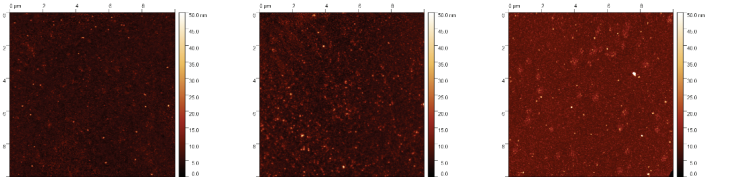
Grafted block copolymer thickness = 8.9 ± 4.6 nm RMS = 7.8 ± 5.3 nm	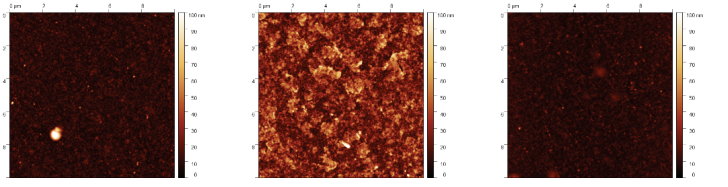
Grafted block copolymer thickness = 15.4 ± 2.1 nm RMS = 11.4 ± 1.1	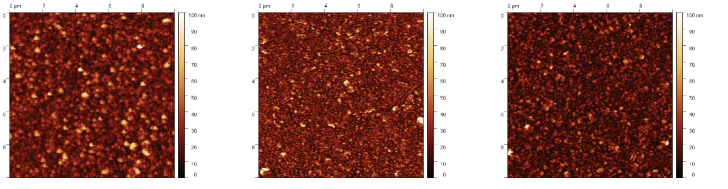
Grafted block copolymer thickness = 14.3 ± 2.9 nm RMS = 14.9 ± 2.1 nm	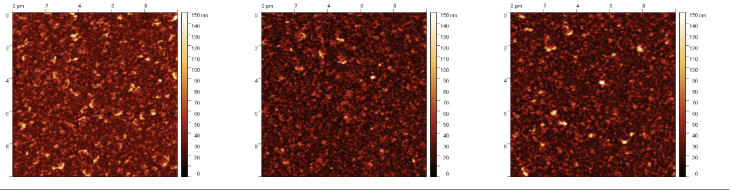

Supp. Figure 4.19 AFM images measured to determine the average roughness values (RMS) for poly(dopamine) films deposited from NaOAc buffer (pH 7) in the presence of 10 mM $NaIO_4$ and subsequently modified with poly(GMA)$_{20}$-*b*-poly(NIPAM)$_{404}$.

Grafted block copolymer thickness = 5.9 ± 1.7 nm RMS = 2.2 ± 0.5 nm	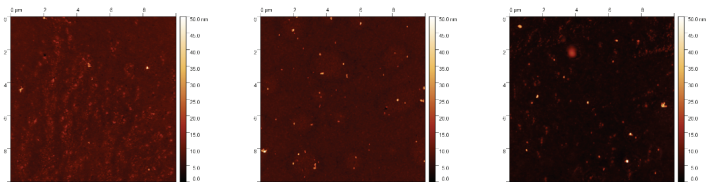
Grafted block copolymer thickness = 9.7 ± 4.5 nm RMS = 2.2 ± 0.1 nm	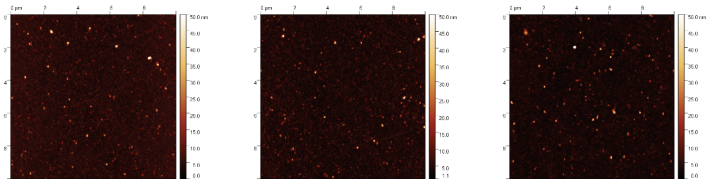
Grafted block copolymer Thickness = 8.3 ± 1.5 nm RMS = 4.6 ± 0.2 nm	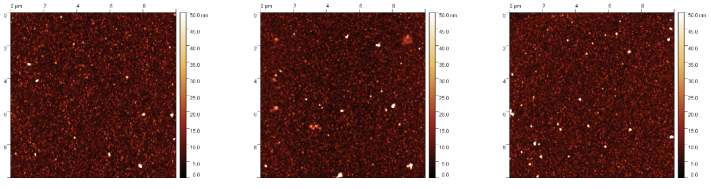
Grafted block copolymer thickness = 12.6 ± 1.7 nm RMS = 11.8 ± 0.6	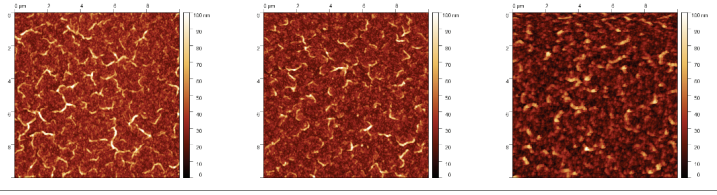
Grafted block copolymer thickness = 12.4 ± 4.3 nm RMS = 24.4 ± 5.4 nm	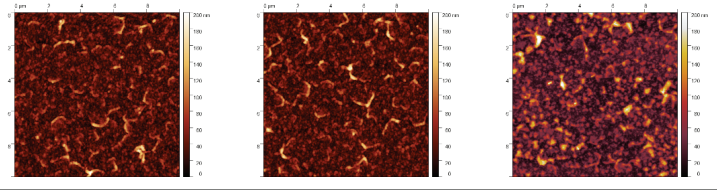

Supp. Figure 4.20 AFM images measured to determine the average roughness values (RMS) for poly(dopamine) films deposited from NaOAc buffer (pH 7) in the presence of 10 mM $NaIO_4$ and subsequently modified with poly(GMA)$_{20}$-*b*-poly(NIPAM)$_{566}$.

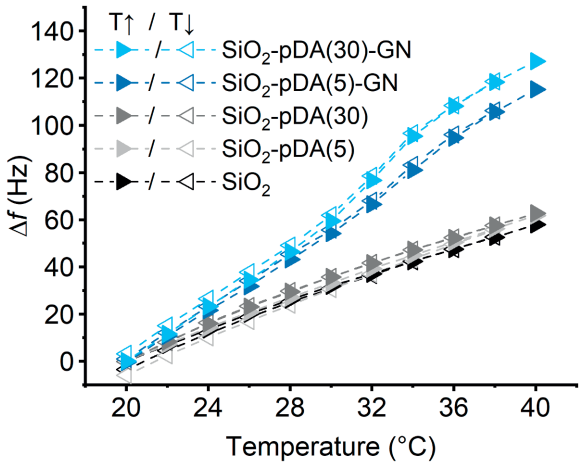

Supp. Figure 4.21 Frequency change as a function of temperature, measured by QCM-D.

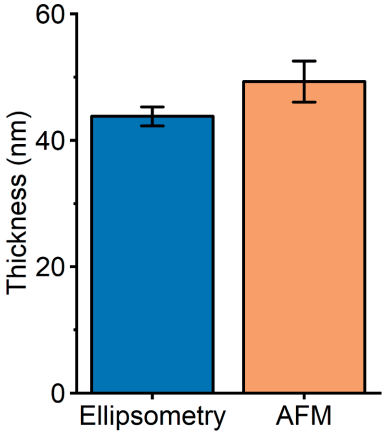

Supp. Figure 4.22 Comparison between thickness values obtained using spectroscopic ellipsometry and AFM.

pH 7 poly(dopamine) modified with poly(GMA)-*b*-poly(NIPAM) Scratch area 1	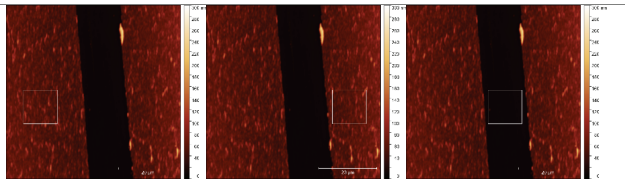
pH 7 poly(dopamine) modified with poly(GMA)-*b*-poly(NIPAM) Scratch area 2	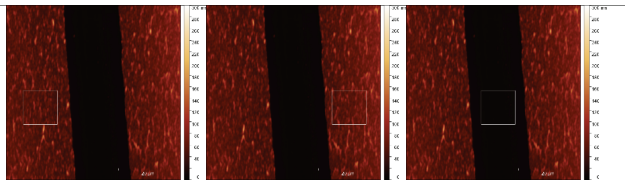
pH 7 poly(dopamine) modified with poly(GMA)-*b*-poly(NIPAM) Scratch area 3	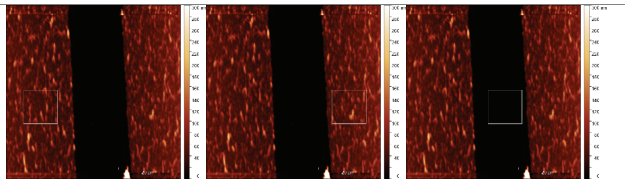

Supp. Figure 4.23 AFM images measured to determine the thickness of the poly(dopamine)–poly(GMA)-*b*-poly(NIPAM) layer. A scratched area is imaged and three areas of interest are selected: Two for the organic layer on each side of the brush and one for the scratched area. The thickness is calculated by subtraction of the mean height of the region of interest in the scratched area from the mean height of the regions of interest for the organic layers.

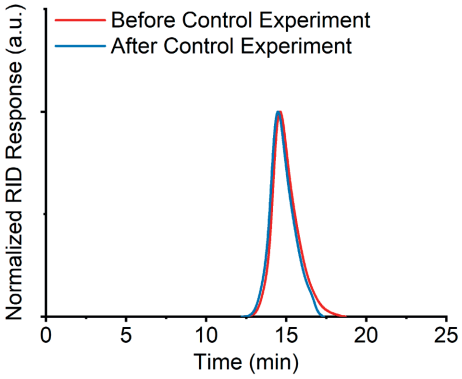

Supp. Figure 4.24 GPC traces of poly(GMA)$_{20}$-*b*-poly(NIPAM)$_{210}$ before and after control experiment to determine occurrence of cross-linking under grafting conditions in the absence of a poly(dopamine) substrate (overnight in DMF with 5% TEA at 80 °C).

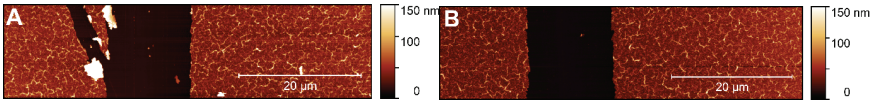

Supp. Figure 4.25 AFM study to investigate potential rupture effects for poly(GMA)$_{20}$-*b*-poly(NIPAM)$_{566}$-modified substrate. AFM images show the substrate which was scratched with a medical needle to calculate film thickness **(A)** before (average thickness 32.7 nm) and **(B)** after sonication in acetone for 10 minutes (average thickness 34.4 nm). No sign of rupture was observed upon sonication.

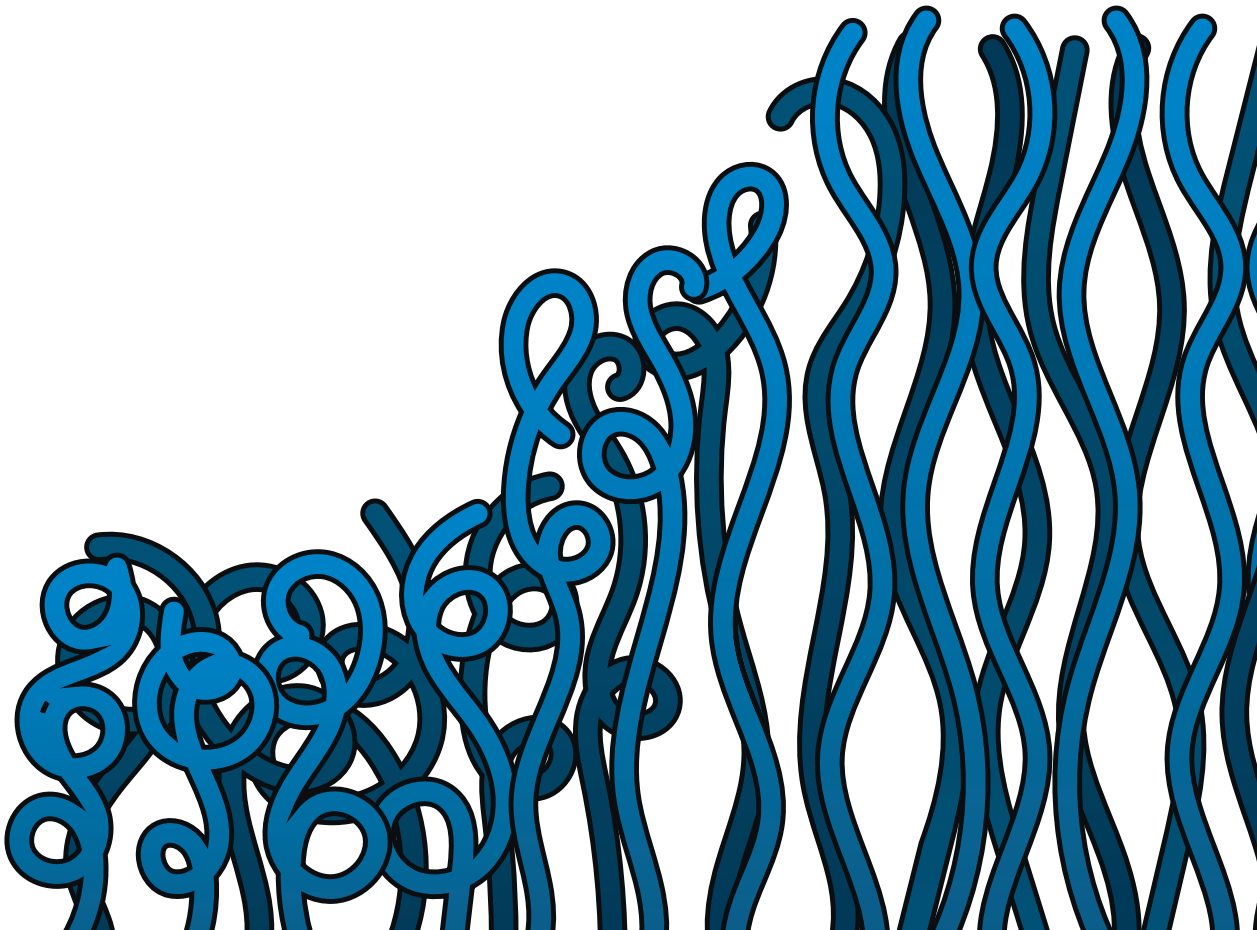

Chapter 5

Modular and Substrate-Independent Grafting-to Procedure for Functional Polymer Coatings

Teunissen, L. W., Smulders, M. M. J. & Zuilhof, H.,
Modular and Substrate-Independent Grafting-to Procedure for Functional Polymer Coatings
Langmuir, Manuscript Accepted (2023).

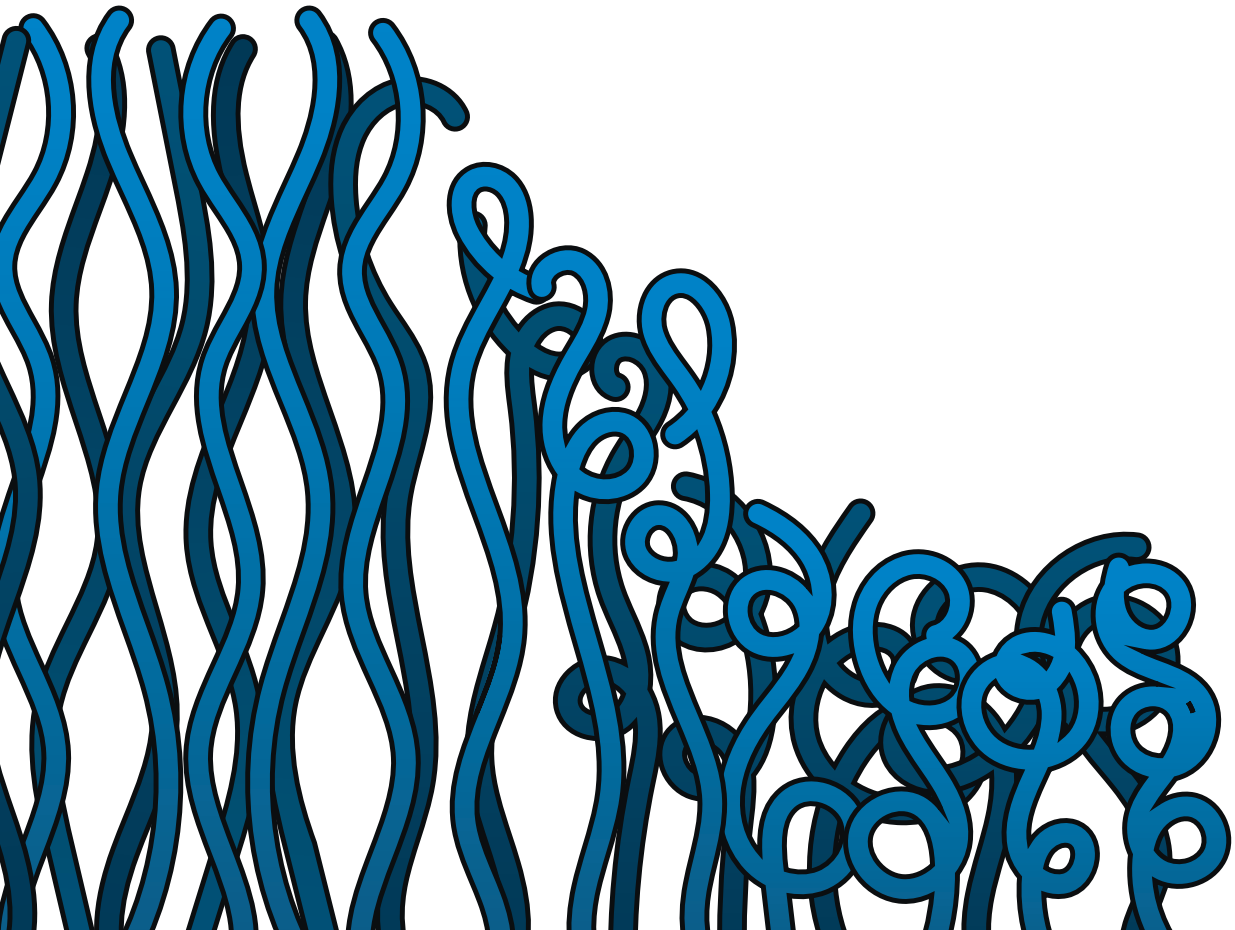

Abstract

The ability to tailor polymer brush coatings to the last nanometer has arguably placed them among the most powerful surface modification techniques currently available. Generally, the synthesis procedures for polymer brushes are designed for a specific surface type and monomer functionality, and cannot be easily employed otherwise. In this Chapter, we describe a modular and straightforward two-step grafting-to approach that allows introduction of polymer brushes of a desired functionality onto a large range of chemically different substrates. To illustrate the modularity of the procedure, gold, silicon oxide (SiO_2) and polyester-coated glass substrates were modified with five different block copolymers. In short, the substrates were first modified with a universally applicable poly(dopamine) primer layer. Subsequently, a grafting-to reaction was performed on the poly(dopamine) films using five distinct block copolymers, all of which contained a short poly(glycidyl methacrylate) segment and a longer segment of varying chemical functionality. Ellipsometry, X-ray photoelectron spectroscopy and static water contact angle measurements confirmed successful grafting of all five block copolymers to the poly(dopamine)-modified gold, SiO_2 and polyester-coated glass substrates. In addition, our method was used to provide direct access to binary brush coatings, by simultaneous grafting of two different polymer materials. The ability to synthesize binary brush coatings further adds to the versatility of our approach and paves the way towards production of novel multifunctional and responsive polymer coatings.

5.1 Introduction

Polymer coatings are employed ubiquitously to introduce specific surface properties required for an intended application. Control over coating properties, such as chemical functionality, polymer density and film thickness can be achieved especially using polymer brushes.[1–3] This type of coating consists of end-tethered polymer chains, densely packed on a material's surface. Generally, these polymers are either grown from surface-immobilized initiator molecules, commonly known as the grafting-from approach, or synthesized in solution and subsequently attached to the target substrate, called the grafting-to approach.[2,4]

Evidently, the chemical and physical characteristics of the target substrate vary significantly for different materials. Due to these characteristics, the synthesis procedures for polymer brush coatings are typically substrate-dependent and cannot be applied modularly.[5,6] For example, initiator molecules regularly employed for surface-initiated polymerizations typically contain disulfide/thiol or silane anchoring groups, and are applied specifically to noble metal and hydroxyl-terminated substrates, respectively.[2,7–9] The same consideration has to be taken into account for grafting-to procedures, in which anchoring motifs present in the presynthesized polymers are required to bind to reactive groups present on the substrate's surface.[4] Such complementary reactive groups are not inherently present on all surface types and treatment with a primer layer can be necessary to introduce these.[6,10] Naturally, to ensure a high durability of the coating, this primer layer requires a strong affinity for the substrate it is applied to.

The number of surface modification reactions that can be applied universally to any surface type is small.[5] The procedure that has perhaps gained most traction over the past years is modification of surfaces with poly(dopamine) films.[11–14] Inspired by mussel adhesive proteins, poly(dopamine) films have been demonstrated to successfully bind to virtually any surface type ranging from high energy surfaces such as noble metals and steel, to low-energy surfaces including polyethylene and polystyrene.[11] Moreover, deposition does not require prior activation through, for example, wet etching or plasma treatment.[15–18] The functional groups present in poly(dopamine) films, such as hydroxyl and amine groups, allow the layers to be used as primer material to perform subsequent surface modifications through formation of stable covalent bonds. In fact, the combination of broad applicability towards different surface types, procedural simplicity and low cost of the deposition procedure has resulted in a large number of reports in which poly(dopamine) was employed to synthesize polymer brush coatings.[19–35]

Polymer brush coatings that were produced using poly(dopamine) as a primer layer were predominantly synthesized using the grafting-from approach, during which poly(dopamine) is functionalized with initiator molecules from which surface-initiated polymerization is then performed.[19,20,24,25,27–30] In addition, there are several examples of polymers synthesized in solution and subsequently successfully grafted onto poly(dopamine) primer layers.[32–34,36] The main advantages to this strategy are the ease of application and the possibility to fully characterize polymer properties before attachment to the substrate. Moreover, grafting-to represents the most straightforward approach to produce binary and ternary polymer brush systems, *i.e.*, polymer brushes in which several chemical different polymer chains are attached onto the surface in one step.[37–40]

Development of a standardized grafting-to procedure that can successfully bind different polymer types to poly(dopamine) primer layers would further remove a bottleneck in polymer brush synthesis methods. That procedure would allow the introduction of effectively any surface property to a substrate, irrespective of the chemical nature of the substrate or polymer. Two approaches that demonstrate modular surface modifications have been reported in recent years. The first procedure relies on one-step codeposition of dopamine with acrylate monomers that bear different functional groups.[41,42] It was suggested that the monomers are incorporated in the poly(dopamine) structure during the polymerization of dopamine, yielding a covalent poly(dopamine)/mono-acrylate network.[42] Although this approach is appealing due to its unmatched simplicity, the presence of dopamine throughout the entire network will strongly influence the surface properties of the resulting layer. A second procedure for modular surface modification involves block copolymers carrying glycidyl methacrylate (GMA) units that were reacted with (3-aminopropyl)triethoxysilane (APTES) functionalized substrates.[43] As mentioned above, silane monolayers can be used to modify several types of surfaces, but cannot be employed as universally as poly(dopamine) films.[6] The APTES monolayers were introduced following acid and plasma activation of the substrate, and then modified with various block copolymers.[43] Using this procedure, a broad range of surface functionalities on silicon substrates was obtained successfully and then tested extensively. Although the method worked well for silicon substrates, the modification of different substrate types revealed inconsistent surface properties, indicating that the procedure is not substrate-independent.

Using the insights developed in the above studies, our group developed an approach to overcome the aforementioned limitations. In Chapter 3 and Chapter 4, we have presented a two-step grafting-to procedure that consists of poly(dopamine) deposition on SiO_2 followed by grafting of poly(GMA)-*b*-poly(NIPAM) block copolymers.[44,45] In contrast to the two coating strategies described above, we demonstrated that our procedure could

achieve polymer brush coatings of appreciable grafting density, and with thicknesses up to 19 nm. Yet, the procedure was exclusively performed on SiO_2 substrates using poly(GMA)-*b*-poly(NIPAM). In this Chapter, we broaden the scope of that procedure and demonstrate that it can be employed modularly, irrespective of surface type or polymer functionality (Scheme 5.1).

Scheme 5.1 Illustration of the grafting-to reaction employed in this study. A range of block copolymers (shown in red) of various compositions is grafted to poly(dopamine)-modified SiO_2, gold and PE substrates.

To illustrate the scope of the grafting-to procedure presented in this study, three substrate types with widely varying chemical characteristics were selected as target substrates: gold (as, *e.g.*, relevant for biomedical applications like surface plasmon resonance (SPR) sensing.[46–48]), silicon with a native silicon oxide layer (SiO_2) (given its use in biomedical applications and photovoltaics[49,50]), and polymer-coated glass (PE), to demonstrate that the procedure can be applied to polymeric substrates, which are generally difficult to efficiently functionalize.[17] To further illustrate the modularity of the procedure, five different block copolymers were synthesized via radical addition-fragmentation chain-transfer (RAFT) polymerization, all of which contained a short poly(glycidyl methacrylate) (poly(GMA)) segment that was incorporated to bind to the amine groups present in the poly(dopamine) film. The monomers used for the longer, second segment vary within the series of block copolymers, and were selected to give rise to widely different surface properties in the final polymer coatings. The produced coatings were analyzed using spectroscopic ellipsometry, static water contact angle (SWCA) measurements and X-ray photoelectron spectroscopy (XPS). The procedure was finally employed to simultaneously graft two different block copolymers to one substrate to achieve binary brushes, which expands the applicability of our approach for facile preparation of advanced polymer coatings even further.[37,38,51]

5.2 Results and Discussion

5.2.1 Synthesis of block copolymers

For this study, a library of five different diblock copolymers was synthesized via RAFT polymerization. Each block copolymer contains a fixed segment of GMA units. The monomers that were used for the second segment differ for al block copolymers and were selected based on their distinct chemical properties as well as their wide-spread use in the field of polymer brush research (Scheme 5.2).

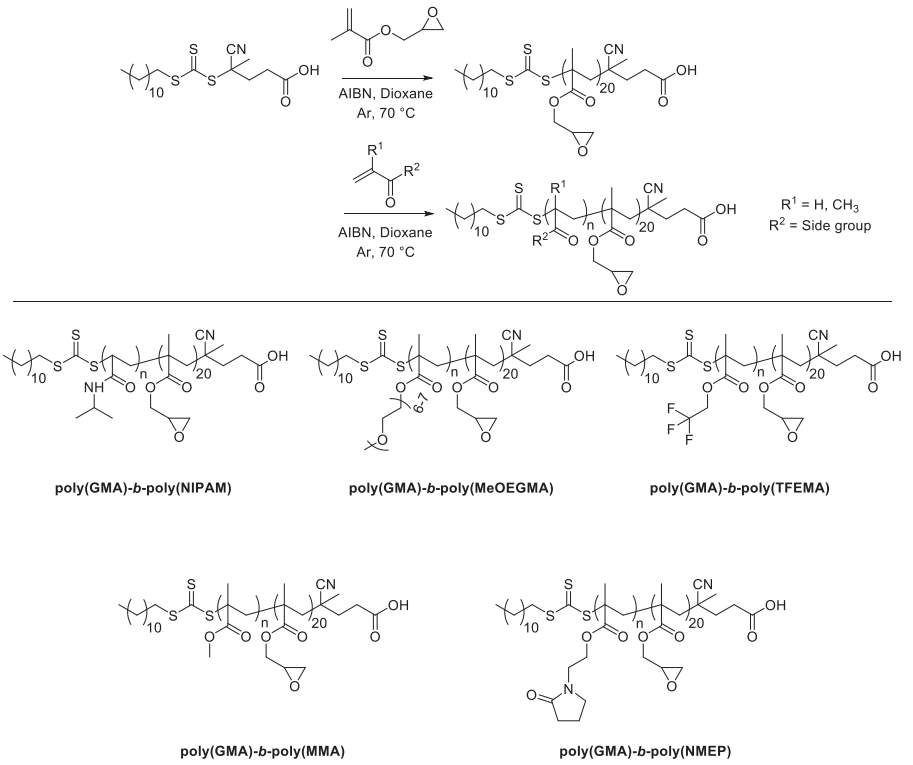

Scheme 5.2 Molecular structure of the block copolymers that were synthesized using RAFT polymerization and employed in the grafting-to reactions in this study.

Methyl methacrylate (MMA) is one of the most commonly employed monomers in polymerization literature and widely used in day-to-day applications, such as dentures, acrylic glass and electronics.[52] (Oligo ethylene glycol) methyl ether methacrylate (MeOEGMA)

was selected as it is the precursor to a hydrophilic polymer frequently used in anti-biofouling surfaces.[53–55] In contrast, trifluoroethyl methacrylate (TFEMA) is known to produce inert, hydrophobic polymer brushes that can be used to produce low-friction[56,57] and anti-polymer fouling surfaces.[58] The *N*-isopropylacrylamide (NIPAM) monomer was included due to the well-known thermoresponsive character of poly(NIPAM).[59,60] Similarly, *N*-(2-methacryloyloxy)ethyl pyrrolidone (NMEP) was added due to its potential towards thermoresponsive, antifouling surfaces (as was reported in Chapter 2).[61–63]

Synthesis of the block copolymers was carried out in two steps (Scheme 5.2). First, GMA was polymerized to produce short polymer chains that contained approximately 20 repeating units (Table 5.1). Based on work reported in Chapter 3, both the nature and length of this GMA block is optimal for the grafting-to step of reacting with of the $-NH_2$ moieties of the poly(dopamine)-modified substrates.[44,64,65] Following the first polymerization step, the poly(GMA) was used as a macro-RAFT agent in a subsequent polymerization reaction with one of the aforementioned monomers. All polymerization reactions were carried out under identical conditions varying only in reaction time over a range from 4 – 48 h, in order to achieve polymer blocks with roughly 250 repeating units. The produced block copolymers were characterized using ^{1}H-NMR, GPC and Fourier-transform infrared spectroscopy (FT-IR) (Table 5.1 and Supporting Information).

Table 5.1 Summary of the block copolymers synthesized in this study and analyzed using GPC.

	M_n (kDa)	M_w (kDa)	Đ
Poly(GMA)	3.6	4.6	1.27
Poly(GMA)-*b*-poly(MMA)	31.5	39.9	1.27
Poly(GMA)-*b*-poly(MeOEGMA)	59.5	89.7	1.51
Poly(GMA)-*b*-poly(TFEMA)	43.4	55.7	1.28
Poly(GMA)-*b*-poly(NIPAM)	28.5	37.2	1.30
Poly(GMA)-*b*-poly(NMEP)	56.8	83.1	1.46

5.2.2 Poly(dopamine) deposition

Poly(dopamine) deposition was performed by dip-coating of the substrates in a solution of dopamine in NaOAc buffer (pH 7) in the presence of oxidizing agent $NaIO_4$.[45] The deposition reaction was performed until approximately 10 nm of poly(dopamine) could be measured on gold and SiO_2 by spectroscopic ellipsometry (Figure 5.1A and B). For the PE substrates, the thickness of the poly(dopamine) layer could not be determined

using spectroscopic ellipsometry as the applied film could not be differentiated from the polyester material underneath. Verification of the presence of poly(dopamine) on PE was therefore performed using XPS analysis (Figure 5.1C). After deposition, a distinct N 1s signal appeared in the XPS wide scan spectra of the PE substrates originating from the poly(dopamine) films. Likewise, the emergence of the nitrogen signal was observed for the gold and SiO_2 substrates. Contact angle measurements were performed before and after poly(dopamine) deposition reactions (Figure 5.1D). Whereas the pristine samples exhibited large differences in contact angles, the poly(dopamine)-modified substrates all showed static water contact angles of approximately 50°, consistent with reported data in literature.[11] These observations imply that the surface modifications on all three substrates yielded similar poly(dopamine) primer layers.

5.2.3 Block copolymer grafting

Following the poly(dopamine) depositions, the block copolymers were grafted to the modified substrates. The surfaces were submerged in solutions of the appropriate block copolymer in DMSO and heated to 80 °C overnight, together with triethylamine (5% v/v) to catalyze the reaction between the amine groups present in poly(dopamine) and the epoxides present in the block copolymers.[66]

After the grafting-to reactions, the layer thicknesses of the gold and SiO_2 surfaces were determined using spectroscopic ellipsometry (Figure 5.1A and B). A substantial increase in layer thickness was observed for both surface types following attachment of the block copolymers. On the poly(dopamine)-modified gold substrates, the block copolymer layer thickness varied between roughly 9 and 13 nm. The average thickness increase was highly similar for the grafting reactions on poly(dopamine)-modified SiO_2 substrates, albeit with a larger variance between samples. Comparison of layer thicknesses on the different substrates did not reveal significant differences in grafting reactivity between the five block copolymers. It was therefore concluded that the reactivity towards grafting is similar for all block copolymers and the differences in observed layer thicknesses are mostly the result of experimental variation.

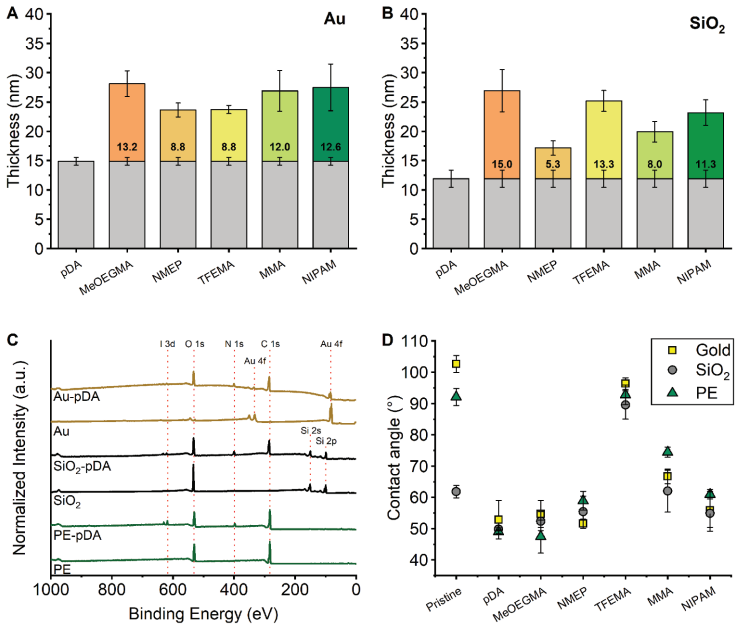

Figure 5.1 Layer thickness of poly(dopamine) film (gray bars) and block copolymers grafted to the poly(dopamine)-modified gold **(A)** and SiO_2 **(B)** substrates, as determined by spectroscopic ellipsometry. **(C)** XPS wide scan spectra for pristine and poly(dopamine)-modified PE, SiO_2 and gold samples. Note the appearance of the characteristic N 1s signal for the modified surfaces. **(D)** Static water contact angles for pristine substrates, poly(dopamine)-modified substrates and poly(dopamine)-modified substrates after grafting of block copolymers.

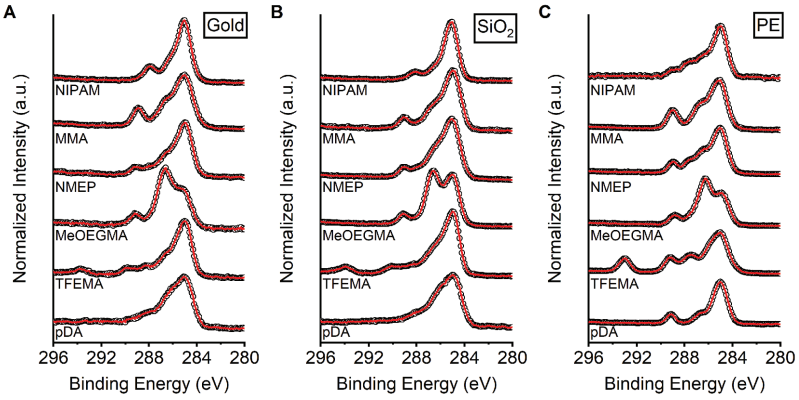

Figure 5.2 XPS C1s narrow scan spectra of gold **(A)**, SiO_2 **(B)** and PE **(C)** after modification with poly(dopamine) and after subsequent grafting of poly(GMA)-*b*-poly(TFEMA), poly(GMA)-*b*-poly(MeOEGMA), poly(GMA)-*b*-poly(NMEP), poly(GMA)-*b*-poly(MMA) and poly(GMA)-*b*-poly(NIPAM).

Static water contact angles that are characteristic for the grafted polymers were observed for all substrates, irrespective of substrate nature (Figure 5.1D). Grafting of poly(GMA)-*b*-poly(MeOEGMA) and poly(GMA)-*b*-poly(NMEP) resulted in hydrophilic surfaces with average contact angles of 51 ± 4° and 55 ± 4°, respectively, which agrees with values reported in literature for poly(MeOEGMA) and poly(NMEP) brushes.[63,67,68] Grafting of poly(GMA)-*b*-poly(TFEMA) and poly(GMA)-*b*-poly(MMA) resulted in more hydrophobic surfaces, with average water contact angles of 93 ± 3° and 68 ± 6°, respectively. These observations were in agreement with literature data for the polymer brush coatings of poly(TFEMA) and poly(MMA).[56,69,70] Lastly, the grafting of thermoresponsive poly(GMA)-*b*-poly(NIPAM) resulted in an average water contact angle of 57 ± 3°, characteristic for surfaces modified with poly(NIPAM).[71]

XPS measurements were performed to further characterize the produced surfaces and confirm the presence of the block copolymers on the substrates. Specifically, C 1s narrow scan spectra were collected to identify signals that are characteristic for the grafted block copolymers (Figure 5.2). In general, the spectra showed highly comparable results, irrespective of the substrate type. The spectra for poly(dopamine)-modified gold and SiO_2 substrates were near-identical and were in agreement with binding energies found previously for poly(dopamine) films.[44,72,73] The C 1s spectrum for poly(dopamine)-modified PE displayed slightly different binding energies, which were attributed to electrons originating from the underlying polyester layer. Following grafting of poly(GMA)-*b*-poly(TFEMA) to the poly(dopamine) substrates, the emergence of a peak at 293.5 eV was observed, which is typical for the C–F bonds present in TFEMA.[58,74,75] Additionally, the successful grafting of the block copolymer was confirmed by the emergence of the F 1s signal in the wide scan spectra (see Supporting Information). The attachment of poly(GMA)-*b*-poly(MeOEGMA) was deduced from the appearance of strong signals at 286.5 eV that arise from the multiple C–O bonds present in the oligo(ethylene glycol) side group.[76] The binding energies arising from attachment of poly(GMA)-*b*-poly(NMEP) were less distinct, although the presence of both the ester (–C(=O)–O) and cyclic amide (–C(=O)–N) could be observed by the increase in intensity at 289.0 eV and 288.0 eV, respectively.[63] More apparent was the N 1s peak in the wide scan spectra, arising from the cyclic amide (see Supporting Information). The substrates that were modified with poly(GMA)-*b*-poly(MMA) showed a distinct ester peak (–C(=O)-O) at 289.0 eV.[77,78] Finally, the presence of poly(GMA)-*b*-poly(NIPAM) was confirmed via the presence of amide (–C(=O)–NH) signal in the C 1s spectra at 288.0 eV, as well as the strong N 1s signal in the wide scan spectra (see Supporting Information).

The analysis of the produced surfaces using spectroscopic ellipsometry, static water contact angle measurements and XPS confirms that the two-step procedure employed

in this study is both modular with respect to substrate type, as well as functional groups of the grafted polymers. Since identical conditions were employed for the grafting reactions of all block copolymers, the method could potentially be used to synthesize binary brushes. Such coatings have become of increasing interest as they commonly exhibit switchable surface properties that can be applied in responsive coatings.[37,38,51,79–81] The ability to easily synthesize such mixed polymer systems on any substrate would greatly enhance the applicability of responsive coatings.

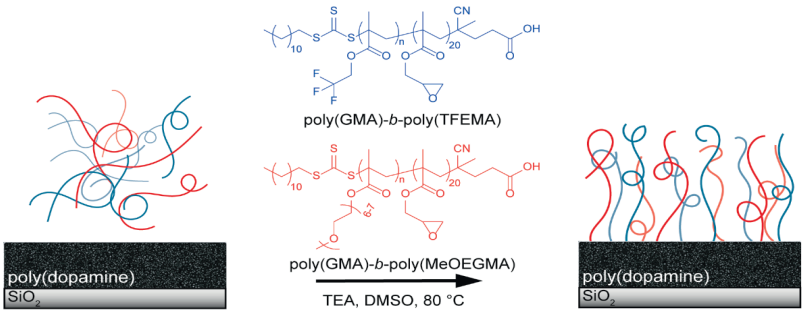

Scheme 5.3 Illustration of the synthesis of binary brush systems. Poly(GMA)-*b*-poly(TFEMA) and poly(GMA)-*b*-poly(MeOEGMA) copolymers, displayed as red and blue chains, respectively, were grafted to poly(dopamine)-modified SiO_2 substrates.

5.2.4 Binary brush synthesis

To study the possible synthesis of binary brushes, grafting reactions using mixed polymer solutions of poly(GMA)-*b*-poly(TFEMA) and poly(GMA)-*b*-poly(MeOEGMA) were performed on poly(dopamine)-modified SiO_2. The polymer mixtures were prepared with ratios poly(GMA)-*b*-poly(TFEMA) to poly(GMA)-*b*-poly(MeOEGMA) of 1:3, 1:1 and 3:1. The grafting step was carried out in the same manner as described for the single block copolymer solutions.

The thickness of the resulting coatings was determined using spectroscopic ellipsometry (Figure 5.3A). The layer of attached block copolymer was in the same thickness range as was previously observed for the single-polymer brushes. XPS C 1s spectra were measured to confirm incorporation of both block copolymers during the grafting step (Figure 5.3B). Both block copolymers have distinctive binding energies originating from C–F at 293.5 eV in TFEMA and from C–O at 286.5 eV in MeOEGMA, which are apparent in the 0:1 and 1:0 spectra, respectively. In the spectrum of the 3:1 sample, signals at 293.5

eV and 286.5 eV can be seen clearly, indicating the presence of both the block copolymers on the surface. With increasing relative amount of poly(GMA)-*b*-poly(TFEMA) with respect to poly(GMA)-*b*-poly(MeOEGMA), the intensity for the C–O signal at 286.5 eV decreases whereas the intensity of the C–F at 293.5 eV in TFEMA increases (Note: due to the underlying polydopamine layer, this trend is difficult to quantify by looking at the respective peak areas). The carbon narrow scan spectra confirm that binary brushes can be synthesized using this simple procedure and that the ratio between the block copolymers on the surface can be easily tuned by variation of the ratio of block copolymers in the grafting solution. The ability to synthesize binary brushes with controlled composition enables the production of tunable responsive coating materials that exhibit, for example, switchable wetting behavior, morphology and interactions with biological components.[39,40,79]

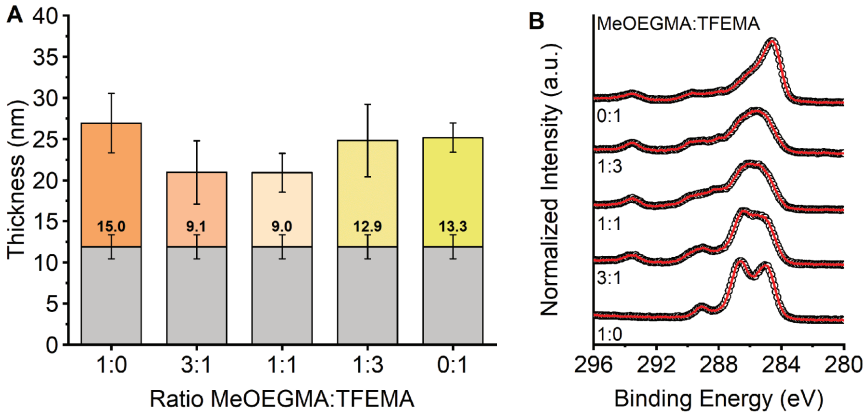

Figure 5.3 (A) Layer thickness of poly(dopamine) film (gray bars) and poly(GMA)-*b*-poly(MeOEGMA)/poly(GMA)-*b*-poly(TFEMA) binary brush systems on SiO_2. **(B)** XPS carbon narrow scan spectra of poly(GMA)-*b*-poly(MeOEGMA)/poly(GMA)-*b*-poly(TFEMA) binary brushes grafted on poly(dopamine)-modified SiO_2.

5.3 Conclusions

We developed a surface-independent, easy-to-apply and modular two-step grafting-to procedure to synthesize polymer brushes. This yielded on gold, SiO_2 and PE-coated grafted-to polymer brushes up to 15 nm, using a poly(dopamine) film as a primer layer. The grafting-to reactions were performed using block copolymers that carried a poly(GMA)

segment, and allows freedom in the nature of the other segment of the copolymer, from hydrophobic to hydrophilic. Moreover, the method was used to synthesize binary brush systems by simply mixing in two block copolymers in the grafting solution.

The highly straightforward nature of the grafting reactions as well as its universal applicability in terms of substrate type and polymer functionalities enables the introduction of wide range of surface properties to effectively any substrate type. The additional possibility to produce binary brush systems in a trivial manner gives this method further potential in the field of surface engineering.

5.4 Materials and Methods

5.4.1 Materials

All chemical reagents were used without further purification unless otherwise specified. Triethylamine (TEA), 2,2′-azobis(2-methylpropionitrile) (AIBN) (98%), poly(ethylene glycol)methyl ether methacrylate (MeOEGMA)(average M_n = 300, stabilized), methyl methacrylate (MMA)(99%, stabilized), NaOAc (> 99%) and 1,4-dioxane (99.8%, anhydrous, non-stabilized) were purchased from Sigma-Aldrich. 4-Cyano-4-[(dodecylsulfanylthiocarbonyl)sulfanyl]pentanoic acid (CDPA) (> 95.0%), dopamine.HCl (> 98.0%), 2,2,2-trifluoroethyl methacrylate (TFEMA)(> 98.0%, stabilized) and *N*isopropylacrylamide (NIPAM) (> 98.0%, stabilized) were purchased from TCI Chemicals Europe. Glycidyl methacrylate (GMA) (97%, stabilized) and methacryloyl chloride (97%, stabilized) were purchased from Thermo Fisher Scientific. $NaIO_4$ (99%) was purchased from ACROS Organics. Deionized water was produced with Milli-Q Integral 3 system Millipore, Molsheim, France (Milli-Q water). Silicon single side-polished wafers (Si(100), N-type, phosphorus-doped) were obtained from Siltronix. Silicon wafers coated with a 200 nm gold layer were acquired from Ssens. Polyester-coated glass samples were kindly provided by Tata Steel Europe, IJmuiden, Netherlands.

Prior to use, GMA was purified by washing with 0.1% m/v KOH solution and NIPAM was recrystallized from hexane. MeOEGMA, TFEMA and MMA were passed over a basic alumina plug. NMEP was synthesized following a synthesis procedure described in Chapter 2.[40]

5.4.2 RAFT polymerization of poly(GMA)$_{20}$

The RAFT polymerization of GMA was performed according to the procedure described in Chapter 3.[41] The product, a fine yellow powder, was obtained through filtration and dried over air. **^{1}H NMR** (400 MHz, $CDCl_3$) δ 4.38 – 4.24 (m, 19H), 3.86 – 3.72 (m, 20 H), 3.26 – 3.19 (m, 20 H), 2.87 – 2.79 (m, 19H), 2.68 – 2.59 (m, 19 H), 2.17 – 1.72 (m, 34 H), 1.45 – 1.23 (m, 18 H), 1.11 – 1.07 (s, 19 H), 0.94 – 0.80 (s, 34 H). **IR** ν = 1740–1720 cm^{-1} (–C(=O)–O), 1470–1430 cm^{-1} (–CH_3), 1260 cm^{-1} (C–O), 903 cm^{-1} (epoxide C–O).[59–61]

5.4.3 Block copolymerization reactions

The polymerization reactions were carried out in an identical manner for all monomers. In short, to 100 mL Schlenk flasks was added AIBN (2.0 mg; 0.0023 mmol; 0.2 equiv.), pGMA$_{20}$ (32 mg; 0.012 mmol; 1 equiv.), monomer (3.45 mmol; 300 equiv.) and 1,4-dioxane (3 mL). The solutions were deoxygenated by three freeze-pump-thaw cycles. After the last cycle, the flask was charged with argon. The flask was then heated at 70 °C and left to stir.

The polymerization MeOEGMA was stopped after 4 h by removing the flask from the heat source and opening the reaction mixture to the atmosphere. To the solution was then added acetone (10 mL), after which the polymer was purified by addition to cold hexane, centrifugation and decantation of the hexane layer. A viscous, transparent and colorless product was obtained. **^{1}H NMR** (400 MHz, $CDCl_3$) δ 4.08 (s, 2 H), 3.82 – 3.47 (m, 16 H), 3.38 (s, 3 H), 1.84 (m, 2 H), 0.95 (m, 3 H). **IR** ν = 2970–2830 cm^{-1} (C–H), 1726 cm^{-1} (–C(=O)–O), 1097 cm^{-1} (C–O–C).[62,63]

The polymerization of NIPAM was stopped after 4 h by removing the flask from the heat source and opening the reaction mixture to the atmosphere. To the solution was then added acetone (10 mL), after which the polymer was purified by two-fold precipitation from cold diethyl ether and filtration. A white powder was obtained. **^{1}H NMR** (400 MHz, $CDCl_3$) δ 4.00 (s, 1 H), 2.58 (s, 1 H), 1.45 – 0.96 (m, 6 H). **IR** ν = 3297 cm^{-1} (N–H), 1640 cm^{-1} (–C(=O)–NH), 1542 cm^{-1} (N–H).[64,65]

The polymerization of MMA was stopped after 48 h by removing the flask from the heat source and opening the reaction mixture to the atmosphere. To the solution was then added acetone (10 mL), after which the polymer was purified by two-fold precipitation from cold diethyl ether and filtration. A white powder was obtained. **^{1}H NMR** (400 MHz, $CDCl_3$) δ 3.62 – 3.58 (m, 3 H), 1.81 (m, 2 H), 0.94 (m, 3 H). **IR** ν = 1730 cm^{-1} (–C(=O)–O), 1470–1430 cm^{-1} (–CH_3), 1260 cm^{-1} (C–O), 1190–1150 cm^{-1} (C–O–C), 988 cm^{-1} (O–CH_3).[66]

The polymerization of TFEMA was stopped after 24 h by removing the flask from the heat source and opening the reaction mixture to the atmosphere. To the solution was then

added acetone (10 mL), after which the polymer was purified by two-fold precipitation from cold diethyl ether and filtration. A white powder was obtained. **^{1}H NMR** (400 MHz, $CDCl_3$) δ 4.37 (s, 2 H), 2.00 (m, 2 H), 1.04 (m, 3 H). **IR** ν = 1743 cm^{-1} (–C(=O)–O), 1280 cm^{-1} (C–F), 655 cm^{-1} (C–F).[67,68]

The polymerization of NMEP was stopped after 6 h by removing the flask from the heat source and opening the reaction mixture to the atmosphere. To the solution was then added acetone (10 mL), after which the polymer was purified by two-fold precipitation from cold diethyl ether and filtration. A white powder was obtained. **^{1}H NMR** (400 MHz, $CDCl_3$) δ 4.07 (s, 2 H), 3.54 (m, 4 H), 2.43 (s, 2 H), 2.12 (m, 2 H), 1.57 (s, 2 H), 0.96 (m, 3 H). **IR** ν = 1726 cm^{-1} (–C(=O)–O), 1664 cm^{-1} (–C(=O)–N), 1268 cm^{-1}, 1424 cm^{-1} (C–H), 1267 cm^{-1} (C–N), 1147 cm^{-1} (C(=O)–O).[40,69]

5.4.4 Modification of gold, SiO_2 and PE substrates with poly(dopamine)

1 × 1 cm substrates were rinsed using acetone, ethanol and Milli-Q and then dried under a gentle stream of argon. The substrates were placed in a petri dish containing freshly prepared solution of dopamine.HCl (2 mg/mL) and $NaIO_4$ (20 mM). The petri dish was closed, sealed using parafilm and placed on an automated shaker at RT, 60 RPM. The surfaces were removed from the solution after the appropriate time, which was 10 min for gold, 20 min for silicon oxide and 30 min for PE. They were then thoroughly rinsed with Milli-Q and subsequently dried.

5.4.5 Grafting of polymers to poly(dopamine)-modified substrates

The grafting-to reaction of the block copolymers was carried out according to the protocol described in Chapter 3.[41]

5.4.6 Gel permeation chromatography (GPC)

The polymer molecular weight and polydispersity index (PDI) were determined using gel permeation chromatography (Agilent 1200 Organic GPC + refractive index detector, equipped with PLgel 5 μm MIXED-D column), The column was calibrated with a poly(methyl methacrylate) polymer set. The selected eluent was THF for poly(GMA)$_{20}$, poly(GMA)-*b*-poly(MeOEGMA), poly(GMA)-*b*-poly(TFEMA) and poly(GMA)-*b*-poly(MMA); and DMF + 0.1% LiBr for poly(GMA)-*b*-poly(NIPAM) and poly(GMA)-*b*-poly(NMEP), which were pumped at a constant flow of 0.5 mL/min.

5.4.7 Ellipsometry

Ellipsometric angles Δ and Ψ of the synthesized polymer brushes were measured using an EP4 imaging ellipsometer (Accurion, Germany). The measurements were performed in air at room temperature in the wavelength range of λ = 491 – 761.3 nm at an angle of incidence of 50°. The acquired Δ and Ψ were fitted in the EP4 modeling software using a multilayer model to obtain dry polymer brush thickness and refraction index values. The poly(dopamine) layer was described using a Cauchy-Urbach model to account for the light absorption of poly(dopamine).

$$n(E) = A + BE^2; \qquad k(E) = \alpha e^{\beta(E-E_b)}$$

The following parameters were used: A = 1.54, B = 3000 nm^2, α = 0.161 ± 0.58, β = 0.242 ± 0.121 and E_b = 3.0 eV. The poly(GMA)-*b*-poly(NIPAM) layer for polymer-modified substrates was described using a Cauchy model with parameters A = 1.50 and B = 3000 nm^2. The poly(GMA)-*b*-poly(TFEMA) layer for polymer-modified substrates was described using a Cauchy model with parameters A = 1.41 and B = 3000 nm^2. The poly(GMA)-*b*-poly(MMA) layer for polymer-modified substrates was described using a Cauchy model with parameters A = 1.49 and B = 3000 nm^2. The poly(GMA)-*b*-poly(MeOEGMA) layer for polymer-modified substrates was described using a Cauchy model with parameters A = 1.45 and B = 3000 nm^2. The poly(GMA)-*b*-poly(NMEP) layer for polymer-modified substrates was described using a Cauchy model with parameters A = 1.49 and B = 3000 nm^2. Addition of an outermost layer to account for the roughness of the measured substrates using Bruggeman's effective medium approximation (EMA) did not improve the fit of the model.[70]

5.4.8 X-ray photoelectron spectroscopy

XPS measurements were performed as described in Chapter 2.

5.4.9 ATR FT-IR spectroscopy

FT-IR spectra were measured as described in Chapter 4.

5.4.10 Static water contact angle measurements

Static water contact angle measurements were performed as described in Chapter 2.

5.4.11 Statistical analysis

All statistical results were calculated using Origin 2019 software. Data were displayed as average values ± standard deviation.

5.5 Acknowledgements

This research was carried out under project number C16030a in the framework of the Partnership Program of the Materials innovation institute M2i (www.m2i.nl) and the NWO Domain Science, which is part of the Netherlands Organization for Scientific Research (www.nwo.nl).

5.6 References

1. Chen, W. L., Cordero, R., Tran, H. & Ober, C. K. 50th Anniversary Perspective: Polymer Brushes: Novel Surfaces for Future Materials. *Macromolecules* **50**, 4089–4113 (2017).
2. Zoppe, J. O. *et al.* Surface-Initiated Controlled Radical Polymerization: State-of-the-Art, Opportunities, and Challenges in Surface and Interface Engineering with Polymer Brushes. *Chem. Rev.* **117**, 1105–1318 (2017).
3. Azzaroni, O. Polymer brushes here, there, and everywhere: Recent advances in their practical applications and emerging opportunities in multiple research fields. *J. Polym. Sci. Part A Polym. Chem.* **50**, 3225–3258 (2012).
4. Zdyrko, B. & Luzinov, I. Polymer brushes by the 'grafting to' method. *Macromol. Rapid Commun.* **32**, 859–869 (2011).
5. Wei, Q. & Haag, R. Universal polymer coatings and their representative biomedical applications. *Mater. Horizons* **2**, 567–577 (2015).
6. Pujari, S. P., Scheres, L., Marcelis, A. T. M. & Zuilhof, H. Covalent surface modification of oxide surfaces. *Angew. Chemie - Int. Ed.* **53**, 6322–6356 (2014).
7. Barbey, R. *et al.* Polymer brushes via surface-initiated controlled radical polymerization: synthesis, characterization, properties, and applications. *Chem. Rev.* **109**, 5437–5527 (2009).
8. Olivier, A., Meyer, F., Raquez, J. M., Damman, P. & Dubois, P. Surface-initiated controlled polymerization as a convenient method for designing functional polymer brushes: From self-assembled monolayers to patterned surfaces. *Prog. Polym. Sci.* **37**, 157–181 (2012).
9. Krishnamoorthy, M., Hakobyan, S., Ramstedt, M. & Gautrot, J. E. Surface-Initiated Polymer Brushes in the Biomedical Field: Applications in Membrane Science, Biosensing, Cell Culture, Regenerative Medicine and Antibacterial Coatings. *Chem. Rev.* **114**, 10976–11026 (2014).
10. Ryu, D. Y., Shin, K., Drockenmuller, E., Hawker, C. J. & Russell, T. P. A Generalized Approach to the Modification of Solid Surfaces. *Science* **308**, 236–239 (2005).
11. Lee, H., Dellatore, S. M., Miller, W. M. & Messersmith, P. B. Mussel-Inspired Surface Chemistry for Multifunctional Coatings. *Science* **318**, 426–430 (2007).
12. Kang, S. M. *et al.* One-step multipurpose surface functionalization by adhesive catecholamine. *Adv. Funct. Mater.* **22**, 2949–2955 (2012).
13. Ryu, J. H., Messersmith, P. B. & Lee, H. Polydopamine Surface Chemistry: A Decade of Discovery. *ACS Appl. Mater. Interfaces* **10**, 7523–7540 (2018).
14. Faure, E. *et al.* Catechols as versatile platforms in polymer chemistry. *Prog. Polym. Sci.* **38**, 236–270 (2013).
15. Liebscher, J. Chemistry of Polydopamine – Scope, Variation, and Limitation. *European J. Org. Chem.* **2019**, 4976–4994 (2019).
16. Saiz-Poseu, J., Mancebo-Aracil, J., Nador, F., Busqué, F. & Ruiz-Molina, D. The Chemistry behind Catechol-Based Adhesion. *Angew. Chemie Int. Ed.* **58**, 696–714 (2019).
17. Yang, J., Cohen Stuart, M. A. & Kamperman, M. Jack of all trades: Versatile catechol crosslinking mechanisms. *Chem. Soc. Rev.* **43**, 8271–8298 (2014).
18. Kord Forooshani, P. & Lee, B. P. Recent approaches in designing bioadhesive materials inspired by mussel adhesive protein. *J. Polym. Sci. Part A Polym. Chem.* **55**, 9–33 (2017).

19. Rodriguez-Emmenegger, C. *et al.* Controlled Cell Adhesion on Poly(dopamine) Interfaces Photopatterned with Non-Fouling Brushes. *Adv. Mater.* **25**, 6123–6127 (2013).

20. Li, N. *et al.* Universal Strategy for Efficient Fabrication of Blood Compatible Surfaces via Polydopamine-Assisted Surface-Initiated Activators Regenerated by Electron Transfer Atom-Transfer Radical Polymerization of Zwitterions. *ACS Appl. Mater. Interfaces* **12**, 12337–12344 (2020).

21. Sundaram, H. S. *et al.* One-Step Dip Coating of Zwitterionic Sulfobetaine Polymers on Hydrophobic and Hydrophilic Surfaces. *ACS Appl. Mater. Interfaces* **6**, 6664–6671 (2014).

22. Gao, C. *et al.* Functionalizable and ultra-low fouling zwitterionic surfaces via adhesive mussel mimetic linkages. *Biomaterials* **31**, 1486–1492 (2010).

23. Sun, F. *et al.* Paper Sensor Coated with a Poly(carboxybetaine)-Multiple DOPA Conjugate via Dip-Coating for Biosensing in Complex Media. *Anal. Chem* **89**, 10999–11004 (2017).

24. Alas, G. R., Agarwal, R., Collard, D. M. & García, A. J. Peptide-functionalized poly[oligo(ethylene glycol) methacrylate] brushes on dopamine-coated stainless steel for controlled cell adhesion. *Acta Biomater.* **59**, 108–116 (2017).

25. Hafner, D. & Jordan, R. Substrate-independent Cu(0)-mediated controlled radical polymerization: Grafting of block copolymer brushes from poly(dopamine) modified surfaces. *Polym. Chem.* **11**, 2129–2136 (2020).

26. Zobrist, C. *et al.* Functionalization of titanium surfaces with polymer brushes prepared from a biomimetic RAFT agent. *Macromolecules* **44**, 5883–5892 (2011).

27. Yang, W. J. *et al.* Biomimetic anchors for antifouling and antibacterial polymer brushes on stainless steel. *Langmuir* **27**, 7065–7076 (2011).

28. Liu, C., Lee, J., Ma, J. & Elimelech, M. Antifouling Thin-Film Composite Membranes by Controlled Architecture of Zwitterionic Polymer Brush Layer. *Environ. Sci. Technol.* **51**, 2161–2169 (2017).

29. Yang, Y. *et al.* Metal-Free Photoinduced Electron Transfer–Atom Transfer Radical Polymerization Integrated with Bioinspired Polydopamine Chemistry as a Green Strategy for Surface Engineering of Magnetic Nanoparticles. *ACS Appl. Mater. Interfaces* **9**, 13637–13646 (2017).

30. Jin, X., Yuan, J. & Shen, J. Zwitterionic polymer brushes via dopamine-initiated ATRP from PET sheets for improving hemocompatible and antifouling properties. *Colloids Surfaces B Biointerfaces* **145**, 275–284 (2016).

31. Asha, A. B., Chen, Y. & Narain, R. Bioinspired dopamine and zwitterionic polymers for non-fouling surface engineering. *Chem. Soc. Rev.* **50**, 11668–11683 (2021).

32. Pop-Georgievski, O. *et al.* Poly(ethylene oxide) layers grafted to dopamine-melanin anchoring layer: Stability and resistance to protein adsorption. *Biomacromolecules* **12**, 3232–3242 (2011).

33. Pop-Georgievski, O. *et al.* Nonfouling poly(ethylene oxide) layers end-tethered to polydopamine. *Langmuir* **28**, 14273–14283 (2012).

34. Sileika, T. S., Kim, H.-D., Maniak, P. & Messersmith, P. B. Antibacterial Performance of Polydopamine-Modified Polymer Surfaces Containing Passive and Active Components. *ACS Appl. Mater. Interfaces* **3**, 4602–4610 (2011).

35. Li, G. *et al.* Ultra low fouling zwitterionic polymers with a biomimetic adhesive group. *Biomaterials* **29**, 4592–4597 (2008).

36. Asha, A. B. *et al.* Dopamine Assisted Self-Cleaning, Antifouling, and Antibacterial Coating via Dynamic Covalent Interactions. *ACS Appl. Mater. Interfaces* **14**, 9557–9569 (2022).

37. Kumar Vyas, M., Schneider, K., Nandan, B. & Stamm, M. Switching of friction by binary polymer brushes. *Soft Matter* **4**, 1024–1032 (2008).

38. Uhlmann, P. *et al.* Surface functionalization by smart coatings: Stimuli-responsive binary polymer brushes. *Prog. Org. Coatings* **55**, 168–174 (2006).

39. LeMieux, M. C. *et al.* Ultrathin Binary Grafted Polymer Layers with Switchable Morphology. *Langmuir* **20**, 10046–10054 (2004).

40. Feng, L., Gu, A., Chen, M. & Wu, L. Synthesis and surface properties of poly(methyl methacrylate)/ poly(ethylene glycol) binary brushes. *Macromol. Mater. Eng.* **292**, 754–761 (2007).

41. Qiu, W. Z., Yang, H. C. & Xu, Z. K. Dopamine-assisted co-deposition: An emerging and promising strategy for surface modification. *Adv. Colloid Interface Sci.* **256**, 111–125 (2018).

42. Zhang, C. *et al.* Dopamine-triggered one-step polymerization and codeposition of acrylate monomers for functional coatings. *ACS Appl. Mater. Interfaces* **9**, 34356–34366 (2017).

43. Mao, S., Zhang, D., Zhang, Y., Yang, J. & Zheng, J. A Universal Coating Strategy for Controllable Functionalized Polymer Surfaces. *Adv. Funct. Mater.* **30**, 2004633 (2020).

44. Teunissen, L. W., van den Beukel, J., Smulders, M. M. J. & Zuilhof, H. Thermoresponsive Polymer Brushes for Switchable Protein Adsorption via Dopamine-Assisted Grafting-To Strategy. *Adv. Mater. Interfaces* **9**, 2201198 (2022).

45. Teunissen, L. W., Smulders, M. M. J. & Zuilhof, H. 19 nm-Thick Grafted-To Polymer Brushes onto Optimized Poly(Dopamine)-Coated Surfaces. *Adv. Mater. Interfaces* **Submitted**, (2022).

46. Homola, J., Yee, S. S. & Gauglitz, G. Surface plasmon resonance sensors: review. *Sensors Actuators, B Chem.* **54**, 3–15 (1999).

47. Homola, J. Surface plasmon resonance sensors for detection of chemical and biological species. *Chem. Rev.* **108**, 462–493 (2008).

48. Oliverio, M., Perotto, S., Messina, G. C., Lovato, L. & De Angelis, F. Chemical Functionalization of Plasmonic Surface Biosensors: A Tutorial Review on Issues, Strategies, and Costs. *ACS Appl. Mater. Interfaces* **9**, 29394–29411 (2017).

49. Stegemann, B. *et al.* Ultra-thin silicon oxide layers on crystalline silicon wafers: Comparison of advanced oxidation techniques with respect to chemically abrupt SiO 2 /Si interfaces with low defect densities. *Appl. Surf. Sci.* **395**, 78–85 (2017).

50. Shergujri, M. A. *et al.* Paper-Based Sensors for Biomedical Applications. in *Biomedical Engineering and its Applications in Healthcare* **19**, 355–376 (Springer Singapore, 2019).

51. Chen, C. *et al.* A binary mixed polymer brush coating with adjusted hydrophobic property to control protein adsorption. *Mater. Adv.* **2**, 2120–2131 (2021).

52. Darabi Mahboub, M. J., Dubois, J. L., Cavani, F., Rostamizadeh, M. & Patience, G. S. Catalysis for the synthesis of methacrylic acid and methyl methacrylate. *Chem. Soc. Rev.* **47**, 7703–7738 (2018).

53. Brown, A. A., Khan, N. S., Steinbock, L. & Huck, W. T. S. Synthesis of oligo(ethylene glycol) methacrylate polymer brushes. *Eur. Polym. J.* **41**, 1757–1765 (2005).

54. Ma, H., Li, D., Sheng, X., Zhao, B. & Chilkoti, A. Protein-resistant polymer coatings on silicon oxide by surface-initiated atom transfer radical polymerization. *Langmuir* **22**, 3751–3756 (2006).

55. Hucknall, A. *et al.* Versatile synthesis and micropatterning of nonfouling polymer brushes on the wafer scale. *Biointerphases* **4**, FA50–FA57 (2009).

56. Bhairamadgi, N. S., Pujari, S. P., Leermakers, F. A. M., Van Rijn, C. J. M. & Zuilhof, H. Adhesion and friction properties of polymer brushes: Fluoro versus nonfluoro polymer brushes at varying thickness. *Langmuir* **30**, 2068–2076 (2014).

57. Bhairamadgi, N. S., Pujari, S. P., Van Rijn, C. J. M. & Zuilhof, H. Adhesion and friction properties of fluoropolymer brushes: On the tribological inertness of fluorine. *Langmuir* **30**, 12532–12540 (2014).

58. van Dam, A., Smulders, M. M. J. & Zuilhof, H. Self-healing antifouling polymer brushes: Effects of degree of fluorination. *Appl. Surf. Sci.* **579**, 152264 (2022).

59. Nagase, K., Okano, T. & Kanazawa, H. Poly(N-isopropylacrylamide) based thermoresponsive polymer brushes for bioseparation, cellular tissue fabrication, and nano actuators. *Nano-Structures & Nano-Objects* **16**, 9–23 (2018).

60. Halperin, A., Kröger, M. & Winnik, F. M. Poly(N -isopropylacrylamide) Phase Diagrams: Fifty Years of Research. *Angew. Chemie Int. Ed.* **54**, 15342–15367 (2015).

61. Peng, Y. *et al.* Facile Synthesis and Thermoresponsive Behaviors of a Well-Defined Pyrrolidone Based Hydrophilic Polymer. *Macromolecules* **41**, 3007–3014 (2008).

62. Savelyeva, X. & Marić, M. Pyrrolidone-functional smart polymers via nitroxide-mediated polymerization. *J. Polym. Sci. Part A Polym. Chem.* **52**, 2011–2024 (2014).

63. Teunissen, L. W., Kuzmyn, A. R., Ruggeri, F. S., Smulders, M. M. J. & Zuilhof, H. Thermoresponsive, Pyrrolidone-Based Antifouling Polymer Brushes. *Adv. Mater. Interfaces* **9**, 2101717 (2022).

64. Gauthier, M. A., Gibson, M. I. & Klok, H. A. Synthesis of functional polymers by post-polymerization modification. *Angew. Chemie - Int. Ed.* **48**, 48–58 (2009).

65. Edmondson, S. & Huck, W. T. S. Controlled growth and subsequent chemical modification of poly(glycidyl methacrylate) brushes on silicon wafers. *J. Mater. Chem.* **14**, 730–734 (2004).

66. Benaglia, M., Alberti, A., Giorgini, L., Magnoni, F. & Tozzi, S. Poly(glycidyl methacrylate): A highly versatile polymeric building block for post-polymerization modifications. *Polym. Chem.* **4**, 124–132 (2013).

67. Kuzmyn, A. R., Nguyen, A. T., Teunissen, L. W., Zuilhof, H. & Baggerman, J. Antifouling Polymer Brushes via Oxygen-Tolerant Surface-Initiated PET-RAFT. *Langmuir* **36**, 4439–4446 (2020).

68. Kuzmyn, A. R. *et al.* Diblock and Random Antifouling Bioactive Polymer Brushes on Gold Surfaces by Visible-Light-Induced Polymerization (SI-PET-RAFT) in Water. *Adv. Mater. Interfaces* **9**, 2101784 (2022).

69. Xu, F. J., Zhao, J. P., Kang, E. T. & Neoh, K. G. Surface functionalization of polyimide films via chloromethylation and surface-initiated atom transfer radical polymerization. *Ind. Eng. Chem. Res.* **46**, 4866–4873 (2007).

70. Patil, R. R., Turgman-Cohen, S., Šrogl, J., Kiserow, D. & Genzer, J. On-Demand Degrafting and the Study of Molecular Weight and Grafting Density of Poly(methyl methacrylate) Brushes on Flat Silica Substrates. *Langmuir* **31**, 2372–2381 (2015).

71. Yu, Y. *et al.* Stretching of collapsed polymers causes an enhanced dissipative response of PNIPAM brushes near their LCST. *Soft Matter* **11**, 8508–8516 (2015).

72. Zangmeister, R. A., Morris, T. A. & Tarlov, M. J. Characterization of polydopamine thin films deposited at short times by autoxidation of dopamine. *Langmuir* **29**, 8619–8628 (2013).

73. Rella, S. *et al.* Investigation of polydopamine coatings by X-ray Photoelectron Spectroscopy as an effective tool for improving biomolecule conjugation. *Appl. Surf. Sci.* **447**, 31–39 (2018).

74. Cheng, Z., Zhu, X., Kang, E. T. & Neoh, K. G. Modification of poly(ether imide) membranes via surface-initiated atom transfer radical polymerization. *Macromolecules* **39**, 1660–1663 (2006).

75. Pester, C. W. *et al.* Ambiguous anti-fouling surfaces: Facile synthesis by light-mediated radical polymerization. *J. Polym. Sci. Part A Polym. Chem.* **54**, 253–262 (2016).

76. Kuzmyn, A. R. *et al.* Exploiting end group functionalization for the design of antifouling bioactive brushes. *Polym. Chem.* **5**, 4124 (2014).

77. Kong, X., Kawai, T., Abe, J. & Iyoda, T. Amphiphilic polymer brushes grown from the silicon surface by atom transfer radical polymerization. *Macromolecules* **34**, 1837–1844 (2001).

78. Chen, J. K. *et al.* Using solvent immersion to fabricate variably patterned poly(methyl methacrylate) brushes on silicon surfaces. *Macromolecules* **41**, 8729–8736 (2008).

79. Delcroix, M. F. *et al.* Design of Mixed PEO/PAA Brushes with Switchable Properties Toward Protein Adsorption. *Biomacromolecules* **14**, 215–225 (2013).

80. Delcroix, M. F., Demoustier-Champagne, S. & Dupont-Gillain, C. C. Quartz crystal microbalance study of ionic strength and pH-dependent polymer conformation and protein adsorption/desorption on PAA, PEO, and mixed PEO/PAA brushes. *Langmuir* **30**, 268–277 (2014).

81. Minko, S. *et al.* Synthesis of adaptive polymer brushes via 'grafting to' approach from melt. *Langmuir* **18**, 289–296 (2002).

3.7 Supporting Information

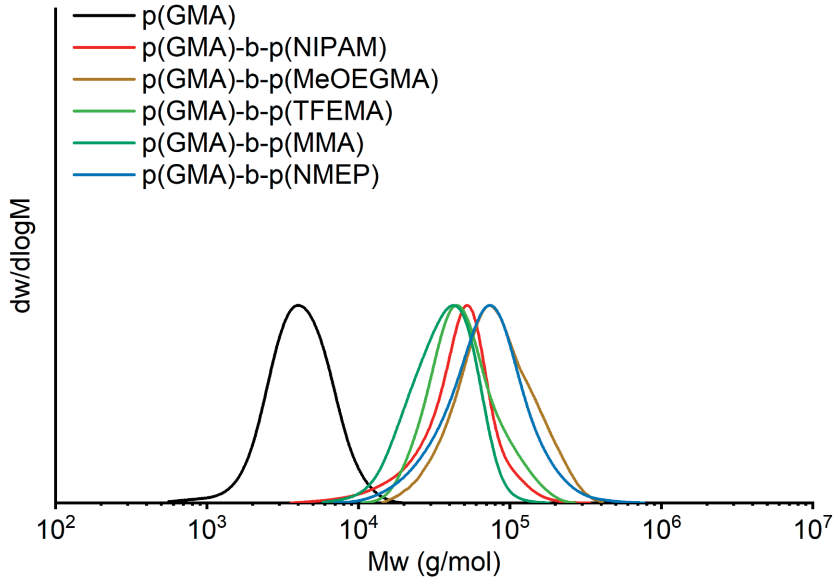

Supp. Figure 5.1 GPC traces for poly(GMA)$_{20}$ and block copolymers.

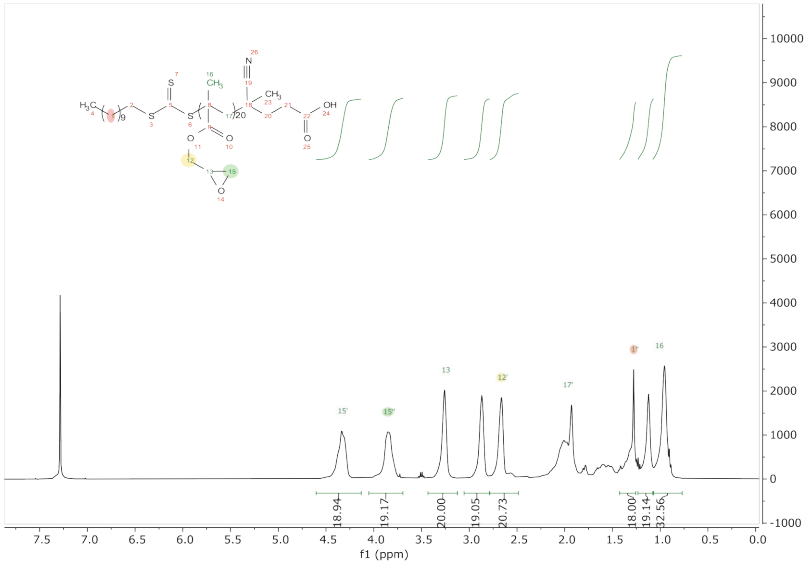

Supp. Figure 5.2 ^{1}H NMR spectrum of poly(GMA)$_{20}$ (in $CDCl_3$, 400 MHz, 298K)

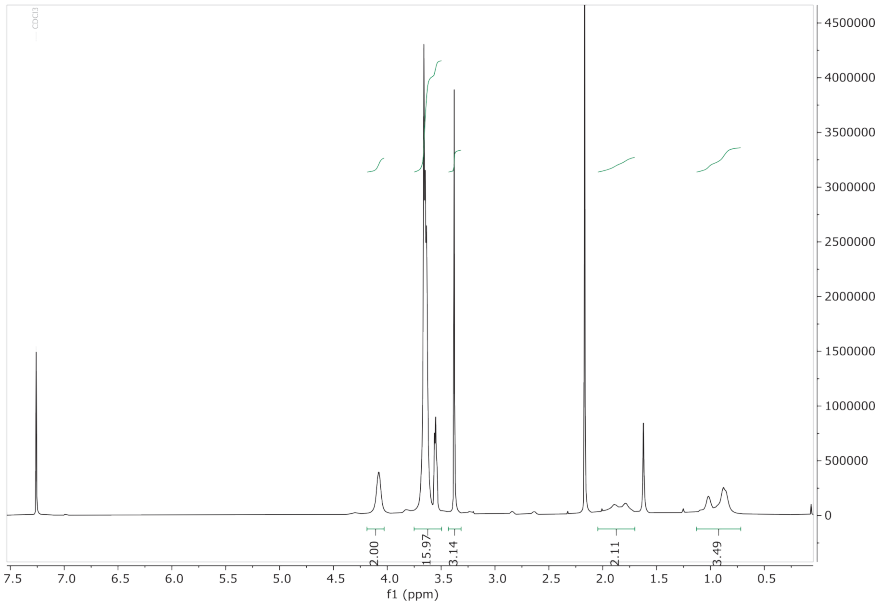

Supp. Figure 5.3 ^{1}H NMR spectrum of poly(GMA)-*b*-poly(MeOEGMA) (in $CDCl_3$, 400 MHz, 298K).

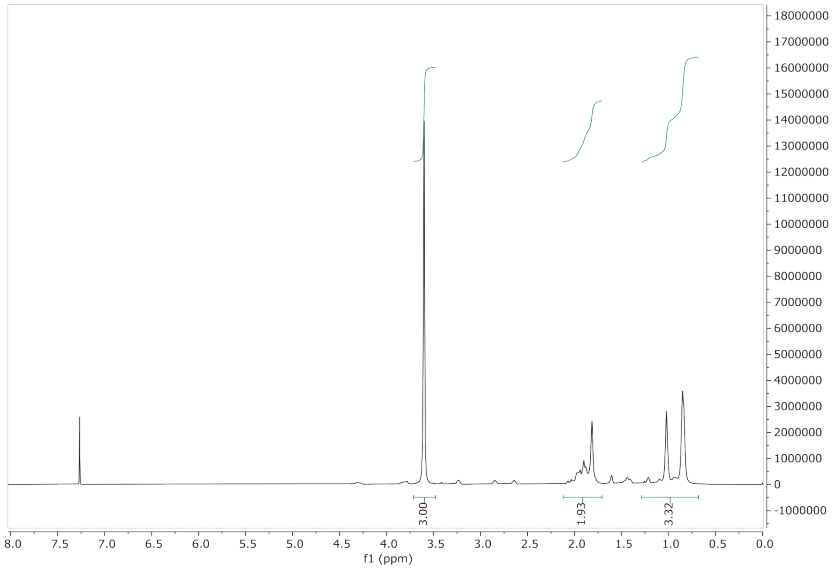

Supp. Figure 5.4 ^{1}H NMR spectrum of poly(GMA)-*b*-poly(MMA) (in $CDCl_3$, 400 MHz, 298K).

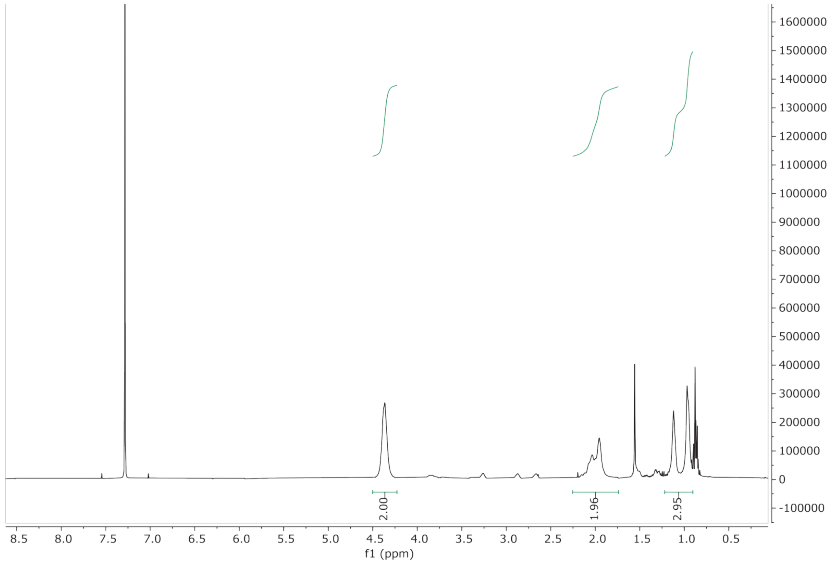

Supp. Figure 5.5 ^{1}H NMR spectrum of poly(GMA)-*b*-poly(TFEMA) (in $CDCl_3$, 400 MHz, 298K).

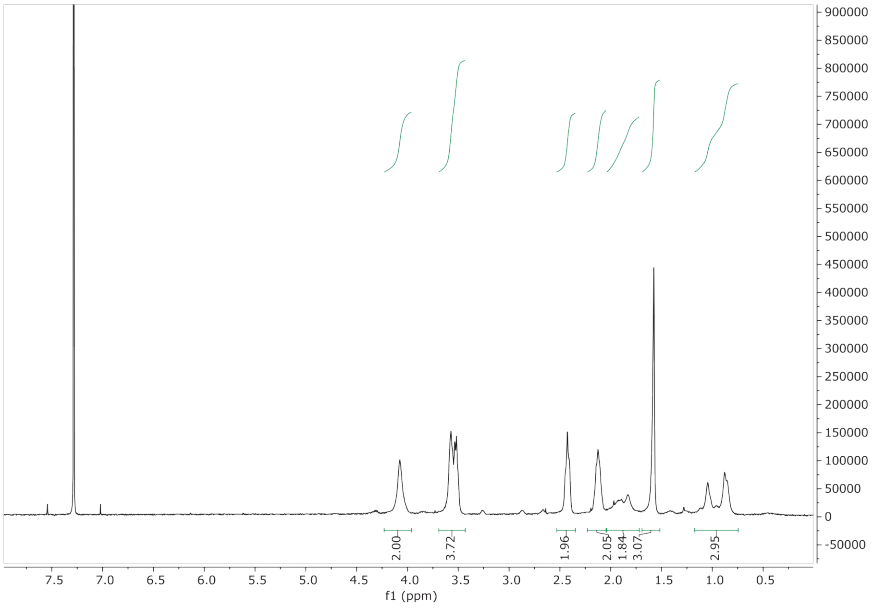

Supp. Figure 5.6 ^{1}H NMR spectrum of poly(GMA)-*b*-poly(NMEP) (in $CDCl_3$, 400 MHz, 298K).

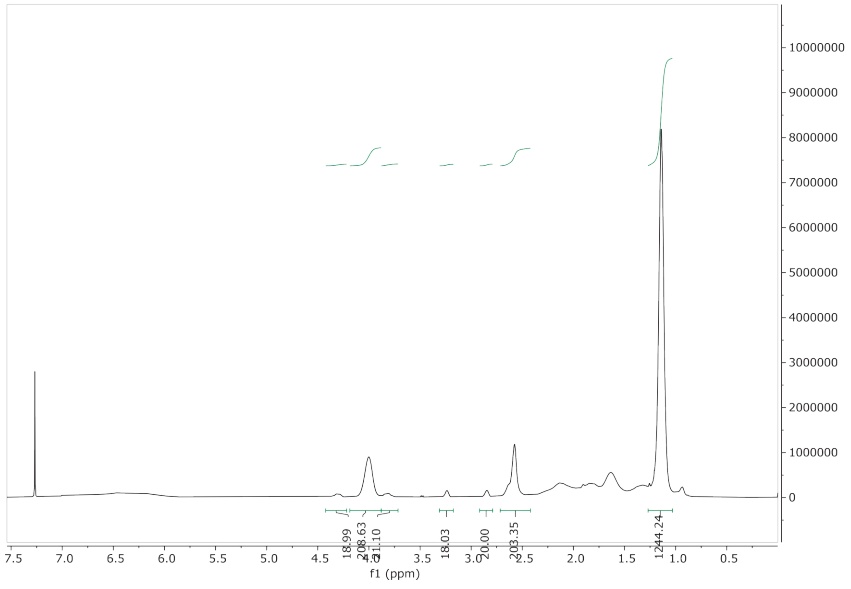

Supp. Figure 5.7 ^{1}H NMR spectrum of poly(GMA)-*b*-poly(NIPAM) (in $CDCl_3$, 400 MHz, 298K).

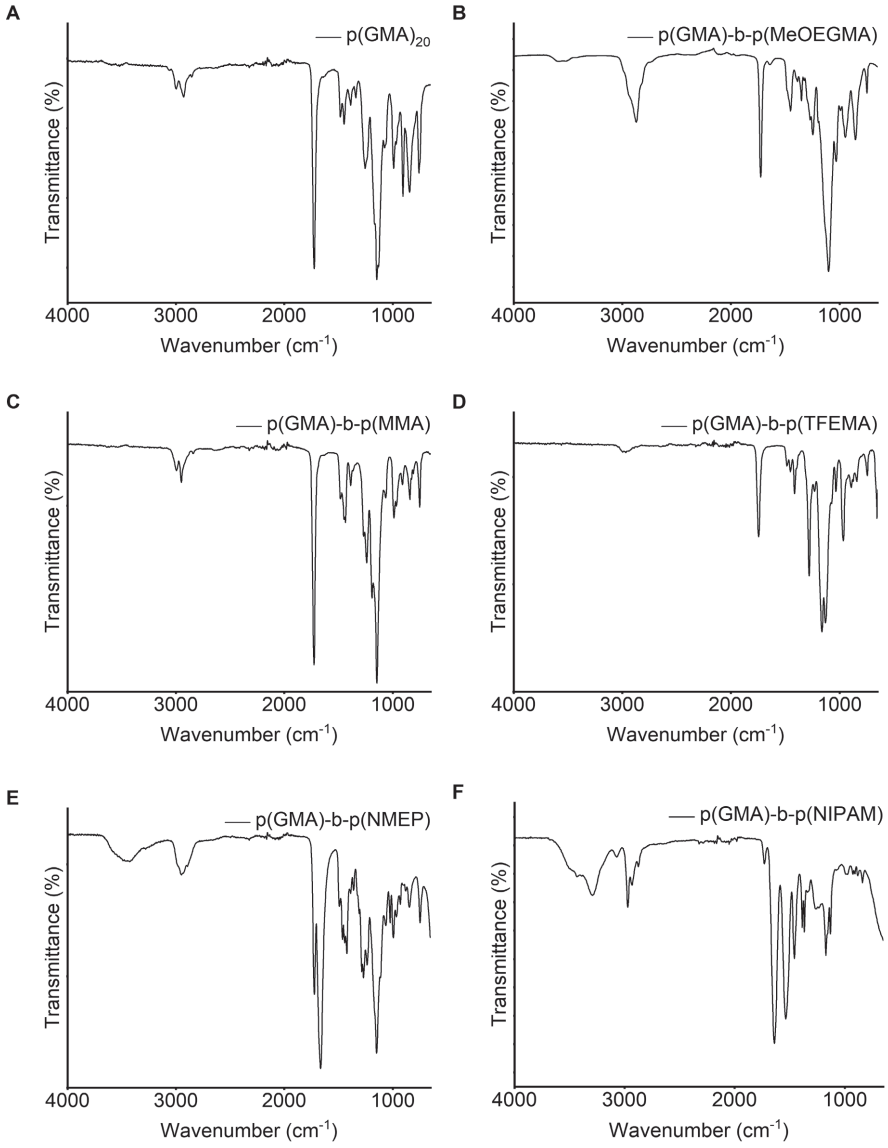

Supp. Figure 5.8 FT-IR spectra of **(A)** poly(GMA)$_{20}$, **(B)** poly(GMA)-*b*-poly(MeOEGMA), **(C)** poly(GMA)-*b*-poly(MMA), **(D)** poly(GMA)-*b*-poly(TFEMA), **(E)** poly(GMA)-*b*-poly(NMEP), and **(F)** poly(GMA)-*b*-poly(NIPAM).

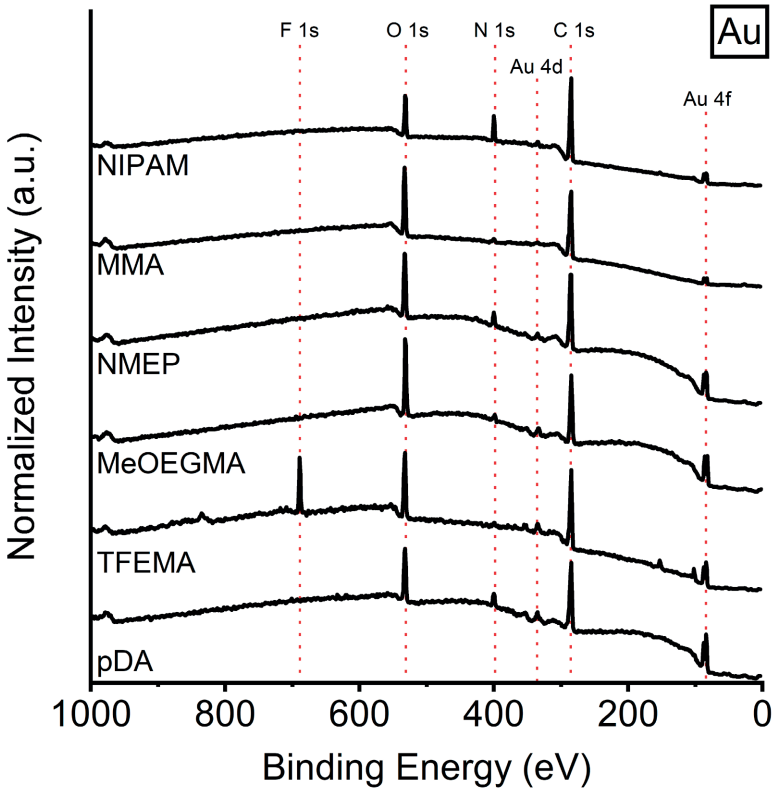

Supp. Figure 5.9 XPS wide scan spectra for gold substrates after modification with poly(dopamine) and after subsequent grafting of poly(GMA)-*b*-poly(TFEMA), poly(GMA)-*b*-poly(MeOEGMA), poly(GMA)-*b*-poly(NMEP), poly(GMA)-*b*-poly(MMA) and poly(GMA)-*b*-poly(NIPAM).

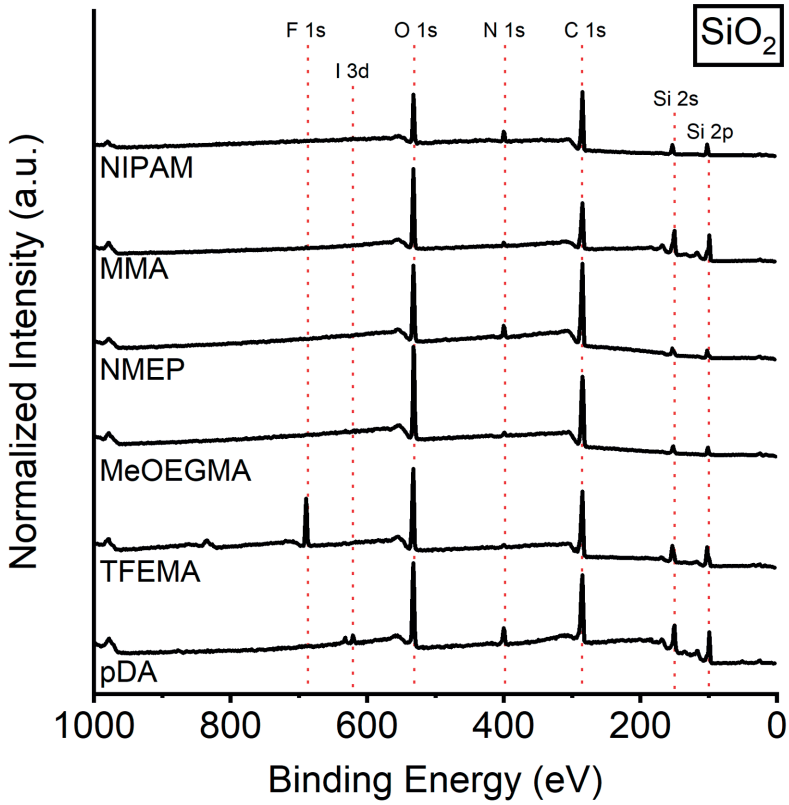

Supp. Figure 5.10 XPS wide scan spectra for SiO_2 substrates after modification with poly(dopamine) and after subsequent grafting of poly(GMA)-*b*-poly(TFEMA), poly(GMA)-*b*-poly(MeOEGMA), poly(GMA)-*b*-poly(NMEP), poly(GMA)-*b*-poly(MMA) and poly(GMA)-*b*-poly(NIPAM).

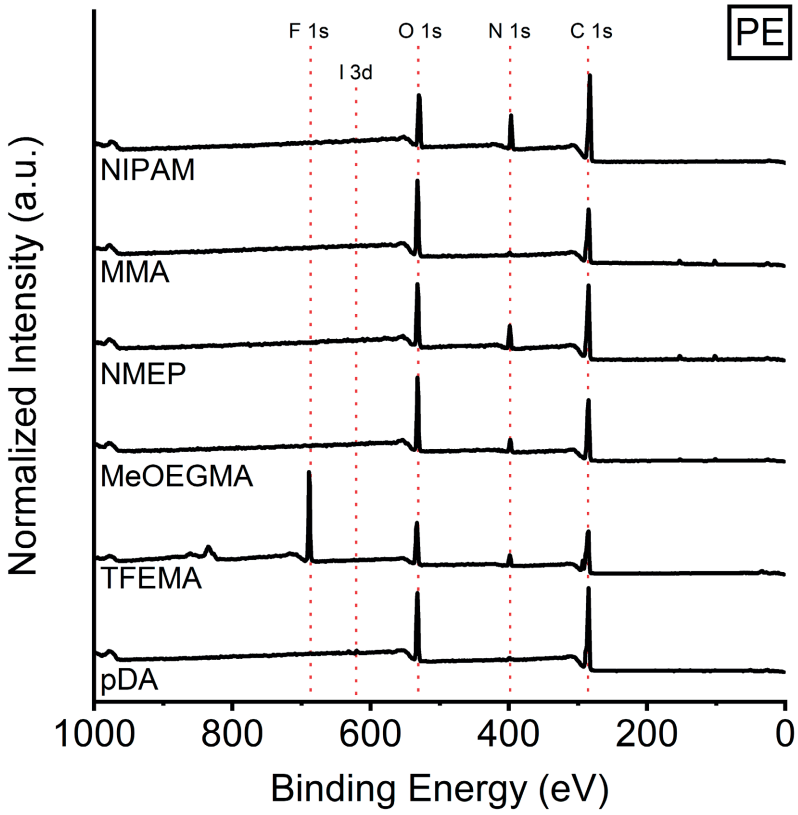

Supp. Figure 5.11 XPS wide scan spectra for PE substrates after modification with poly(dopamine) and after subsequent grafting of poly(GMA)-*b*-poly(TFEMA), poly(GMA)-*b*-poly(MeOEGMA), poly(GMA)-*b*-poly(NMEP), poly(GMA)-*b*-poly(MMA) and poly(GMA)-*b*-poly(NIPAM).
Note: The wide scan spectra presented for PE substrates modified with block copolymers poly(GMA)-*b*-poly(TFEMA) and poly(GMA)-*b*-poly(MeOEGMA) showed minor N 1s signals. A control experiment was performed in which poly(dopamine)-modified substrates are submerged in DMSO at 80 °C overnight without block copolymer or TEA (Supp. Figure 17). Still, the N 1s signal appears, which implies that the nitrogen-containing compound was already present within the PE polymer layer and had migrated towards the surface.

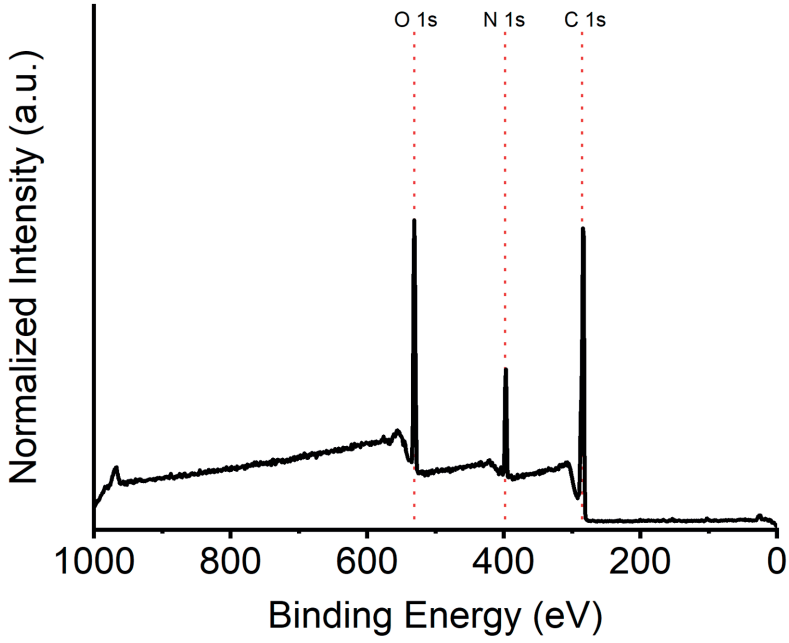

Supp. Figure 5.12 XPS wide scan spectra for control experiment involving immersion of PE substrate in DMSO overnight at 80 °C. The emergence of the N 1s signal implies that a nitrogen-containing compound was present within the PE polymer layer and had migrated towards the surface.

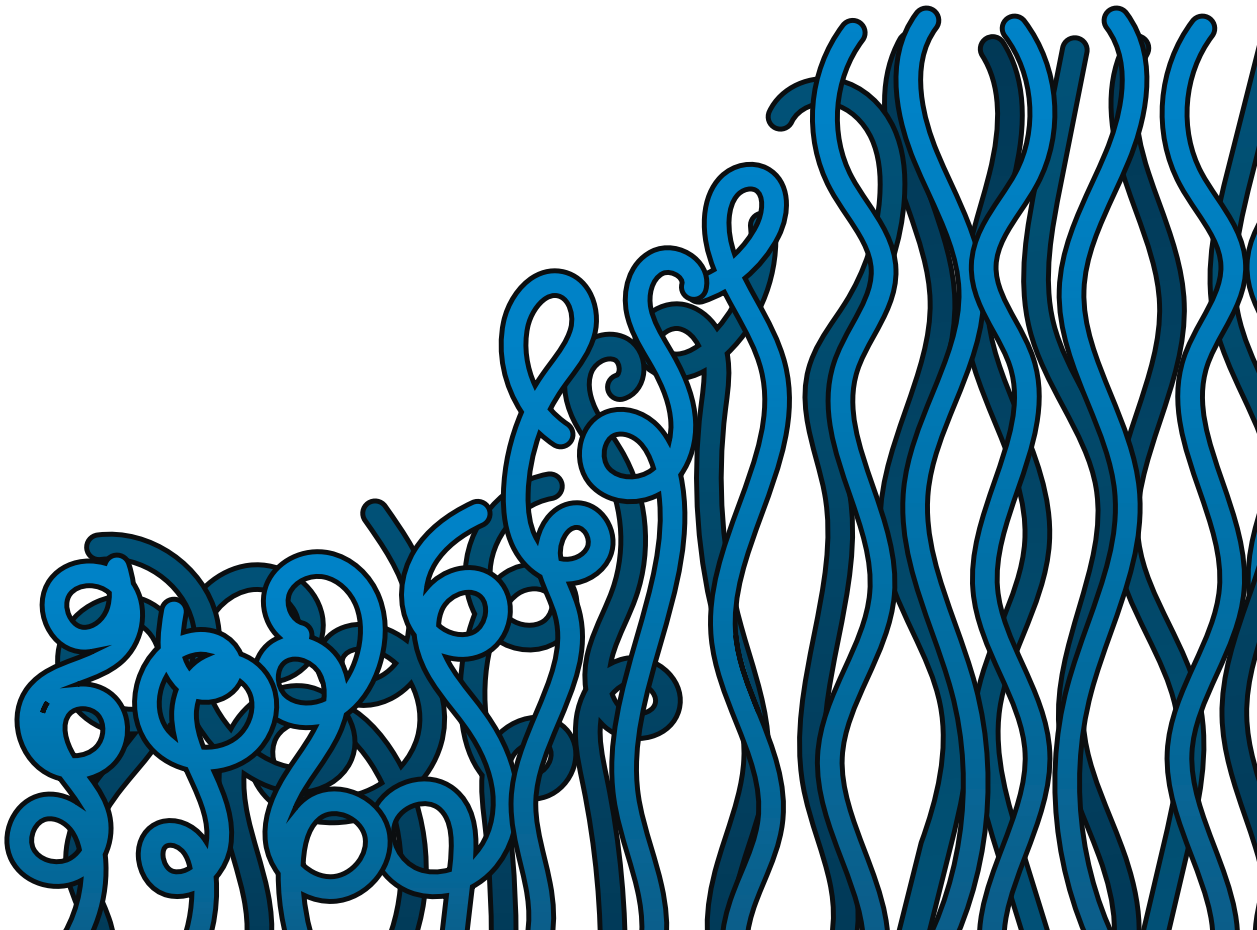

Chapter 6

General Discussion

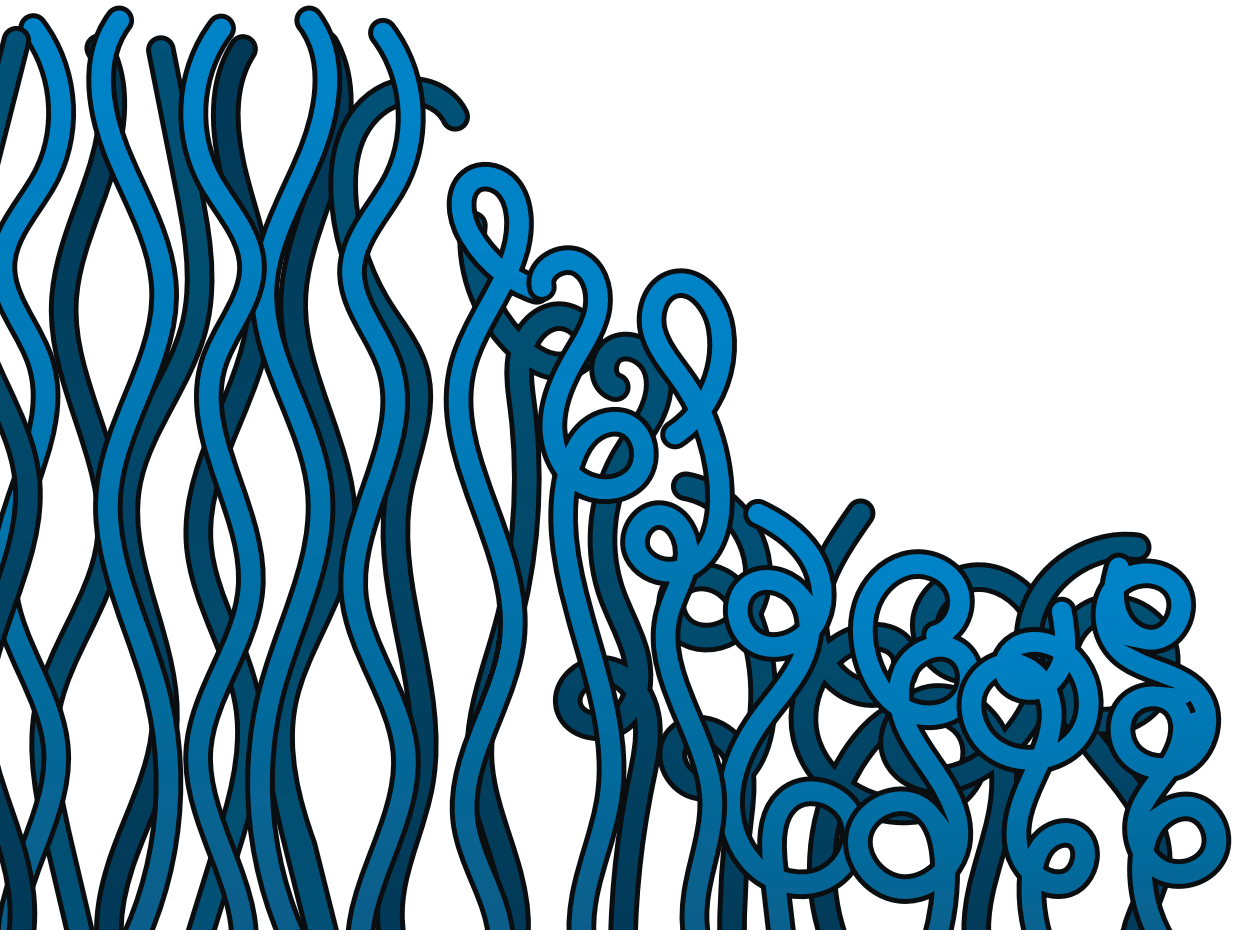

6.1 The loose ends to grafting-to

As amply demonstrated in this thesis, the grafting-to strategy provides several advantages in comparison to the grafting-from approach, and it is hoped that this can inspire researchers to select it for polymer brush synthesis. Polymerization reactions in solutions are easier to perform experimentally and the efficiency of solution polymerization lies significantly higher than that of surface-initiated polymerization reactions. The two-step grafting-to strategy presented in this thesis exhibits these features and is a promising addition to the currently available synthesis procedures. Following our studies, however, a number of aspects remain that demand further investigation.

6.1.1 Brush density

The most apparent disadvantage to grafting-to polymer brush synthesis is the relatively low grafting density that can be obtained in comparison with grafting-from strategies. The limitation in film thickness that can be achieved originates from the excluded volume interactions that prevent attachment of polymers at high grafting densities.[1] As a consequence, studies that describe grafting-to strategies in which polymers are attached to a substrate from solution typically report dry polymer brush thicknesses of several nanometers, at most.[2–7] The self-limiting effect can be viewed as a positive feature of the grafting-to approach, as it facilitates the synthesis of highly uniform polymer brush coatings with a reproducible thickness.[8,9] Still, many studies are designed to minimize this effect to obtain the highest possible grafting densities. That objective is particularly relevant for antifouling polymer brush coatings, which have been reported to benefit from a high chain surface density.[10]

The grafting densities and film thickness that we reported for the two-step grafting-to procedure presented in this thesis are relatively high for grafting-to procedures. In **Chapter 4**, we demonstrate that after optimization of poly(dopamine) deposition conditions, poly(GMA)-*b*-poly(NIPAM)$_{210}$ layer thickness of 19 ± 3 nm and grafting densities of 0.48 ± 0.07 chains/nm^2 were achieved. Both values redefine the state-of-the-art in this field. Although these results are thus highly encouraging in terms of the value of the method for polymer brush synthesis methods, the origin of the high chain density remains unknown. A review of grafting-to studies reveals there are several reports that show polymer brush coatings of similarly high grafting densities, but these were synthesized by grafting under cloud-point conditions or melt conditions.[2,3,7,11–21] Under cloud-point conditions, also known as θ-conditions, the solubility of the polymers is minimal and the chains adopt a more tight conformation resulting in an increase in achievable grafting densities at the

surface.[2,3,7,15,17,18,22,23] Excluded volume interactions are screened out when grafting from melt, which further enables production of high grafting density polymer brushes.[11,19,20,24–26]

One of the factors that potentially could contribute to the high grafting density of the polymer brushes prepared using the grafting-to procedure presented in this study is the relatively high concentration that is employed. Several studies have indicated that chain density on the surface increases substantially with polymer concentration during the grafting step.[27,28] For the grafting-to reactions described in **Chapter 4**, the concentration of poly(GMA)-*b*-poly(NIPAM)$_{210}$ (37.9 kDa) is approximately 0.26 mM (10 mg/mL). However, comparison with other studies indicate that similar concentrations have been employed in grafting-to reactions but yielded significantly lower grafting densities.[2,3] Evidently, there must be additional causes for the high grafting density of the block copolymers that was found in this study.

The primary distinctive feature of the block copolymers that are employed in our procedure is the presence of a large and multivalent anchoring motif. All of the polymers that were employed were equipped with twenty repeating units of GMA to facilitate covalent attachment to the poly(dopamine) film. The multivalency of these segments that is displayed over an extended spatial range – 20 monomer units – is expected to play an essential role in the efficient binding of the block copolymers to the poly(dopamine) film. Unfortunately, there are but few reports that discuss the relation between number of anchoring groups in the grafted polymer and grafting density. The studies that did investigate this dependence indicated that the relation is not straightforward. For shorter anchoring segments (with degree of polymerization DP_n = 1–4), it was found that grafted thickness increased with the number of anchoring groups.[12,29] The increased grafting efficiency could be explained by increased enthalpic gain of the adhesion.[9,29] Since the adhesion of polymers to a surface is believed to be a thermodynamic equilibrium governed by enthalpic attraction and entropic repulsion interactions, incorporation of additional adhesive groups increases surface affinity and therefore grafting density.[9,30] Conversely, studies of much larger anchoring segments (DP_n = 34–2850) indicated that a lower number of reactive groups yielded higher grafting densities.[31,32] This result was attributed to the large surface area that is covered by the longer anchoring segments, which covers many reactive sites on the surface and prevents other polymers from binding. The findings of these studies imply that there likely is an optimum for the number of repeating units that balances the enthalpic gain and the area covered on the surface. With respect to our grafting-to procedure, this conclusion warrants additional research in which the number of repeating GMA units is systematically varied. Such a study of this variable will not only be an addition to the optimization of the procedure presented in this thesis, but will perhaps

contribute to the understanding of this relatively underinvestigated aspect of grafting-to approaches in general.

In addition to the length of the anchoring segment, the results presented in **Chapter 4** indicate that the thickness of the poly(dopamine) film plays a prominent role during the grafting step. With increasing poly(dopamine) thickness, the amount of block copolymer that is grafted to the film also increases. To be specific, under otherwise identical conditions, the thickness of the grafted polymers could be raised from 6 nm to 19 nm when the poly(dopamine) thickness was increased from 5 to 23 nm. Interestingly, a similar effect has been observed in previous grafting-to studies.[13,33] For the grafting-to reactions in those studies, which were performed from melt, it was found that higher grafting densities were achieved on thicker anchoring layers. It was hypothesized that with higher thickness of the anchoring layer, the number of binding sites increases and therefore it is possible to achieve higher grafting densities. Although those results clearly correspond with the observations that we made in our grafting experiments, it remains an open question whether an increase in the number of reactive sites contributes as significantly in grafting-to reactions from solution. The excluded volume effects, present in reactions in solution, will most likely have a stronger limiting effect on the grafting density than the number of reactive sites.

Clearly, the grafting densities that are achieved using the grafting-to procedure presented here are promising and at the same time surprising. Although there are indications that the long anchoring motif and increased poly(dopamine) film thickness contribute to the outstanding grafting efficiency, it is necessary to further investigate grafting reactions to fully determine the origins of the success. The starting point for these investigations should be the study of different sizes of the poly(GMA) anchoring segment (*e.g.*, DP_{GMA} = 5, 10, 15, 20, 30, 40, 50) and their effect on grafting efficiency. Such a study would indicate to what extent the poly(GMA) blocks contribute to the high grafting densities observed in our studies and, at the same time, whether the grafting density can be increased even more. Additionally, it would be of interest to perform kinetics experiments to determine the time frame in which the grafting reactions reach their plateau values.[27] Grafting-to reactions typically adhere to a three-regime reaction profile, which consists of initial grafting, followed by a dormant period and then a final grafting process.[27] A kinetics study will give insight into whether the grafting-to procedure presented in our studies behaves accordingly. The results obtained by these experiments are expected to contribute to understanding of the grafting densities observed for the grafting-to procedure presented in this thesis.

The availability of grafting-to techniques that yield high grafting densities as demonstrated in this thesis presents a large opportunity for the community due to its easy application, scalability and reproducibility. This advancement can therefore be of tremendous value in the production of high-end coatings in various applications such as biomedical devices, membranes and photovoltaics.

6.1.2 Modularity

Apart from the high grafting densities that can be obtained using the two-step grafting-to procedure presented in this thesis, the modularity of the approach is its most appealing aspect. In short, this procedure provides two types of modularity, that is with respect to surface type as well as polymer functionality.

The substrate-independent applicability of the approach allows modification of any surface type. Although the study presented in **Chapter 5** is limited to the description of the modification of gold, silicon oxide and polyester-coated glass, it can be expected that the approach can be applied to a much larger range of surface types. This assumption is primarily based on the numerous studies that describe the successful deposition of poly(dopamine) films on countless materials, which ranges from metals to polymers, and from high surface energy to low surface energy substrates.[34–36] Furthermore, in a recent study by Svoboda *et al.*, it was demonstrated that although the substrate's nature will affect the chemical and physical properties of the poly(dopamine) film in the first few nanometers, the grafted layers display near-identical features with increased film thickness.[37] It is therefore likely that the method presented here can be easily translated to poly(dopamine) deposited on different surface types.

The diversity that can be obtained in polymer functionality was described in **Chapter 5** by preparing five block copolymers of varying functionality and subsequently grafting them to the poly(dopamine)-modified substrates. The produced coatings exhibit distinct surface properties, which was plainly illustrated by the markedly different wettability throughout the surfaces. The conditions for the RAFT polymerizations were purposely kept constant for each block copolymer, aside from addition of the correct monomer and variation of the reaction time. Whereas this experimental procedure was appropriate for synthesis of the reported block copolymers, it may require several modifications should the block copolymer library be extended. For instance, it is conceivable that a different solvent, RAFT agent or radical initiator may be required to incorporate a strongly hydrophilic or hydrophobic polymer block. Fortunately, examples of such block copolymers and their synthesis procedures are available.

6.2 Thermoresponsive polymer brushes in biomedical devices

The majority of studies that involve thermoresponsive polymer brushes is concluded by praising their huge potential for future application in biomedical devices. This section will focus on the most promising developments in this field.

6.2.1 Emerging applications

The incorporation of thermoresponsive polymers in coating materials has led to many innovations in polymer brush science.[38] As mentioned in **Chapter 1**, of all thermoresponsive polymers, poly(NIPAM) is by far the most intensively researched thermoresponsive polymer, due to its LCST at approximately 32 °C. The application of poly(NIPAM) as polymer brush coating has sparked the production of innovative technologies in the scientific field. Several of these technologies have been studied intensively and exhibit highly promising features. Specifically, the application of poly(NIPAM) polymer brushes in cell culture dishes, protein purification and kill-and-release coatings is of great interest.[38–40]

Transplantation of cell sheets is a procedure that can be employed to replace or restore cell tissue.[41,42] These cell sheets are typically grown in cell culture dishes and eventually detached from the dish surface by either mechanical scraping or trypsinization.[43] These methods are relatively aggressive and are likely to damage a fraction of the cells.[43] By growing the cell sheets on thermoresponsive polymers, the phase transition behavior can be employed to trigger their release without inflicting any damage.[39] Cell culture dishes coated with poly(NIPAM) hydrogels are currently produced on a large scale via electron beam polymerization, and are commercially available.[39] The advantages of using poly(NIPAM) polymer brushes instead of hydrogels for this purpose have been investigated.[44–46] It became apparent that the interaction of cell lines with the poly(NIPAM) brushes can be tuned by tailoring grafting density and chain length,[44] which evidently adds to their functionality. Another promising feature is the ability to produce cell tissue of specific orientations by micropatterning the brush coating.[45] The main limitation of using poly(NIPAM) in cell culture dishes is the relatively poor affinity of the polymer towards different types of cell lines.[43] Hence, this technology can currently exclusively be employed for specific cell lines.

In addition to regulation of interactions with cells, the difference between surface properties of thermoresponsive polymer brushes above and below LCST can be employed to steer protein adsorption, as we also demonstrated in **Chapter 3**.[47,48] The switchable interaction has been utilized for purification of protein mixtures.[38,49,50] Reverse phase liquid chromatography is commonly used to separation and purification of protein mixtures.[49]

Typically, this technique relies on hydrophobic or ionic interactions of proteins with the stationary phase.[50] To achieve separation, the strength of interactions between analyte and column is modulated through the mobile phase by addition of organic solvent or variation of salt concentration. A drawback of using high salt concentrations and organic solvents is that they may inflict irreversible damage to the analyte. Introduction of poly(NIPAM) to the column has allowed modulation of the interactions between analyte and stationary phase via temperature.[49,50] Consequently, pure water can be used as a mobile phase that does not alter the properties of the analyte.

The final application of interest that will be discussed here are thermoresponsive polymer brushes that employ the so-called "kill-release" strategy.[51–57] These dual-functional coatings combine bactericidal and antifouling properties to kill bacteria and subsequently release the dead bacterial cells.[53] To achieve this dual functionality, poly(NIPAM) brushes are commonly copolymerized with a second monomer or synthesized as binary brushes to introduce a bactericidal unit or polymer.[51] The "kill-release" working mechanism relies on the phase transition of the thermoresponsive poly(NIPAM). At temperatures above the LCST, the brushes are collapsed and bacteria are able to approach the surface. Apart from enabling adsorption, the collapse of the polymer brushes results in exposure of the bactericidal units in the coating.[55] The bacterial cells are therefore killed upon adsorption on the surface. The dead cells can then be released from the surface coating by decreasing the temperature below the LCST. The poly(NIPAM) polymers swell and induce the detachment of the dead cells from the surface to prevent biofilm formation on the surface. This type of coating can potentially be employed to diminish the chance of bacterial infections in biomedical devices.

The applications of poly(NIPAM) polymer brushes mentioned here are but a grasp of the exciting technologies that have been and are currently developed. Naturally, there are also a few aspects related to thermoresponsive brush coatings that require further attention. A commonly encountered phenomenon, discussed for many of these technologies, is that both grafting density and polymer size strongly affect the properties of the polymer brush and its interactions with the surroundings. Mere modulation of the poly(NIPAM) brush thickness, for instance, results in large differences in cell adhesion.[58] Similarly, cell adhesion occurs more readily on poly(NIPAM) brushes of low grafting density, than on those of high grafting density.[59] These examples illustrate how brush properties affect the performance of thermoresponsive brushes in cell sheet dishes. It is safe to assume that such effects will also play a role in other types of applications. Evidently, it is of crucial importance that these parameters are thoroughly studied to ensure successful and standardized implementation in future applications. Ideally, a straightforward technique

to determine grafting densities and polymer size of polymer brushes will be developed in the near future.[1] Until then, it will be crucial for any of the technologies mentioned above to perform extensive analysis of device performance as a function of brush density and polymer chain length. We argue that in the coming years, the focus should be on mapping the effect of these properties on device performance as accurately as possible. These studies will optimize the performance of these technologies and prepare them for future application.

6.2.2 Potential of poly(NMEP) brushes

With the synthesis and characterization of poly(NMEP) brushes, described in **Chapter 2**, we presented a new member to the library of thermoresponsive polymer brush coatings. The main goal of our study was to find an alternative to poly(NIPAM) that could be incorporated in copolymer structures more easily. By reinitiation of a poly(NMEP) brush and addition of a poly(MeOEGMA) block, we confirmed that poly(NMEP) can indeed be easily copolymerized with other monomers. The measurements performed using AFM in aqueous environment indicated that the LCST of poly(NMEP) brushes lies between 40 °C and 50 °C, notably higher than the LCST for poly(NIPAM).

The introduction of thermoresponsive features using poly(NMEP) brushes in biomedical devices is not as apparent due to its relatively high LCST. The onset temperature of protein denaturation is 40–45 °C, which implies that application of thermoresponsive features of poly(NMEP) brushes in biological media is likely to cause irreversible damage to the proteins.[60] Fortunately, it is possible to alter the LCST of a polymer by introduction of comonomers in its structure. For instance, copolymerization of NIPAM and NMEP was performed to produce copolymers with LCSTs ranging from 34–36 °C, depending on monomer ratio.[61] In fact, these copolymers were then applied as a coating in cell culture dishes and showed both good cell adhesion as well as efficient temperature-induced detachment. To expand on this result, we envision that investigation of the compatibility of poly(NMEP) brushes with different cell lines may indeed prove its complementary features to poly(NIPAM) in cell culture dish application (Figure 6.1).

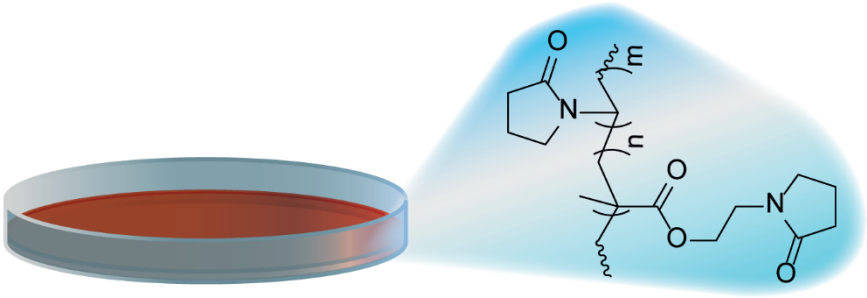

Figure 6.1 Potential application of NMEP as component in thermoresponsive copolymer brush with *N*-vinylpyrrolidone in cell culture dishes.

A particularly interesting candidate for copolymerization with NMEP is its vinylic analog, *N*–vinylpyrrolidone. Poly(*N*-vinylpyrrolidone) (PVP) has been used in biomedical applications for nearly a century due to its high biocompatibility and inertness.[62] Among these applications, PVP polymer brushes have been employed as an antifouling surface coating to prevent adsorption of various proteins.[63–65] By copolymerization of NMEP with the more hydrophilic *N*-vinylpyrrolidone, the LCST will most likely be lower than the LCST of poly(NMEP), which makes it more suitable for potential application in physiological media.[61,66]

In conclusion, we believe that NMEP has great potential in biomedical applications, specifically as a component in copolymer brush structures. To verify this premise, a substantial amount of research with regards to LCST optimization and biocompatibility studies is yet to be performed. Based on those studies, the added value of poly(NMEP) to the library of thermoresponsive polymers can be reassessed.

6.3 Prospects for Polymer Brushes

In spite of the vast number of studies that have been performed since polymer brushes were first described 50 years ago, the field is still far from broad commercial application.[67]

The progress in the field of polymer brushes depends for a large part on innovations that are made in controlled radical polymerization techniques. For a long time, these polymerization methods required an oxygen-free environment, which greatly hampered large-scale application.[68,69] Several oxygen-tolerant techniques, such as photoelectron transfer reversible addition-fragmentation chain-transfer polymerization (PET-RAFT) and activators regenerated by electron transfer atom transfer radical polymerization (ARGET ATRP), have been developed during the past years.[70,71] These techniques, as well as their corresponding surface-initiated procedures, have taken away a major obstacle standing in

the way of industrial production of polymer brushes.[69,72] Unfortunately, additional obstacles remain, such as the practical challenges that arise with polymer brush synthesis on large or non-flat substrates. A number of procedures has been developed in an attempt to overcome these challenges and bring upscaling one step closer.[67,73,74] Oxygen-tolerant ARGET SI-ATRP techniques were used to perform "paint-on" and roll-to-roll polymer brush synthesis on substrates of 30 × 10 cm and 50 × 50 cm, respectively.[73,74] Using these techniques, polymer brush coatings of different functionality and appreciable layer thicknesses (> 30 nm) were achieved. Industrial application of these techniques is not yet feasible, mainly due to the long reaction times required to produce the coatings. Nevertheless, it is this type of developments made in scientific research that brings the field one step closer to the market.

Aside from the polymerization method, the attachment strategy is of critical importance for eventual commercial applications. Ideally, the strategy is substrate-independent and able to bind the polymer chains strongly to the surface. As we have discussed and demonstrated in this thesis, one of the prime candidates for this task is poly(dopamine). Various studies have indeed indicated that the substrate-independent adhesion of the poly(dopamine) films is outstanding and as yet unmatched by any other material.[34,36,75] The strength and durability of this adhesion, however, has rarely been investigated. In fact, our own practical experiences working with poly(dopamine) match those of Ryu *et al.*, as they comment on the typically poor abrasion or delamination resistance of the films.[36] Extensive stability tests per surface type in various environments will need to be performed before poly(dopamine) can be considered for commercial applications.

As was mentioned in **Chapter 1**, polymer brush coatings are arguably the most powerful tool to functionalize a material's surface. The ability to precisely tailor polymer properties provides the producer with seemingly infinite possibilities to produce state-of-the-art coating formulations. The recent developments in controlled radical polymerization techniques and surface adhesives have brought application of polymer brushes closer than ever. It is our expectation that, especially in biomedical applications, polymer brush coatings will become increasingly prominent in the coming years. More specifically, we envision that, in the biomedical field, polymer brush coatings will predominantly be applied to prevent biofilm formation, due to their superior antifouling capabilities. Applications are expected to range from small substrates, such as biosensor interface and membranes, to much larger materials, such as medical implants. Thermoresponsive polymer brushes are anticipated to be applied in more specialized and intricate equipment. In fact, we believe that the application of thermoresponsive brushes in cell sheet dishes will be realized in the near future.

6.4 References

1. Michalek, L., Barner, L. & Barner-Kowollik, C. Polymer on Top: Current Limits and Future Perspectives of Quantitatively Evaluating Surface Grafting. *Adv. Mater.* **30**, 1706321 (2018).
2. Schweigerdt, A., Heinen, S., Stöbener, D. D. & Weinhart, M. Grafting Density-Dependent Phase Transition Mechanism of Thermoresponsive Poly(glycidyl ether) Brushes: A Comprehensive QCM-D Study. *Langmuir* **37**, 7087–7096 (2021).
3. Heinen, S. & Weinhart, M. Poly(glycidyl ether)-Based Monolayers on Gold Surfaces: Control of Grafting Density and Chain Conformation by Grafting Procedure, Surface Anchor, and Molecular Weight. *Langmuir* **33**, 2076–2086 (2017).
4. Chan, J. W., Huang, A. & Uhrich, K. E. Self-Assembled Amphiphilic Macromolecule Coatings: Comparison of Grafting-From and Grafting-To Approaches for Bioactive Delivery. *Langmuir* **32**, 5038–5047 (2016).
5. Sofia, S. J., Premnath, V. & Merrill, E. W. Poly(ethylene oxide) grafted to silicon surfaces: Grafting density and protein adsorption. *Macromolecules* **31**, 5059–5070 (1998).
6. Heinen, S. *et al.* Transfer of functional thermoresponsive poly(glycidyl ether) coatings for cell sheet fabrication from gold to glass surfaces. *J. Mater. Chem. B* **6**, 1489–1500 (2018).
7. Wang, Y. M. *et al.* Grafting density and antifouling properties of poly[N-(2-hydroxypropyl) methacrylamide] brushes prepared by "grafting to" and "grafting from". *Polym. Chem.* **13**, 3815–3826 (2022).
8. Chiarcos, R. *et al.* Short vs. long chains competition during " grafting to " process from melt. *Polym. Chem.* **13**, 3904–3914 (2022).
9. Chiarcos, R., Perego, M. & Laus, M. Polymer Brushes by Grafting to Reaction in Melt: New Insights into the Mechanism. *Macromol. Chem. Phys.* **2200400**, (2022).
10. Dai, W. *et al.* A negative correlation between water content and protein adsorption on polymer brushes. *J. Mater. Chem. B* **7**, 2162–2168 (2019).
11. Pop-Georgievski, O. *et al.* Nonfouling poly(ethylene oxide) layers end-tethered to polydopamine. *Langmuir* **28**, 14273–14283 (2012).
12. Dalsin, J. L. *et al.* Protein resistance of titanium oxide surfaces modified by biologically inspired mPEG-DOPA. *Langmuir* **21**, 640–646 (2005).
13. Iyer, K. S. & Luzinov, I. Effect of macromolecular anchoring layer thickness and molecular weight on polymer grafting. *Macromolecules* **37**, 9538–9545 (2004).
14. Laradji, A. M., McNitt, C. D., Yadavalli, N. S., Popik, V. V. & Minko, S. Robust, Solvent-Free, Catalyst-Free Click Chemistry for the Generation of Highly Stable Densely Grafted Poly(ethylene glycol) Polymer Brushes by the Grafting To Method and Their Properties. *Macromolecules* **49**, 7625–7631 (2016).
15. Emilsson, G. *et al.* Strongly stretched protein resistant poly(ethylene glycol) brushes prepared by grafting-to. *ACS Appl. Mater. Interfaces* **7**, 7505–7515 (2015).
16. Kingshott, P., Thissen, H. & Griesser, H. J. Effects of cloud-point grafting, chain length, and density of PEG layers on competitive adsorption of ocular proteins. *Biomaterials* **23**, 2043–56 (2002).
17. Ortiz, R., Olsen, S. & Thormann, E. Salt-Induced Control of the Grafting Density in Poly(ethylene glycol) Brush Layers by a Grafting-to Approach. *Langmuir* **34**, 4455–4464 (2018).
18. Ghezzi, M. *et al.* Protein micropatterns by PEG grafting on dewetted PLGA films. *Langmuir* **30**, 11714–11722 (2014).

19. Luzinov, I., Julthongpiput, D., Malz, H., Pionteck, J. & Tsukruk, V. V. Polystyrene layers grafted to epoxy-modified silicon surfaces. *Macromolecules* **33**, 1043–1048 (2000).

20. Minko, S. *et al.* Synthesis of adaptive polymer brushes via 'grafting to' approach from melt. *Langmuir* **18**, 289–296 (2002).

21. Michalek, L., Mundsinger, K., Barner, L. & Barner-Kowollik, C. Quantifying Solvent Effects on Polymer Surface Grafting. *ACS Macro Lett.* **8**, 800–805 (2019).

22. Ogaki, R., Alexander, M. & Kingshott, P. Chemical patterning in biointerface science. *Mater. Today* **13**, 22–35 (2010).

23. Unsworth, L. D., Sheardown, H. & Brash, J. L. Protein-resistant polyethylene oxide-grafted surfaces: Chain density-dependent multiple mechanisms of action. *Langmuir* **24**, 1924–1929 (2008).

24. Jones, R. A. L., Lehnert, R. J., Schönherr, H. & Vancso, J. Factors affecting the preparation of permanently end-grafted polystyrene layers. *Polymer (Guildf).* **40**, 525–530 (1999).

25. Minko, S. *et al.* Bidisperse mixed brushes: Synthesis and study of segregation in selective solvent. *Macromolecules* **36**, 7268–7279 (2003).

26. Pop-Georgievski, O. *et al.* Poly(ethylene oxide) layers grafted to dopamine-melanin anchoring layer: Stability and resistance to protein adsorption. *Biomacromolecules* **12**, 3232–3242 (2011).

27. Sha, X., Xu, X., Sohlberg, K., Loll, P. J. & Penn, L. S. Evidence that three-regime kinetics is inherent to formation of a polymer brush by a grafting-to approach. *RSC Adv.* **4**, 42122–42128 (2014).

28. Taylor, W. & Jones, R. A. L. Producing high-density high-molecular-weight polymer brushes by a 'grafting to' method from a concentrated homopolymer solution. *Langmuir* **26**, 13954–13958 (2010).

29. Gillich, T. *et al.* Self-assembly of focal point oligo-catechol ethylene glycol dendrons on titanium oxide surfaces: Adsorption kinetics, surface characterization, and nonfouling properties. *J. Am. Chem. Soc.* **133**, 10940–10950 (2011).

30. Feuz, L., Leermakers, F. A. M., Textor, M. & Borisov, O. Adsorption of Molecular Brushes with Polyelectrolyte Backbones onto Oppositely Charged Surfaces: A Self-Consistent Field Theory. *Langmuir* **24**, 7232–7244 (2008).

31. Belder, G. F., Ten Brinke, G. & Hadziioannou, G. Influence of anchor block size on the thickness of adsorbed block copolymer layers. *Langmuir* **13**, 4102–4105 (1997).

32. Nunnery, G. A., Jacob, K. I. & Tannenbaum, R. Reactive adsorption of PS-PMMA block copolymers on concave alumina surfaces. *Langmuir* **28**, 14960–14967 (2012).

33. Zdyrko, B., Swaminatha Iyer, K. & Luzinov, I. Macromolecular anchoring layers for polymer grafting: Comparative study. *Polymer (Guildf).* **47**, 272–279 (2006).

34. Lee, H., Dellatore, S. M., Miller, W. M. & Messersmith, P. B. Mussel-Inspired Surface Chemistry for Multifunctional Coatings. *Science* **318**, 426–430 (2007).

35. Dreyer, D. R., Miller, D. J., Freeman, B. D., Paul, D. R. & Bielawski, C. W. Perspectives on poly(dopamine). *Chem. Sci.* **4**, 3796–3802 (2013).

36. Ryu, J. H., Messersmith, P. B. & Lee, H. Polydopamine Surface Chemistry: A Decade of Discovery. *ACS Appl. Mater. Interfaces* **10**, 7523–7540 (2018).

37. Svoboda, J., Král, M., Dendisová, M., Matějka, P. & Pop-Georgievski, O. Unraveling the influence of substrate on the growth rate, morphology and covalent structure of surface adherent polydopamine films. *Colloids Surfaces B Biointerfaces* **205**, 111897 (2021).

38. Nagase, K., Okano, T. & Kanazawa, H. Poly(N-isopropylacrylamide) based thermoresponsive polymer brushes for bioseparation, cellular tissue fabrication, and nano actuators. *Nano-Structures & Nano-Objects* **16**, 9–23 (2018).

39. Nagase, K., Yamato, M., Kanazawa, H. & Okano, T. Poly(N-isopropylacrylamide)-based thermoresponsive surfaces provide new types of biomedical applications. *Biomaterials* **153**, 27–48 (2018).

40. Li, D., Xu, L., Wang, J. & Gautrot, J. E. Responsive Polymer Brush Design and Emerging Applications for Nanotheranostics. *Adv. Healthc. Mater.* **10**, 2000953 (2021).

41. Ohki, T. *et al.* Prevention of Esophageal Stricture After Endoscopic Submucosal Dissection Using Tissue-Engineered Cell Sheets. *Gastroenterology* **143**, 582-588.e2 (2012).

42. Sato, M., Yamato, M., Hamahashi, K., Okano, T. & Mochida, J. Articular cartilage regeneration using cell sheet technology. *Anat. Rec.* **297**, 36–43 (2014).

43. Nash, M. E., Healy, D., Carroll, W. M., Elvira, C. & Rochev, Y. A. Cell and cell sheet recovery from pNIPAm coatings; Motivation and history to present day approaches. *J. Mater. Chem.* **22**, 19376–19389 (2012).

44. Takahashi, H., Nakayama, M., Yamato, M. & Okano, T. Controlled Chain Length and Graft Density of Thermoresponsive Polymer Brushes for Optimizing Cell Sheet Harvest. *Biomacromolecules* **11**, 1991–1999 (2010).

45. Takahashi, H., Nakayama, M., Itoga, K., Yamato, M. & Okano, T. Micropatterned Thermoresponsive Polymer Brush Surfaces for Fabricating Cell Sheets with Well-Controlled Orientational Structures. *Biomacromolecules* **12**, 1414–1418 (2011).

46. Takahashi, H. & Okano, T. Cell Sheet-Based Tissue Engineering for Organizing Anisotropic Tissue Constructs Produced Using Microfabricated Thermoresponsive Substrates. *Adv. Healthc. Mater.* **4**, 2388–2407 (2015).

47. Nagase, K. *et al.* Thermo-responsive protein adsorbing materials for purifying pharmaceutical protein on exposed charging surface. *J. Mater. Chem.* **21**, 2590–2593 (2011).

48. Xue, C. *et al.* Protein adsorption on poly(N-isopropylacrylamide) brushes: Dependence on grafting density and chain collapse. *Langmuir* **27**, 8810–8818 (2011).

49. Tan, I., Roohi, F. & Titirici, M. M. Thermoresponsive polymers in liquid chromatography. *Anal. Methods* **4**, 34–43 (2012).

50. Nagase, K. Thermoresponsive interfaces obtained using poly(N-isopropylacrylamide)-based copolymer for bioseparation and tissue engineering applications. *Adv. Colloid Interface Sci.* **295**, 102487 (2021).

51. Wei, T., Qu, Y., Zou, Y., Zhang, Y. & Yu, Q. Exploration of smart antibacterial coatings for practical applications. *Curr. Opin. Chem. Eng.* **34**, 100727 (2021).

52. Wang, X. *et al.* Temperature-Responsive Hierarchical Polymer Brushes Switching from Bactericidal to Cell Repellency. *ACS Appl. Mater. Interfaces* **9**, 40930–40939 (2017).

53. Wei, T., Tang, Z., Yu, Q. & Chen, H. Smart Antibacterial Surfaces with Switchable Bacteria-Killing and Bacteria-Releasing Capabilities. *ACS Appl. Mater. Interfaces* **9**, 37511–37523 (2017).

54. Jiang, R. *et al.* Thermoresponsive Nanostructures: From Mechano-Bactericidal Action to Bacteria Release. *ACS Appl. Mater. Interfaces* **13**, 60865–60877 (2021).

55. Yu, Q., Wu, Z. & Chen, H. Dual-function antibacterial surfaces for biomedical applications. *Acta Biomater.* **16**, 1–13 (2015).

56. Yu, Q., Ista, L. K. & López, G. P. Nanopatterned antimicrobial enzymatic surfaces combining biocidal and fouling release properties. *Nanoscale* **6**, 4750–4757 (2014).

57. Yu, Q., Cho, J., Shivapooja, P., Ista, L. K. & López, G. P. Nanopatterned smart polymer surfaces for controlled attachment, killing, and release of bacteria. *ACS Appl. Mater. Interfaces* **5**, 9295–9304 (2013).

58. Lian, J. *et al.* Tunable Adhesion of Different Cell Types Modulated by Thermoresponsive Polymer Brush Thickness. *Biomacromolecules* **21**, 732–742 (2020).

59. Lilge, I. & Schönherr, H. Control of Cell Attachment and Spreading on Poly(acrylamide) Brushes with Varied Grafting Density. *Langmuir* **32**, 838–847 (2016).

60. Bischof, J. C. & He, X. Thermal stability of proteins. *Ann. N. Y. Acad. Sci.* **1066**, 12–33 (2006).

61. Nash, M. E. *et al.* Synthesis and characterization of a novel thermoresponsive copolymer series and their application in cell and cell sheet regeneration) Synthesis and characterization of a novel thermoresponsive copolymer series and their application in cell and cell sheet. *J. Biomater. Sci. Polym. Ed.* **24**, 253–268 (2013).

62. Teodorescu, M. & Bercea, M. Poly(vinylpyrrolidone) – A Versatile Polymer for Biomedical and Beyond Medical Applications. *Polym. Plast. Technol. Eng.* **54**, 923–943 (2015).

63. Yu, Q. *et al.* Protein adsorption on poly(N-isopropylacrylamide)-modified silicon surfaces: Effects of grafted layer thickness and protein size. *Colloids Surfaces B Biointerfaces* **76**, 468–474 (2010).

64. Wu, Z. *et al.* Poly(N-vinylpyrrolidone)-modified poly(dimethylsiloxane) elastomers as anti-biofouling materials. *Colloids Surfaces B Biointerfaces* **96**, 37–43 (2012).

65. Wu, Z. *et al.* Protein Adsorption on Poly(N-vinylpyrrolidone)-Modified Silicon Surfaces Prepared by Surface-Initiated Atom Transfer Radical Polymerization. *Langmuir* **25**, 2900–2906 (2009).

66. Becer, C. R. *et al.* Libraries of methacrylic acid and oligo(ethylene glycol) methacrylate copolymers with LCST behavior. *J. Polym. Sci. Part A Polym. Chem.* **46**, 7138–7147 (2008).

67. Buhl, K. B. *et al.* Polymer Brush Coating and Adhesion Technology at Scale. *Polymers (Basel).* **12**, 1475 (2020).

68. Destarac, M. Industrial development of reversible-deactivation radical polymerization: Is the induction period over? *Polym. Chem.* **9**, 4947–4967 (2018).

69. Li, M. *et al.* SI-PET-RAFT: Surface-Initiated Photoinduced Electron Transfer-Reversible Addition–Fragmentation Chain Transfer Polymerization. *ACS Macro Lett.* **8**, 374–380 (2019).

70. Szczepaniak, G., Fu, L., Jafari, H., Kapil, K. & Matyjaszewski, K. Making ATRP More Practical: Oxygen Tolerance. *Acc. Chem. Res.* **54**, 1779–1790 (2021).

71. Xu, J., Jung, K., Atme, A., Shanmugam, S. & Boyer, C. A robust and versatile photoinduced living polymerization of conjugated and unconjugated monomers and its oxygen tolerance. *J. Am. Chem. Soc.* **136**, 5508–5519 (2014).

72. Matyjaszewski, K., Hongchen, D., Jakubowski, W., Pietrasik, J. & Kusumo, A. Grafting from surfaces for 'everyone': ARGET ATRP in the presence of air. *Langmuir* **23**, 4528–4531 (2007).

73. Dunderdale, G. J., Urata, C., Miranda, D. F. & Hozumi, A. Large-scale and environmentally friendly synthesis of pH-responsive oil-repellent polymer brush surfaces under ambient conditions. *ACS Appl. Mater. Interfaces* **6**, 11864–11868 (2014).

74. Sato, T., Dunderdale, G. J., Urata, C. & Hozumi, A. Sol-Gel Preparation of Initiator Layers for Surface-Initiated ATRP: Large-Scale Formation of Polymer Brushes Is Not a Dream. *Macromolecules* **51**, 10065–10073 (2018).

75. Lee, H. A., Ma, Y., Zhou, F., Hong, S. & Lee, H. Material-Independent Surface Chemistry beyond Polydopamine Coating. *Acc. Chem. Res.* **52**, 704–713 (2019).

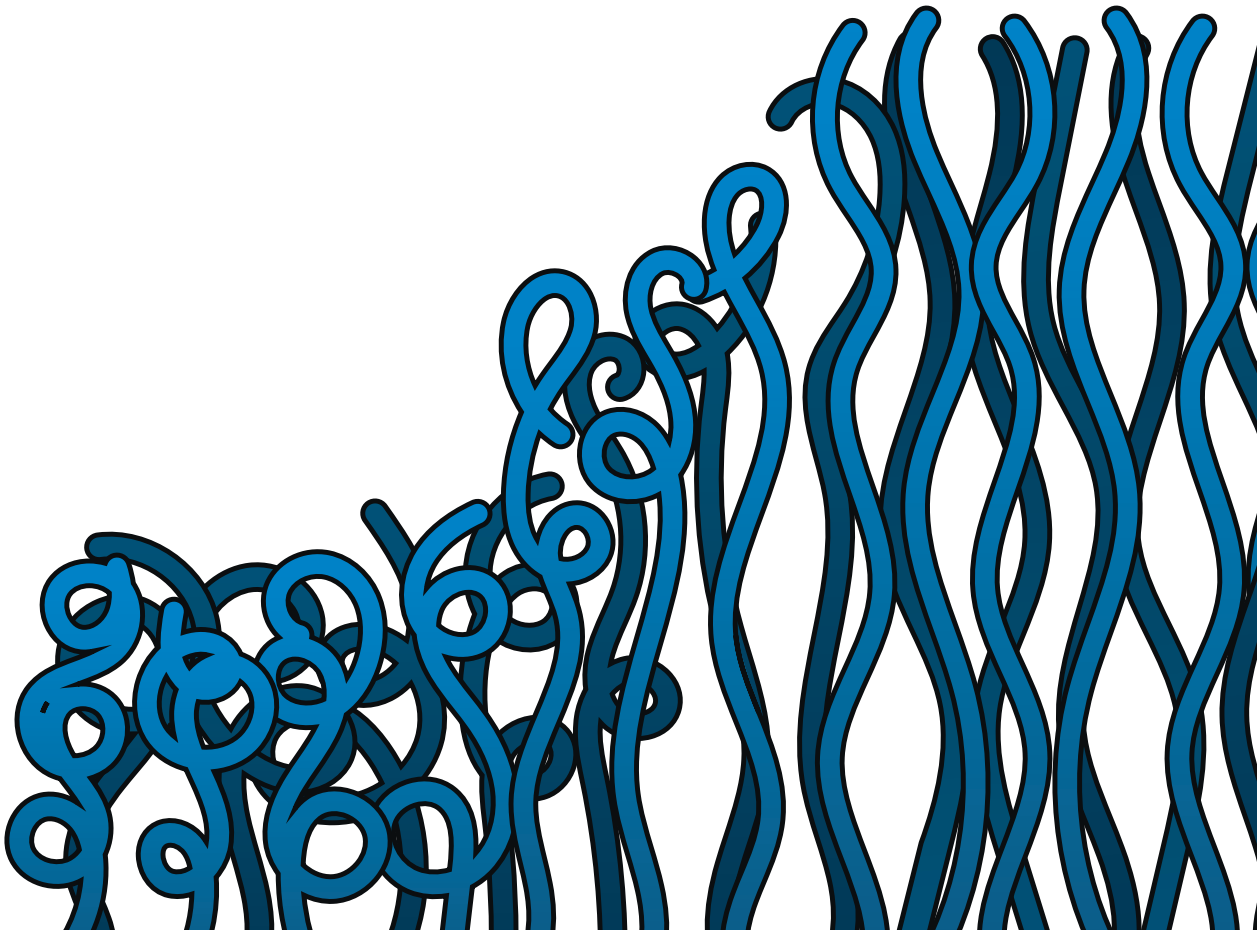

Summary

Summary (English)
Samenvatting (Nederlands)

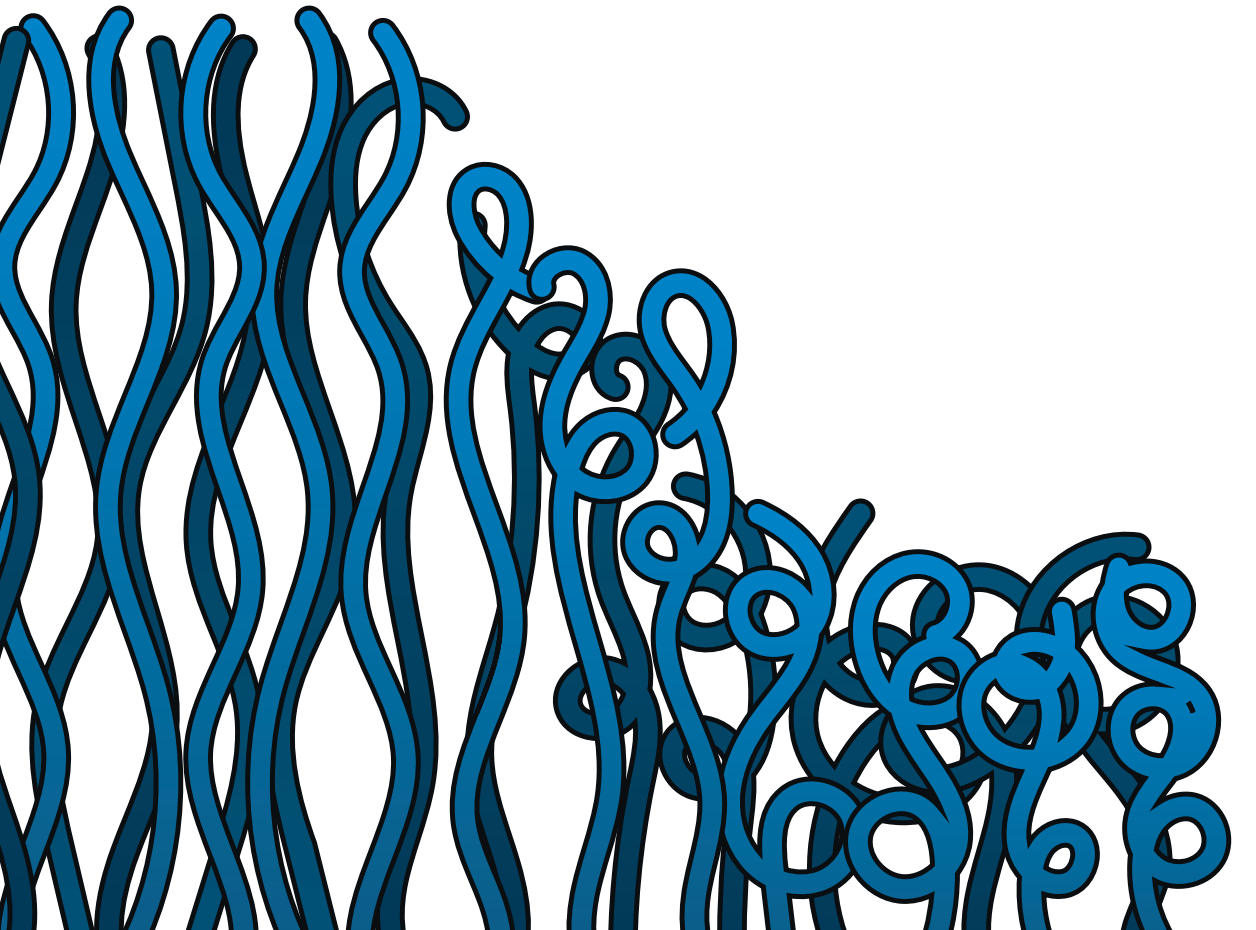

Summary

Control over interactions between biological media and a device's surface is essential for development of biomedical applications. Such control can be achieved by modification of a surface using polymer brush coatings. Introduction of thermoresponsive properties to these polymer brush coatings enables steering of the interactions with the surroundings by application of temperature changes. In this thesis, we describe multiple aspects of polymer brush research, including the synthesis and characterization of novel thermoresponsive polymer brushes, thorough investigation of thermoresponsive properties of these polymer brush coatings and the development of a substrate-independent, modular grafting-to procedure.

Chapter 1 introduces biological fouling and its implications in the production and application of biomedical devices. The main strategies to control the interactions of a surface with biological media are discussed with a particular focus on polymer brush coatings. The concept and typical features of antifouling polymer brush coatings are explained and the current state-of-the-art materials are examined. Moreover, we discuss the properties of thermoresponsive polymer brush coatings and their potential applicability in biomedical devices. Lastly, we zoom in on the currently available synthesis techniques of polymer brush coatings in general.

The majority of thermoresponsive polymer brushes is based on poly(*N*isopropylacrylamide) (poly(NIPAM)), mainly due to its convenient lower critical solution temperature (LCST) at 32 °C. NIPAM is, however, known to suffer from several drawbacks that complicate copolymerization reactions. Therefore, in **Chapter 2**, we present a novel thermoresponsive polymer brush that was synthesized from (*N*(2methacryloyloxyethyl) pyrrolidone (NMEP) using a grafting-from approach. The ability to reinitiate the brush to form block copolymer structures was confirmed by polymerization of a second monomer on top of the poly(NMEP) brushes. Furthermore, we demonstrate that poly(NMEP) brushes exhibit reversible thermoresponsive behavior and that the LCST lies between 40–50 °C. The coated substrates were finally subjected to protein fouling studies, which indicated that poly(NMEP) brushes possess promising antifouling properties.

Thermoresponsive properties in polymer brushes can be employed to control interactions of the brush with its environment. In **Chapter 3**, the synthesis of thermoresponsive polymer brush coatings via a simple two-step grafting-to procedure is described. Silicon oxide substrates were coated with a poly(dopamine) film that acted as a primer for subsequent functionalization. The grafting-to step was then performed using poly(glycidyl methacrylate)-*b*-poly(*N*isopropylacrylamide) (poly(GMA)-*b*-poly(NIPAM)) block copo-

lymers in which the length of the poly(NIPAM) block was varied. This synthesis method is shown to produce polymer brushes of relatively high grafting densities. The differences in thermoresponsive behavior between the three grafted block copolymers is illustrated in detail. Then, we describe that the thermoresponsive properties of the polymer brushes can be employed to control adsorption of proteins from biological media. The methodology developed in Chapter 3 was used for further research, as described in Chapters 4 and 5.

The grafting-to procedure was optimized by investigating the influence of the poly(dopamine) deposition conditions, as described in **Chapter 4**. The deposition reactions were performed at pH ranging from 4–7 from NaOAc buffer in the presence of $NaIO_4$, and at pH 8.5 from Tris buffer. The resulting poly(dopamine)-modified surfaces were then modified with poly(GMA)-*b*-poly(NIPAM) block copolymers. We show that both grafting efficiency as well as film stability are strongly affected by poly(dopamine) deposition conditions. Deposition at pH 7 in the presence of $NaIO_4$ was found to be most appropriate for the subsequent grafting-to reactions. Under these conditions, the thickness of the grafted block copolymer layer could reach up to 19 nm.

In **Chapter 5**, we broaden the scope of the two-step grafting-to procedure by showing that this method can be employed independent of substrate type and monomer functionality. The substrate independence is demonstrated by modification of gold, silicon oxide and polyester-coated glass substrates. The modularity with respect to monomer functionality was illustrated by grafting five distinct block copolymers, all of which contained a short poly(glycidyl methacrylate) segment and a longer segment of varying chemical functionality. To add to its versatility, we show that this procedure can easily be employed to synthesize binary brush coatings.

Finally, in **Chapter 6** we discuss the potential value of the work described in this thesis. The main findings are examined in terms of applicability and several suggestions are provided for further research. Additionally, we review the current status of polymer brush research and speculate on its development in the coming years.

Samenvatting

Het controleren van interacties tussen biologische oplossingen, zoals bloed, en het oppervlak van een apparaat is van essentieel belang bij de ontwikkeling van biomedische apparatuur. Die controle is mogelijk door het aanbrengen van coatings, bestaande uit zogenaamde polymeerborstels. Polymeerborstels bestaan uit lange ketens die met één uiteinde aan het oppervlak vastzitten. Vanwege de hoge dichtheid van de ketens op het oppervlak ontstaat de karakteristieke borstelachtige structuur, waaraan deze coatings hun naam ontlenen. De verwerking van thermoresponsieve polymeren in deze polymeerborstels maakt het mogelijk de interacties van dit oppervlak met de omgeving te beïnvloeden door simpelweg de temperatuur te veranderen. In dit proefschrift beschrijven we onderzoek naar verschillende aspecten van coatings gebaseerd op polymeerborstels, waaronder de synthese en karakterisering van een nieuwe thermoresponsieve polymeerborstel, grondig onderzoek naar de thermoresponsieve eigenschappen van polymeerborstelcoatings en de ontwikkeling van een algemeen protocol om de coatings vast te zetten op het oppervlak dat onafhankelijk is van zowel het aard van het oppervlak als ook van het type polymeer.

Hoofdstuk 1 behandelt aspecifieke adsorptie van biologisch materiaal op oppervlakken en de bijbehorende gevolgen voor productie en toepassing van biomedische apparatuur. De voornaamste strategieën om interacties tussen oppervlakken en biologische oplossingen te sturen worden toegelicht met bijzondere aandacht voor polymeerborstels. Het concept en de eigenschappen van niet-vervuilbare polymeerborstels worden hierin uiteengezet en de nieuwste ontwikkelingen op dit vlak worden beschreven. Verder worden de eigenschappen van thermoresponsieve polymeerborstels en hun toepasbaarheid in biomedische apparatuur bediscussieerd. Tenslotte bespreken we de hedendaagse synthesemethoden voor polymeerborstels in het algemeen.

Het merendeel van thermoresponsieve polymeerborstels is gebaseerd op poly(*N*-isopropylacrylamide) (poly(NIPAM)), voornamelijk vanwege de gunstige lagere kritische oplossingstemperatuur (LKOT) van 32 °C. Van NIPAM zijn echter verscheidene nadelen bekend welke copolymerisatiereacties bemoeilijken. Daarom presenteren wij in **Hoofdstuk 2** een nieuwe thermoresponsieve polymeerborstel, gesynthetiseerd uit het monomeer (*N*-(2-methacryloyloxyethyl)pyrrolidon) (NMEP), met behulp van een zogenaamde grafting-from procedure, waarbij de keten vanaf het oppervlak wordt gegroeid. Het was mogelijk om een tweede monomeer vanaf de bestaande poly(NMEP) ketens te polymeriseren, om zo blokcopolymeren te maken. We toonden ook aan dat de poly(NMEP) borstels reversibele thermoresponsieve eigenschappen bezitten en dat de LKOT tussen de 40 en 50 °C ligt. De gecoate substraten zijn tenslotte blootgesteld

aan eiwitoplossingen, waarbij bleek dat poly(NMEP) borstels veelbelovende antifouling eigenschappen bezitten.

Thermoresponsieve eigenschappen in polymeerborstels kunnen worden toegepast om de interacties tussen de borstel en zijn omgeving te sturen. In **Hoofdstuk 3** wordt een simpele procedure voor de synthese van thermoresponsive polymeerborstel coatings beschreven. Silica substraten werden voorzien van een laag poly(dopamine) die fungeert als een grondlaag voor verdere modificatie. Met behulp van een grafting-to methode, waarbij bestaande polymeren aan een oppervlak worden gezet, zijn verschillende blokcopolymeren met een segment poly(glycidylmethacrylaat) (poly(GMA)) – gebruikt om met de poly(dopamine) laag te reageren – en een segment poly(NIPAM) vastgezet, waarbij de lengte van het poly(NIPAM) blok varieerde. Deze synthesemethode maakte het mogelijk om polymeerborstels van relatief hoge dichtheid te produceren. De verschillen in thermoresponsieve eigenschappen van de drie blokcopolymeren worden in detail toegelicht. Vervolgens laten we zien dat de thermoresponsieve eigenschappen van de polymeerborstels kunnen worden gebruikt om adsorptie van eiwitten uit biologische media te sturen. De methodologie gepresenteerd in Hoofdstuk 3 is gebruikt voor verder onderzoek, zoals wordt beschreven in Hoofdstukken 4 en 5.

De grafting-to procedure werd geoptimaliseerd door de invloed van de depositie-omstandigheden van poly(dopamine) te onderzoeken, zoals beschreven in **Hoofdstuk 4**. De depositiereacties werden uitgevoerd bij pH-waarden tussen 4 en 7 uit een natriumacetaatbuffer in de aanwezigheid van $NaIO_4$, en bij pH 8.5 uit een Trisbuffer. De resulterende, met poly(dopamine) bedekte substraten werden vervolgens gemodificeerd met poly(GMA)-*b*-poly(NIPAM) blokcopolymeren. We tonen aan dat zowel de dichtheid als de stabiliteit van de polymeerborstels sterk worden beïnvloed door de depositie-omstandigheden van poly(dopamine). Depositie bij pH 7 in de aanwezigheid van $NaIO_4$ was het meest geschikt voor de grafting-to reacties. Onder deze omstandigheden bereikt de dikte van de gekoppelde blokcopolymeerlaag 19 nanometer.

In **Hoofdstuk 5** verbreden we de toepasbaarheid van de tweestaps grafting-to procedure door aan te tonen dat deze gebruikt kan worden ongeacht het substraattype of het gekozen monomeer. De substraatonafhankelijkheid wordt aangetoond door goud, silica en met polyester bedekt glas te modificeren. De modulariteit ten aanzien van monomeerkeuze wordt bewezen door vijf verschillende blokcopolymeren aan de substraten te koppelen. Elke van deze blokcopolymeren bevatte een kort segment van poly(GMA) en een langer segment van het desbetreffend monomeer. Verder laten we zien dat deze procedure eenvoudig kan worden toegepast om binaire polymeerborstels te maken.

Tenslotte bespreken we de potentie van het werk dat wordt beschreven in deze thesis in **Hoofdstuk 6**. De voornaamste bevindingen van dit werk worden bediscussieerd met het oog op toepasbaarheid en er worden suggesties gegeven voor vervolgonderzoek. Daarnaast beschouwen we de huidige status van het onderzoeksveld gericht op polymeerborstels en speculeren over toekomstige ontwikkelingen.

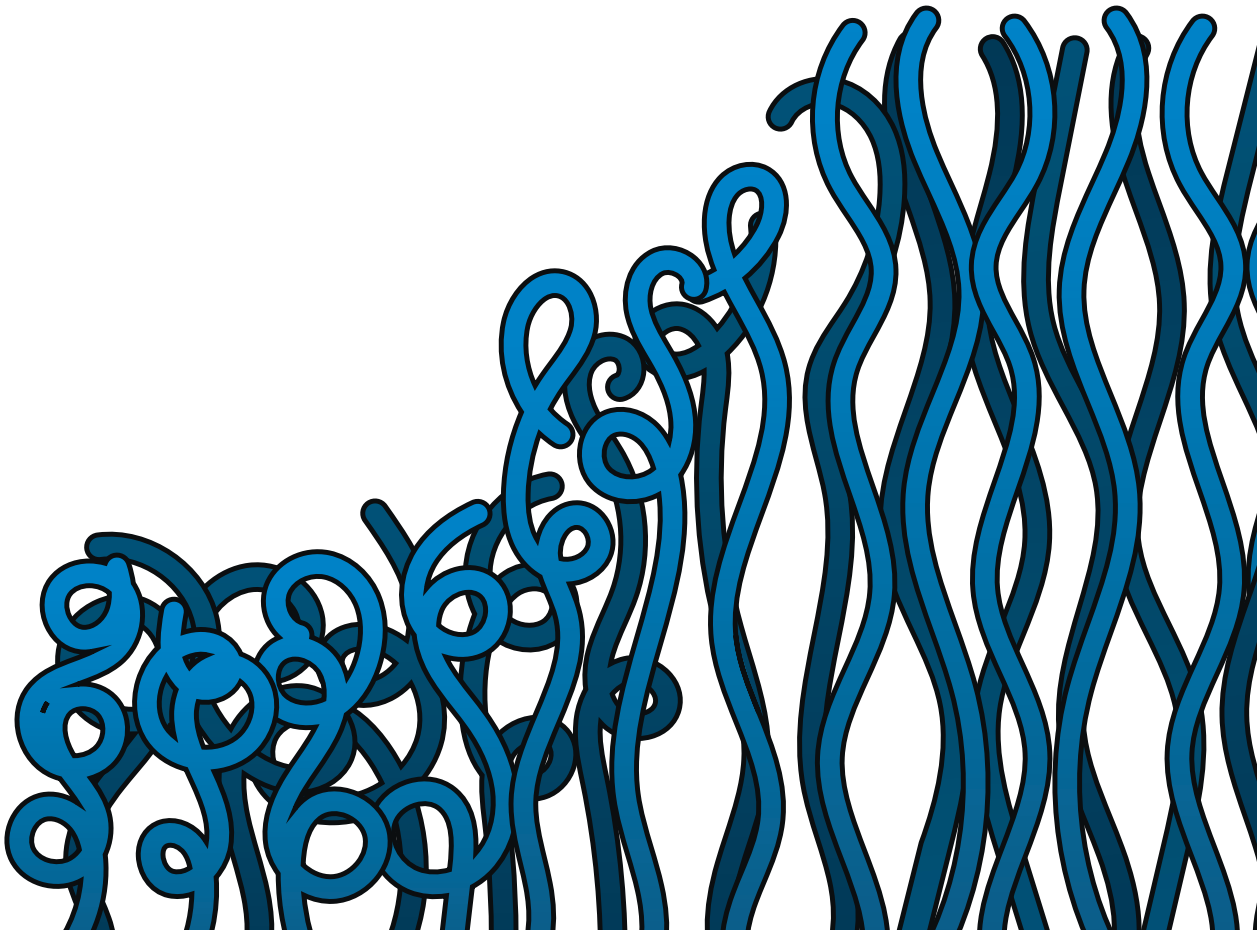

About the author

Curriculum Vitae
List of publications
Overview of completed training activities

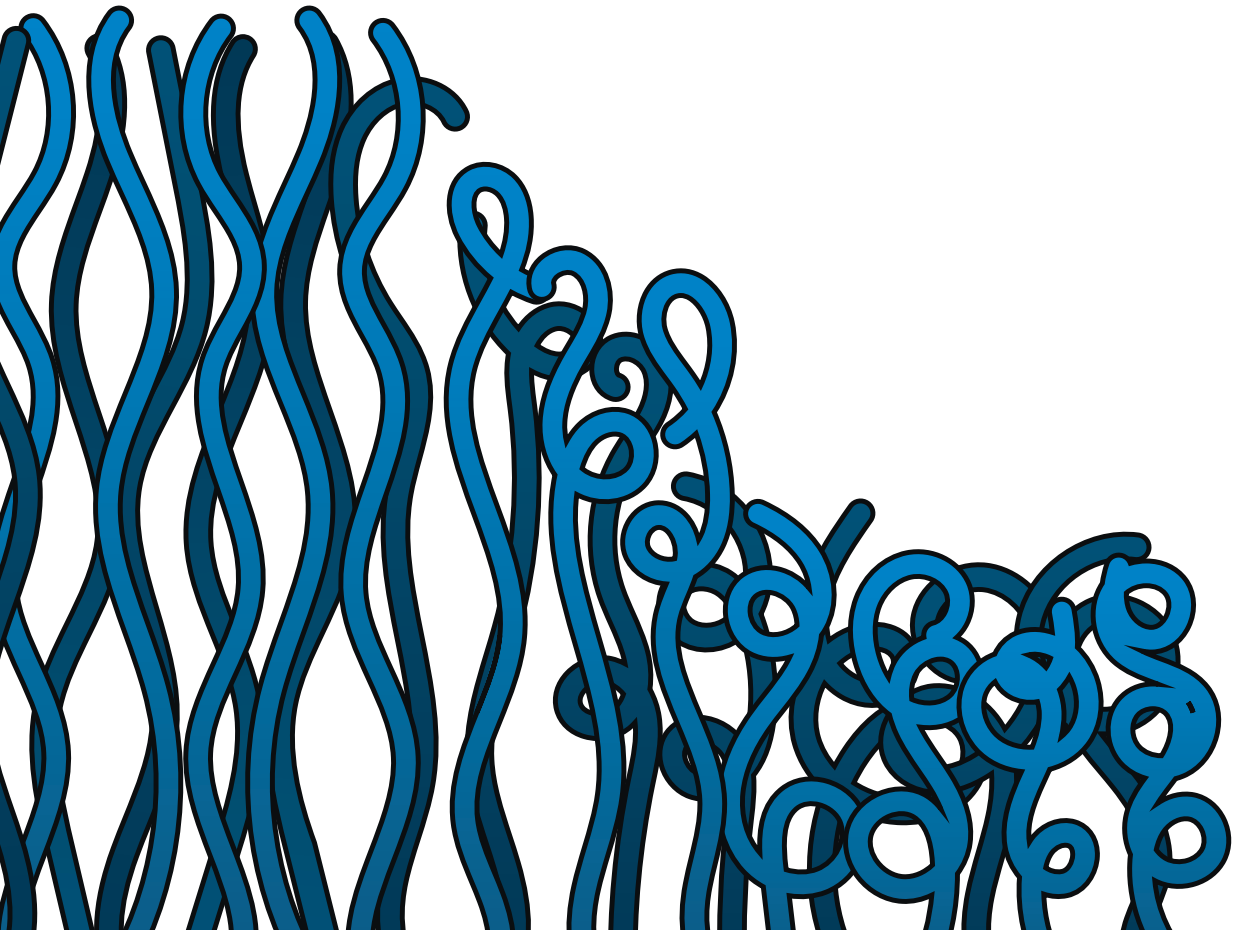

Curriculum vitae

Lucas Willem Teunissen was born on September 19, 1994 in Gouda, The Netherlands. He finished his high school education (Coornhert Gymnasium, Gouda) in 2012 and subsequently started his studies in Chemistry at Utrecht University. The third year of his BSc program, he spent abroad at the University of Glasgow, Scotland. He conducted his BSc thesis project in the Van 't Hoff Laboratory for Physical and Colloid Chemistry, Utrecht, (supervisors: Dr. P.G. Moerman and Prof. Dr. W.K. Kegel), where he studied charge prediction for viral capsid proteins. Following his BSc studies, Lucas followed the Master's program Nanomaterials at Utrecht University, during which he performed an internship at Croda, Gouda. His MSc thesis research was carried out at the Inorganic Chemistry and Catalysis group (supervisors: Dr. C.S. Lancefield and Prof. Dr. P.C.A. Bruijnincx) and was aimed towards the development of novel lignin depolymerization procedures using homogeneous catalysis. Lucas received his MSc degree in 2018 and in the same year he started his PhD project at the Laboratory of Organic Chemistry at Wageningen University & Research under the supervision of Dr. Ir. M.M.J. Smulders and Prof. Dr. Han Zuilhof. The most important results of this research are described in this thesis.

List of publications

Teunissen, L. W., Smulders, M. M. J. & Zuilhof, H. Modular and Substrate-Independent Grafting-to Procedure for Functional Polymer Coatings. *Langmuir*, in press. (2023)

Teunissen, L. W., Smulders, M. M. J. & Zuilhof, H. 19 nm-Thick Grafted-To Polymer Brushes onto Optimized Poly(Dopamine)-Coated Surfaces. *Adv. Mater. Interfaces*, in press., (2023).

Teunissen, L. W., van den Beukel, J., Smulders, M. M. J. & Zuilhof, H. Thermoresponsive Polymer Brushes for Switchable Protein Adsorption via Dopamine-Assisted Grafting-To Strategy. *Adv. Mater. Interfaces* **9**, 2201198 (2022).

Teunissen, L. W., Kuzmyn, A. R., Ruggeri, F. S., Smulders, M. M. J. & Zuilhof, H. Thermoresponsive, Pyrrolidone-Based Antifouling Polymer Brushes. *Adv. Mater. Interfaces* **9**, 2101717 (2022).

Kuzmyn, A. R., Teunissen, L. W., Fritz, P., van Lagen, B., Smulders, M. M. J., Zuilhof, H., Diblock and Random Antifouling Bioactive Polymer Brushes on Gold Surfaces by Visible-Light-Induced Polymerization (SI-PET-RAFT) in Water. *Adv. Mater. Interfaces* **9**, 2101784 (2022).

Kuzmyn, A. R., Teunissen, L. W., Kroese, M. V, Kant, J., Venema, S., Zuilhof, H., Antiviral Polymer Brushes by Visible-Light-Induced, Oxygen-Tolerant Covalent Surface Coating. *ACS Omega* **7**, 38371–38379 (2022).

Kuzmyn, A. R., Nguyen, A. T., Teunissen, L. W., Zuilhof, H. & Baggerman, J. Antifouling Polymer Brushes via Oxygen-Tolerant Surface-Initiated PET-RAFT. *Langmuir* **36**, 4439–4446 (2020).

Lancefield, C. S., Teunissen, L. W., Weckhuysen, B. M. & Bruijnincx, P. C. A. Iridium-catalysed primary alcohol oxidation and hydrogen shuttling for the depolymerisation of lignin. *Green Chem.* **20**, 3214–3221 (2018).

Overview of completed training activities

Discipline specific activities	Organizing institute	Year
Advanced Organic Chemistry	ORC (VLAG)	2018 - 2022
Chains (CHemistry As INnovating Science)	NWO	2019 - 2021
Intern. Conference on Bio-inspired and Zwitterionic Materials	ICBZM	2019
Dutch Polymer Days	PTN	2019
M2I Conference	M2I	2019 - 2022
Brightlands Polymer Days	Brightlands	2021

General courses	Organizing institute	Year
VLAG PhD week	VLAG	2019
Project and time management	WGS	2020
Online Presenting Materials Science	4TU.HTM/BW Science	2021
Efficient Writing Strategies	In'to Languages	2022
Effective behaviour in your professional surroundings	GS WIAS	2022
Introduction to Latex	PE&RC	2022
Career Assessment	Meijer en Meijaard	2023

Optionals	Organizing institute	Year
Preparation of research proposal	ORC/VLAG	2018
PhD study tour to Israel	ORC	2019
Weekly group meetings	ORC	2018 - 2023

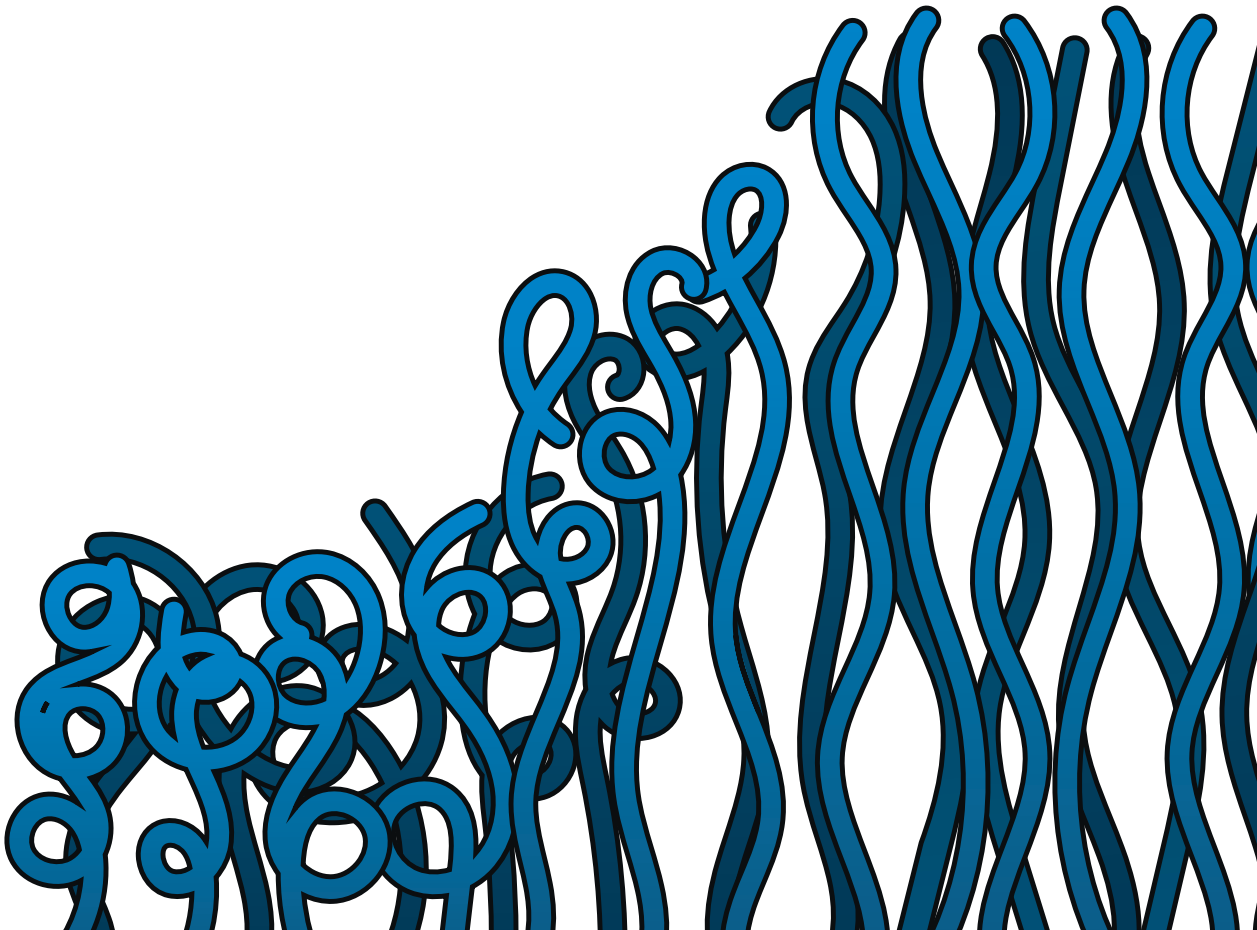

Acknowledgements

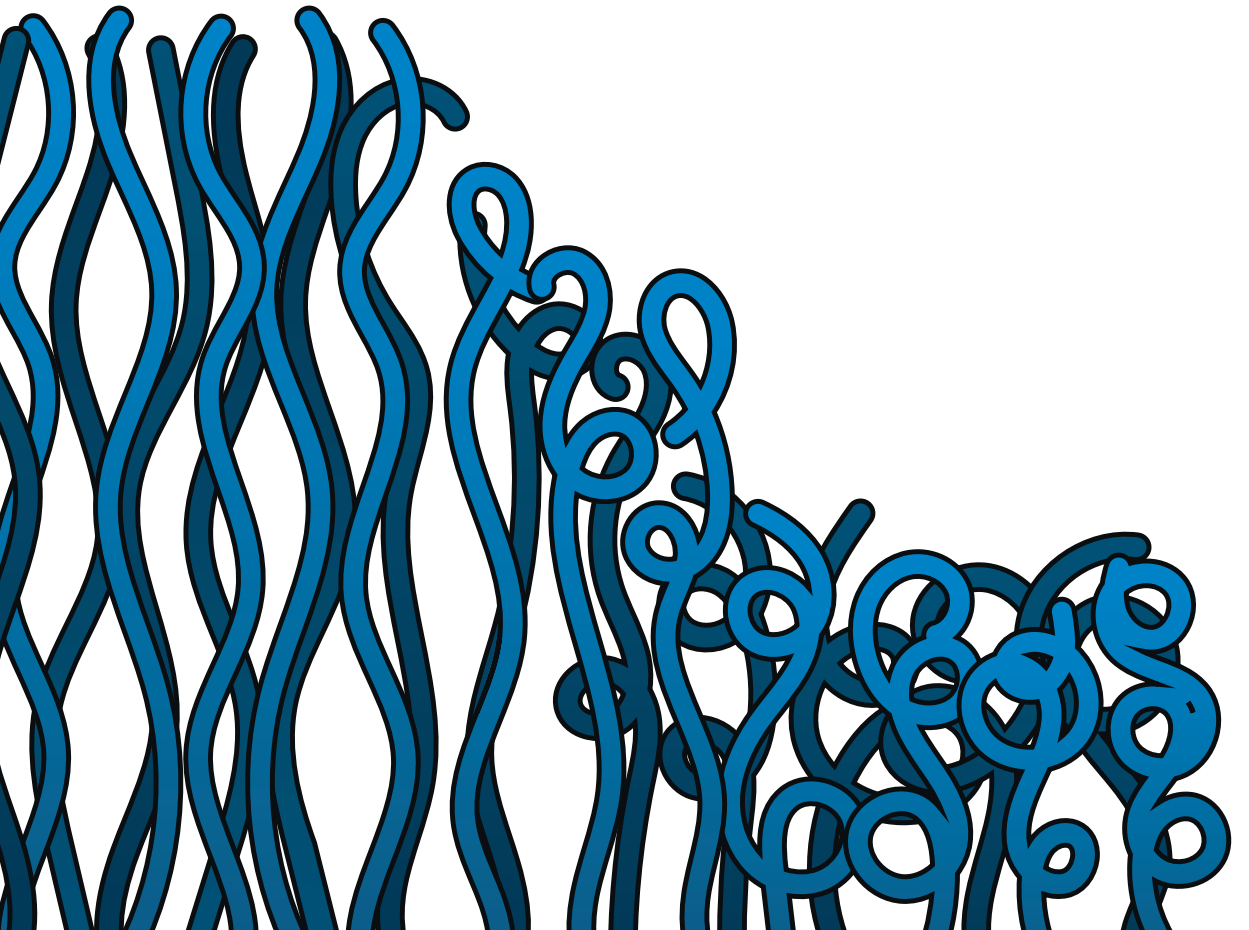

Acknowledgements

It's incredible to have arrived at this point, to write this part of my thesis and look back at the time I have spent in Wageningen. Four and a half years ago, I started my PhD project at ORC. For me, that meant working on a new and unfamiliar research topic in a new and unfamiliar research group. Frankly, I had no idea of what I was getting myself into. Fortunately, I can now say that I am glad to have started at ORC. It has been a great experience and an equally great challenge; and it is only due to the support of my colleagues, friends and family that I have indeed made it to this point.

First, I would like to thank my promotor, Han. Despite my lack of experience working with polymer brushes or surface chemistry, you allowed me to start the project and join your research group. I am very thankful for that opportunity and for the support that you have provided along the way. Additionally, I would like to thank you for your valuable input on the design and wording of manuscripts, which has taught me a lot.

Maarten, my copromotor, I am incredibly grateful to have had you as my daily supervisor. From the start you have been supportive, understanding and approachable. Our interactions were always pleasant, with room for both small talk and more serious issues. In the last months, when I needed input quite frequently, you were always happy to help. I still do not understand how you combine your speed of reply with such attention to detail. It really was a pleasure to have been working with you.

Fredérique and Julian, I am extremely happy that you have agreed to be my paranymphs. Dear Fredérique, I'm proud to say that since we met at the very beginning of our chemistry careers, you have become one of my dearest friends. We weren't too bad when working with each other on study projects, but we work particularly well together outside of class. We've made such good memories (festivals, carnaval, chin stitching, unemployment afternoon, Dutch champions cycling quiz for mixed teams, etc.) and I am already looking forward to adding to that list.

Dear Julian, your positive attitude is unmatched, something I believe everyone around you can testify to. It has been great to have someone in ORC to share a passion for sports and the outdoors with. I've really enjoyed our running and climbing sessions as well as our shared lunches, which you also prefer to have outdoors, oftentimes regardless of poor weather conditions. It's a shame we just missed each other in Thailand, but hopefully we'll meet many times to come in equally beautiful places.

To all members of my thesis committee, Prof. Dr. J.R. de Vries, Prof. Dr Ir. J. Huskens, Prof. Dr. M. Weinhart and Dr. Ir. H. Van der Weijde; thank you for finding the time to validate my PhD thesis.

My career at ORC was jumpstarted by joining the PhD trip last minute, I couldn't have imagined a better way to start in the group and get to know my colleagues. Since then, I have had the pleasure to work with so many great PhD students, postdocs, technicians and guest researchers. Andriy, you have been of such great help during my project. During the first few months, you taught me how to perform polymerizations in the first place. Later, you became the best sparring partner to discuss experimental results or advancements in the field, either in the office, over drinks, or on the bike. I am very grateful for that! Alice, thank you so much for the lovely dinners at your place in Wageningen, car rides from Ede-Wageningen and simultaneous Italian swear word orations, and providing me with your and your mother's advice on Sicily; you are great. The LFOTM of the month drinks we organized have yet to be topped, it was great to run that with you, Sybren. Although we never went, I'm quite sure that our PhD-trip would have been great, had it taken place, Ellen, Canan and Simon. Jay, I really enjoyed hanging out during lunches, between experiments and over drinks; such a shame we never got the chance to go to the mysterious International Club. Yuri, I'm happy that I could always find you to discuss two of the most important talking points there are: Previous weekend stories and plans for the next. For many more great times, I would like to thank Jasper, Tunan, Alyssa, Jorick, Ian, Esther, Annemieke, Bas, Jordi, Hamit, Michel, Dongdong, Rafael, Si, Thijmen, Tjerk, Natassa, Muthu, Pepijn, Kaustub…

The findings in this thesis would not have been there if it weren't for the help of a few very appreciated colleagues. Simone, thank you for helping out with AFM measurements, you came in at exactly the right time. Barend, you have been a great help with using the XPS and many other pieces of equipment. Sidhu, thank you for running XPS experiments and our discussions on surface modifications. Sevil, your extensive introductory lessons and colorful notes to the QCMD are very much appreciated. Hans, you were always there when I had GPC issues or just for a good chat at the ORC drinks, I appreciate that! Judith, thanks a lot for guiding me through supervising practicals only one week after joining ORC.

My collaborators at Tata Steel are acknowledged for their contributions during meetings as well as conferences. Ganesan, I'd like to personally thank you for your involvement and advice throughout the entire four years.

For important contributions to my research project, intriguing questions and educational collaborations, I want to thank my students Koen, Rui, Axel, Eline, Joram and Jelle. I wish you the best of luck with your future careers!

Many can probably agree, the time of the pandemic was not great. Thankfully, I got to spend a lot of time with my flat mates at the Koekoek. With a dart board, smoke machine and disco light, we turned our stamp-sized living room into the smallest café of Utrecht where we could have a drink after work, watch NAC and discover the magic of the statafel.

In Utrecht, the seed was planted for the success that is this PhD thesis. I would like to thank the friends that I made there, Daniël, Jasper, Laura, Nienke, Sander, Thomas and Sophie; who have been an important part of my life since. Likewise, I want to thank my high school friends, with whom I have had so many special moments throughout the years and who I consider some of my closest friends, in particular Jorik, Just, Luc, Olaf and Sam. Additionally, I want to thank San en Mir, you will always be the best neighbors, wherever you may be. Roland and Julie, I want to thank you for being so incredibly welcoming and kind.

One group of people that is too big to name personally, but definitely deserve a honorable mention are the many friends that I have made at USVV Odysseus '91 and USV Hercules. A big thank you to my friends from Hercu Zat 2, I could not wish for a better team.

My family has been a constant source of support for me. Mathijs and Nadine, it's cool to see how all three of us have found our own way after moving away from Gouda. I am glad we see each other quite frequently though and am proud to have you as my siblings. To my parents, papa en mama, I strongly feel that this PhD thesis would not have been here were it not for you. Throughout my entire life, you have been nothing but loving and supportive. The solid foundation that you have provided has allowed me the freedom to pursue my academic as well as personal interests, and ultimately brought me where I am now. I am and always will be grateful for that.

Finally, Karen, lieve Ka, I want to thank you for your consistent care, support and love during the past years. Even though you do not consider yourself patient, you have been precisely that when I was spending a lot of time and energy on work. As I am writing this, we have embarked on our big adventure and I enjoy every moment with you. You are absolutely amazing and I am so excited for everything that lies ahead of us.

This research was carried out under project number C16030a in the framework of the Partnership Program of the Materials innovation institute M2i (www.m2i.nl) and the NWO Domain Science, which is part of the Netherlands Organization for Scientific Research (www.nwo.nl).

Financial support from Wageningen University & Research for printing this thesis is gratefully acknowledged.

Cover design by Lucas Teunissen
Printed by Ipskamp Printing | proefschriften.net
Layout and design: Erwin Timmerman, persoonlijkproefschrift.nl